A STUDY ON REAL-TIME MEDIUM-RANGE CARRIER-PHASE-BASED GPS MULTIPLE REFERENCE STATIONS

HORNG-YUE CHEN

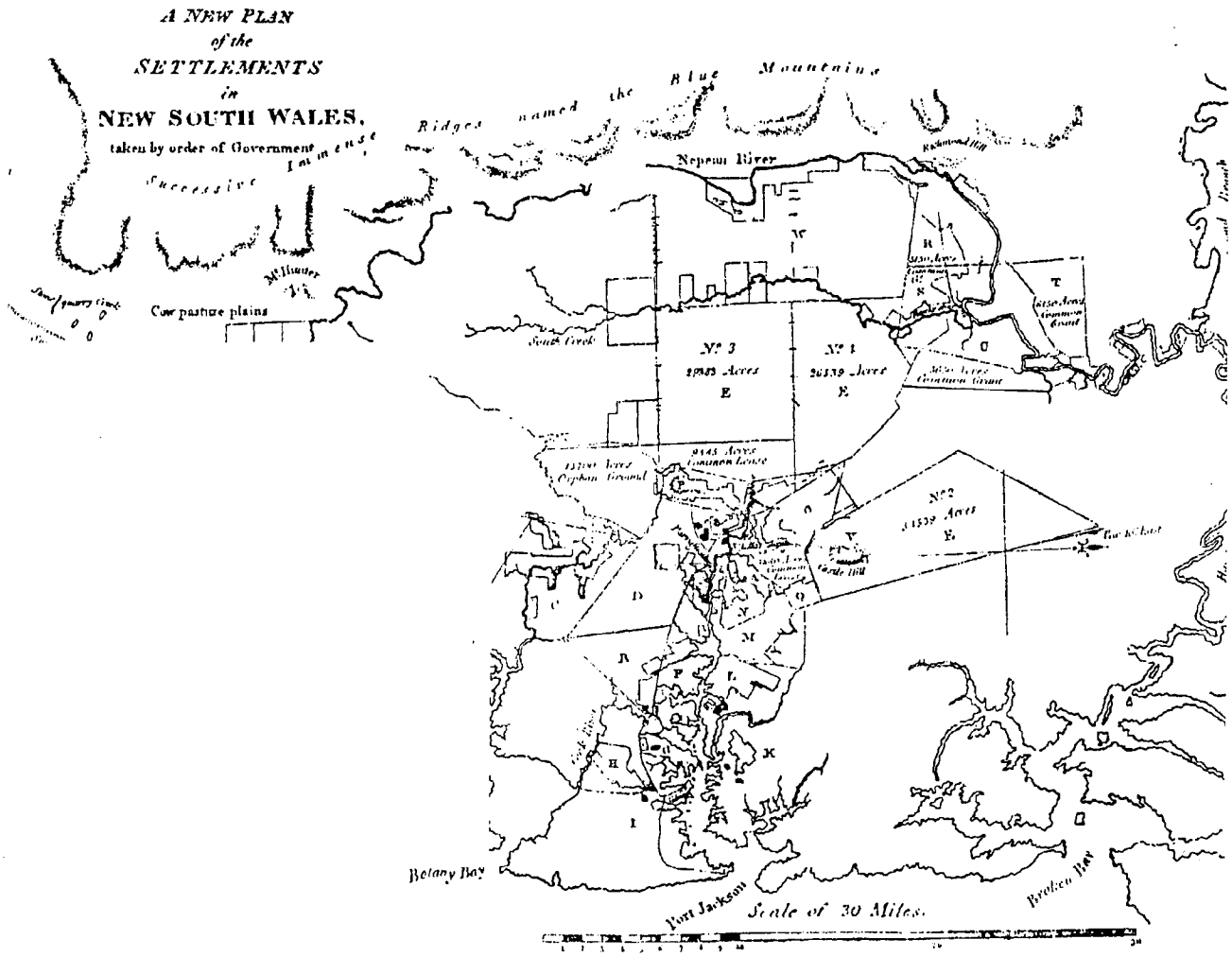

UNISURV S-64, 2001

Reports from

SCHOOL OF SURVEYING
AND SPATIAL INFORMATION SYSTEMS

THE UNIVERSITY OF NEW SOUTH WALES UNSW SYDNEY NSW 2052 AUSTRALIA

UNISURV REPORT S-64, 2001

A STUDY ON REAL-TIME MEDIUM-RANGE CARRIER-PHASE-BASED GPS MULTIPLE REFERENCE STATIONS

HORNG-YUE CHEN

Received: August 2001
Accepted: September 2001

SCHOOL OF SURVEYING AND SPATIAL INFORMATION SYSTEMS
(formerly GEOMATIC ENGINEERING)
UNIVERSITY OF NEW SOUTH WALES
UNSW SYDNEY NSW 2052
AUSTRALIA

UNISURV REPORTS

Series Editor: Dr. J. M. Rüeger

National Library of Australia

Card No. and ISBN 0 - 7334 - 1842 - 2

FOREWORD

Researchers have extensively used GPS measurements for geodetic applications, such as the study of crustal plate motion and deformation monitoring, since the early 1980s. In such applications, geodesists typically measure the baselines within special deformation networks on a regular (usually annual) basis. These techniques have become highly developed so that nowadays sophisticated scientific GPS software packages are used to rigorously compute baselines. Such software, when combined with state-of-the-art, dual-frequency hardware and specialised operational procedures, are capable of delivering relative accuracies at the few tens parts-per-billion level, from which station motions are deduced. Recently there has been an increased interest in permanent, continuously operating GPS networks. This thesis reports on the research undertaken to make operations of continuous GPS networks more efficient, and to support several user applications. Three different data processing techniques have been developed for this purpose.

A 'fast static' algorithm to effect a form of hardware *densification* of a network of dual-frequency GPS receivers through the deployment of an array of low-cost, single-frequency GPS receivers has been developed. This algorithm was tested using several data sets from the permanent GPS network of Japan's Geographical Survey Institute, and from a network operated by Taiwan's Institute of Earth Sciences, Academia Sinica. Data from a variety of geographical regions, with different inter-receiver distances, and collected at different seasons of the year, were used. The results confirm that such a spatial densification using single-frequency receivers can achieve relative accuracies similar to dual-frequency static positioning techniques over inter-receiver distances up to almost 100 km.

This research also addressed the main challenge of continuous GPS network operations, namely the need to keep resolving the ambiguities instantaneously (or with minimum delay) when tracking to a satellite that experiences cycle slips, or a long data gap, or when a new satellite rises above the horizon. A three-step strategy, which is suitable for implementation in real-time, was proposed. Finally, improvements have been made to the data processing algorithm for user-reference receiver baseline determination. An algorithm similar to triple-differences formed between one epoch with unknown ambiguities and another epoch with the fixed ambiguities can be used to derive the relative ambiguity values, which are ordinarily equal to zero (or to the number of cycles that have 'slipped' when loss-of-lock has occurred). Because of the temporal correlation characteristics of the error sources, the cycle slips can be easily 'recovered' using the proposed functional model.

To test the performance of this algorithm, an experiment for the precise positioning of an aircraft, over distances ranging from a few hundred metres up to a few hundred kilometres, was carried out. The results indicate that the proposed technique can successfully resolve the relative ambiguity (or cycle slips) over long distances in an efficient manner.

In summary, this report describes a number of innovative techniques to enhance the positioning performance with the aid of multi-GPS reference receiver networks.

Chris Rizos

August 2001

ABSTRACT

Researchers have extensively used GPS measurements for geodetic applications, such as the study of tectonic plate motion and crustal deformation, since the early 1980s. In such applications, geodesists typically measure the baselines within special deformation networks on a regular (usually annual) basis. These techniques have become highly developed so that nowadays sophisticated scientific GPS software packages are used to rigorously compute baselines. Such software, when combined with state-of-the-art, dual-frequency hardware and specialised operational procedures, are capable of delivering relative accuracies at the few tens parts-per-billion level, from which station motions are deduced. Recently there has been an increased interest in permanent, continuously operating GPS networks. Three techniques that make the operations of GPS networks more efficient, and support several user applications, have been proposed in this thesis.

A 'fast static' algorithm to effect a form of hardware densification of a network of dual-frequency GPS receivers is tested. This involves the deployment of a permanent array of low-cost, single-frequency GPS receivers to increase the receiver network spatial resolution. A variation of this integration strategy permits the use of cost effective operational procedures based on single-frequency receivers with relatively short station occupation times. This integration methodology was tested using several data sets from the permanent GPS network of Japan's Geographical Survey Institute, and from a network operated by Taiwan's Institute of Earth Sciences, Academia Sinica. Data from a variety of geographical regions, with different inter-receiver distances, and collected at different seasons of the year, were used. The results confirm that this methodology can achieve relative accuracies similar to dual-frequency static positioning techniques over inter-receiver distances up to almost 100km.

In practice, the ambiguities associated with the network data processing can be correctly resolved during some sort of 'initialization' procedure. However, the main challenge is to keep on fixing the ambiguities instantaneously (or with minimum delay) when tracking to a satellite that experiences cycle slips, or a long data gap, or when a new satellite rises above the horizon. A three-step strategy, which is suitable for implementation in real-time, is proposed for addressing these challenges. In the first step, the high correlation of the atmospheric delay between adjacent epochs is used to assist cycle slip 'recovery' and ambiguity resolution. Then such an atmosphere model is used in a predictive manner to correct the double-differenced observations, on an epoch-by-epoch and satellite-by-satellite basis. Finally, the atmosphere model is applied in a kinematic data processing algorithm to fix the ambiguities during situations when there is a long data gap, or when a new satellite rises between the tracking horizon of the reference stations.

Due to the presence of the ionospheric signal delay, satellite orbit errors and the troposphere delay, so-called 'absolute' ambiguity resolution "on-the-fly" for long-range positioning applications becomes very difficult, and largely impossible. However, all of these errors exhibit a high degree of spatial and temporal correlation. In the case of short-range ambiguity resolution, because of the high spatial correlation, their effect can be neglected, but their influence will dramatically increase as the baseline length increases. However, between discrete measurement epochs they will still exhibit a large degree of similarity for short time spans. An algorithm similar to triple-differences formed between one epoch with unknown ambiguities and another epoch with the fixed ambiguities can be used to derive the relative ambiguity values, which are ordinarily equal to zero (or to the number of cycles that have 'slipped' when loss-of-lock has occurred). Because of the temporal correlation characteristics of the error sources, the cycle slips can be easily 'recovered' using the proposed functional model. In order to test the performance of this algorithm an experiment for the precise positioning of an aircraft, over distances ranging from a few hundred metres up to a few hundred kilometres, was carried out in October 1999. The results indicate that the proposed technique can successfully resolve the relative ambiguity (or cycle slips) over long distances in an efficient manner that can potentially be implemented in real-time.

TABLE OF CONTENTS

LIST OF TABLES

Table

LIST OF FIGURES

Figure

ACKNOWLEDGEMENTS

As I complete this thesis, I would like to express my sincere gratitude to those who have enabled this study to be accomplished.

To my supervisor Prof. Chris Rizos, the main reason that I came to The University of New South Wales, Australia, for his valuable advice and encouragement which was given to me throughout this study.

To my co-supervisor Dr. Shaowei Han, who has been always helpful in my research, and who especially helped me to understand his multiple reference station concept.

To members of the Satellite Navigation and Positioning (SNAP) group, Craig Roberts, Linlin Ge, Volker Janssen, Chalermchon Satirapod, Ip Ki Choi, Michael Moore, Clement Ogaja, Jun Zhang and Liwen Dai, for assistance in collection GPS data and much valued discussion. To Mr. Liwen Dai, Linlin Ge and Jun Zhang in particular, for their assistance and programming support.

To the Republic of Taiwan's Institute of Earth Sciences, Academia Sinica, who supported a study grant to help me to study towards a Ph.D. at the School of Geomatic Engineering, UNSW.

To Prof. Shui-Beih Yu. Your encouragement is greatly appreciated, because it was you who helped me take my first steps to study abroad.

To all of my friends, especially Wang-Shung Chung and Long-Chen Kuo. Your unselfish teaching and support was a most valuable assistance in my studies.

To my parents, who freely give everything and keep on encouraging me in my studies. Also to my children, Arick and Alice.

To my wife, Piin-Shiow Wang, who supported me unwaveringly and who ably substituted for my absence in caring for my family.

Chapter 1
INTRODUCTION

1.1 GPS and Deformation Monitoring

1.1.1 Background

Since 1990, the full constellation of Global Positioning System (GPS) satellites ensures that at least five (and usually more) satellites are visible anywhere on earth, on a 24 hour basis. The GPS system has therefore been adopted for worldwide navigation, as well as for many other applications where precise positioning is required, such as in surveying, mapping and other scientific applications. After Selective Availability (SA) was turned off at UTC 2 May 2000 04:00 by order of the President of the United States, the accuracy of the Standard Positioning Service (SPS) increased from about 100m horizontal and 156m height (at the 95% confidence level) to less than 10 metres (Rizos et al. 2001). While such accuracy is a welcome boon to many SPS users such as outdoor and boating enthusiasts, the turning off of SA has had no impact on precise relative positioning applications such as those generally referred to by the generic label of 'geodesy'.

Compared with traditional surveying methods, using GPS to address geodetic applications such as deformation monitoring has many advantages. For example, GPS provides an all-weather, 24 hour a day, globally available, independent of line-of-sight requirements, precise positioning tool, that has now become an indispensable technology for a wide range of surface and building deformation monitoring systems.

The *coverage* of a deformation monitoring system is of course very dependent on the application requirements. For example, to measure tectonic plate motion, a global network of monitoring stations is required. To monitor a specific feature, such as a volcano, a regional network is used. To monitor an active fault, a local network may be utilised. Nevertheless, in general, the objective of a deformation monitoring system is to detect the relative motion of stations, objects or benchmarks within a network especially established for such a purpose.

The *accuracy* of the relative positioning information derived by GPS is influenced by many factors, most notable of which are geometry (satellites and stations), data collection

strategy, data processing strategy and level of errors and biases. These include: satellite geometry, orbit error, atmospheric effects, and how they impact on different baseline lengths (which may be casually identified as being of the 'short', 'medium' or 'long' baseline class), multipath bias, the mode of positioning (static or kinematic mode), observation time span, and others. However, once the purpose and configuration of the monitoring network has been defined, the appropriate positioning algorithm and estimation parameter strategy can be identified.

Many researchers have contributed to the definition of a reliable, effective and standard methodology for processing GPS measurements in order to address geodetic applications. Thousands of research publications, conference papers and books have been published on topics concerned with sophisticated GPS data processing. Topics range from space segment errors (e.g. orbit errors, reference systems), GPS signal transmission and other errors (e.g. atmospheric effects, multipath bias and observation noise), ambiguity resolution procedures (e.g. functional model, stochastic model and reliability), studies of observation time span (as a function of baseline length and relative position accuracy), accounting for hardware biases (e.g. receiver inter-channel bias and antenna phase centre variation), to ground monument, reference frame definitions, and the special demands of different locations (equator, mid-latitude or auroral area) in general, and the specifications of particular applications.

1.1.2 The requirements of deformation monitoring systems

There are so many requirements to decide the deformation monitoring systems. From the GPS-based point of view, the most common factors are: the content coverage, high performance and accuracy.

1.1.2.1 Content coverage

The International GPS Service (IGS) coordinates the operation of a network of global GPS tracking stations, and generates several products from the GPS measurements: GPS satellite ephemerides, earth rotation parameters, IGS tracking station coordinates and velocities, GPS satellite and IGS tracking station clock information, and zenith path delay estimates (IGS, 2001). From an analysis of the changes in the tracking station coordinates, the motion of the tectonic plates can be deduced (as it can also directly from the estimated station velocities). The European reference frame (EUREF) GPS network is the European regional densification of the IGS network. The main purpose of the EUREF network is to estimate on a weekly basis the coordinates, and associated covariance information, of all tracking stations within the network, from which the plate motion of the European continent can be estimated (EUREF, 2000). The Japanese GEONET (GPS Earth Observation Network) has a similar function, and its primary product is a vector map, depicting the distance and coordinate changes of the GPS stations across Japan (GEONET,

2000). Hence, GPS plays a major role in geodynamic studies, with spatial resolutions ranging from the global (inter-station distances of several hundreds to thousands of kilometres in the case of the IGS), down to national scales (several tens of kilometres in the case of the GEONET).

1.1.2.2 High performance

Some of the GPS monitoring systems are set up to detect changes in station coordinates that might be precursors to hazards, such as in the case of systems that monitor volcanoes, active faults or manmade structures. The basic requirement of such monitoring systems is the acquisition of GPS coordinate solutions in real-time, perhaps with a high data rate. With an unobstructed sky view at the monitoring station, the current constellation of GPS satellites ensures that 5 to 8 satellites are in view anywhere on earth. Furthermore, the current generation dual-frequency receivers operate at very fast rates (up to 20Hz, or 0.05 second data sample rate), so that kinematic positioning techniques can output independent coordinates as fast as the data rate.

There are many GPS-based deformation monitoring systems being used to study the geodynamics of volcanoes or earthquakes. For example, scientists at the Hawaiian Volcano Observatory use a variety of techniques to measure ground deformation around volcanoes in Hawaii, including GPS. During a brief eruptive episode of the Kilauea Volcano that began on 30 January 1997, continuously recording GPS receivers measured significant ground deformation near the eruption site along part of the volcano's east rift zone. The stations moved apart about 36cm during the volcanic activity, and continued to move apart at a slower rate after the activity stopped on 31 January 1997. More than half of the extension between the GPS sites actually occurred during a period of volcanic tremor that began about 8 hours before the eruption started. This suggests that the magma took about 8 hours to reach the surface once it started to move (HVO, 2000).

In another example, an M7.1 earthquake occurred at 2:46am local time on 16 October 1999 was captured by the Southern California Integrated GPS Network (SCIGN Analysis Committee Report September, 2000). The event was located in a remote, sparsely-populated part of the Mojave Desert, approximately 47 miles east-southeast of Barstow and 32 miles north of Joshua Tree. The SCIGN is a cooperative project of the U.S. Geological Survey (USGS), the Jet Propulsion Laboratory (JPL), and the Scripps Institution of Oceanography (SIO). There are now approximately 140 SCIGN stations operating in Southern California; and an additional 110 are planned. Fortunately, several recently-installed GPS stations were near the Hector Mine epicentre. In the case of the SCIGN, the USGS is in charge of earthquake response. As part of that responsibility USGS computed the coseismic displacements. Significant coseismic displacements were observed at stations as distant as Blythe and Palomar, and of course throughout the Mojave Desert region. The largest motion occurred at Landers Elementary School - that site has permanently shifted 19cm towards the north-northeast. The static displacements from these rather far off sites are consistent with very simple, uniform-slip dislocation models (USGS, Earthquake Hazards Program-South California, 1999)

In these two examples, GPS has shown itself to be a reliable, all-weather geodetic measuring tool that can be used by earth scientists to study the continuously deforming earth. When combined with other scientific methodologies, GPS is expected to contribute significantly to research into the mitigation of volcanic and seismic hazards.

1.1.2.3 Accuracy

Although monitoring systems may operate over different scales, in different areas, with minor variations in design, sufficient accuracy to satisfy the detection of the deformation is the basic requirement. Table 1-1 (Rizos et al., 2000) lists the faulting lengths associated with earthquake activity and their maximum displacements. It is obvious that the maximum seismic displacement can be easily detected after a major event using GPS monitoring networks. In general, the assured accuracy of the GPS-derived coordinates from static processing is under one centimetre, once the carrier cycle ambiguities have been fixed to their true integer values.

Table 1-1. Earthquake surface faulting (Rizos et al. 2000)

Locality	Date (dd/mm/yy)	Magnitude (M)	Length (km)	Maximum displacement (m)	
				Horizontal	Vertical
Chedrang Fault, India	12/06/1897	8.7	19	N/A	11.0
Formosa	16/03/1906	7.1	48	2.5	1.3
California, USA	18/04/1906	8.3	434	6.4	1.0
Nevada, USA	03/10/1915	7.8	32	N/A	4.5
Murchison, New Zealand	16/06/1929	7.6	4	N/A	4.6
Chile	22/05/1960	8.3	1600	N/A	N/A
Alaska, USA	28/03/1964	8.5	900	6.0	6.0
Iran	31/08/1968	7.4	27	4.0	N/A
Taiwan	20/09/1999	7.3	100	9.0	5.5

*N/A: Not Available

For earthquake motion studies, the pre-seismic deformation is often more important than post-seismic displacement information. The challenge therefore is to detect precursor motion, with uniform high accuracy, across a wide range of spatial scales (Mervart, 1995; Yu et al., 1997). For example, because of the unpredictable characteristics of earthquakes such as that occurred in Taiwan on 20 September 1999 (earthquake magnitude 7.3 in which more than 2000 people were killed), together with the sparsely distributed GPS stations within an active fault monitoring system, the efficiency of such monitoring systems is not as good as volcano deformation monitoring systems. Although volcano eruptions are also difficult to predict, a GPS-based monitoring system is much easier to set up for such a localised phenomenon.

1.2 Motivation

The carrier phase-based multiple reference station concept has been proposed by Han & Rizos (1995a), Raquet & Lachapelle (1997), Wanninger (1995), Wübbena et al. (1996), and others, for high precision positioning applications that extend over many tens of kilometres. In such applications it is assumed that the objective is to determine the (relative) positions of GPS receivers at arbitrarily located user stations within the area defined by the reference station network (whose locations are assumed fixed, and whose coordinates are known). The technique is therefore similar to the pseudorange-based differential GPS (DGPS) systems, such as the Wide Area Augmentation System (WAAS) and Wide Area Differential GPS (WADGPS)(Figure1-1, 1-2) (Parkinson et al., 1996). That is, the multiple reference station networks can be used to generate "correction data or messages" that, when used in the data analysis of observations made by both user and reference receivers, reduces or eliminates the effect of distance dependent biases (principally orbit error and atmospheric delay) that typically plague relative positioning.

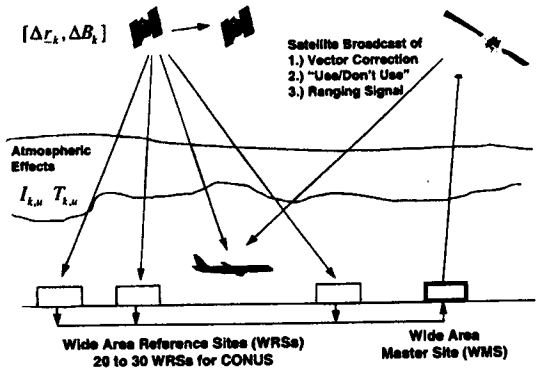

Figure 1-1. Wide area augmentation system.

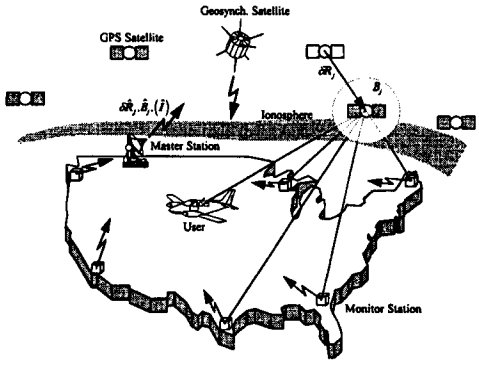

Figure 1-2. Wide area differential GPS.

(all adapted from Parkinson et al., 1996)

Compared to the process by which the pseudorange correction data/messages are generated (for WAAS and WADGPS), in the case of the carrier phase-based network concept an extra complication is the need to resolve the "ambiguity" terms that must be estimated during between-reference receiver data processing. This is crucial if the required positioning accuracy is at the centimetre level. The carrier phase-based multiple reference station methodology was successfully used for single-epoch kinematic solutions (Han, 1997), for "fast static" solutions during active solar maximum conditions (Wanninger, 1999), and for single-frequency receiver solutions (Rizos et al., 1998; 2000), even for baseline lengths up to one hundred kilometres. For the short or medium range GPS positioning with long observation period, the ambiguities do not need to be all fixed in integer (float solution solutions) which still can acquire precise enough relative positioning,

because through the long enough observation period the biases causing by ambiguity terms become very small.

Permanent GPS receiver networks are increasingly being established for multi-functional uses, including to support carrier phase-based GPS positioning for surveying or precise navigation applications. In such an implementation the generation of carrier phase "correction messages", in a manner analogous to WADGPS, requires that the ambiguities present in the models of double-differenced measurements between GPS reference stations be resolved to their integer values in real-time, and that these values be derived on a continuous basis. Although the ambiguities could be resolved at the beginning of network operation, the challenge remains: how to recover an integer ambiguity if a cycle slip or data gap occurs, or if a new satellite rises?

1.3 Research Objectives

The main research objectives in this thesis are to: (1) analyse the performance of low-cost single-frequency GPS receivers for geodetic applications using the multiple reference station methodology, (2) develop an algorithm to consider the circumstances of 'new' satellites, or long data gaps, for real-time ambiguity resolution within the reference station network, and (3) integrate the 'ambiguity recovery method' to allow the multiple reference station service to operate in real-time.

Three main objectives are described below:

1.3.1 Analysing the performance of low-cost single-frequency GPS receivers for geodetic applications using the multiple reference station methodology

Researchers have used GPS for geodetic applications for many years. In such applications, where there are no continuously operating GPS receivers, geodesists typically measure the baselines within special deformation networks on a regular (usually annual) basis. The GPS analysis techniques have become highly developed so that nowadays scientific GPS software packages are used to compute the baselines. Such software, when combined with state-of-the-art, dual-frequency hardware and specialised operational procedures, are capable of delivering relative accuracies at the few tens parts-per-billion level (approximately sub-centimetre error in a baseline of 100km or so in length).

Over the last decade or so there has been an increasing interest in establishing permanent, continuously operating GPS (CGPS) networks. One geodetic implementation being studied at The University of New South Wales (UNSW) is a form of *densification* of a sparse network of dual-frequency GPS receivers in which a permanent array of low-cost, single-

frequency GPS receivers is deployed to increase the spatial resolution of the monitoring network (Rizos et al., 2000). A variation of this integration strategy permits the use of cost effective operational procedures based on single-frequency receivers with relatively short station occupation times.

Conventional CGPS networks, such as the GEONET established in Japan to precisely measure earth surface movement, are very expensive; the high cost being primarily due to the fact that dual-frequency GPS receivers are used. Note that Japan's nationwide GEONET network is the world's largest, numbering nearly 1000 receiver stations, with an average station spacing of the order of 30km (Rizos et al., 2000).

In order to densify such CGPS networks (important when high spatial resolution is required for the monitoring of particular deformation phenomena), and to promote the use of the CGPS technique in lesser developed countries, a significantly cheaper system architecture is needed. The proposed UNSW design is an integrated, dual-mode network consisting of single-frequency GPS receivers across the area of interest, surrounded by a sparser network of dual-frequency GPS receivers. Initial tests of data collected at selected stations in the GEONET network have already shown that, through enhanced data processing algorithms, a CGPS network containing both single-frequency and dual-frequency receivers would be able to deliver better than centimetre level accuracies, at considerably lower cost than present systems based exclusively on dual-frequency instrumentation.

The first field test of this CGPS system design was carried out in the Tsukuba area of Japan, in August 1999. The test network consisted of: (a) several stations of the GEONET network surrounding (b) an inner network of four single-frequency Canadian Marconi GPS receivers installed by UNSW researchers. The data from both the GEONET and the UNSW receivers were processed using a modified version of the Bernese GPS Software Package. The software first processes the GEONET GPS station data in order to generate empirical data "corrections", which are then applied to the double-differenced data of the GPS baselines located within the test area enclosed by the GEONET stations. These corrections have the effect of improving baseline solution accuracy by up to an order of magnitude, even for baselines ranging up to 100km in length.

The baselines connecting the inner network to the surrounding GEONET stations are processed in a number of modes, including 24hr files (as is the standard practice for geodynamic applications) and hourly data files (as in local deformation monitoring applications). The results indicate that single-frequency-with-correction processing can achieve accuracies of better than 5mm in the horizontal components and 3cm in height, while the dual-frequency results can achieve accuracies better than 2mm in the horizontal components and 6mm in height. Therefore, for many geodetic applications, there are no significant differences between the single-frequency-with-correction results and the

standard dual-frequency results, especially as far as the measurement of horizontal components is concerned.

1.3.2 Developing an algorithm to consider the rise of 'new' satellites, or long data gaps, for real-time ambiguity resolution within the reference station network

For high accuracy real-time (or near real-time) applications, the multiple reference station network needs to output the data corrections on a continuous basis, to ensure that the user stations can immediately apply the corrections to help resolve the integer ambiguities instantaneously (or nearly so). Hence, there are two major challenges: to operate the *multiple reference station network on a continuous basis*, and to optimize the use of data corrections *in the user receivers* to ensure precise positioning at all times.

For medium-sized reference station networks, the estimated ambiguities, because the distance between the stations may be many tens of kilometres, are contaminated by atmospheric biases. Therefore it is a significant challenge to resolve the correct integer ambiguities, in real-time (or near real-time). Li & Gao (1998), Rabah & Leinen (1999), and others, have suggested algorithms for fixing the integer ambiguities estimated from the processing of data from medium-sized reference station networks.

At the user stations, as the distance dependent biases in double-differenced observables linking user and reference stations can, in principle, be accounted for by the reference network-derived data corrections, then the integer ambiguities can be resolved more easily and precise positioning can be assured. For example, Wübbena & Bagge (1996), Han & Rizos (1997b) and Wanninger (1997) have addressed the problem of using multiple reference stations to reduce the impact of unmodelled atmospheric biases.

However, for real-time high accuracy applications, although the integer ambiguities of the reference station networks can be fixed at the beginning of network operation by using data collected over several hours, they have to be resolved again when the tracked satellite has a cycle slip, or a long data gap occurs, or when a new satellite rises.

This thesis focuses on the development of an algorithm to resolve integer ambiguities in real-time (or near real-time) for the reference stations, by using the atmospheric delay derived at initialization and the predicted atmospheric biases from previous epochs. The main challenges for real-time implementation are:

1. Repairing cycle slips for tracked satellites at the reference stations from the atmospheric delay of previous epochs, in order to assist the resolution of ambiguities for reference station data processing.

2. Prediction of the ionospheric and tropospheric delay for existing satellites at the reference stations using previous measurements. When the tracked satellite has a long data gap, the atmospheric delay can, to some extent, be predicted for the purpose of aiding the resolution of the ambiguities.

3. Prediction of the tropospheric delay for a newly-risen satellite at the reference stations using a prediction model based on measurements from other tracked satellites. The estimation of the tropospheric delay for a newly-risen satellite can help fix the associated integer ambiguities.

Tests involving several CGPS networks have shown that the proposed methodology can provide reliable integer ambiguities for medium-sized reference station networks.

1.3.3 Integrating the 'ambiguity recovery method' to allow the reference station service to operate in real-time

A triple-difference-type approach has been proposed for "ambiguity recovery". For medium-range (and long-range) the ambiguities are hard to resolve to their correct integer values because of the effects of distance dependent residual biases, especially for real-time (or near real-time) applications. The correct ambiguities may be referred to as the 'absolute' ambiguities. However, there are high correlations of the distance-dependent biases between epochs, hence it is easier to solve for the 'relative' ambiguities than for the 'absolute' values. A triple-difference-type 'ambiguity recovery' technique can be used to generate the data corrections from multiple reference station networks, and can be implemented in real-time.

1.4 Research Methodology

The research **methodology** of this thesis are to perform the three categories: (1) analysing the performance of low-cost single frequency receiver in geodetic applications using the multiple reference station algorithm. (2) developing the algorithm when the new satellite rises or long data gap for real-time ambiguity resolution between reference stations. (3) integrating the ambiguity recovery method to help the reference stations operating in real-time or near real-time.

1.4.1 Analysing the performance of low-cost single frequency receiver in geodetic applications using the multiple reference station algorithm.

The algorithm discussed in the chapter 3 will show that from the linear observable combination for determining the user stations, the major error sources such as orbit bias, ionospheric delay, the tropospheric delay and multipath bias have been reduced or eliminated.

The data processing procedure consists of the following three steps (Rizos et al., 1998):

1. Perform the ambiguity resolution for the reference stations and derive the residual vectors.

2. Determine the linear combination coefficients (the α values) from the approximate position of any user stations (single-frequency receivers) and the reference stations, then the correction term is obtained.

3. Apply this correction term to the double-differenced carrier phase observations. The standard rapid static positioning procedure can then be used to resolve integer ambiguities and to derive the user station coordinates.

1.4.2 Developing the algorithm when the new satellite rises or long data gap for real-time ambiguity resolution between reference stations.

At the beginning of operation, the integer ambiguities can be acquired within the reference stations with the known coordinates. Hence, the double differenced ionospheric and tropospheric delay can be estimated and then predicted to assist ambiguity resolution for next epoch. The linear combinations commonly used in real-time medium range carrier phase ambiguity resolution are wide-lane, L1 or ionospheric-free linear combinations.

The data processing procedure can be divided into four steps:

1. At the beginning of the operation, the coordinates and the ambiguities need to be known at the reference stations. It means that the reference stations have to acquire the known coordinates and integer ambiguities in initialization.

2. After fixing the integer ambiguities of the reference stations, the ionospheric and tropospheric delay can be estimated. Although the RTZD (Relative Troposphere Zenith Delay) can be computed in every epoch at Step 1, the variation in RTZD value still can be up to a few centimetres because of the observation noise and tropospheric delay residuals. The RTZD values will have to be computed in every 5min to acquire the stable model values.

3. For the next epoch, the observations can apply the ionospheric and tropospheric delay values from previous epoch to help fixing the current ambiguities, using the ionosphere free linear combination (first fixing wide lane integer ambiguity then L1 integer ambiguity (the effective wavelength is 10.7cm)). If there is a long data gap or instantaneously a new satellite is rising, the tropospheric delay can be predicted by the RTZD value. At the reference stations, the coordinated is known, the orbit error will slightly affect ambiguity resolution when the predict orbit is applied and the multipath error can be reduced by hardware and software techniques. Therefore the main error source of the ionospheric-free linear combination is the tropospheric delay as the wide lane integer ambiguities is acquired.

4. Using the ionosphere free linear combination, after fixing the wide lane integer ambiguity and then try to fix the L1 integer ambiguity. However, the effective wavelength in L1 only is 10.7cm and the observation noise combined with the

tropospheric delay have a large variation, hence accumulating the observations in low elevation satellite for fixing integer ambiguity is necessary.

1.4.3 Integrating the ambiguity recovery method to help the reference stations operating in real-time or near real-time.

From the computational point of view, the distance dependent biases have a high temporal correlation. This means that between two consecutive observation epochs the GPS signals have been affected by almost the same atmospheric propagation conditions. Hence, the triple-differenced observables are similarly affected. They can be used to 'link' one epoch with unknown ambiguities to another epoch with fixed ambiguities, in order to derive the 'relative' ambiguity values. They are ordinarily equal to zero (or to the number of cycles that have 'slipped' when loss-of-lock occurred).

The triple-differenced approach for 'ambiguity recovery' can be used in any kind of linear combination to determine the 'relative' integer ambiguities. The remained biases still have a significant effect, hence some strategies for implementing the 'ambiguity recovery' technique should be developed to improve the success rate of ambiguity resolution.

The triple-difference-type ambiguity recovery procedure can be performed in 5 steps:

1. Read the observation, ephemeris data and initial integer ambiguities.

2. Detect the cycle-slips using widelane and monster widelane linear combinations. If no cycle-slips occur, using the ionosphere-free linear combination to estimate the user coordinates and computing the triple-difference-type residuals of the dual-frequency observations.

3. If cycle-slips occur, apply the triple-difference-type residuals of the previous epoch.

4. According the error propagation of the widelane and monster widelane linear combinations to determine the ambiguity search space in φ_1 and φ_2.

5. Ambiguity resolution using the determined search space.

1.5 Outline of the Thesis

This thesis consists of seven chapters.

Chapter 1. Introduction. This chapter introduces the research topic, the motivation for this research, the research objectives, the methodology and the contributions of the research.

Chapter 2. Network-based precise GPS positioning techniques and applications. This chapter introduces the continuously operating GPS networks, and the categorisation of carrier phase-based positioning techniques for precise deformation monitoring.

Descriptions are given of the successful application of GPS for geodynamics research using a global network (International GPS Service), regional networks (Southern California Integrated GPS Network, or the GPS Earth Observation Network in Japan), or a local network (Taiwan GPS Network, in Taiwan). Emphasis is placed on the advantages of multiple reference station techniques not only from the accuracy point of view, but also in thinks of economic and logistical considerations. A study of several current implementations of network-based algorithms, such as the Network Solution (Lachapelle, Canada), Virtual Reference Station Approach (Wanninger, Germany) and the Multiple Reference Station Approach (Han & Rizos, Australia), is made.

Chapter 3. Multiple reference station processing in support of precise, medium-range GPS positioning. This chapter describes the geometry of multiple reference stations and the network densification applications. The operational procedure for generating network data corrections, including the initialisation of reference stations, determination of coordinates and ambiguities, and the generation of correction terms, is outlined. The basic functional model and the modified model for multiple reference stations are presented, suitable for the generation of the data corrections, and their application to both dual-frequency or single-frequency users. Some experimental results of the application to kinematic and fast static mode positioning are described.

Chapter 4. Real-time atmospheric bias prediction for resolving ambiguity resolution between reference stations. This chapter compares two different methods to solve the real-time application deflects of the continuously-operating multiple reference station networks. The main requirement for continuously-operating multiple reference station networks is that the integer ambiguities between the reference stations need to be known at all times. Even though these ambiguities can be resolved at the beginning of network operation, the challenge remains: how to recover an integer ambiguity if a cycle slip, or data gap occurs, or if a new satellite rises? Hence, two algorithms have been proposed. The first one, using the correlation between previous information concerning the atmospheric bias, can improve the success rate by about 20% for newly-risen satellites (compared with not applying this atmosphere information). The second method estimates the tropospheric delay using the tracking satellite information from the multiple reference stations. Tests indicate that the ambiguity resolution success rate can be increased by up to 90%.

Chapter 5. Ambiguity recovery using triple-difference-type observables for reference station processing. This chapter proposals an concept, which is due to the presence of the ionospheric signal delay, satellite orbit errors and the tropospheric delay, so-called 'absolute' ambiguity resolution "on-the-fly" (OTF-AR) for distances up to and beyond 100km becomes very difficult, if not impossible. However, all of these biases exhibit a high degree of spatial and temporal correlation. In the case of short-range ambiguity resolution, because of the high spatial correlation, their effect can be neglected, but their influence will dramatically increase as the baseline length increases. However, between

discrete trajectory epochs they will still exhibit a large degree of similarity for short time spans. In this chapter the similar triple-differences formed between one epoch with unknown ambiguities and another epoch with fixed ambiguities can be used to derive the 'relative' ambiguity values, which are ordinarily equal to zero (or equal to the number of cycles that have 'slipped' when loss-of-lock occurred). In order to test the performance of this algorithm, an experiment for the precise positioning of an aircraft, over distances ranging from a few hundred metres up to 700 kilometres, was carried out in October 1999. The results indicate that the proposed technique can successfully resolve the relative ambiguities (or cycle slips) over long distances, in an efficient manner that can be implemented in 'real-time'.

Chapter 6. Medium-range network-based geodetic monitoring systems. This chapter confirms the feasibility of using single-frequency GPS receivers for medium-range precise positioning, with the aid of data corrections derived from the multiple reference station algorithm. This algorithm makes high precision relative positioning accuracy possible, using data from single-frequency receivers installed within a sparse permanent GPS network, even if the baseline lengths are of the order of a few tens of kilometres or more. In this section, various scenarios for testing the multi-reference station methodology of Han & Rizos (1997b), for sub-part-per-million, single-frequency receiver positioning, are discussed. The second experiment verifies the performance of medium-range kinematic positioning. The instantaneous OTF-AR algorithms can be used for kinematic GPS positioning, at the same time ensuring high accuracy, availability and reliability for critical applications. Data from different areas, and for varying baseline lengths, were tested.

Chapter 7. Summary, conclusions and recommendations. The final chapter of the thesis contains a summary of research findings, some conclusions and recommendations for further research.

1.6 Contributions of the Research

The contributions of this research can be summarised as follows:

1. A continuously-operating, carrier phase-based multiple reference station methodology as proposed here requires that the ambiguities between the reference stations be resolved to their integer values at all times. Although the ambiguities associated with the reference station data can be estimated during initialisation, the remain challenges are: the 'recovery' of an integer ambiguity if a cycle slip or long data gap occurs, or if a new satellite rises. Hence, two algorithms have been proposed. The first one uses the correlation between the previous information concerning the atmospheric bias. The second method estimates the tropospheric delay using tracking information from the multiple reference stations.

2. The extended functional model for medium-range, carrier phase-based GPS positioning, based on the application of data corrections derived from an analysis of multiple reference station data, can accommodate more than one user receiver operating simultaneously. In the processing procedure, by forming the double-differences between the user stations, and using the data corrections from the CGPS network, the user station coordinates can be determined without using any reference station observation data directly.

3. A new integrated 'ambiguity recovery' method is proposed using a type of triple-differenced observable, which when combined with the 'ambiguity recovery' algorithm suggested by Han (1997), is more effective even during periods of ionospheric disturbances.

4. A wide range of single-frequency data was analysed to test the performance of the algorithm for 'fast static', medium-range precise positioning using the multiple reference station methodology. The data sets were selected so that the integrated, dual-mode networks are located at different latitudes, traversing large station elevations, involve data collected during different seasons, employ single-frequency receivers of different makes, and use baselines of different lengths.

5. Medium-range kinematic results derived from the application of the multiple reference station methodology have been analysed. The instantaneous OTF-AR algorithm can be used for kinematic GPS positioning over several tens of kilometres, at the same time ensuring high accuracy, availability and reliability for critical applications.

Chapter 2

NETWORK-BASED PRECISION GPS POSITIONING TECHNIQUES AND APPLICATIONS

2.1 Introduction

Continuously-operating GPS networks have been used for many years to address geodetic applications such as the determination of crustal motion on local, regional and continental scales. Many hundreds of permanent GPS stations around the world contribute data to the International GPS Service (IGS). One example of a continental scale network is the Australian Fiducial Network (AFN), comprising less than ten GPS receivers (AUSLIG, 1999). Some of the inter-station distances in this network are over a thousand kilometres. Many other networks have been established to study local ground deformation due to tectonic faulting. Examples of such networks include the Southern California Integrated GPS Network (SCIGN) (Bock et al., 1997), and the Geographical Survey Institute's (GSI) network in Japan. The latter now consists of almost 1000 permanent GPS stations (Sagiya et al., 1997). Such networks are operated according to similar principles, for example they collect and archive dual-frequency carrier phase data on a daily basis. This chapter will describe some network-based GPS positioning techniques and applications.

2.2 Carrier Phase-Based Positioning Techniques

2.2.1 Short-range, medium-range and long-range positioning

For carrier-based GPS positioning techniques the average baseline length can be used to categorise them into *short-range*, *medium-range* and *long-range* techniques. From the ambiguity resolution point of the view, these categorise match the difficulty in resolving the integer ambiguities in the double-differenced observables for the baseline connecting the two receiver stations. Typically the 'short-range' baselines are defined as being between about 10km (Rothacher et al., 1996) and 20km (Rizos, 1996). The average length is dependent on the level of ionospheric activity, as this impacts on ambiguity resolution and the resultant position accuracy obtained using comparatively simple observable models. When the level of ionospheric activity is high (as during periods of solar maximum), then

the average baseline length defining the 'short-range' category is shortened, and conversely during periods of 'quiet' ionospheric activity. The 'medium-range' techniques may be taken as those that address regional scale applications, and hence the range of baseline lengths is generally limited to being less than about 100km. Baseline lengths over 100km may therefore be regarded as belonging to the 'long-range' category.

These categories are also important as far as defining the positioning techniques to be used for different applications. For instance, the short-range technique(s) can be used for the monitoring of buildings, dams, bridges, and other structures. On the other hand, regional scale geodetic applications such as the monitoring of a volcano, an active fault or a plate boundary deformation zone, require medium-range GPS positioning techniques. While global applications such as the determination of crustal deformation clearly require the use of long-range positioning techniques.

2.2.2 Modes of positioning

The static mode of relative positioning assumes that the receiver antennas are stationary during the period of observation. Although it is possible to estimate the ambiguities, and to resolve them to their integer values, with a few epochs of data, for geodetic applications it is generally conceded that the length of observation time span is closely linked to the accuracy requirement. Figure 2-1 shows the change in quality of the estimated baseline components for different observation session lengths, for both an ambiguity-free solution (where the ambiguities are estimated as real-valued quantities) and an ambiguity-fixed solution (where the estimated ambiguities are resolved to their correct integer values) (taken from Mervart, 1995). Figure 2-2 also illustrates the relationship between a number of different observation session lengths and the resulting positioning repeatability (ibid, 1995).

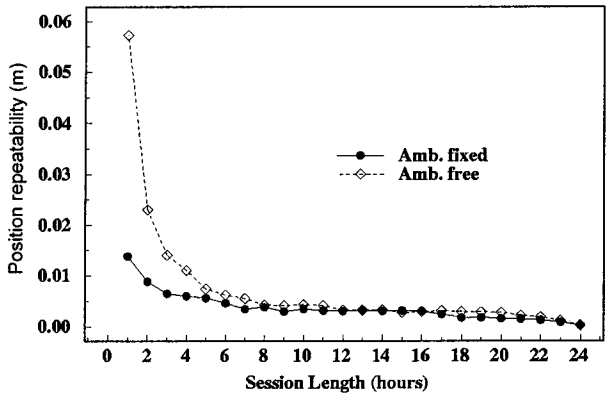

Figure 2-1. The change in quality of long range (from 180 to 1380 km) baseline components, comparing an ambiguity-free solution to an ambiguity-fixed solution, with varying observation session length (adapted from Mervart, 1995).

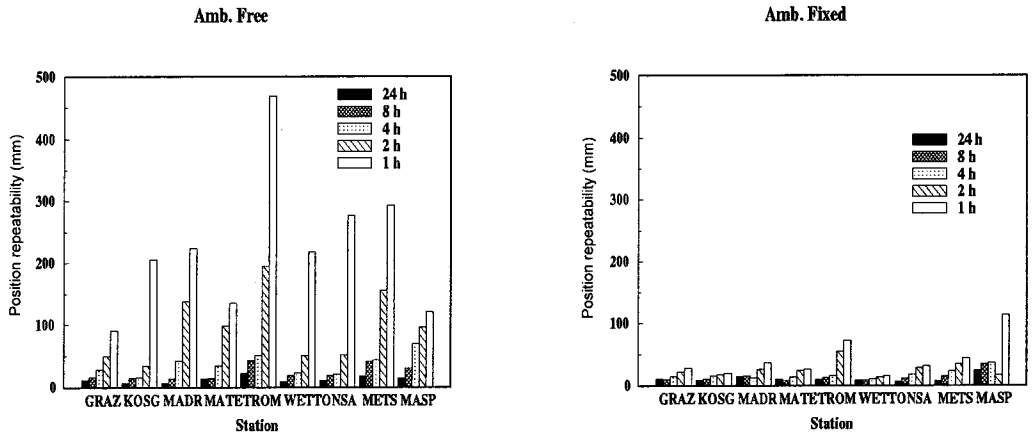

Figure 2-2. Day to day repeatability of the long range (from 180 to 1380 km) horizontal position (ϕ,λ) for different session lengths: stations of the European Core Network (adapted from Mervart, 1995).

What do these plots indicate? Obviously to correctly estimate the ambiguities is the first step in high accuracy positioning. However this requires that the various biases in the carrier phase observations, such as orbit error, ionospheric and tropospheric delays, and multipath disturbance, must be accounted for in the processing algorithm. Lengthening the observation session is the most obvious means of improving accuracy (Figure 2-2). In addition, the challenge of ambiguity resolution can be mostly easily addressed through prolonging the observation session. However, when the ambiguities have been resolved the positioning accuracy can reach a few centimetres, even for baselines up to several hundred kilometres in length. Yet while the difference between the ambiguity-free and ambiguity-fix solution for short observation sessions (1-4 hours) is significant, for long observation sessions there is hardly any difference in accuracy (Figure 2-1).

Centimetre level repeatability for estimated baseline components have been demonstrated for the Taiwan GPS network (Figure 2-3). These results involve 131 stations, surveyed 4-6 times from 1990-1995, with observation sessions of 6-14 hour duration. The standard deviation of an observed baseline length, with its linear trend removed, is in the range of 6-10mm for 3-120km long baselines (Yu et al., 1997).

The standard relative kinematic positioning procedure usually has the GPS receivers starting at two known stations. One receiver (at the *reference* station) remains stationary while the other receiver (the *rover* unit) visits the points whose positions are to be determined, or follows a trajectory that must be coordinated. Both receivers need to operate continuously during the survey period. Commencing the survey on a known baseline makes the ambiguities easier to resolve for short baselines. If during the survey no cycle slips occur, and observations to at least four satellites are made, the coordinates of the points or the trajectory can be estimated using a single epoch of data. Ambiguity resolution "on-the-fly" is now an accepted carrier phase-based technique for kinematic

positioning over short baselines (Abidin, 1993). Hence the coordinates of the points, or the trajectory, can be estimated without the constraint of a static start on a known station.

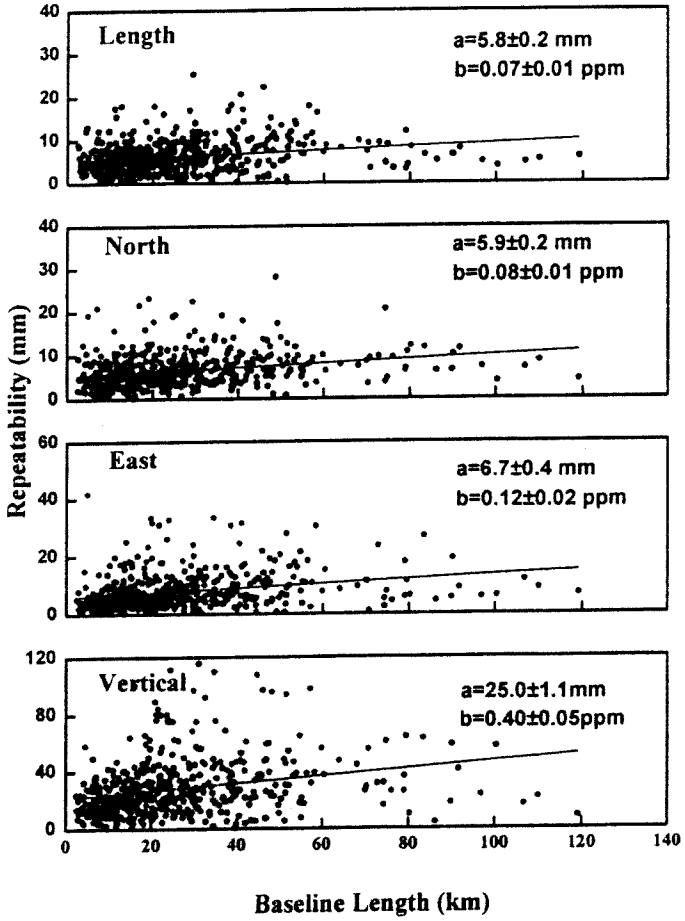

Figure 2-3. Long-term repeatability for annually surveyed baselines of the Taiwan GPS Network (Yu et al., 1997). The recursive function is represented in R=a+b*L (L is baseline length (km)). The a is the constant value and the b is the rate of the linear trend.

However, in addition to kinematic positioning, single epoch solutions can be used for deformation monitoring. Figure 2-4 displays the single epoch results for a baseline in the Chukuo network, Taiwan. Note the difference in the vertical axis scale for plot 3 (the height component). The standard deviation in the horizontal components (east and north component) is less than 15mm and 30mm in the hight component

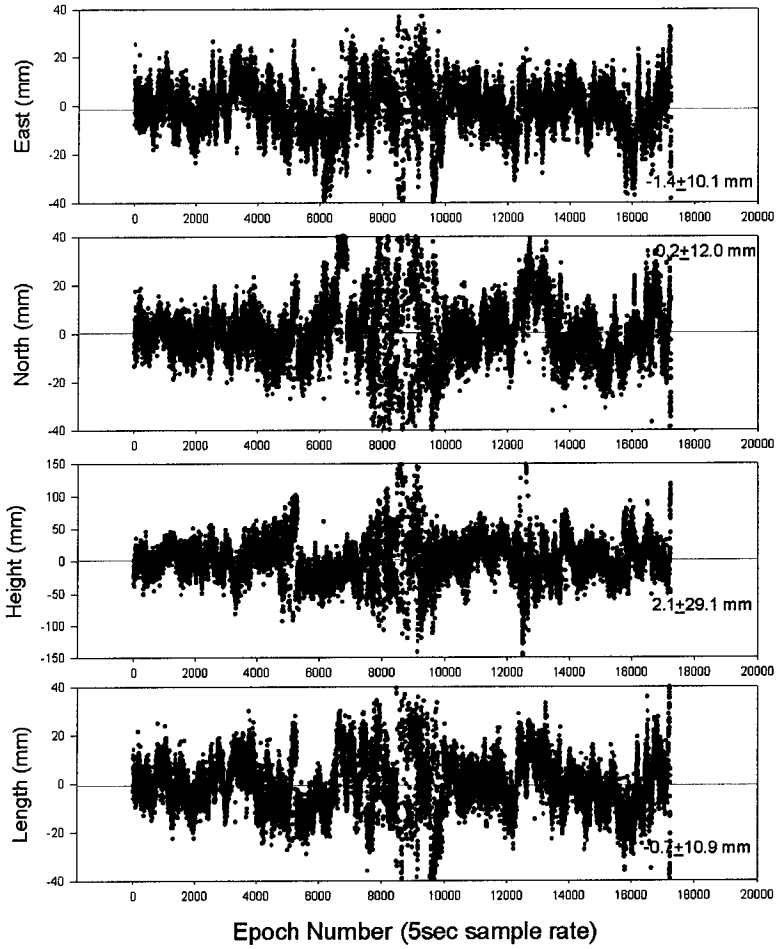

Figure 2-4. The single epoch solution computed from station S011 to KULN (21km baseline), Chukuo network, Taiwan. The numbers on the right hand side of the each graph represent the mean values and their standard deviations. (Chen, 1999)

2.2.3 Baseline and network-based determination

Compared with the EDM traverse technique, the GPS technology has many advantages; one of the most significant being no requirement for line-of-sight between stations. In addition, the repeatability of the baseline determination using geodetic GPS techniques is under 0.1 parts per million (ppm) (Figure 2-3), even for baseline lengths up to several hundreds of kilometres. For deformation monitoring applications, repeated baseline determination can be used to measure the horizontal and vertical movement of a GPS station. Through automatic data downloading, transfer and processing, such a GPS-based monitoring system can deliver reliable relative positioning on a continuous basis.

Network-based GPS techniques use a small number of receivers to coordinate a large number of stations. The area of survey operations may span distances from a few kilometres (as on an engineering site), to several hundred kilometres, or even thousands of kilometres in the case of geodynamical surveys. A typical GPS survey, such as for

mapping or control densification, involves distances of the order of several tens of kilometres. The survey may be carried out using conventional static GPS survey techniques, or the so-called 'high productivity' techniques such as 'rapid static' or 'stop & go'. However, the principles of network processing are the same whether a small number of baselines are observed over several days using the static GPS technigue over a long observation session, or many baselines observed in a matter of a few hours (Rizos, 1996). Individually processed baselines, linking GPS receivers, are combined in a secondary adjustment. Network processing is not a rigorous geodetic methodology.

The first GPS control networks were established in the early 1980's and exhibited internal accuracies approaching 1 ppm, but disagreements with the conventionally established control networks were up to 10 ppm or more in many cases. This discrepancy was not surprising to the geodesists responsible for the establishment of such the control networks, but it did concern GPS surveyors because they could not obtain accurate position checks on their work. Hence, the concept of a 'supernet' or sparse network of high accuracy control points established by GPS was developed. Many such 'supernets' have now been established all over the world (Hofmann-Wellenhof et al., 1998)

Nowadays, for global applications, daily sets of observations from the IGS network are used to estimate precise GPS orbits, polar motion parameters, station coordinates and velocities, and other products. This kind of processing is considerably more sophisticated than used for standard baseline-based GPS surveying techniques, for example, to account for the correlations between the baselines observed in a single session.

For regional scale applications, data from a network of reference receivers can be used to estimate satellite orbit errors, ionospheric and tropospheric delay 'corrections'. Once these distance-dependent biases have been accounted for by correcting the data, coordinate solutions can be obtained with the same level of performance (accuracy, observation session length, etc.) as for the short-range baseline case.

2.3 GPS Reference Station Networks for Geodetic Applications

2.3.1 The IGS network

The International GPS Service (IGS) coordinates the global network of tracking stations and the analysis of the measurements to generate products such as the GPS satellite ephemerides, earth rotation parameters, tracking station coordinates and velocities, and so on. The primary mission of the IGS is (IGS, 2001): "To provide a service to support, through GPS data products, geodetic and geophysical research activities. Cognisant of the immense growth in GPS applications the secondary objective of the IGS is to support a

broad spectrum of activities performed by governmental and selected commercial organisations. The service also develops the necessary standards/specifications and encourages international adherence to its conventions."

The accuracies of the various IGS products are listed in Table 2-1 (IGS, 2001):

Table 2-1. The IGS products in the "Final", "Rapid" and "Predicted" stages and their accuracies.

	Final (2 weeks)	Rapid (2 days)	Predicted (real time)
Ephemerides	5 cm	10 cm	50 cm
Satellite Clocks	0.3 ns	0.5 ns	150 ns
Pole coordinates	0.1 mas	0.2 mas	--
Pole Rates	0.2 mas/day	0.4 mas/day	--
UT1-UTC	50 μs	300 μs	--
Length of Day	30 μs/day	60 μs/day	--

The IGS collects, archives, and distributes GPS observation data sets to address the needs of a wide range of applications. For example, these data sets are used by the IGS analysis centres to generate the data products mentioned above, which are then made available to users via the Internet. The quality of the IGS products is sufficient for the improvement and extension of the International Terrestrial Reference Frame (ITRF), the monitoring of solid earth deformations, earth rotation, and variations in the liquid earth (sea level, ice-sheets, etc.), for scientific satellite orbit determination, ionosphere monitoring, and the estimation of precipitable water vapour in the troposphere. The IGS products are available from their web site (http://igscb.jpl.nasa.gov/).

2.3.2 EUREF and a precise coordinate frame

The EUREF reference frame (Figure 2-5) is one of the successful network-based precise GPS applications for realizing the regional reference frame (or datum) of the International Terrestrial Reference System (ITRS).

The main product of the EUREF permanent GPS network is the weekly estimates of the coordinates of the EUREF tracking stations (and their covariance information). This so-called "combined EUREF solution" is based on sub-network solutions submitted by the EUREF Local Analysis Centres (LAC). All exchange of sub-network solutions is done using the Software Independent Exchange Format (SINEX) (Kouba, 1995).

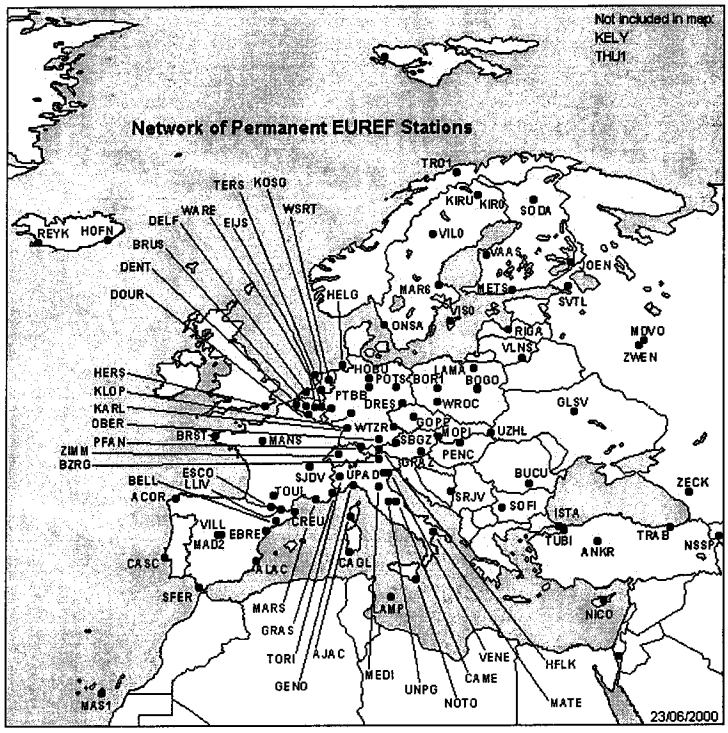

Figure 2-5. The network of permanent EUREF stations. (http://epncb.oma.be)

2.3.3 Examples of operational GPS deformation monitoring networks

GEONET – Japan

Japan's Geographical Survey Institute (GSI) established in 1869 is the national surveying and mapping organisation, operating under the Ministry of Construction. The GSI conducts basic surveying and mapping, as well as dealing with any land use and ownership matters in Japan. GSI has the following responsibilities: (http://www.gsi-mc.go.jp/ENGLISH/index.html/):

1. Survey administration based on the Survey Act.
2. Implementation of survey works.
3. Research and development of survey and mapping.
4. International cooperation for survey and mapping.

Since 1994 GSI has operated the world's largest permanent GPS receiver network (http://www.gsi-mc.go.jp/ENGLISH/ABOUT/OUTLINE/out-his.htm). Continuously-operating GPS stations currently cover most of the Japanese islands with an average spacing of about 30km. The main purpose of this nationwide GPS array is to monitor crustal deformation, so as to assist in the study (and hopefully the prediction) of large earthquakes and volcanic eruptions. The data collected at each station are transferred to GSI's data processing centre in Tsukuba via telephone line. These data are processed with a cluster of workstations to yield the position of each station with an accuracy of a few centimetres, or better, in a global reference frame. GSI monitors daily variations of station

position in order to detect any abnormal changes in estimated crustal strain. GSI also plans to support those who use GPS for public or engineering surveys by providing GEONET observation data for their own processing.

Tectonic events such as large earthquakes or seismic swarms cause sudden and large deformations of the crust, whereas plate motions or magma movements deform the crust slowly and gradually. Hence for the *prediction* of earthquakes or volcanic eruptions, the detection of the slow deformation is essential. Because of its continuous and highly accurate positioning capability, the nationwide GEONET array is an ideal instrument for detecting slow deformation. The GEONET is expected to play a key role in earthquake prediction studies in the Tokai area, which has a high risk of M8 class earthquake in the near future.

From September to October 1995, a seismic swarm hit the eastern part of the Izu Peninsula. The permanent GPS array successfully monitored the slow crustal deformation resulting from the swarm. The results from GPS detected the cessation of the swarm activity in October 1995 (Figure 2-6, 2-7, and 2-8) (http://www.gsi-mc.go.jp/ENGLISH/ ABOUT/OUTLINE/out-his.htm).

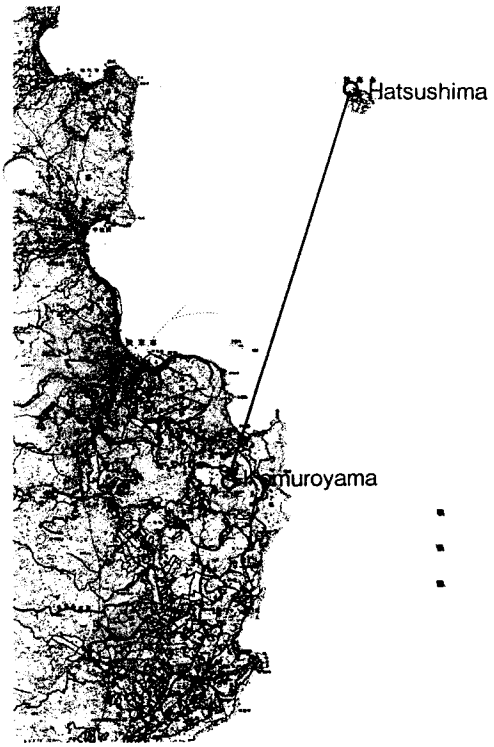

Figure 2-7. Location of GPS stations near Ito

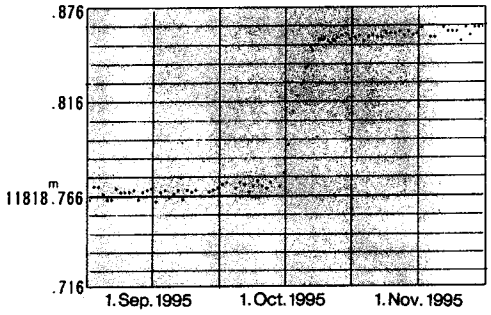

Figure 2-6. Distance between Hatushima and Komuroyama

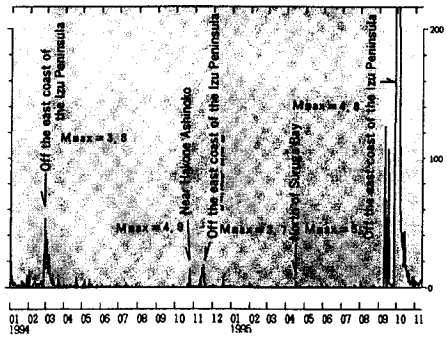

Figure 2-8. Number of Earthquakes per day at Kamada, Ito

SCIGN – US

The Southern California Integrated GPS Network (SCIGN) is a collaborative project to install and operate about 250 continuously recording GPS receivers in and around the Los Angeles basin, to provide accurate deformation information that hopefully will improve knowledge of earthquake hazards. Major participants in the SCIGN include NASA/JPL, The United States Geological Survey (USGS), and The University of California San Diego, operating under the umbrella of the Southern California Earthquake Center (SCEC). Chief sponsors of the SCIGN network are the Keck Foundation, The National Science Foundation, NASA, and the USGS. The major objectives of the SCIGN are (http://www.scign.org/):

1. To provide regional coverage for estimating earthquake potential throughout Southern California.
2. To identify active blind thrust faults and test models of compressional tectonics in the Los Angeles region.
3. To measure local variations in strain rate that might reveal the mechanical properties of earthquake faults.
4. In the event of an earthquake, to measure permanent crustal deformation not detectable by seismographs, as well as the response of major faults to the regional change in strain.

From 24 hour files of GPS data the coordinates of each receiver can be computed to an accuracy of a few mm. Time series graphically illustrate the evolution of receiver positions from day to day. Each plot includes the estimated positions with error bars, the best fit line, and the residual scatter which is an indication of the daily measurement precision. The motion of each site is due to a combination of inter-seismic, co-seismic, and post-seismic effects (http://milhouse.jpl.nasa.gov/).

Co-seismic displacements from SCIGN for the Hector Mine earthquake on 16 October 1999 were published in Seismological Research Letters (http://www.socal.wr.usgs.gov/hector/hector_srl.html), and can be seen in Figure 2-9.

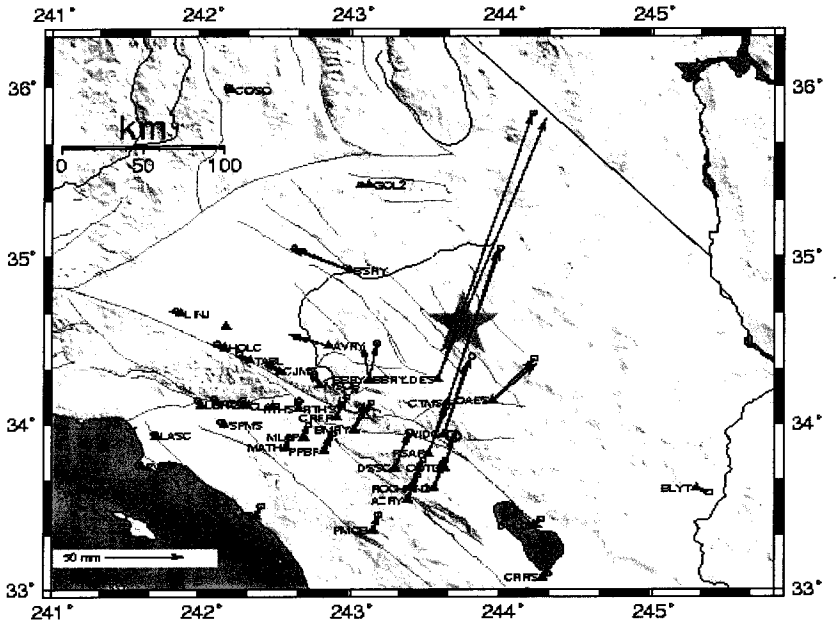

Figure 2-9. Co-seismic and model offsets from the M7.1 Hector Mine earthquake. (http://milhouse.jpl.nasa.gov/hector/)

TAIWNET - Taiwan

The island of Taiwan is located at the junction between the southeast-facing Ryukyu arc-trench system and the west-facing Luzon Arc-Manila Trench system. The Philippine Sea Plate subducts northward beneath the Eurasian Plate at the Ryukyu Trench, and overrides the crust of the South China Sea at the Manila Trench, which extends from the Philippines to about 20°N off southwestern Taiwan. Between the two opposite-facing Ryukyu and Luzon arcs, the Longitudinal Valley in eastern Taiwan is considered the suture zone of the active collision between the Luzon Arc and the Chinese continental margin (Yu et al., 1997). Taiwan is divided into several geologic provinces which trend mainly north-northeast. In general, all of the stations of the Taiwan GPS Network (TAIWNET) are located at stable sites which exhibit little possibility of local movement, and which can be preserved for many years. Most of them also have good sky visibility for elevation angles greater than 15°.

As at the end of 2000 there were more than 150 occasional and 45 permanent GPS stations established for deformation monitoring purposes in the Taiwan region (Figure 2-10).

Currently, there are a total of 45 permanent GPS stations operated by the Ministry of Interior, the Central Weather Bureau (CWB), IESAS and other institutions. 100 CGPS stations will be established in Taiwan by the year 2003. These stations will be densely deployed near the active faults and potential earthquake source areas. In contrast, the additional 50 new stations of the CWB will be evenly distributed around the Taiwan Island. The enormous quantity of CGPS data collected by the array will give Taiwanese scientists

an unprecedented opportunity to study crustal deformation at different space and time scales. The near real-time spatial and temporal variations of crustal stain can be estimated and their correlation with seismic activity will be analysed. By incorporating the continuous GPS data with the near-fault intensive GPS observations, it will be possible to identify the active blind thrust faults under the plains area, and measure the associated fault-slip rates. These data are important for estimating earthquake potential in the Taiwan region. In the event of a major earthquake, the CGPS array could provide precise measurements of pre-seismic, co-seismic and post-seismic deformations. This would assist in understanding the process of strain accumulation and energy release through an earthquake cycle. Researchers will then be able to measure local variations in strain rate, that might reveal the mechanical properties of earthquake faults. With a better understanding of the earthquake generating mechanism, the possibility of developing some form of earthquake prediction can be furthered.

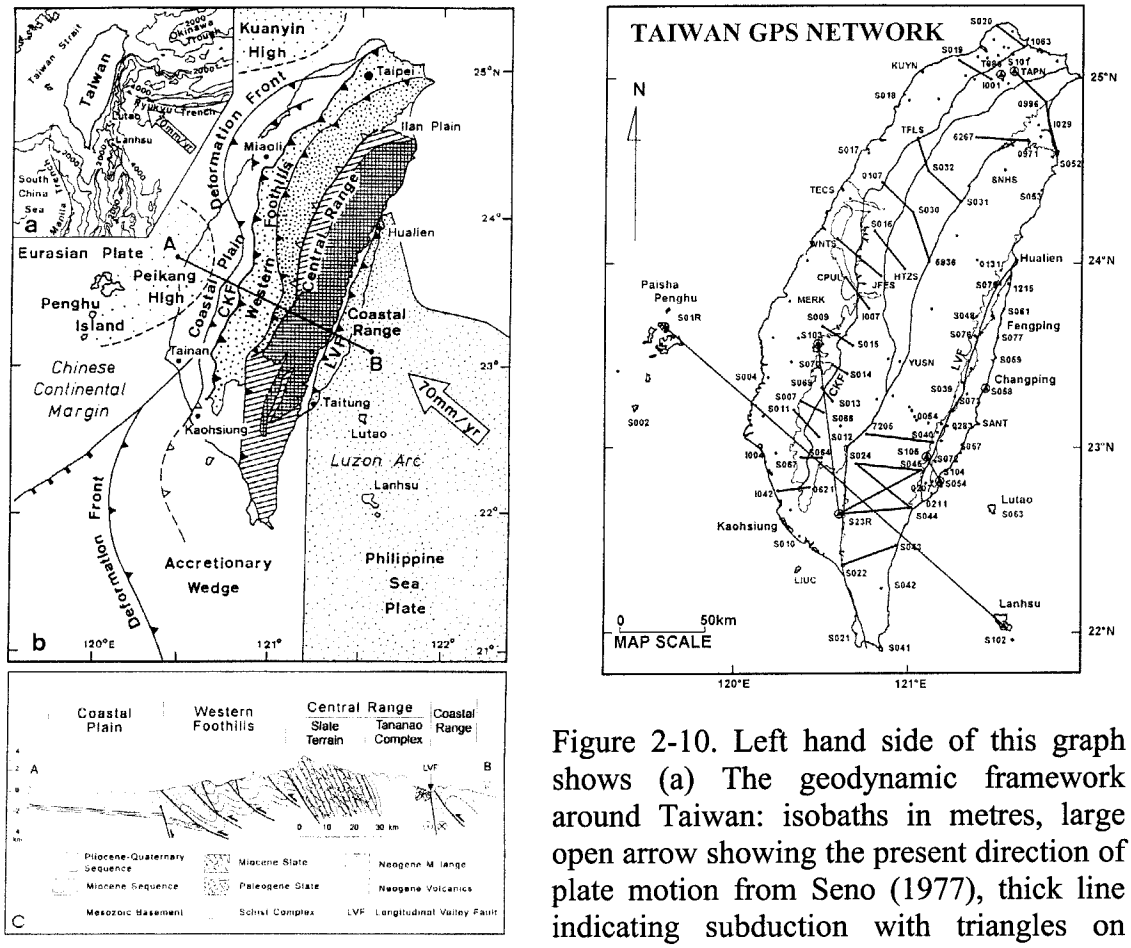

Figure 2-10. Left hand side of this graph shows (a) The geodynamic framework around Taiwan: isobaths in metres, large open arrow showing the present direction of plate motion from Seno (1977), thick line indicating subduction with triangles on overriding side. (b) The geologic provinces in Taiwan: major thrust faults with triangles on the upthrust side, CKF=Chukou Fault=Longitudinal Valley fault. (c) Schematic cross-section of Taiwan (location shown in (b)). Right hand side of this graph displays the Taiwan GPS network. The small dots represent annually surveyed stations, while the solid triangle inside circles indicate permanent or semi-permanent stations. The thick lines show major faults, and the straight lines indicate the baseline with their observed length plotted (Yu et al., 1997).

Since 1989, the semi-permanent stations have been surveyed at least once a year. These field surveys take more than 5 months of the year to complete. Such surveys provide information on the detailed plate motion characteristics of the Taiwan landmass, permitting the deformation of the Taiwan area to be studied (Yu et al., 1994; 1995 and 1997). Since November 1991, four continuously recording permanent GPS stations at Paisha of Penghu (S01R), Taipei (T986 or TAIW), Pingtung (S23R) and Lanhsu (S102) have been operated by the Institute of Earth Science, Academia Sinica (IESAS). Another five semi-permanent GPS stations at S058, S103, S101, S104 and S105, also established by the IESAS, were mostly occupied 7-10 months a year before 1994, a period without field surveys.

2.3.4 Natural disaster applications: monitoring volcanoes

Another geodetic application of network-based precise GPS positioning is the study of volcanoes and active faults. Although GPS is just one of the tools for monitoring ground surface deformation, the advantages of GPS are such that it is nowadays the 'first choice' technology for such applications. For such geodetic applications, the GPS position information can be acquired on a daily, hourly or continuous basis, depending on the application requirements. For volcano monitoring, GPS receivers are set up over several control marks and observations collected. For a small deformation area, most of the biases associated with the delay of the signal through the atmosphere, and due to orbit errors, can be assumed to be common to all receiver sites. Hence relative simple data models may be used, and yet still assure that the positions can be determined relative to one another to sub-centimetre accuracy. In general, the positions of the volcano monitoring control marks are computed on a regular basis. However, increasingly *continuous* GPS (CGPS) measurements are being made at active volcanoes. The pattern and time evolution of displacements may enable volcanologists to estimate the location, depth, and volume of magma intrusion.

The U.S. Geological Survey uses GPS for several geodetic applications. Scientists at the Hawaiian Volcano Observatory (HVO) use a variety of techniques to measure ground deformation on volcanoes in Hawaii, including GPS. Continuously recording GPS receivers are operating at 16 sites on the Kilauea, Mauna Loa and Mauna Kea volcanoes; data are sampled every 30 seconds and downloaded once a day to calculate one-day average positions. In addition, more than 100 other sites are surveyed intermittently using GPS receivers; each survey or data point is compared with previously sampled data to determine accumulated ground deformation and to calculate strain rates or velocities.

During a brief eruptive episode of the Kilauea Volcano that began on 30 January 1997, continuously recording GPS receivers measured significant ground deformation near the eruption site along part of the volcano's east rift zone. (For an overview of Kilauea's 1983-

present deformation visit HVO's Kilauea eruption summary (http://hvo.wr.usgs.gov/kilauea/summary/main.html.) This survey, and the results from other CGPS stations, clearly show that even a relatively small eruption (about 300,000 m^2) was associated with a much larger volume of magma that intruded into the east rift zone, and remained below ground. Continuously-operating GPS receivers operated by scientists of the HVO and Stanford University about 3 km uprift from the Napau Crater recorded a widening of the rift zone by 36cm (Figures 2-11, 2-12).

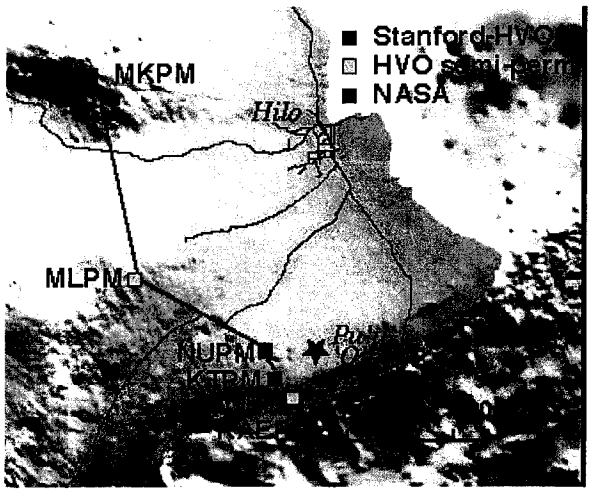

Figure 2-11. Map showing the location of several GPS receivers on the Island of Hawaii. The two nearest continuously-operating GPS receivers - NUPM and KTPM - span the east rift zone of Mauna Kilauea, about 6 km from Pu`u `O`o. MLPM is located on the southeast flank of Mauna Loa, and MKPM is located on the summit of Mauna Kea. (http://volcanoes.usgs.gov/About/What/Monitor/Deformation/GPSKilauea.html)

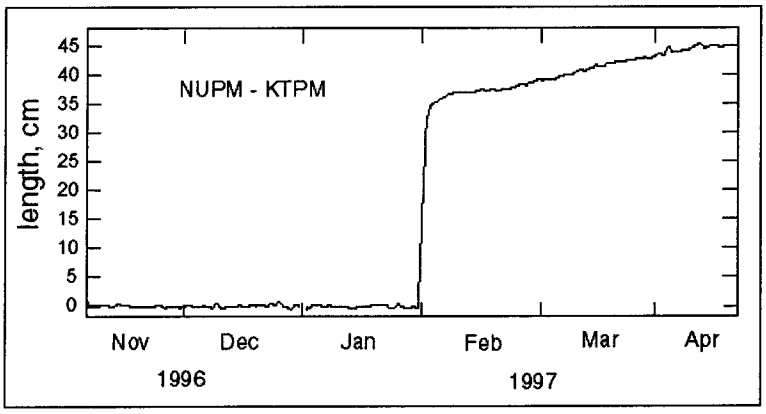

Figure 2-12. Graph showing the increase in distance between NUPM and KTPM during the intrusion of magma into the east rift zone and eruption of lava from the Napau Crater on 30 January 1997. As magma forced its way into the rift beneath the Napau Crater, these two GPS moved apart about 36cm during the activity, and continued to move apart at a slower rate after the activity stopped on 31 January. (http://volcanoes.usgs.gov/About/What/Monitor/Deformation/GPSKilauea.html)

2.4 Benefits of Multiple Reference Station Techniques

Carrier-phase measurements are the most precise observables of the GPS signals. To take advantage of these low noise measurements the standard positioning mode involves two simultaneously observing stations. This can be referred to as the 'single-baseline' mode. One of the stations is identified as the 'reference station/receiver' or 'base station/receiver' whose coordinate is assumed known and held fixed during data processing. The processing of the 'double-differenced' observables (formed from the data collected by both GPS receivers) permits the determination of the coordinate of the other GPS receiver station and the double-differenced "ambiguity" terms.

However, the *differential* atmospheric refraction effects (remaining in the double-differenced observable) due to both the ionosphere and troposphere will increase in magnitude as the inter-station distance (i.e. baseline length) gets larger. This will impact on the quality of both the estimated coordinate and ambiguity parameters, which in turn will make the ambiguity terms harder to fix to their correct integer values (i.e. ambiguity resolution). Hence the baseline solution will be biased. The conventional way to ensure that the ambiguities will be correctly resolved in cases where the residual atmospheric delay is significant is: (a) to increase the length of the observation period, (b) to form linear combinations of the observations to reduce the effect of the ionospheric delay, (c) to estimate the tropospheric delay as an additional parameter, or (d) all of the above. Another option is to apply a model to account for the residual atmosphere effect. However, this requires that the ionospheric and tropospheric delays are measured or modelled precisely.

It must be emphasised that residual atmospheric delays are only a concern when the inter-station distances are large enough so that the tropospheric and/or ionospheric delay at both the receivers (at the same instant of time, and for observations made to the same satellite) are no longer similar. A rule-of-thumb would define this magnitude as being of the order of a quarter of a cycle (approximately 5cm) or greater. However, it is not possible to say precisely what the corresponding baseline length is. For extreme circumstances (e.g. active ionosphere, large elevation difference between the two receivers, etc.) baselines as short as 10-15km might experience significant residual atmospheric delays (i.e. greater than about 0.25 cycles). In other words, to process data for baselines of this length, or longer, the residual atmospheric delay must be accounted for in some way (i.e. not to be ignored). In other circumstances the baseline length may be as long as 30-50km before the atmospheric effect becomes significant. Hence, residual atmospheric delays are *distance-dependent*, but not in some linear or easily predictable manner. The 'dividing line' between short-range (i.e. baseline lengths below which the residual atmospheric delay is negligible) and medium-(or long-)range (i.e. beyond which the atmospheric effect is no longer negligible) positioning is hard to define. In this study it is set rather arbitrarily at 30km.

In the Wide Area Differential GPS (WADGPS) technique a model for the residual atmospheric delay is computed across an area of interest from observations made at a network of continuously-operating GPS receivers. An estimate of the atmospheric delay is then transmitted to users in the form of 'correction terms' which are applied to the raw pseudorange observations (before processing). In a similar manner as the WADGPS technique, the carrier phase data from multiple reference stations can be processed to estimate the 'correction terms' which account for this atmospheric effect (i.e. eliminate or significantly reduce its magnitude in the double-differenced observables).

2.4.1 Error mitigation

Reference station network processing algorithms have been developed which can effectively eliminate or mitigate the distance-dependent biases such as the residual atmospheric delays (Han & Rizos 1996c, Raquet et al., 1998; Wanninger 1997; Wübbena et al., 1996). As mentioned earlier, the main bias which will affect baseline estimation and ambiguity resolution for medium-range (>30km) precise (carrier phase-based) relative positioning is the residual atmospheric delay. Hence, if the ionospheric and tropospheric delay within the coverage of the reference stations can be modelled in some way, the ambiguity parameters can be determined (for the double-differenced observables between the reference stations and user stations), after applying the appropriate 'corrections'.

Han (1997) described an experiment to test this algorithm for carrier phase-based, kinematic positioning. The distance between the reference stations was from 29km to 35km, and the ambiguity resolution success rate on a *single-epoch* basis was 100%. Using the single-baseline mode such success rates would only be expected for baselines less than 10km.

Wanninger (1997) also reported an experiment for single-epoch ambiguity resolution using multiple reference stations, and concluded that "Under standard conditions (undisturbed ionosphere effect) single-epoch ambiguity resolution succeeded for more than 99% of the observations, and produced incorrect results for just 0.01% of the data. Under disturbed conditions the success rate decreased to about 95%, with the percentage of incorrect result increasing to about 0.5%."

Hernández-Pajares et al. (1999) proposed a new approach for global ionospheric determination, and applied his technique to medium-range, ambiguity resolution using multiple reference stations (see also Colombo et al., 1999). The kinematic "on-the-fly" (OTF) ambiguity resolution success rate was 100% (the user station was 116km away from the nearest reference station).

2.4.2 High precision

Fixing the correct integer ambiguities is the first step in precise relative positioning. As already discussed, for short baselines the observation biases are almost entirely eliminated by constructing the double-differenced GPS observables. However, for medium- or long-range relative positioning, even if the ambiguities can be resolved under standard conditions (e.g. assuming an undisturbed atmosphere), the positioning results still will be biased due to distance-dependent effects that contaiminate the double-differenced observables.

Therefore a multiple reference station algorithm that generates the 'corrections' referred to earlier, not only can help resolve the correct integer ambiguities, but can also improve the positioning accuracy itself. Tables 2-2 and 2-3 compare the positioning results that were obtained by two investigators, with and without applying the 'corrections' that account for the distance-dependent biases.

Table 2-2. Ambiguity resolution and positioning errors with 5 minute observation sample, for 29km baseline length, using the single-baseline approach (top row) and the multi-reference station approach (bottom row) (Wanninger, 1997).

Baseline		No of samples	Success Rate Ambiguity Resolution	Positioning Errors RMS dN/dE/dH (cm) L1	Liono.
HVLB-STEN (29km)	Standard Cond.	864	89%	N/A	1.1/0.7/2.5
	Iono. Disturb.	119	87%	N/A	1.3/0.8/2.8
	Tropo. Disturb.	106	89%	N/A	1.6/0.8/7.8
	Large Orbit Err.	126	97%	N/A	1.3/0.8/2.7
Virtual Reference station-STEN	Standard Cond.	864	98%	0.9/0.6/1.9	1.0/0.6/2.4
	Iono. Disturb.	119	96%	1.5/0.9/2.7	1.1/0.7/2.7
	Tropo. Disturb.	106	100%	1.4/0.7/1.7	1.4/0.6/2.4
	Large Orbit Err.	126	99%	0.8/0.7/1.7	0.9/0.6/2.2

Table 2-3. Summary of baseline results, the 'before' and 'after' columns indicate the results obtained before and after applying ionospheric 'corrections' derived from a GPS network (Gao et al., 1997).

	Before (cm)		After (cm)	
	Mean	Rms	Mean	Rms
Latitude	3.8	16.3	0.4	4.5
Longitude	2.6	9.4	2.5	3.8
Height	21.9	36.1	6.1	7.4

2.4.3 High performance

Applying 'corrections' derived from processing data from medium-scale GPS reference networks, not only is the positioning accuracy improved, but in addition the length of the observation session can be reduced. For static medium-range or long-range baseline determination typically several hours of obvservations are required (Mervart, 1995; Liu et al., 1999), although some claim that as a few as tens of minutes is sufficient to estimate the integer ambiguities and the coordinates for baselines several tens of kilometres in length using single-baseline techniques (Odijk, 1999). However, single-epoch ambiguity resolution for precise, medium-range, kinematic positioning requires multi-reference station techniques (Han, 1997).

A single-frequency GPS receiver, because the increase in baseline length means the ionospheric delay bias cannot be accounted for through the use of the ionosphere-free linear combination (of L1 and L2 observations), cannot be used for medium-range positioning. However, using the 'rapid static' positioning mode, and applying 'corrections' generated from a multiple reference station network, it has been found that the high quality positioning results can be reliably determined. Chen et al. (1999; 2000) report cm-level accuracy in the horizontal components and 3-5cm in the height component, even for baseline lengths up to a hundred kilometres. Hence, the multiple reference station method can be used to generate 'corrections' that eliminate (or reduce), the effect of distance-dependent biases such as the residual atmospheric delay, and to make possible high accuracy positioning even with single-frequency GPS receivers.

2.4.4 Multi-functional

The global ensemble of GPS tracking stations comprising the 'core' network of the International GPS Service (IGS) is an example of a multi-reference receiver network. However, the data is not streamed to a computation centre in real-time. On the other hand, the real-time, pseudorange-based WADGPS services such as those provided by organisations such as RACAL (the "Landstar" service) and FUGRO (the "Omnistar" service) utilise a network of reference stations permanently connected to a central computation centre.

Use of multiple GPS reference stations allows for "network-based" positioning solutions, rather than the conventional single-baseline (two receiver) approach. Network-based GPS is of course the mode used in ultra high accuracy GPS geodesy applications, such as the determination ground fault motion through the integrated processing of data collected by a network of simultaneously operating GPS receivers. Some applications that take advantage of network-based positioning techniques are (Rizos et al., 1999):

Single-epoch or "instantaneous" on-the-fly ambiguity resolution (IOTF-AR), even when the distance separating the user receiver and the reference receiver(s) is several tens of kilometres. (Single-baseline IOTF-AR techniques typically only work over short distances, generally less than 10km.) However, dual-frequency, so-called 'third generation' GPS receivers are required.

'Rapid-static' techniques (observation sessions of the order of ten minutes or less) for baselines up to several tens of kilometres in length, to deliver cm-level accuracy, even when using single-frequency GPS receivers. (An attractive option for a low-cost GPS surveying system.)

Precise ground or structural deformation monitoring to sub-cm-level accuracy, using either single-frequency or dual-frequency GPS receivers.

Various combinations of static and kinematic positioning modes are possible, in either real-time (if there is a data communication channel available to the user) or post-processing mode. Furthermore, users need not own and operate their own reference stations. The latter is a significant advantage, as it permits the development of network services for users.

2.5 Implementations of the Network-Based Positioning Concept

2.5.1 General description

As noted earlier, considerable savings could be won if a surveyor need only purchase a single GPS receiver, and to use data collected by a third party at GPS reference station(s). The surveyor could collect data at the points of interest (using the static or kinematic positioning mode), and then upon returning to the office could download the data from the nearest GPS 'service centre', and perform the necessary baseline computation(s). However, as discussed in section 1.1 and 1.2, standard 'high-productivity' GPS techniques require the reference receiver be within 10 or so kilometres of the survey area. Across a large country, the establishment of a network of GPS reference receivers at a density to support all (or most) GPS surveys is hardly feasible. For example, Japan's GSI network has an average receiver spacing of 20-30km. In some states of Germany, GPS reference stations have been established by survey authorities with similar spacings. In Australia, the state of Victoria will also establish a reference station network to support GPS surveys with average receiver spacing of 20km. However, it was envisaged that these networks would support single-baseline determination techniques, such as are implemented within commercial GPS data processing software. *These are less efficient than using multi-reference station, or network-based techniques.*

The advantages of carrier phase-based, multi-reference station GPS positioning techniques can be summarised as being:

(a) Rapid static and kinematic GPS positioning techniques can be used over baselines up to a hundred kilometres in length.

(b) Instantaneous OTF-AR algorithms can be used for kinematic GPS positioning, at the same time ensuring high accuracy, availability and reliability for critical applications.

(c) Rapid static positioning is possible using low-cost, single-frequency GPS receivers, even over tens of kilometres.

Hence the question of "how to improve GPS carrier phase-based positioning performance?" is answered in various ways. If the baseline length constraint is the crucial factor impacting on static or kinematic GPS, then overcoming this constraint through the use of multi-reference station techniques results in significant performance improvements. If "improving performance" is related to lowering receiver costs, then a reference receiver network would allow the use of single-frequency GPS receivers instead of expensive dual-frequency receivers for static positioning. If "time-to-ambiguity resolution" (AR) is the critical performance indicator, then a reference receiver network approach would contribute to faster AR (including single-epoch AR) as well as enhance the reliability of AR, even for baselines several tens of kilometres in length. However, the implementation of a GPS positioning technique based on data from reference station network is much more complicated than the standard single reference receiver scenario.

In order to win the performance improvements mentioned above more than two dual-frequency GPS receivers would need to be used to support the survey. Rarely would the benefits of improved positioning performance be great enough for a single user that they would be compelled to establish and operate their own reference receiver network. It is therefore assumed that a multi-reference station *service* would be provided by a government agency or private organisation. This may be a "fee-for-service" or the reference receiver data may be provided free of charge. Furthermore, in order to justify such an infrastructure, it is envisaged that the reference receiver network would be established in order to service the GPS survey needs of a large metropolitan area, such as that centred on Sydney or Melbourne. In such a scenario three or four GPS reference receivers would be deployed on the outskirts of the city so that they would form a polygon surrounding the area in which GPS positioning would typically take place. It is envisaged that some or all of the following services could be offered across a metropolitan area:

(a) The 'minimalist' option is for the user to simply download (via the Internet) the necessary data files from the reference station network. No modification is needed to

present, government-run GPS services such as GSI's or AUSLIG's. The user, however, requires the appropriate post-mission data processing software to perform the multi-station processing. This is not commercially available from the GPS manufacturers.

(b) One of the more innovative implementations of multi-reference station processing is not to require the surveyor to download *any* GPS reference receiver data. Rather, the user logs the GPS data locally and then submits (or uploads) the data file to a central server for processing via an Internet Web page (the web browser software necessary for this may be found on a mobile phone or a palmtop/PDA). The implementation of such a service requires the establishment of the appropriate GPS reference station data links to the central server, a database management system and the web-based data processing 'engine'. This service has the additional advantage in that it obviates the need for users to maintain their own PC-based GPS data processing software. Furthermore, this service is ideally suited for the more sophisticated data processing necessary when using all the data from the reference station network. Examples of such services are currently provided by AUSLIG (http://www.auslig.gov.au/cgi-bin/gps.cgi), UCSD-SIO (http://sopac. ucsd.edu/processing), and the JPL Precise Point Positioning service (through ftp/e-mail interface: ag@cobra.jpl.nasa.gov). (The former two are relative positioning services.) All are free.

(c) The other type of service would be for real-time users. Unfortunately this implementation is more complex for a number of reasons. Firstly, the distance(s) from reference receiver(s) to user may be several tens of kilometres, resulting in communication link issues becoming critical. Secondly, because more than one GPS reference receiver is used, a network-generated correction message must be transmitted. This is not unlike a WADGPS scenario, except that carrier phase data is used for positioning instead of pseudoranges. In WADGPS services a satcom link is typically used, and a special decoder is necessary (for which a subscription fee is paid) because the correction message that must be input to the user's RTK receiver is *location dependent*. Such services may not be too far off. For example, FUGRO and RACAL have announced long-range positioning services, with several decimetre accuracy. The first commercial implementation of a RTK network-based technique was announced by Trimble in late 2000: the *Trimble VRS system*.

2.5.2 Network solution (Raquet & Lachapelle, Canada)

The basic assumption is that for short baselines, forming the double-differenced observable can effectively eliminate or reduce observation biases such as satellite and receiver clock errors, orbit bias, ionospheric and tropospheric delay biases. The main errors that remain are the multipath signal disturbance and measurement noise. After the relative positions of the reference stations have been precisely determined, the multipath error can be accurately

estimated on an epoch-by-epoch basis using the Least Squares Condition Adjustment method (Raquet, 1996).

Raquet (1997) extended this methodology, now referred to as the *NetAdjust method* (Figure 2-13), to use multiple reference receivers to generate 'corrections' to the measurements from a single reference receiver. With the NetAdjust method, a Least Squares Condition Adjustment is applied at each measurement epoch, resulting in corrections for every measurement. The condition to be satisfied is that all the double-differences of the adjusted measurements minus the calculated ranges be zero (which would only be true if there were no errors or residual biases). (The calculated range is the distance between the known receiver and satellite positions -- as calculated from the ephemeries data.)

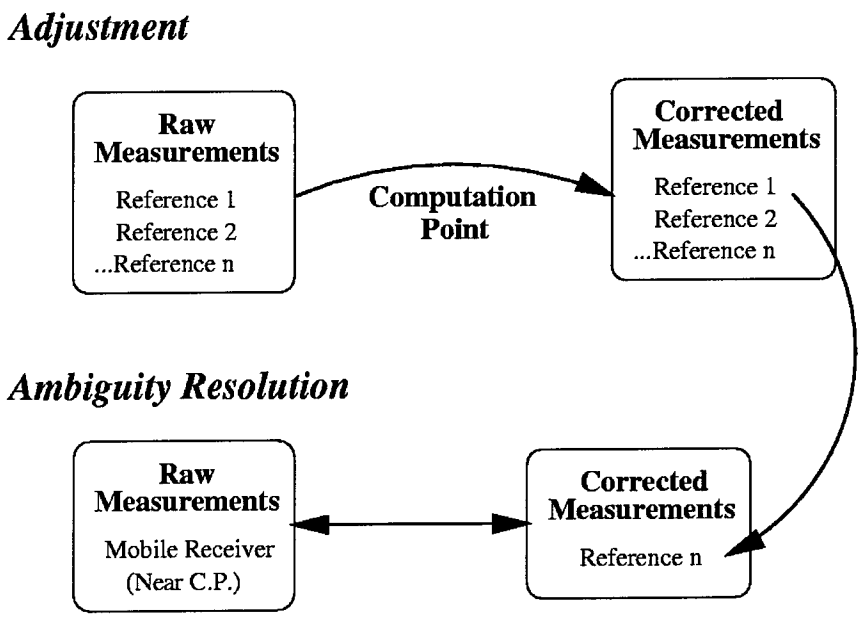

Figure 2-13. The NetAdjust concept (Raquet, 1997).

Raquet et al. (1998) describe the NetAdjust method as being based on a 'minimum variance of error estimator', and demonstrated it to be effective for lengthening the distance over which carrier phase ambiguities can be correctly resolved. In essence, the NetAdjust method encapsulates all the network information into the measurements of a single reference receiver, so that standard single-baseline GPS algorithms can be used for ambiguity resolution and positioning.

2.5.3 'Virtual Reference Station 'approach (Wanninger, Germany)

Wanninger (1995) claimed that the efficiency of ambiguity resolution can be improved by applying differential ionospheric corrections. The ionospheric correction is computed by a

network of GPS reference stations, and then using the known coordinates of the reference stations and the approximate coordinate of the user receiver, interpolate the ionospheric correction for the user station. The basic elements of the algorithm are indicated in Figure 2-14.

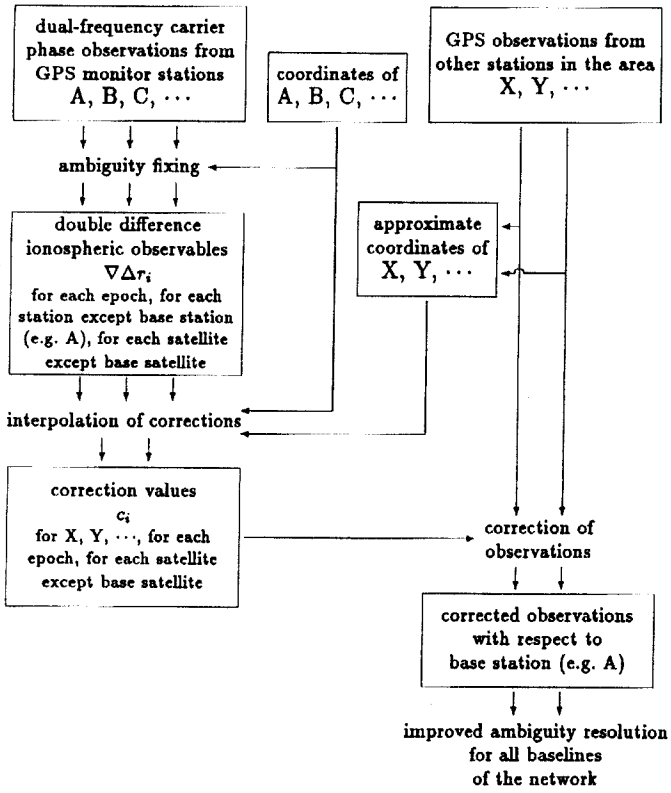

Figure 2-14. The algorithm for generating differential ionospheric corrections from a GPS reference station network (Wanninger 1995).

Wanninger (1997) described his concept as a 'virtual reference station' (unlike Raquet's 'real' reference receiver with 'corrected' measurements). After fixing the ambiguities in the reference network data processing, the ionospheric correction can been derived from the ionospheric linear combination, and the orbit and tropospheric correction quantity can then been calculated from the ionosphere-free linear combination. These corrections are applied to the measurements of a selected reference station. The observations of the 'virtual reference station' can then be constructed, as shown in Figure 2-15. Wanninger (1999) investigated the performance of this algorithm under solar maximum conditions.

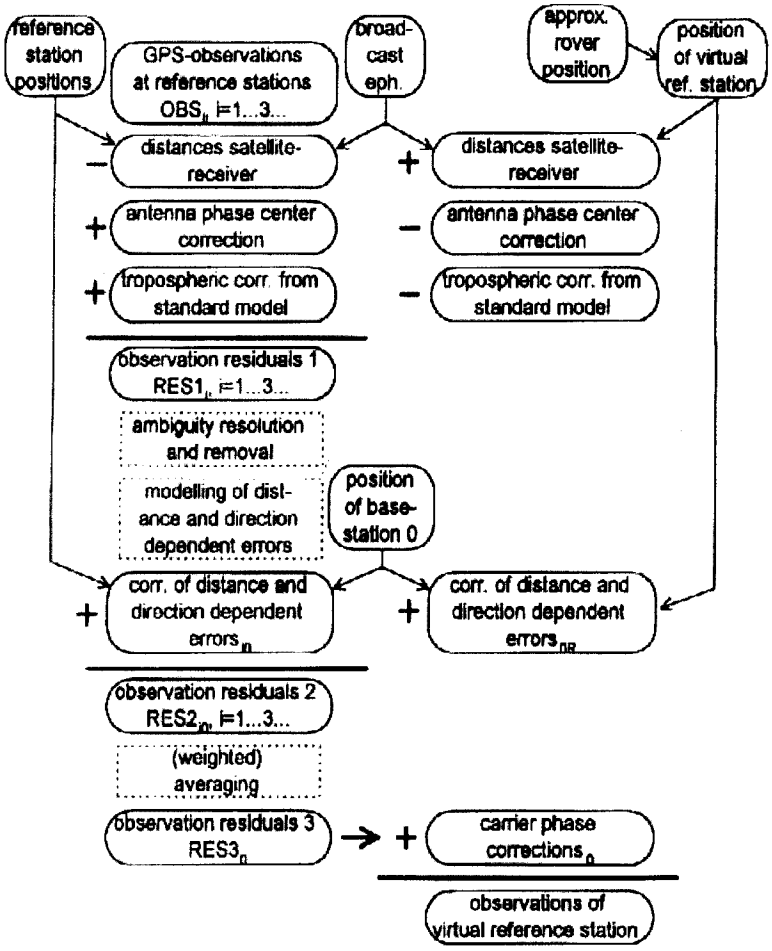

Figure 2-15. Generating the observables of a 'virtual reference station' (Wanninger, 1997).

2.5.4 Multiple reference station approach (Han & Rizos, Australia)

Han & Rizos (1995b) described an algorithm for long-range kinematic ambiguity resolution based on multiple reference stations. In 1996 the same authors proposed a GPS network design for continuous GPS monitoring systems that also relied on using a GPS reference station network (Han & Rizos, 1996c). The main feature of this algorithm was the use of single-differenced functional model to eliminate the orbit bias, ionospheric delay, and to reduce the tropospheric delay biases and other errors. The proposed technique contained a three-step procedure that resulted in reliable positioning for baselines many tens of kilometres in length. The proposed real-time stochastic model estimation procedure is a refinement of the fidelity of the functional and stochastic models, and makes the estimation results more reliable. The proposed procedure for discriminating between the integer ambiguity sets that generate the minimum quadratic form of the residuals and the second minimum one has rigorous statistical meaning and is very efficient for practical use. Finally, a global measure related to the neighbouring epochs (the variation in the Total Electron Content quantity) has been used to define necessary conditions to enhance the

reliability of the result. This adaptive procedure is very powerful and leads to maximum positioning success rates (Han & Rizos, 1996c; 1997b; Han, 1997).

Rizos et al. (1998) analysed the 'rapid static' mode for medium-range positioning, using single-frequency data. An extension of the functional model for multiple reference stations was developed to accommodate more than one user receiver operating simultaneously (Chen et al., 1999). The feasibility of low-cost densification of permanent GPS networks using single-frequency user receivers was studied by Chen et al. (2000).

2.5.5 Comparison of implementation strategies

The common requirement for all these multi-reference station techniques is that the coordinates and integer ambiguities associated with the data processing for the network of GPS reference stations need to be known. (In addition, the approximate location of the user station(s) are also required for the computation of the appropriate 'corrections'.) A comparison of the implementation algorithms, the error mitigation strategies, the ambiguity resolution technique and the positioning accuracy achieved, for the various techniques is made below.

Error mitigation

Because the coordinates of the reference stations are known, the NetAdjust method (section 2.5.2) first computes the measurement-minus-range quantities, and then forms the linearly independent double-differenced combinations of the measurement-minus-range observables. Then the double-differencing operator matrix for the network and the covariance function is formed. Two 'corrections' are generated, one is to correct the measurement from a single reference receiver, and the other is to correct the measurements of the receiver at the computation point (user station). Finally the ambiguity resolution and positioning task is carried out (see, for example, Raquet et al., 1998). Hence the error modelling algorithm (that defines the 'corrections') does not separate it into different types of error, but is assumed to be only dependent on the position of the user station.

The error mitigation algorithm of the Wanninger (1997) proposal (section 2.5.3) consists of two main parts. One is the error modelling algorithm based on bilinear surfaces, which requires undifferenced observations and the computation of 'virtual observables'. The main error sources are divided into the ionospheric delay bias (based on the ionospheric linear combination and the geometric model), and the tropospheric delay and orbit error (based on the ionosphere-free linear combination) determined by the reference stations. Hence, the error mitigation algorithm accounts for the ionospheric and tropospheric delay biases, and orbit errors, and is also dependent on the location of the user station.

The error mitigation algorithm of the Han & Rizos (1996c) proposal (section 2.5.4) is simpler to the other techniques. After the integer ambiguities and coordinates of the reference stations are known, the double-differenced observable corrections between one reference station and the user station can be computed (with the aid of the approximate coordinates of the user receiver), which in turn aid the resolution of the baseline ambiguities. Hence, the characteristic of this error mitigation algorithm is to introduce a set of parameters to eliminate, or reduce, the orbit error, ionospheric delay, tropospheric delay, multipath and observation noise of the single-difference function model (Han, 1997).

Ambiguity resolution

If the observation errors and biases (orbit error, ionospheric delay, tropospheric delay, multipath and observation noise) can be eliminated, or reduced, between the reference stations and user station(s) in the medium-range positioning case (baselines >30km in length), then the ambiguity resolution task will be *similar* to the short-range positioning case. For example, the ionospheric delay is dependent on such factors as geographic location and level of solar activity. Hence, the coverage of the multiple reference station, and the effectiveness of the error mitigation model, is dependent on the characteristics of the distance-dependent biases (primarily tropospheric and ionospheric delay) at the time.

In cases of no ionospheric disturbances, Raquet (1999) (Figure 2-16), Wanninger (1999) (Table 2-4) and Han (1997) all report high success rates for ambiguity resolution. However, during periods of ionospheric disturbances, Wanninger (1999) and Chen (1999) (Table 2-5) suggest that the ionosphere-free linear combination is more useful for ambiguity resolution.

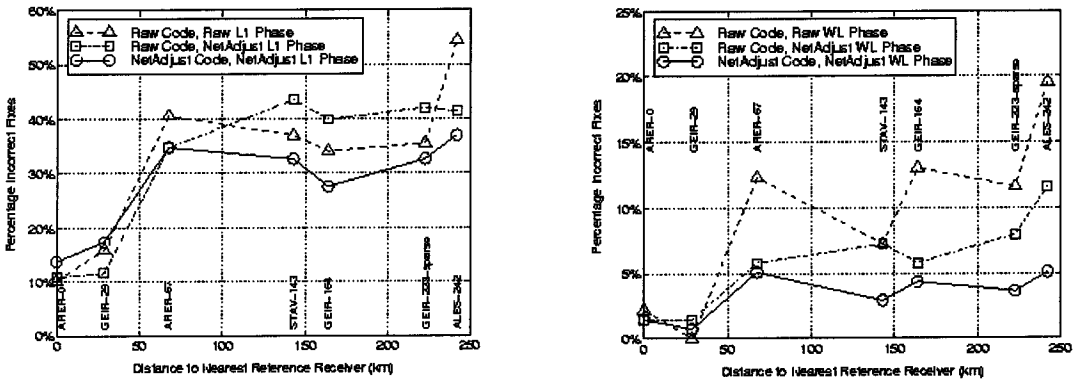

Figure 2-16. Percentage of incorrectly fixed L1 (left-hand graph) and widelane (right-hand graph) ambiguities over seven test networks (Raquet, 1999)

Table 2-4. Left-hand table shows the 'rapid static' result across different reference station networks. Right-hand table displays the ambiguity success rate for different ionospheric conditions, using different commercial software (Wanninger, 1999).

Post. Processing Software	Correct-ness (%)	Reliability (%)	Accuracy 2D/vertical RMS (%)
undisturbed ionosphere default algorithms			
A	97	97	1.0/1.6
B	95	95	1.1/1.8
C	87	98	0.9/2.0
disturbed ionosphere default algorithms			
A	87	87	2.2/2.9
B	80	81	2.1/3.3
C	37	96	2.0/2.7
disturbed ionosphere Algorithms for long baselines(ionosphere-free)			
A	97	97	5/2.8
B	83	86	2.2/3.5
C	37	96	1.4/1.8

Baseline	undisturbed ionosphere		disturbed ionosphere	
	iono-free	L1	iono-free	L1
60 km-network				
closest ref. Sta.(29km)	2.0	2.2	2.1	12.0
virtual station	1.5	0.9	1.6	2.3
100 km-network				
closest ref. Sta.(50km)	2.2	3.2	1.7	23.8
virtual station	1.0	0.8	0.9	3.5
150 km-network				
closest ref. Sta.(29km)	1.7	3.8	2.1	21.4
virtual station	1.4	1.8	1.4	8.5

Table 2-5. Comparing two different methodologies for single-epoch ambiguity resolution with the aid of multiple reference stations (Chen, 1999).

	S011-S106 (17km)		S011-S012 (22km)		S011-KULN (22km)		S011-CHYN (21km)	
	Correctness (%)		Correctness (%)		Correctness (%)		Correctness (%)	
DoY	L1&L2	Iono.-free	L1&L2	Iono.-free	L1&L2	Iono.-free	L1&L2	Iono.-free
335	42.46	94.78	33.69	97.04	40.55	97.19	32.84	90.51
336	41.62	96.02	33.48	97.74	42.05	95.86	34.87	93.54
337	30.36	96.81	27.53	97.10	26.76	97.06	28.02	96.95
338	44.76	95.60	39.70	96.41	43.41	97.20	38.88	96.89

Positioning accuracy

In Raquet (1998), a comparison was made between the positioning accuracy using raw data, and when the data was corrected using the NetAdjust method. The ambiguities were first resolved, resulting in ambiguity-fixed positioning. For L1 and widelane observables, the NetAdjust method reduced the 3-D RMS position errors by approximately 10% for networks with baselines less than 100km in length, and 40% for networks with baselines longer than 100km.

Wanninger (1999) reports that, for 5 minutes 'rapid-static' processing, the 2-D positioning accuracy was about 2.5cm for a 60km network, 2.4cm for a 100km network, and 2.2cm for a 150km network, when there were no ionospheric disturbances; and 2.6cm for the 60km network, 1.9cm for the 100km network and 2.5cm for the 150km network during disturbed conditions (Table 2-3).

Han (1997) reported kinematic results with single-epoch ambiguity resolution success rates reaching 100%, for a 70km network. Another kinematic experiment reported in Rizos et al. (1999), involving the use of 'corrections' derived from a 100km network achieved single-epoch ambiguity success rates ranging from 95% to 97%. For static results, the 2-D positioning accuracy was about 2cm for the 100km network when there were no ionospheric disturbances (Figures 6-15 to 6-22).

Chapter 3

MULTIPLE REFERENCE STATION PROCESSING IN SUPPORT OF PRECISE, MEDIUM-RANGE GPS PRECISE POSITIONING

3.1 Introduction

GPS is an indispensable tool for measuring crustal deformation. As a result, a large number of continuously-operating GPS networks have been established in the USA, Japan, Europe, and many other countries, to address a variety of crustal deformation monitoring applications. Most of these CGPS networks can be described as being 'medium-scale', as they typically have inter-receiver distances of several tens of kilometres, up to about 100km. With these GPS data, researchers can use special carrier phase processing techniques to achieve relative station coordinate accuracies as high as a few tens of parts-per-billion. Since the atmospheric signal delays are the main measurement biases that impact accuracy within medium-scale networks, researchers have focussed on the problem of modelling or estimating these biases.

In this chapter a multiple reference station methodology is described by which a network of dual-frequency GPS receivers is "densified" by an array of 'inner' single-frequency GPS receivers. In this way the GPS receiver network's spatial resolution is significantly increased, but at a significantly reduced capital cost compared to using only dual-frequency instrumentation. A linear combination model proposed by Han (1997) and Han & Rizos (1996c) can not only account for orbit bias and ionospheric delay, but also mitigate tropospheric delay, multipath and measurement noise across the network. This mixed receiver system can achieve a similar level of accuracy as using dual-frequency GPS receivers for medium-range baselines. Permanent GPS reference stations can be used to generate empirical 'correction terms' for double-differenced carrier phase observables formed between the 'inner' user receivers and a single reference receiver. This makes possible the implementation of the algorithm using commercial 'off-the-shelf', single-reference-receiver, static and kinematic data processing software.

3.2 Functional Models

3.2.1 Basic model

In the processing of between-receiver carrier phase observables the remaining dominant errors and biases are orbit error, ionospheric delay, tropospheric delay, multipath and observation noise. Consider the scenario of three or more reference stations (equipped with dual-frequency receivers) surrounding a user station (equipped with a single-frequency receiver). The single-differenced carrier phase observable between the user and a reference station can be written as (Han, 1997):

$$\Delta\phi_i = \Delta\rho_i + \Delta d\rho_i - c\cdot\Delta dT_i + \lambda\cdot\Delta N_i - \Delta d_{ion,i} + \Delta d_{trop,i} + \Delta d^{\phi}_{mp,i} + \varepsilon_{\Delta\phi_i} \qquad (3\text{-}1)$$

where $\Delta(\cdot) = (\cdot)_u - (\cdot)_i$; i indicates the reference station, and u the user station; ϕ is the carrier phase observation in units of metres; $\rho = \left\|X^s - X\right\|$, where X^s is the satellite position vector and X is the station position vector; $d\rho$ is the effect of orbit error; dT is the receiver clock error with respect to GPS time; d_{ion} is the ionospheric delay; d_{trop} is the tropospheric delay after model correction; d^{ϕ}_{mp} is the multipath on the carrier phase measurement; $\varepsilon_{\Delta\phi}$ is the carrier phase observation noise; λ is the wavelength of the carrier wave; and N is the integer ambiguity.

For the multiple reference station system, there are several of single-differenced carrier phase observables between the user and the reference stations can be made as Equation 3-1. In order to eliminate the distance dependent errors (orbit error, ionospheric delay and tropospheric delay) in Equation 3-1, the weights are chosen to be inversely proportional to the baseline lengths. By choosing weights properly, a method is to average out the differenced distance between the user and the reference station positions. This idea was suggested by Wu, 1994 and Han & Rizos, 1996. In the case that there are three reference stations, a set of parameters can be computed such that the following conditions are satisfied:

$$\sum_{i=1}^{3}\alpha_i\left(\bar{X}_u - \bar{X}_i\right) = 0 \qquad (3\text{-}2)$$

where $\bar{X}_u$ and $\bar{X}_i$ are the coordinates of the user receiver and reference receiver in the Gaussian plane coordinate system respectively and α_i is the weight for the i reference station.

To average out the difference distances, the sum of weights is required in 1.

$$\sum_{i=1}^{3} \alpha_i = 1 \tag{3-3}$$

In order to minimize α_i, another constraint should be added:

$$\sum_{i=1}^{3} \alpha^2_i = \min \tag{3-4}$$

If more reference stations are available, the parameter α_i can be determined using Equations (3-2), (3-3) and (3-4) so as to make the standard deviation of the linear combination observations a minimum. Through the application of the Condition Method:

$$B\,\alpha = w, \text{ with weight matrix } P \tag{3-5}$$

where B is the design matrix.

The least squares estimate is based on satisfying the condition in Equation (3-4). A solution is obtained by introducing the vector of Lagrange multipliers K, and minimising the function:

$$F(V,K) = P - 2K^T(B\alpha - w) \tag{3-6}$$

Equation (3-6) is a function of two variables, namely α and K. A necessary condition for the minimum is that the partial derivatives must be zero:

$$P\alpha - B^T K = 0 \tag{3-7}$$

$$\alpha = P^{-1}B^T K \tag{3-8}$$

By substituting Equation (3-8) into (3-5), the Lagrange multiplier vector K can be derived:

$$K = \left(BP^{-1}B^T\right)^{-1} w \tag{3-9}$$

$$\text{then } \alpha = P^{-1}B^T(BP^{-1}B^T)^{-1} \cdot w \tag{3-10}$$

In general, P is an Identity matrix, hence:

$$\alpha = B^T(BB^T)^{-1} \cdot w \tag{3-11}$$

where B is the design matrix, containing the partial derivatives of Equations (3-2) and (3-3) with respect to the α values, α are the parameter values, and w is the misclose vector.

Using Equation (3-1), the user station coordinate can be determined on a site-by-site basis, with respect to the reference station 3. This technique can be used not only in a single user receiver mode but also in the case of multiple user receiver arrays.

Single-Differenced Model

The linear combination of the single-differenced observables can be written as:

$$\sum_{i=1}^{3}\alpha_i\cdot\Delta\phi_i=\sum_{i=1}^{3}\alpha_i\cdot\Delta\rho_i+\sum_{i=1}^{3}\alpha_i\cdot\Delta d\rho_i\ -c\cdot\sum_{i=1}^{3}\alpha_i\cdot\Delta dT_i+\lambda\cdot\sum_{i=1}^{3}\alpha_i\cdot\Delta N_i$$
$$-\sum_{i=1}^{3}\alpha_i\cdot\Delta d_{ion,i}+\sum_{i=1}^{3}\alpha_i\cdot\Delta d_{trop,i}+\sum_{i=1}^{3}\alpha_i\cdot\Delta d^{\phi}_{mp,i}+\varepsilon_{\sum_{i=1}^{3}\alpha_i\cdot\Delta\phi_i} \tag{3-12}$$

According to Equation 3-2, the orbit error term has been shown to be:

$$\sum_{i=1}^{3}\alpha_i\cdot\Delta d\rho_i\approx 0 \tag{3-13}$$

The ionospheric delay can be written as:

$$\sum_{i=1}^{3}\alpha_i\cdot\Delta d_{ion,i}=d_{ion,u}-d_{ion,3}-\begin{bmatrix}\alpha_1\\ \alpha_2\end{bmatrix}^{T}\begin{vmatrix}d_{ion,1}-d_{ion,3}\\ d_{ion,2}-d_{ion,3}\end{vmatrix} \tag{3-14}$$

When the distance between the reference stations increases, the residual error will become greater due to errors in the ionospheric delay interpolation.

If the tropospheric delay can be interpolated from the residual tropospheric delay at the reference stations, the tropospheric delay can be represented as:

$$\sum_{i=1}^{3}\alpha_i\cdot\Delta d_{trop,i}=d_{trop,u}-d_{trop,3}-\begin{bmatrix}x_u & y_u\end{bmatrix}\begin{bmatrix}x_1 & y_1\\ x_2 & y_2\end{bmatrix}^{-1}\begin{vmatrix}d_{trop,1}-d_{trop,3}\\ d_{trop,2}-d_{trop,3}\end{vmatrix} \tag{3-15}$$

where $(x_1\quad y_1),(x_2\quad y_2)$ and $(x_u\quad y_u)$ are the north and east coordinate components relative to reference station 3 in the Gaussian plane coordinate system. How close it is to zero depends on the spatial correlation of the tropospheric delay. The residual tropospheric delay is mostly contributed by to the wet component of the troposphere, which shows strong variation with height, time and location. It can be expected that the term $\sum_{i=1}^{3}\alpha_i\cdot\Delta d_{trop,i}$ will be mitigated to an extent that is an unknown function of the distance between stations.

The multipath term can be represented as:

$$\sum_{i=1}^{3}\alpha_i \cdot \Delta d^{\phi}_{mpi} = d^{\phi}_{mpu} - \sum_{i=1}^{3}\alpha_i \cdot d^{\phi}_{mpi} \qquad (3\text{-}16)$$

The last term $\sum_{i=1}^{3}\alpha_i \cdot \Delta d^{\phi}_{mpi}$ on the right hand side of Equation (3-16) is the weighted mean value of the multipath values at the three reference receivers for this satellite. Due to the random nature of multipath at different receivers, the weighted mean value will be significantly reduced if all $\alpha_i (i = 1,2,3)$ are positive and less than 1, although the weight α_i is not derived from its standard deviation. On the other hand, the multipath at the user receiver will become a high frequency bias, and mostly will be close to random noise (Zhang & Schwarz, 1996). Therefore, the multipath term can be assumed to have been significantly reduced and will consequently be ignored in the functional model.

The standard derivation of the one-way carrier phase observation can be considered, as a first approximation, a function of the elevation angle. Since all stations are located within a region of about 100km radius, the elevation angle to a satellite is approximately the same. The standard deviation of the linear combination of single-differenced observations $\varepsilon_{\sum_{i=1}^{3}\alpha_i \cdot \Delta\phi_i}$ can be expressed as:

$$\sigma_{\sum_{i=1}^{3}\alpha_i \cdot \Delta\phi_i} = \sqrt{1+\alpha_1^2+\alpha_2^2+\alpha_3^3} \cdot \sigma^j \qquad (3\text{-}17)$$

Compared to the standard deviation of the single-frequenced carrier phase observation $\sqrt{2} \cdot \sigma^j$, the standard deviation will become smaller if the user receiver is located within the triangle formed by the reference stations.

The single-differenced functional model can be simplified to:

$$\sum_{i=1}^{3}\alpha_i \cdot \Delta\phi_i = \sum_{i=1}^{3}\alpha_i \cdot \Delta\rho_i - c \cdot \sum_{i=1}^{3}\alpha_i \cdot \Delta dT_i + \lambda \cdot \sum_{i=1}^{3}\alpha_i \cdot \Delta N_i + \varepsilon_{\sum_{i=1}^{3}\alpha_i \cdot \Delta\phi_i} \qquad (3\text{-}18)$$

Double-Differenced Model

Equation (3-18) can be written as:

$$\begin{aligned}
&\Delta\phi_{u,3} - [\alpha_1 \cdot \Delta\phi_{1,3} + \alpha_2 \cdot \Delta\phi_{2,3}] = \\
&\Delta\rho_{u,3} - [\alpha_1 \cdot \Delta\rho_{1,3} + \alpha_2 \cdot \Delta\rho_{2,3}] - c \cdot \sum_{i=1}^{3}\alpha_i \cdot \Delta dT_i + \lambda \cdot \Delta N_{u,3} - \\
&[\alpha_1 \cdot \Delta N_{1,3} + \alpha_2 \cdot \Delta N_{2,3}] + \varepsilon_{\sum_{i=1}^{3}\alpha_i \cdot \Delta\phi_i}
\end{aligned} \qquad (3\text{-}19)$$

The residual vectors are defined as:

$$V_{1,3} = \Delta\nabla\phi_{1,3} - \Delta\nabla N_{1,3} - \Delta\nabla\rho_{1,3}$$
$$V_{2,3} = \Delta\nabla\phi_{2,3} - \Delta\nabla N_{2,3} - \Delta\nabla\rho_{2,3} \qquad (3\text{-}20)$$

The double-differenced observable model can be written as:

$$\Delta\nabla\phi_{u,3} - \left[\alpha_1 \cdot V_{1,3} + \alpha_2 \cdot V_{2,3}\right] = \Delta\nabla\rho_{u,3} + \lambda \cdot \Delta\nabla N_{u,3} + \varepsilon_{\sum_{i=1}^{3}\alpha_i \cdot \Delta\nabla\phi_i} \qquad (3\text{-}21)$$

where $\left[\alpha_1 \cdot V_{1,3} + \alpha_2 \cdot V_{2,3}\right]$ is the correction term for the user stations.

Therefore, after the initialisation of the reference stations, the coordinates and integer ambiguities are known, and the correction vectors $V_{1,3}, V_{2,3}$ can then be computed. For the real-time baseline computation, the correction vectors, *together with the carrier phase and pseudo-range data at a reference station,* can be transmitted to the user.

3.2.2 Modified model for between-user receiver positioning

Figure 3-1 illustrates the geometric relationship between the GPS reference stations and user stations. If there are 5 reference stations, the origin point is set up at the reference station 3 in order to simplify the derivation.

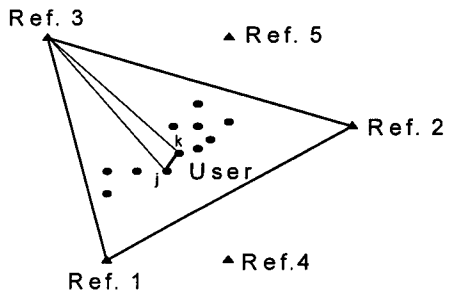

Figure 3-1. The mixed mode network: triangles denote the GPS reference stations, and the dots denote the user stations.

In the case of two user stations j and k, the double-differenced observable equation can be written as:

$$\Delta\nabla\phi_{j,3} - \left[\alpha_1^j \cdot V_{1,3} + \alpha_2^j \cdot V_{2,3}\right] = \Delta\nabla\rho_{j,3} + \lambda \cdot \Delta\nabla N_{j,3} + \varepsilon_{\sum_{i=1}^{3}\alpha_j \cdot \Delta\nabla\phi_j} \qquad (3\text{-}22)$$

$$\Delta\nabla\phi_{k,3} - \left[\alpha_1^k \cdot V_{1,3} + \alpha_2^k \cdot V_{2,3}\right] = \Delta\nabla\rho_{k,3} + \lambda \cdot \Delta\nabla N_{k,3} + \varepsilon_{\sum_{i=1}^{3} \alpha_k \cdot \Delta\nabla\phi_k} \tag{3-23}$$

Forming the linear combination between the user stations (j and k), the following expression is obtained:

$$(\Delta\nabla\phi_{k,3} - \Delta\nabla\phi_{j,3}) - \left(\left[\alpha_1^k \cdot V_{1,3} + \alpha_2^k \cdot V_{2,3}\right] - \left[\alpha_1^j \cdot V_{1,3} + \alpha_2^j \cdot V_{2,3}\right]\right)$$

$$= (\Delta\nabla\rho_{k,3} - \Delta\nabla\rho_{j,3}) + \lambda \cdot (\Delta\nabla N_{k,3} - \Delta\nabla N_{j,3}) + (\varepsilon_{\sum_{k=1}^{3} \alpha_k \cdot \Delta\nabla\phi_k} - \varepsilon_{\sum_{j=1}^{3} \alpha_j \cdot \Delta\nabla\phi_j}) \tag{3-24}$$

Equation (3-24) can be written as:

$$\Delta\nabla\phi_{k,j} - \left[\alpha_1^{k,j} \cdot V_{1,3} + \alpha_2^{k,j} \cdot V_{2,3}\right] = \Delta\nabla\rho_{k,j} + \lambda \cdot \Delta\nabla N_{k,j} + \varepsilon_{k,j} \tag{3-25}$$

Where the $\alpha_1^{k,j}$ is the difference of the α_1 value for user stations k and j ($\alpha_2^{k,j}$ has a similar definition to $\alpha_1^{k,j}$.) and $\left[\alpha_1^{k,j} \cdot V_{1,3} + \alpha_2^{k,j} \cdot V_{2,3}\right]$ is the correction term for user stations j and k.

Comparing Equation (3-25) and (3-21), the advantage of Equation (3-25) is that it can accommodate more than one user receiver operating simultaneously. In the processing procedure, by forming the double-differenced observables between the user stations, and obtaining the residual vectors from the reference station, the user station coordinates can be determined without needing to directly process any reference station data.

3.3 The Procedure for Generating Network 'Corrections'

The 'correction' generating algorithm consists of two main elements: one relates to the precise coordinates and ambiguities of the reference stations, and the other one is the α values. The coordinates and ambiguities associated with the reference stations can be estimated during the initialisation process, while the α values can be computed from Equations (3-2)~(3-4) using the approximate coordinates of the user station (and the known coordinates of the reference stations).

3.3.1 Initialisation of reference station processing

The double-differenced carrier phase observables used in standard GPS processing can be expressed as:

$$\Delta\nabla\phi_1 = \Delta\nabla\rho + \Delta\nabla d\rho - \Delta\nabla I + \Delta\nabla T + \Delta\nabla M + \lambda_1\Delta\nabla n_1 + \Delta\nabla\varepsilon_{\Delta\nabla\phi_1} \quad (3\text{-}26)$$

$$\Delta\nabla P_1 = \Delta\nabla\rho + \Delta\nabla d\rho - \Delta\nabla I + \Delta\nabla T + \Delta\nabla M + \Delta\nabla\varepsilon_{\Delta\nabla\phi_1} \quad (3\text{-}27)$$

$$\Delta\nabla\phi_2 = \Delta\nabla\rho + \Delta\nabla d\rho - \frac{f_1^2}{f_2^2}\Delta\nabla I + \Delta\nabla T + \Delta\nabla M + \lambda_2\Delta\nabla n_2 + \Delta\nabla\varepsilon_{\Delta\nabla\phi_2} \quad (3\text{-}28)$$

$$\Delta\nabla P_2 = \Delta\nabla\rho + \Delta\nabla d\rho - \frac{f_1^2}{f_2^2}\Delta\nabla I + \Delta\nabla T + \Delta\nabla M + \Delta\nabla\varepsilon_{\Delta\nabla\phi_2} \quad (3\text{-}29)$$

where $\Delta\nabla\phi$: the double-differenced carrier phase measurements;
$\Delta\nabla P$: the double-differenced pseudorange measurements;
$\Delta\nabla\rho$: the double-differenced geometric range;
$\Delta\nabla d\rho$: double-differenced orbit error;
$\Delta\nabla I$: the double-differenced ionospheric delay;
$\Delta\nabla M$: the double-differenced multipath error;
$\Delta\nabla T$: the double-differenced tropospheric delay;
λ_1, λ_2: the wavelength of L1 and L2 respectively;
f_1, f_2: the frequency of L1 and L2 respectively;
$\Delta\nabla n$: the double-differenced phase ambiguity;
$\Delta\nabla\varepsilon$: the double-differenced carrier phase noise.

The estimated accuracies of the orbit information based on analyses performed by IGS Analysis Center Coordinator are given in Table 3-1. The rms value of 20cm per coordinate component for the CODE (Center for Orbit Determination in Europe) solution assumes predicted orbits from a 2-4 hour extrapolation (Rothacher & Mervart, 1996). Current accuracies are even higher.

Table 3-1. Estimated quality of GPS orbit information (Rothacher & Mervart, 1996).

Orbit Type	Quality (m)	Delay of Availability	Available at
Broadcast	3.00	Real-time	Broadcast Message
CODE Predicted	0.20	Real-time	CODE via FTP
CODE Rapid	0.10	After 16hrs	CODE via FTP
IGS Rapid	0.10	After 24hrs	IGS data centres
IGS Final	0.05	After 11 Days	IGS data centres

After careful selection of the reference stations, and using both hardware and software multipath error reduction techniques, the effect of multipath error can be assumed to have been significantly mitigated. Hence, the main biases in medium-range positioning are the

ionospheric and tropospheric delays. At the commencement of operation of the reference station network, the ambiguities and the coordinates of the reference stations, together with the parameters of the ionospheric delay and tropospheric delay, can be estimated from several hours of observation data.

3.3.2 Determination of coordinates and ambiguities

Because the distance-dependent biases (i.e. orbit error, ionospheric delay and tropospheric delay) noticeably increase as the baseline length increases beyond 10-20km, the ambiguity resolution process becomes harder. There are two methods for dealing with what is generally considered the dominant bias, the ionospheric delay. The first method is to form a linear combination to eliminate the effect of the ionospheric delay, e.g. use an ionosphere-free linear combination. The other method uses a stochastic model of the ionosphere, which can be mathematically regarded as the addition of pseudo-observations, together with a variance-covariance matrix in which the uncertainty of the ionospheric delay is accounted for, as described in, for example, Odijk (1999) and Rothacher & Mervart (1996). These two procedures are discussed below.

Two-step procedure:

Step 1 - Widelane ambiguity resolution
The double-differenced, widelane linear combination can be written as:

$$\Delta\nabla\phi_{WL} = \frac{f_1}{f_1 - f_2}\Delta\nabla\phi_1 - \frac{f_2}{f_1 - f_2}\Delta\nabla\phi_2$$

$$= \Delta\nabla\rho + \Delta\nabla d\rho + \Delta\nabla T + \Delta\nabla M + \frac{f_1}{f_2}\Delta\nabla I + \frac{c}{f_1 - f_2}(\Delta\nabla n_1 - \Delta\nabla n_2) + \Delta\nabla\varepsilon_{\Delta\nabla\phi_{WL}} \qquad (3\text{-}30)$$

where: c the light of speed;

$\frac{c}{f_1 - f_2}$ the widelane wavelength (86.2cm); and

$(\Delta\nabla n_1 - \Delta\nabla n_2)$ the widelane ambiguity.

An estimate of the widelane ambiguity is:

$$\Delta\nabla n_{WL,FLOAT} = \frac{1}{\lambda_{WL}}(\Delta\nabla\phi_{WL} - \Delta\nabla\rho - \Delta\nabla d\rho - \Delta\nabla T - \Delta\nabla M - \frac{f_1}{f_2}\Delta\nabla I - \Delta\nabla\varepsilon_{\Delta\nabla\phi_{WL}}) \qquad (3\text{-}31)$$

In using Equation (3-30) to resolve the widelane integer ambiguity, the geometric errors and multipath are assumed to have been mitigated at the reference stations by careful selection of station sites and through the use of precise (IGS-derived) ephemeris

information. Although the noise and ionospheric delay relative to L1 are up to 6 and 1.3 times larger respectively, the integer ambiguity can be fixed because of the comparatively long wavelength of this combination.

Step 2 - Ionosphere-free linear combination

The ionosphere-free linear combination can be expressed as:

$$\Delta\nabla\phi_{IONO-FREE} = \frac{f_1^2}{f_1^2 - f_2^2}\Delta\nabla\phi_1 - \frac{f_2^2}{f_1^2 - f_2^2}\Delta\nabla\phi_2$$
$$= \Delta\nabla\rho + \Delta\nabla d\rho + \Delta\nabla T + \Delta\nabla M + \varepsilon_{\Delta\nabla\phi_{IONO-Free}} + \frac{f_1^2}{f_1^2 - f_2^2}\lambda_1\Delta\nabla n_1 - \frac{f_2^2}{f_1^2 - f_2^2}\lambda_2\Delta\nabla n_2 \quad (3\text{-}31)$$

The ionospheric refraction bias can be eliminated by constructing a combined ionosphere-free phase or pseudorange observable from the ϕ_1 and ϕ_2 data. The last term of Equation (3-31) can be written as:

$$\begin{aligned} Bias_{IONO-FREE} &= \frac{f_1^2}{f_1^2 - f_2^2}\lambda_1\Delta\nabla n_1 - \frac{f_2^2}{f_1^2 - f_2^2}\lambda_2\Delta\nabla n_2 \\ &= \frac{c \cdot f_2}{f_1^2 - f_2^2}\Delta\nabla n_{WL} + \frac{c}{f_1 + f_2}\Delta\nabla n_1 \\ &= \frac{f_2 \cdot \lambda_{NL}}{f_1 - f_2}\Delta\nabla n_{WL} + \lambda_{NL}\Delta\nabla n_1 \end{aligned} \quad (3\text{-}32)$$

Therefore, Equation (3-32) can be rewritten as:

$$\Delta\nabla n_{1,FLOAT} = \frac{1}{\lambda_{NL}}(\Delta\nabla\phi_{IONO-FREE} - \Delta\nabla\rho - \Delta\nabla d\rho$$
$$-\Delta\nabla T - \Delta\nabla M - \Delta\nabla\varepsilon_{\Delta\nabla\phi_{IONO-FREE}}) - \frac{f_2}{f_1 - f_2}\Delta\nabla n_{WL} \quad (3\text{-}33)$$

The last term on the righthand side of Equation (3-33) is the widelane ambiguity term. If the widelane ambiguity can be fixed, in subsequent processing the formal wavelength $\lambda_{IONO-FREE}$ is only 10.7cm.

Due to the fact that geometric errors and multipath can be mitigated at the reference stations, the most significant error in the determination of the $\Delta\nabla n_1$ integer ambiguity is then the residual tropospheric delay (after applying a standard tropospheric refraction model).

One-step procedure:

QIF (Quasi Ionosphere-Free) combination

This procedure was proposed by Rothacher & Marvart (1996) and Odijk (1999). The main characteristic of this algorithm is to add ionospheric pseudo-observables (artificial observations) to the observation model.

For baselines longer than about 10km, processing of the two frequencies L1 and L2 separately does not give sufficiently good initial real-valued estimates of n1 and n2 due to the influence of the ionospheric refraction. One ionospheric correction $I_k^i(t_j)$ for satellite i, receiver k and epoch t_j is estimated. Estimating these parameters without any a priori constraints is equivalent to processing the ionosphere-free linear combination. In order to resolve the integer ambiguities, it is necessary to constrain these parameters to within a few decimetres. This constraining may be achieved by introducing an artificial observation:

$$I_k^i(t_j) - I_{k,apr}^i(t_j) = 0 \tag{3-34}$$

for each epoch with a non-zero a priori weight. The actual values $I_{k,apr}^i(t_j)$ may be obtained from an ionosphere model, and in many cases (baselines up to 500km in length) even $I_{k,apr}^i(t_j) = 0$ may be sufficient. It is of course necessary to pre-eliminate all epoch-specific ionospheric parameters $I_{k,apr}^i(t_j)$, I=1,2,..., n_s (n_s is the number of satellites per epoch) after having processed epoch t_j, because a huge number of parameters would otherwise have to be handled in the normal equation system after n_s epochs.

Implementation of the QIF processing strategy

Denote by $b_{1i}, b_{1i_1}, b_{1i_2}$ the (real-valued) double-differenced L1 ambiguities. Similarly $b_{2j}, b_{2j_1}, b_{2j_2}$ are the corresponding L2 ambiguities. The ambiguity pair can be checked in (b_{1i}, b_{2j}) or a pair of differences $(b_{1i_1} - b_{1i_2})$, $(b_{2j_1} - b_{2j_2})$.

which, as a matter of fact, is again a pair of double-differenced ambiguities . It meets the requirement of being close to integers, and may be accepted as the correct pair of integer ambiguities. This procedure needs to be explained in more detail. Compute the rms error for each ionospheric-free linear combination ambiguity bias $\tilde{b}_3$ associated with a pair (b_{1i}, b_{2j}), or with a pair of differences $(b_{1i_1} - b_{1i_2})$, $(b_{2j_1} - b_{2j_2})$:

$$\sigma = \sigma_0 \cdot \sqrt{\beta_1^2 Q_{11} + 2\beta_1\beta_2 Q_{12} + \beta_2^2 Q_{22}} \tag{3-35}$$

where

$$Q_{11} = Q(b_{1i,}b_{1i}),\ Q_{12} = Q(b_{1i,}b_{2j}),Q_{22} = Q(b_{2j,}b_{2j}) \tag{3-36}$$

in the case of pair differences ($b_{1i_1} - b_{1i_2}$), ($b_{2j_1} - b_{2j_2}$). Sort the ambiguity pairs in ascending order of their σ-values. For the ambiguity pair (or pair of differences) with the smallest σ (if this σ is lower than the specified σ_{max}) define the search regions:

$$\begin{aligned}
&\tilde{n}_1 = n\,int(b_1) \pm i, && i=0;\ 1;\ \ldots;\ i_{max}\\
&\tilde{n}_{WIDE} = n\,int(b_1 - b_2) \pm k, && k=0;\ 1;\ \ldots;k_{max}\\
&\tilde{n}_2 = \tilde{n}_1 - \tilde{n}_5
\end{aligned}$$

and for each pair $(\tilde{n}_1, \tilde{n}_2)$ of integers within the search region compute the test value:

$$d_3 = \left|\beta_1(b_1 - \tilde{n}_1) + \beta_2(b_2 - \tilde{n}_2)\right| \tag{3-37}$$

The pair associated with the smallest value d_3 is accepted as a solution, unless

$$d_3 \geq d_{max} \tag{3-38}$$

where d_{max} is a user-defined threshold value. If no ambiguity set is able to pass the test, proceed to the next pair of ambiguities associated with the second smallest σ. After having accepted one pair, the entire least squares adjustment and the procedure described above is repeated. The ambiguities are thus resolved iteratively. All or only a subset of the ambiguity pairs may be resolved in the iteration process.

3.3.3 Generation of 'correction' terms

According to Equations (3-21) or (3-25), the 'correction' terms can be computed after obtaining the residuals and the α values. To compute the residuals in Equation (3-20), it is necessary to have the coordinates and integer ambiguities associated with the reference stations. After the initialisation process the coordinates and ambiguities can be determined. In the case of the α values, computed using Equations (3-5)~(3-11), the approximate coordinate of the user station(s) and the known coordinates of the reference stations are required.

Figure 3-2 shows an example of the 'correction' terms. The α values for baseline 1 & 2 are 0.333 and 0.430 respectively.

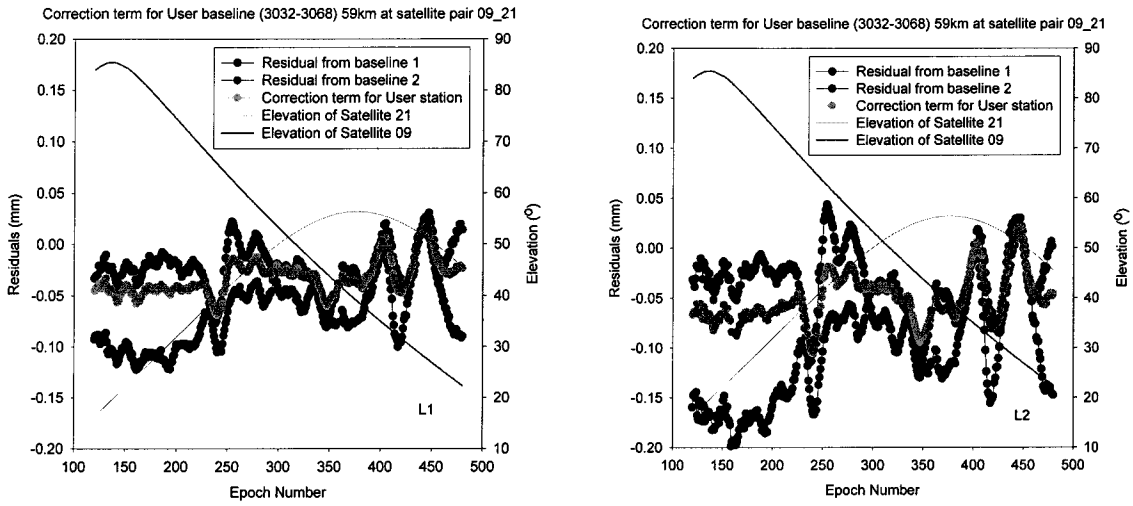

Figure 3-2. Example of the 'correction' terms. The left hand graph contains the L1 corrections and the right hand graph denotes the L2 corrections, for the satellite pair 09_21. The baseline length is 59km, from the epoch number 120 to 480 (UTC 02^{h}:00^{m}~04^{h}:00^{m} + 0900), for day of year 001, 1997, in the Tokai area, Japan.

3.3.4 Summary of the procedure

The data processing procedure consists of the following steps (Figure 3-3):

Step 1. After fixing the ambiguities for the reference stations, derive the residual vectors on an epoch-by-epoch and satellite-by-satellite basis, using Equation (3-13).

Step 2. From the approximate positions of any user station and the reference stations, determine the linear combination coefficients and the α values. Then the 'correction' term is obtained from Equations (3-14) and (3-18).

Step 3. Apply the 'correction' term to the double-differenced carrier phase observations between the user station and reference station, or between pairs of user stations.

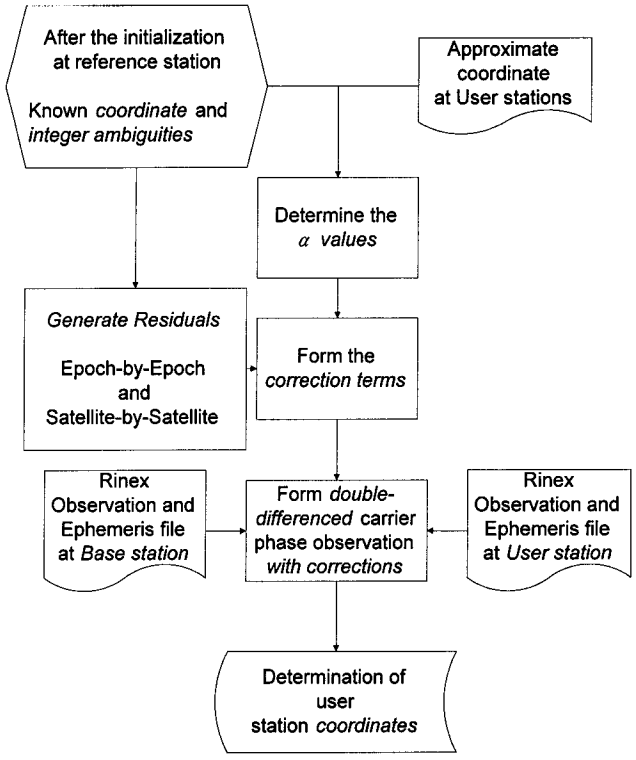

Figure 3-3. Flow chart for the computation and application of the 'correction' terms for the case of computing a user-reference station baseline.

3.4 Corrections and Their Application

3.4.1 Basic mode - L1, L2 corrections

For a dual-frequency receiver, the residual from Equation (3-20) can be represented by different linear combination models, such as L1&L2, widelane, geometry-free or the ionosphere-free combinations. The reference and user stations are assumed to be in the configuration shown in Figure 3-1.

Equation (3-20) defines the residual vectors as:

$$V_{1,3} = \Delta\nabla\phi_{1,3} - \Delta\nabla N_{1,3} - \Delta\nabla\rho_{1,3}$$
$$V_{2,3} = \Delta\nabla\phi_{2,3} - \Delta\nabla N_{2,3} - \Delta\nabla\rho_{2,3}$$

where $V_{1,3}, V_{2,3}$ are the residuals between reference stations 1 to 3 and 2 to 3, in the case of the L1 observable. Hence, for the L1&L2 residuals, they can be rewritten as:

For stations 1,3:

$$V_{1,3}^{L1} = \Delta\nabla\phi_{1,3}^{L1} - \Delta\nabla N_{1,3}^{L1} - \Delta\nabla\rho_{1,3}^{L1}$$
$$V_{1,3}^{L2} = \Delta\nabla\phi_{1,3}^{L2} - \Delta\nabla N_{1,3}^{L2} - \Delta\nabla\rho_{1,3}^{L2} \quad (3\text{-}39)$$

For stations 2,3:

$$V_{2,3}^{L1} = \Delta\nabla\phi_{2,3}^{L1} - \Delta\nabla N_{2,3}^{L1} - \Delta\nabla\rho_{2,3}^{L1}$$
$$V_{2,3}^{L2} = \Delta\nabla\phi_{2,3}^{L2} - \Delta\nabla N_{2,3}^{L2} - \Delta\nabla\rho_{2,3}^{L2} \quad (3\text{-}40)$$

Equations (3-39) and (3-40) contain the orbit bias, tropospheric delay, multipath and ionospheric delay. After combining the α values to form 'corrections' at the user station, the ambiguity resolution (using a dual-frequency user receiver) can be carried out even with only a single epoch of data (Han, 1996; Han& Rizos, 1996a).

3.4.2 Other extension mode – L5, L4 and L3 corrections

Other commonly-used linear combinations, and their residuals, are considered below. In the case of the widelane linear combination ($L5=\frac{1}{f_1 - f_2}(f_1 L_1 - f_2 L_2)$), for station pairs 1-3 and 2-3:

$$V_{1,3}^{L5} = \Delta\nabla\phi_{1,3}^{L5} - \Delta\nabla N_{1,3}^{L5} - \Delta\nabla\rho_{1,3}^{L5}$$
$$V_{2,3}^{L5} = \Delta\nabla\phi_{2,3}^{L5} - \Delta\nabla N_{2,3}^{L5} - \Delta\nabla\rho_{2,3}^{L5} \quad (3\text{-}41)$$

Equation (3-41) contains the orbit bias, tropospheric delay, multipath and ($\frac{f_1}{f_2} \cong 1.28$) times the L1 magnitude of the ionospheric delay.

For the geometry-free linear combination ($L4=(L_1 - L_2)$):

$$V_{1,3}^{L4} = \Delta\nabla\phi_{1,3}^{L4} - (\lambda_1\Delta\nabla N_{1,3}^{L1} - \lambda_2\Delta\nabla N_{1,3}^{L2})$$
$$V_{2,3}^{L4} = \Delta\nabla\phi_{2,3}^{L4} - (\lambda_1\Delta\nabla N_{2,3}^{L1} - \lambda_2\Delta\nabla N_{2,3}^{L2}) \quad (3\text{-}42)$$

Equation (3-42) contains ($\frac{f_2^2 - f_1^2}{f_2^2} \cong 0.647$) times the L1 ionospheric delay.

For the ionosphere-free linear combination (L3=$\frac{1}{f_1^2 - f_2^2}(f_1^2 L_1 - f_2^2 L_2)$):

$$V_{1,3}^{L3} = \Delta\nabla\phi_{1,3}^{L3} - (c\frac{f_2}{f_1^2 - f_2^2}\Delta\nabla N_{1,3}^{L5} - \frac{c}{f_1 + f_2}\Delta\nabla N_{1,3}^{L1})$$

$$V_{2,3}^{L3} = \Delta\nabla\phi_{2,3}^{L3} - (c\frac{f_2}{f_1^2 - f_2^2}\Delta\nabla N_{2,3}^{L5} - \frac{c}{f_1 + f_2}\Delta\nabla N_{2,3}^{L1}) \quad (3\text{-}43)$$

Equation (3-43) contains the orbit bias, multipath and tropospheric delay.

3.5 Corrections and Position Accuracy Analysis

3.5.1 Computing α values and their positioning accuracy

The α values can been estimated in the Gaussian plane coordinate system or the geocentric coordinate system. From Equation (3-3), $(X_u - X_i)$ is the baseline vector from the user u to the reference station i, and the α values are the associated weights for that baseline (Figure 3-4). Hence, the α values are dependent on which coordinate system $(X_u - X_i)$ are expressed in.

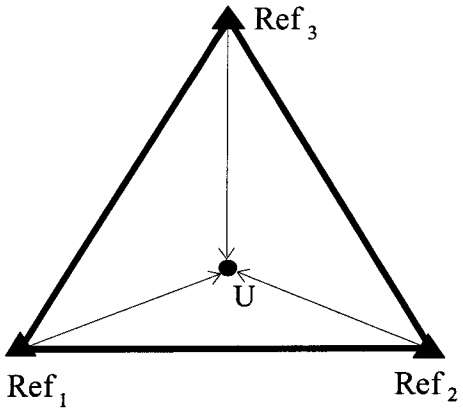

Figure 3-4. Simple configuration of the GPS reference stations (triangles) and the user receiver (circle).

From Equation (3-2):

$$\sum_{i=1}^{3} \alpha_i (\vec{X}_u - \vec{X}_i) = 0$$

the α values are related to the position of the user station and the baseline length. If the size of the triangle is enlarged or reduced, the α values do not change. But for a certain sized triangle, if the position of the user station is changed, the α values will also change:

$$\Delta\alpha \cong \frac{\Delta X_u}{(X_u - X_i)} \tag{3-44}$$

where $\Delta X_u = X_u^{'} - X_u$; ΔX_u is the change in the user station position.

$\Delta\alpha = \alpha^{'} - \alpha$; $\Delta\alpha$ is the change in the α value for the new user station position.

Consider, for example, a user station located at the centre of a triangle of reference stations, with each side 100km in length, then the distance from a reference station to the user station is about 57km. If X_u moves 500m in the X direction, the α value will only change by -0.005 for α_1, by +0.005 for α_2, and α_3 will not change.

In the case illustrated in the Figure 3-4, a user station located at the centre of the reference network, the α values can be computed using Equations (3-2)~(3-4), using either the Gaussian plane coordinate system or the geocentric coordinate system. Their values are listed in Table 3-2 and 3-3.

Table 3-2. Effect of position of user station on a value for the Gaussian plane coordinate system.

	Ref1-2-3 (100-100-100km)	Ref1-2-3 (100-100-100km)	Ref1-2-3 (50-50-50km)	Ref1-2-3 (50-50-50km)
	Ref1-User (in the centre)	Ref1-New User (500m diff in X)	Ref1-User (in the centre)	Ref1-User (500m diff. In X)
α_1	0.33333	*0.32833*	0.33333	*0.32333*
α_2	0.33333	*0.33833*	0.33333	*0.34333*
α_3	0.33333	0.33333	0.33333	0.33333

Table 3-3. Effect of position of user station on a value for the geocentric coordinate system.

	Ref1-2-3 (100-100-100km)	Ref1-2-3 (100-100-100km)	Ref1-2-3 (50-50-50km)	Ref1-2-3 (50-50-50km)
	Ref1-User (in the centre)	Ref1-New User (500m diff in X)	Ref1-User (in the centre)	Ref1-User (500m diff. In X)
α_1	0.33333	*0.33169*	0.33333	*0.33000*
α_2	0.33333	*0.33501*	0.33333	*0.33666*
α_3	0.33333	0.33333	0.33333	0.33333

There are three reference receiver subnets in Figure 3-5. The corresponding α values are listed in Table 3-4. The maximum difference in α values between the Gaussian plane coordinate system and the geocentric coordinate system is 0.06. For a 0.5 cycle residual, the effect is only 0.03 cycle in the 'correction' term (Equation (3-22)).

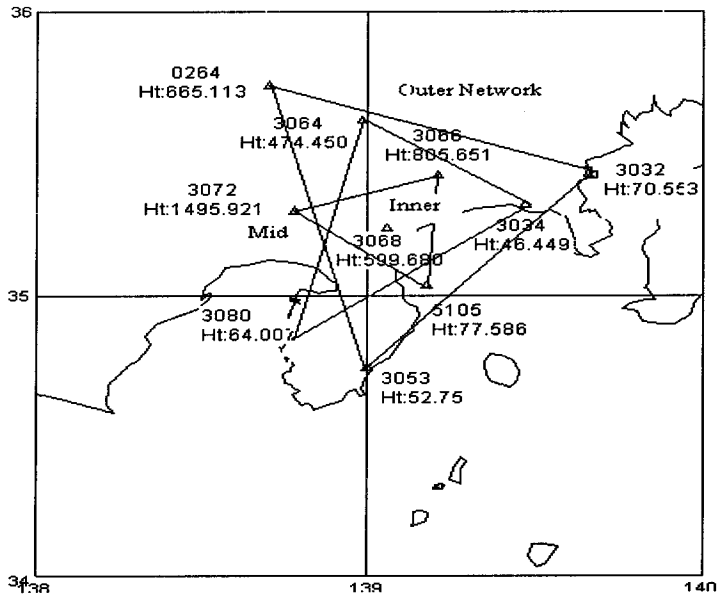

Figure 3-5. Subnets in the Toki GPS network, Japan. The outer network consists of reference stations 3032, 0264 and 3053, the middle network consists of reference stations 3034, 3064 and 3080, and the inner network consists of reference stations 3072, 5105 and 3066. The semi-diameters of these three reference station networks are 100km, 70km and 40km.

Table 3-4. The α values on the Gaussian plane and the geocentric coordinate system for the three Tokai (Japan) GPS reference station networks.

	Gaussian plane coordinate			Geocentric coordinate		
Network	Inner	Mid	Outer	Inner	Mid	Outer
α_1	0.330	0.323	0.237	0.338	0.308	0.182
α_2	0.303	0.243	0.333	0.288	0.216	0.320
α_3	0.367	0.434	0.430	0.374	0.476	0.498

Figure 3-6 displays the L1 different residuals obtained, using different α values computed in either the Gaussian plane coordinate system or the geocentric coordinate system. Comparing the two graphs, there is only a 2mm difference in offset variation due to the different sets of computed α values.

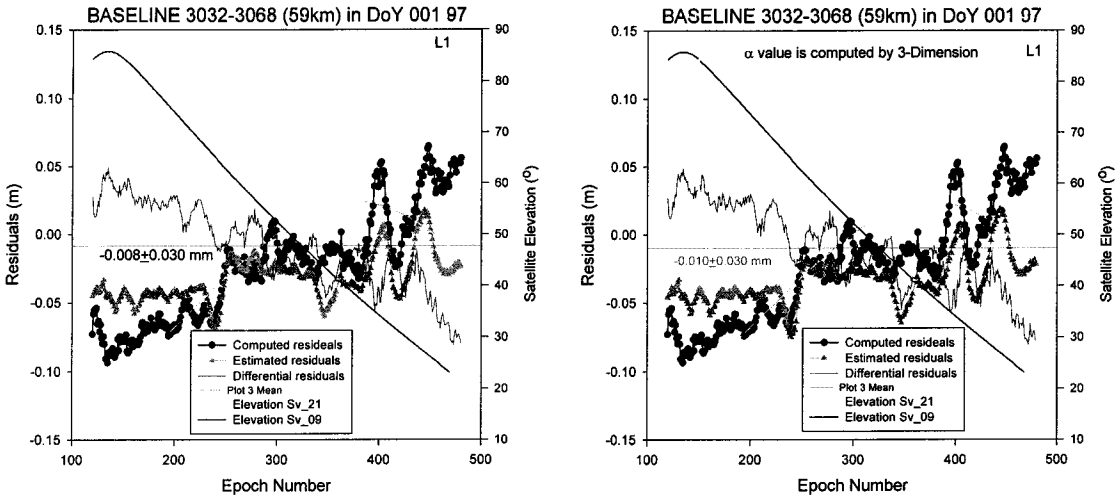

Figure 3-6. Left hand graph illustrates the L1 residual and the α value computed using the Gaussian plane coordinate system. Right hand graph denotes the L1 residual and the α value computed using geocentric coordinates. The satellite pair is 09_21 (Tokai, Japan) and the baseline length (stns 3032-3068) is 59km, from the epoch number 120 to 480 (UTC $02^h:00^m$~$04^h:00^m$ + 0900), for day of year 001 (1997).

3.5.2 Coverage of multiple reference station networks and their positioning accuracy

Regional-scale GPS permanent networks are being established in several countries to support a range of applications, such as:

- high precision, real-time kinematic positioning over medium-range baselines
- 'rapid static' positioning system
- machine control applications, e.g. precision farming
- deformation monitoring, e.g. volcano or structural monitoring

As already indicated, centimetre-level accuracy cannot be assured with a single reference station for baselines more than a few tens of kilometres in length. The advantage of using a multiple reference station technique is that the distance-dependent biases can be (to a certain extent) mitigated, and the ambiguities between the reference and user stations can be more easily resolved, hence resulting in a high precision positioning solution. However, modelling the distance-dependent biases using data from reference station networks can be performed successfully only if the spatial extents of the biases features are of larger scale than the inter-station distances (Wanninger, 1999).

Figure 3-7 shows three different coverage scenarios for the reference stations in the Tokai GPS network, Japan. Three subnets are used in this area: 3032-0264-3053, 3034-3064-3080 and 3072-5105-3066. Using three reference stations, the position of the user station (assumed to be station 3068, equipped with a single-frequency receiver) was estimated from three baselines 3072-3068, 3034-3068 and 3032-3068 (their approximate lengths being 26km, 39km and 58km respectively).

Table 3-5 displays the coordinate results for station 3068 with the 'corrections' generated, in turn, from the three different coverage networks. There were four different time periods (day of year (DoY) 001-007, 091-097, 181-187 and 271-277 in 1997) in these tests. Daily data processing was carried out for the four different periods, corresponding to each season of the year, using the ionosphere-free linear data combination. These results (for receiver coordinates and associated ambiguities) were compared with the single-frequency results after applying the 'correction terms' generated from processing the multi-reference station data. For the horizontal components (latitude and longitude) the position offset for the four data periods are all below 3mm, and in the case of the vertical component (height) the standard deviations are all below 41mm. The standard deviations increase as the reference station network coverage gets larger. As expected, the further apart the reference stations, the worse the positioning accuracy.

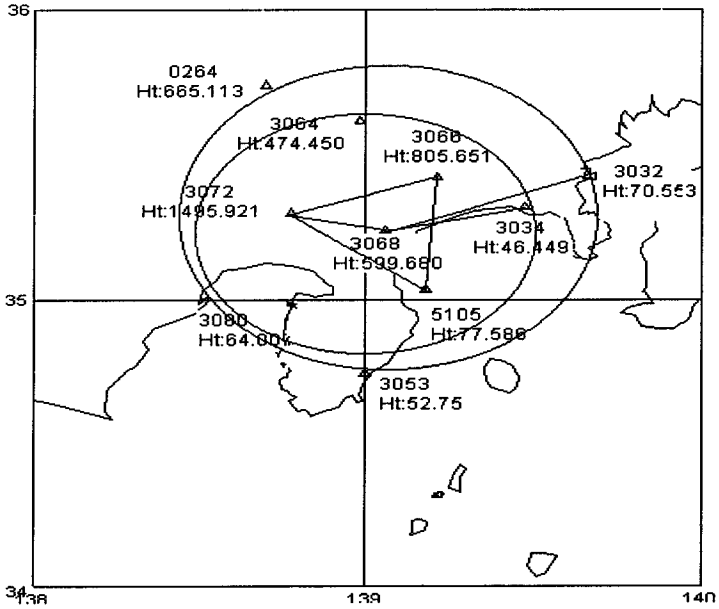

Figure 3-7. Three subnets considered in the Toki GPS network, Japan. The outer circle represents reference stations: 3032, 0264 and 3053, the middle circle denotes reference stations: 3034, 3064 and 3080 and the inner triangle shows reference stations 3072, 5105 and 3066. The semi-diameters of these three subnets are 100km, 70km and 40km.

Table 3-5. Positioning results for station 3068, computed with the aid of different subnets of reference stations (units in mm).

Network / Comp.	From inner network (26km)	From middle network (39km)	From outer network (59km)
Latitude	1.1±0.5	-1.6±3.5	-0.5±2.8
Longitude	2.5±4.1	1.2±4.0	-2.0±6.7
Height	-20.6±7.6	-26.1±8.8	-40.9±12.6
Length	2.8±4.2	1.1±4.3	-1.8±5.8

Figures 3-8, 3-9 and 3-10 show the differences between the computed residuals and the estimated residuals for the three baselines 3032-3068, 3034-3068 and 3072-3068 (only satellite pair 09_21 is shown), from the epoch number 120 to 480 (UTC 02^h:00^m~04^h:00^m), for day of year 001, 1997. The computed residuals are determined after resolving the integer ambiguities. The estimated residuals are generated by the three different reference stations to 'correct' the positioning of the user station 3068 individually (Equation (3-39)). Figures 3-8, 3-9 and 3-10 have the same graph frame, the x-axis is the epoch number, the left hand side of the y-axis is the residual (units in mm), and the right hand side of the y-axis is the satellite elevation (in degrees). The offsets and standard deviations of the L1 and L2 residuals are –0.013±0.014 mm and –0.013±0.016 mm (Figure 3-8) for the 23km baseline (3072-3068), –0.013±0.029 mm and –0.011±0.028 mm (Figure 3-9) for the 39km baseline (3034-3068), and –0.008±0.030 mm and –0.007±0.036 mm (Figure 3-10) for the 59km baseline (3032-3068).

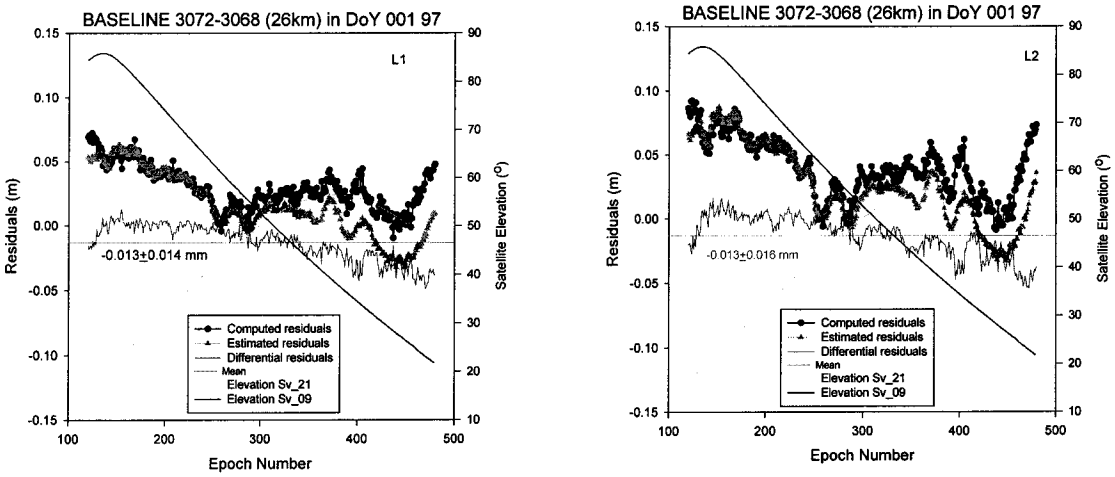

Figure 3-8. Difference between the computed and estimated residuals for station 3068. The left hand graph shows the L1 residuals, and the right hand graph shows the L2 residuals, for satellite pair 09_21. The baseline length (3072 to 3068) is approximately 26km, from the epoch number 120 to 480 (UTC 02^h:00^m~04^h:00^m + 0900), for day of year 001, 1997, Tokai, Japan.

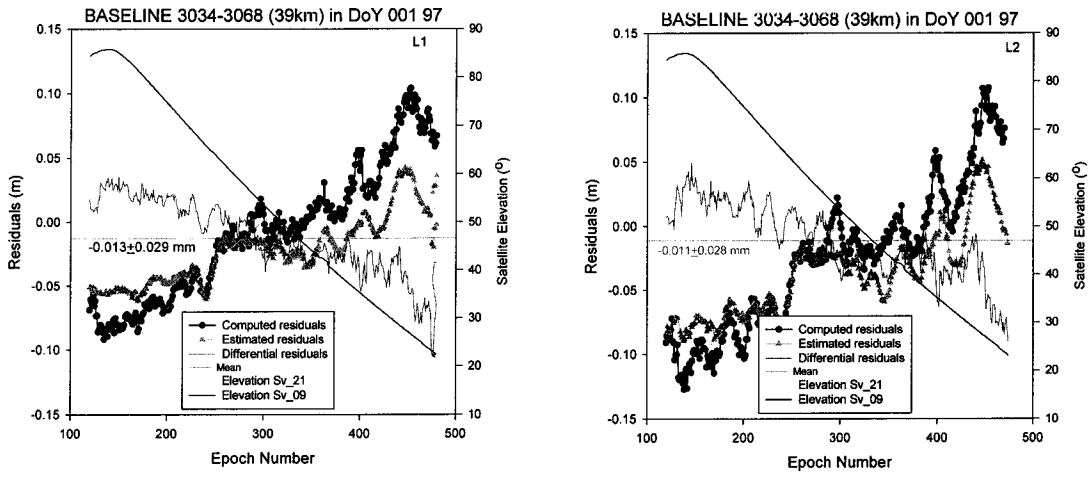

Figure 3-9. Difference between the computed and estimated residuals for station 3068. The left hand graph shows the L1 residuals, and right hand graph shows the L2 residual, for satellite pair 09_21. The baseline length (3034 to 3068) is approximately 39km, from the epoch number 120 to 480 (UTC 02^h:00^m~04^h:00^m + 0900), for day of year 001, 1997, Tokai, Japan.

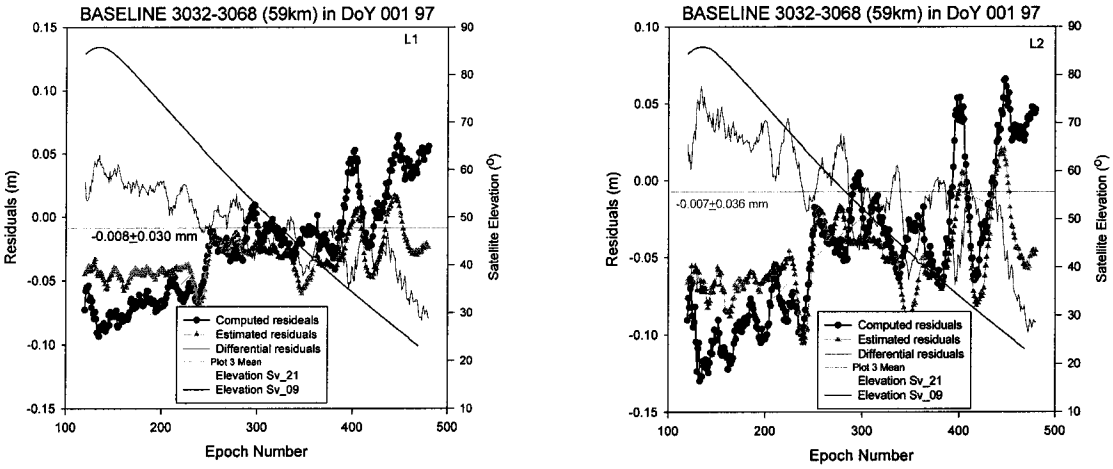

Figure 3-10. Difference between the computed and estimated residuals for station 3068. The left hand graph shows the L1 residuals, and right hand graph shows the L2 residual, for satellite pair 09_21. The baseline length (3032 to 3068) is approximately 59km, from the epoch number 120 to 480 (UTC 02^h:00^m~04^h:00^m + 0900), for day of year 001, 1997, Tokai, Japan.

Hence the accuracy of this positioning mode is related to the extent of coverage of the reference station network. Using the outer reference station network (3032-0264-3053, triangle sides 114km-93km-94km) to determine the user station coordinates is less effective than using the middle network (3034-3064-3080, triangle sides 55km-74km-74km), which itself is worse than using the inner network (3066-3072-5105, triangle sides 47km-42km-43km) (Table 3-5). Figures 3-8, 3-9 and 3-10 also show that the longer the baseline (i.e. greater the distance from the reference station), then the larger the residuals.

3.5.3 Number of reference stations and their positioning accuracy

In August 1999 an experiment was carried out involving the Geographical Survey Institute's (GSI) GEONET GPS receiver network around the city of Tsukuba, in Japan (Figure 3-11) to test the feasibility of using single-frequency GPS receivers (Canadian Marconi Company - CMC) side-by-side with dual-frequency Trimble 4000SSE GPS receivers. The objectives were to test the proposed method of integrated data processing, analyse the coordinate results obtained by this procedure, and establish a test network for future UNSW-GSI tests. Four temporary sites were set up as user stations in the Goka, Hojo, Niihari, and Yatabe districts of Tsukuba, equipped with both CMC and Trimble receivers and with antenna atop two closely spaced tripods. The tripods initially occupied by the CMC antennas are referred to GOKA, HOJO, NIIH, and YATA. The tripods initially occupied by Trimble antennas are referred to GOKT, HOJT, NIIT, and YATT. GEONET stations 93002, 93006, 93012, 960582, 960583, and 960584 were used as reference stations in the experiment.

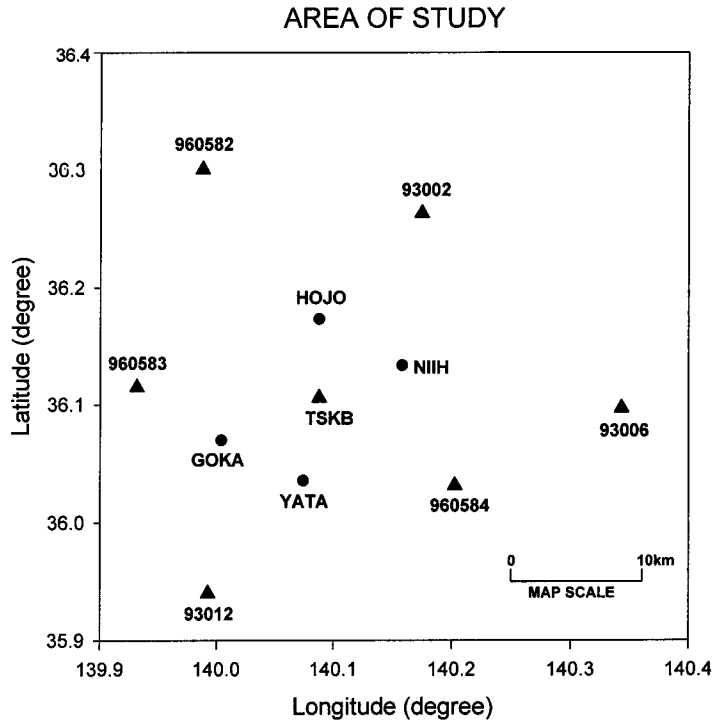

Figure 3-11. The UNSW-GSI test network around the city of Tsukuba, Japan.

The experiment consisted of two phases. First both the UNSW single-frequency receivers and the GSI dual-frequency receivers were operating continuously, side-by-side, for two days. Then the four test sites were divided into two groups, with two sites in each group. An antenna swap test was carried out in the first group (Niihari and Yatabe) (Figure 3-12), while antenna sharing was implemented in the second group (Goka and Hojo) (Figure 3-13). Data were collected for 8 hours each day over a three day period.

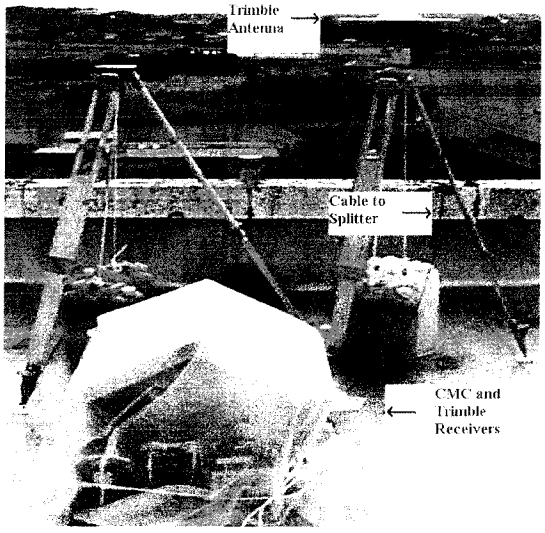

Figure 3-12. Antenna swap site.

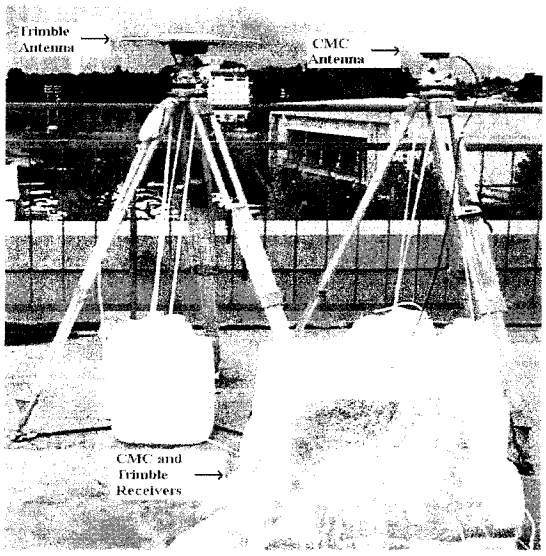

Figure 3-13. Antenna sharing site.

The "true" coordinate values for the four temporary sites were computed using data from the whole campaign (from DoY 214 to 224, 1999). The coordinate of the GEONET station 93012 was held fixed, and in all the following analyses the true values have been subtracted from the estimated latitude, longitude, height and length components (hence only the differences are shown). Comparisons have been made for both the long-session and hour-session solutions. ('Long-session' refers to the 24 and 8 hour data sets for phases 1 and 2, respectively.) In the hour-session processing there were 387 and 475 data files for the dual-frequency (Trimble) and single-frequency (CMC) receivers respectively. (The single-frequency receivers logged data during the weekend of 7-8 August, and therefore there are more single-frequency files.)

Four different types of reference station combination solutions were attempted, represented by the four different symbols in Figure 3-14. According to the statistical results (mean value and standard deviation), there are no significant differences in the four different reference station combinations that were tested. Table 3-6 shows the mean values and standard deviations of the hour-session results for the different reference station combinations. Comparing the mean values and standard deviations derived from the dual-frequency data with those of the single-frequency data (with 'corrections' generated by the reference station network), the horizontal components (latitude, longitude and length) are not significantly different. In the case of the height component, the variations in the single-frequency-with-correction results are larger. In general, single-frequency-with-correction processing can achieve accuracies better than 5mm in the horizontal components, and about 3cm in height.

There is no obvious difference in the offset values and standard deviations in the single-frequency hourly results using different combinations of reference stations (only 1~2mm difference). The horizontal components only have 2~3mm difference from the true values,

except at station HOJO and HOJT where the difference is 8mm. The height component has 2~3cm difference from the true value.

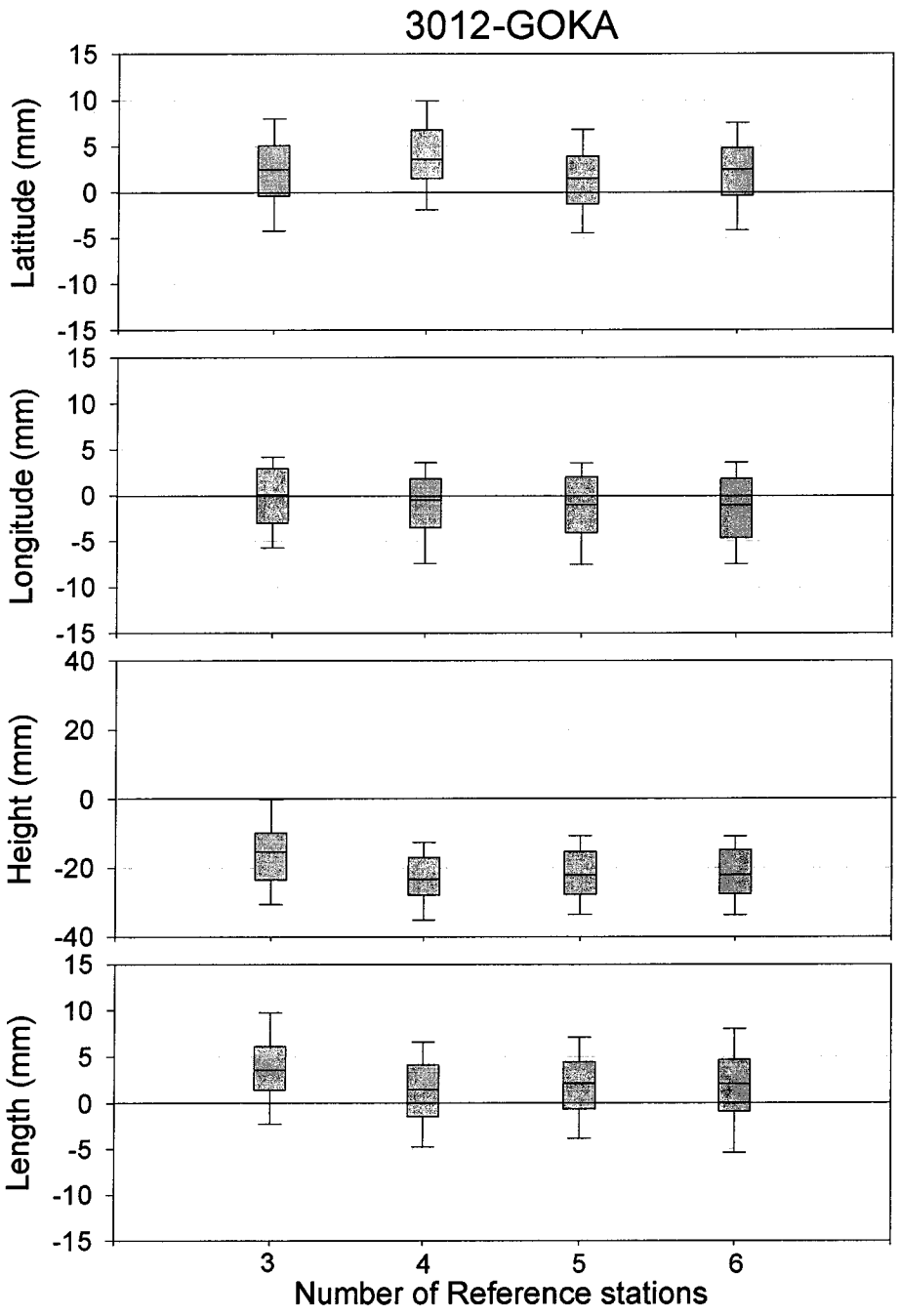

Figure 3-14. Single-frequency hourly results for station GOKA, using different combinations of reference stations to generate the 'corrections'.

Table 3-6. Comparing offsets and standard deviations for difference baselines using different reference station combinations (solutions have had the "true" coordinate values subtracted).

	3 Ref. Stations (3012-3006-0582)	4 Ref. Stations (3012-3006-3002-0583)	5 Ref. Stations (3012-3006-3002-0582-0583)	6 Ref. Stations (3012-0584-3006-3002-0582-0583)
3012-YATA (13km)	0.3±5.4 0.9±6.1 -13.1±12.4 0.8±5.7	-0.7±5.2 -0.9±5.9 -17.1±13.3 -1.0±5.2	-0.8±5.3 -1.0±5.9 -16.7±9.6 -1.2±5.3	-0.4±5.0 -0.0±5.6 -17.9±12.2 -0.3±5.2
3012-YATT (13km)	2.6±4.0 1.4±5.1 -17.3±11.2 2.9±4.2	2.0±5.6 -1.3±4.8 -22.4±11.2 0.8±5.7	1.1±5.9 -0.5±6.0 -23.1±12.2 0.6±5.6	1.1±5.4 0.3±5.4 -23.4±12.4 1.0±5.2
3012-GOKA (14km)	3.9±4.8 -0.1±4.5 -15.6±10.7 3.9±4.7	1.5±4.2 -1.2±4.5 -23.1±9.0 1.4±4.2	2.2±4.3 -1.2±4.3 -22.1±9.6 2.1±4.3	1.9±4.9 -1.9±4.4 -22.0±9.6 1.8±4.9
3012-GOKT (14km)	2.6±5.1 1.7±4.7 -6.8±9.1 2.7±5.1	1.5±4.0 1.4±4.3 -12.3±8.6 1.6±4.0	2.1±3.7 1.2±4.2 -12.9±8.2 2.2±4.1	2.0±3.7 1.4±4.0 -12.8±8.1 2.1±3.7
3012-NIIH (26km)	-1.3±5.0 1.1±5.4 9.9±15.8 -0.4±4.1	-2.5±5.3 -0.5±6.8 13.6±17.5 -2.3±5.4	-1.8±5.2 -0.7±6.0 13.3±17.7 -1.8±4.9	-1.3±5.1 -0.6±4.8 10.9±16.9 -1.4±4.5
3012-HOJO (27km)	-2.0±5.6 -6.0±5.8 -2.1±16.4 -3.8±5.0	-4.1±6.1 -8.2±5.9 -6.5±14.8 -6.4±5.5	-3.3±5.4 -8.4±5.9 -4.1±15.3 -5.7±5.1	-3.5±5.6 -7.4±6.1 -4.4±15.5 -5.7±5.4
3012-HOJT (27km)	-5.5±5.1 -4.0±6.3 14.5±14.1 -6.4±4.9	-7.2±4.5 -5.3±6.1 13.1±14.3 -8.4±4.3	-6.3±5.0 -5.6±5.7 12.7±15.1 -7.7±4.4	-6.0±5.3 -5.0±5.7 12.5±14.4 -7.2±4.8

Unit in mm

3.6 Experimental Results

3.6.1 Kinematic

In order to investigate further the performance of network-based techniques such as that described in this chapter, a set of data was processed in the single epoch (or instantaneous) on-the-fly ambiguity resolution (IOTF-AR) mode, with and without applying the 'correction' terms generated by a reference station network. The results are summarised in Table 3-7. The 2nd and 4th rows are the results of IOTF-AR (without applying the 'correction' terms) for the morning and afternoon sessions respectively. Similarly, the 3rd and 5th rows are the results obtained after applying the 'correction' terms for the morning and afternoon sessions respectively (Rizos et al., 1999).

Table 3-7. Kinematic experiment results, with and without the application of 'correction' terms generated by a network of reference stations.

Time (UT)	No.of epoch	Correction terms	Correct	Wrong	Reject
0:50-2:20	5273	Yes	5125(97.2%)	0(0.0%)	148(2.8%)
0:50-2:20	5273	No	5037(95.5%)	0(0.0%)	236(4.5%)
3:50-5:20	5314	Yes	5155(97.0%)	0(0.0%)	159(3.0%)
3:50-5:20	5314	No	5075(95.5%)	0(0.0%)	239(4.5%)

It can be clearly seen that a higher percentage of correct results can be achieved using the multiple reference station technique.

3.6.2 'Rapid static'

Results from the Kyushu GPS Network (DoY 271-272)

This experiment was designed to test the multiple baseline linear combination model (including Equations (3-21) and (3-25) simultaneously) and to analyse the effect of varying the observation session length for medium-range, 'rapid static' GPS positioning using single-frequency GPS receivers. Figure 3-15 displays one part of GSI's permanent GPS network in Kyushu, Japan.

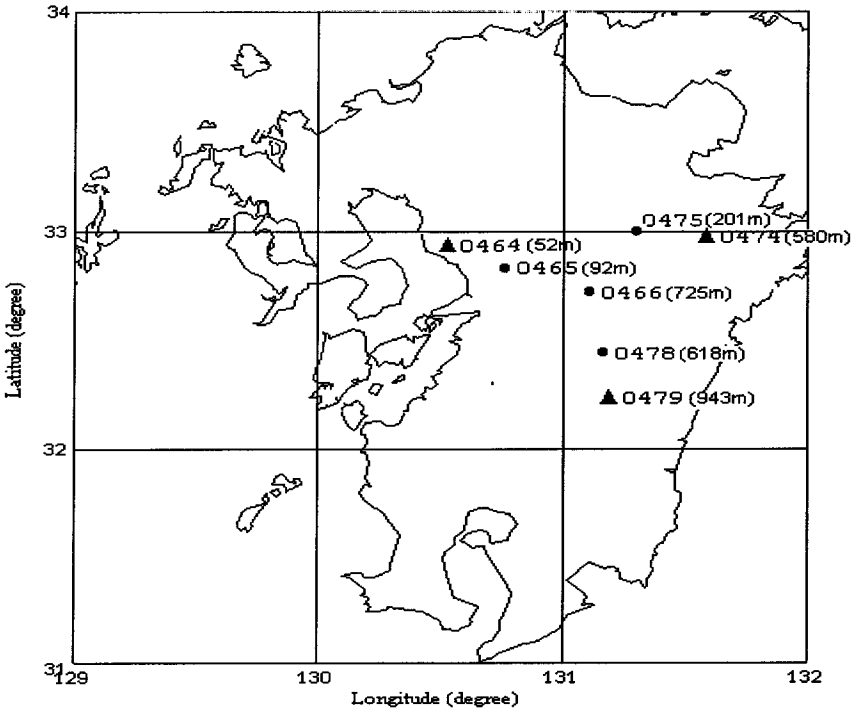

Figure 3-15. Some stations of GSI's Kyushu GEONET GPS network.

Seven stations were selected for tests, all equipped with dual-frequency GPS receivers. All baselines were first processed using the ionosphere-free observable from data over seven days. This result was then considered to be the "true" coordinates against which the results of a two day test period (DoY 271-272) were compared.

In step 1, three reference stations (0479, 0464 and 0474) were selected for the tests. Using the Bernese GPS software package and standard processing, the ambiguities were estimated and resolved to integer values, and the station coordinates were computed. Then the residual vectors were derived using a modified version of the Bernese software, for the two days of the experiment. In step 2, the coefficient values were computed using the station coordinates of the user (approximate values) and the reference stations. Therefore, through the application of Equations (3-21) and (3-25) the 'correction' terms for the L1 carrier phase observations associated with the user-reference station pair and between the various user stations were determined.

Figure 3-16 shows the result for a 77km baseline (between stations 0465-0479) with five different observation session lengths. There are 24 solutions for the 2hr observation sessions, 48 solutions for the 1hr observation sessions, 72 solutions for the 40min observation sessions, 96 solutions for the 30min observation sessions, and 144 solutions for the 20min observation sessions. The upper numbers on each plot are the mean discrepancies for each observation session length and the lower numbers denote the standard deviations of the discrepancies for each baseline component (top to bottom). The

latitude, longitude and baseline components are accurate to 5mm, and the height component accuracy is below the 2cm level.

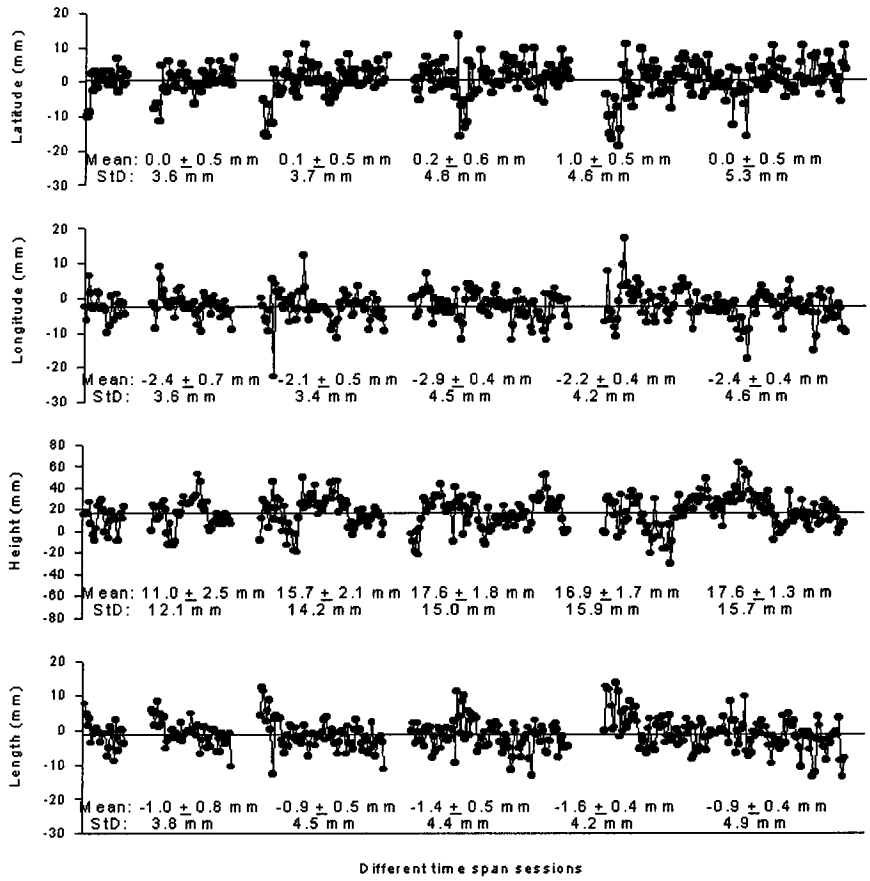

Figure 3-16. Results for five different observation spans: 2hr, 1hr, 40min, 30min and 20min, for a 77km baseline (stations 0465-0479), for DoY 271-272. The clusters along the x-axis represent the five different time spans, and the y-axis is in linear units of mm.

Figure 3-17 shows the mean discrepancies and standard deviations for different observation session spans with user-reference baselines 0478-0479 (23km), 0466-0479 (55km) 0465-0479 (77km) and 0466-0478 (32km). The mean value of a baseline represents the mean of all the single-frequency results for that session. It can be seen that the mean discrepancies in the latitude, longitude and baseline length components are less than 6mm, and the standard deviations in these components are less than 8mm. In contrast to these three components, the mean offset and standard deviation of the height component are at the 1-2cm level. As expected, for a particular baseline, the longer the observation session, the smaller the variations in the mean discrepancies and standard deviations.

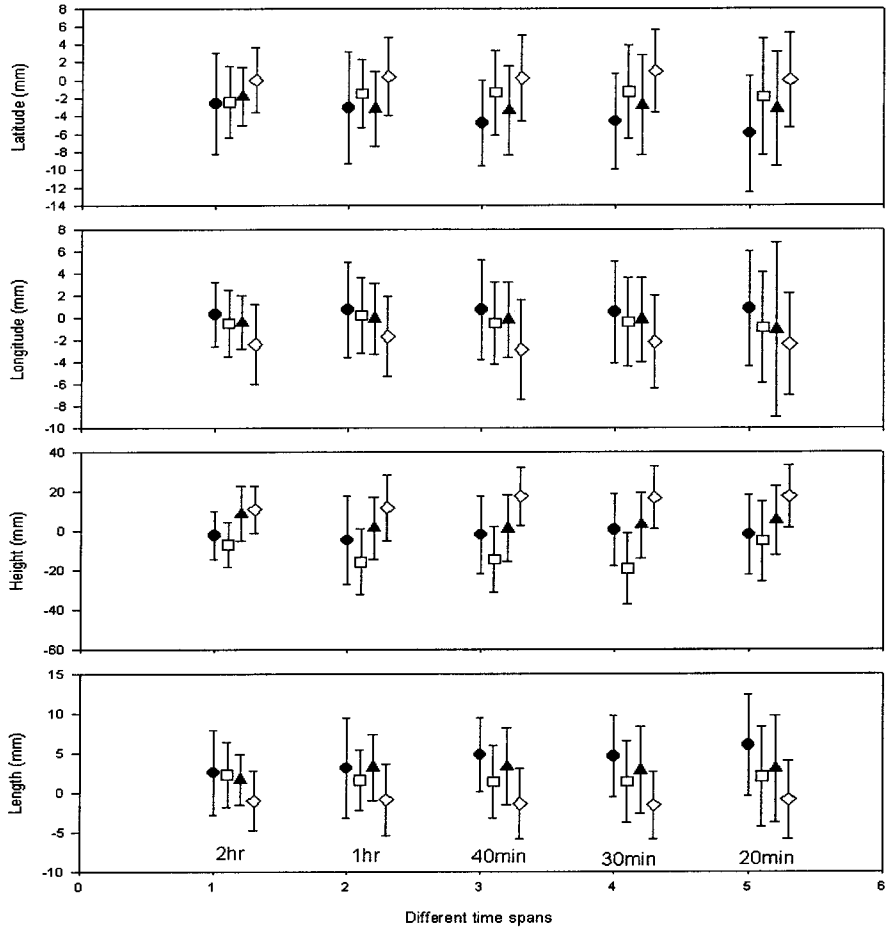

Figure 3-17. The mean discrepancies and standard deviations of discrepancies for different observation sessions lengths. The symbols, •, □, ▲, ◊ represent the different baselines considered: 0478-0479 (23km), 0466-0478 (32km), 0466-0479 (55km), 0465-0479 (77km).

Medium-range GPS 'rapid static' position results using single-frequency data, with observation span of 40 minutes, were derived from two days of continuous data. The 72 observations per baseline were determined and the differences from the "ground truth" values (derived using the ionosphere-free observables) are illustrated in Figure 3-18, for the latitude, longitude, height and baseline length components (from top to bottom). For each plot, the x-axis represents the session number (40 minutes for each session), and the y-axis is in linear units of mm. For each plot the four baselines are represented by white triangles (23km baseline, mean short dash line), solid circles (32km, mean: solid line), white squares (55km, mean: dotted line) and solid squares (77km, mean: long dash). To simplify the relative between the different baseline and their standard deviations, also present in box-and-whisker plot (Figure 3-19). The mean values and the standard deviation are listed in Table 3-8. It can be seen that the mean offsets in the latitude, longitude and baseline length components are less than 5mm, and the standard deviation of the variation in these three components are also less 5mm. In contrast, the mean offset and the standard deviation of the variation in the height component is at the 1-2cm level. The maximum bias

is less than 3cm in the latitude, longitude and baseline length components, and less than 5cm for the height component.

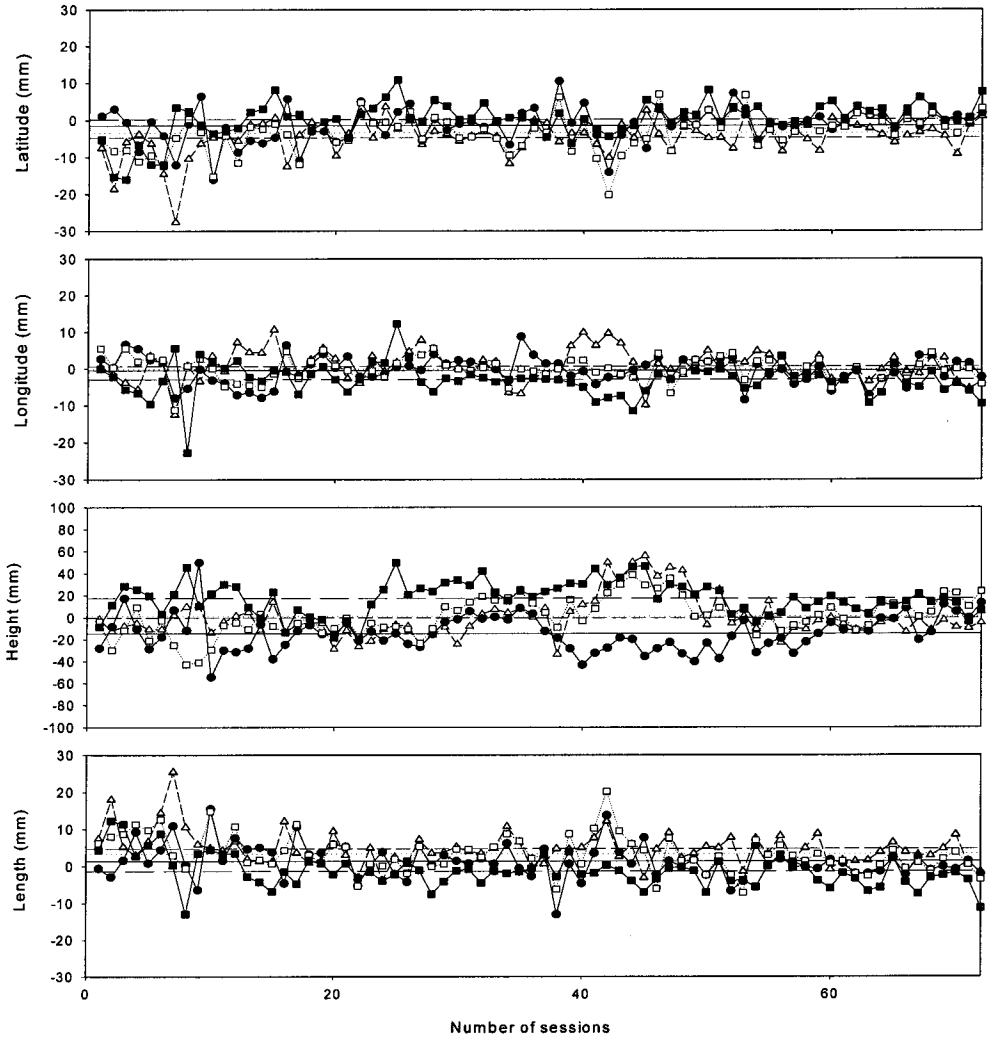

Figure 3-18. The 'rapid static' baseline solutions using the multiple reference station technique (top to bottom): latitude, longitude, height, baseline length) after subtracting from "true" coordinate values. The x-axis represents the session number (40 minute sessions) and the y-axis are in linear units of mm. For each plot the four baseline are represented by white triangles (23km baseline, mean short dash line), solid circles (32km, mean: solid line), white squares (55km, mean: dotted line), and solid squares (77km, mean: long dash).

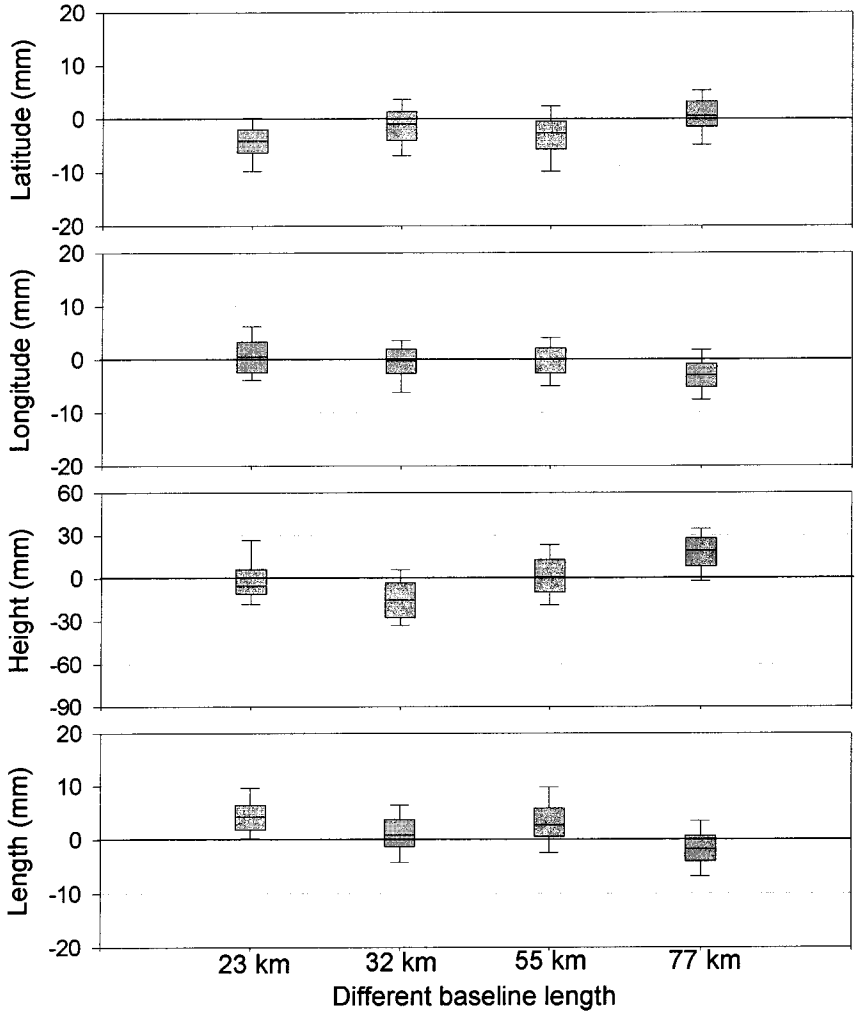

Figure 3-19. The 'rapid static' baseline solutions using the multiple reference station technique (top to bottom): latitude, longitude, height, baseline length) after subtracting from "true" coordinate values. The x-axis represents the different baseline length and the y-axis are in linear units of mm.

Table 3-8. The mean offsets (in mm) and standard deviation (in mm) for each session's (40min) results over two days, for the four baselines in the Kyushu GSI test network, processed using the multiple reference station technique.

Baseline / Comp.	0478-0479 (23km)		0466-0478 (32km)		0466-0479 (55km)		0465-0479 (77km)	
	Mean	StD	Mean	StD	Mean	StD	Mean	StD
Latitude	-4.8	4.8	-1.4	4.7	3.4	5.0	0.2	4.8
Longitude	0.7	4.5	-0.5	3.7	-0.2	3.4	-2.9	4.5
Height	-1.9	20.0	-14.6	16.6	1.3	16.9	17.6	15.0
Length	4.8	4.7	1.4	4.6	3.3	4.9	-1.4	4.4

The ambiguity resolution performance processing with and without 'corrections', and the baseline accuracy, have been compared. For the ambiguity resolution performance comparsion the data was split into 48 1-hour sessions and 72 40-minute sessions. The

number of successful ambiguity resolution sessions are listed in Table 3-9. The baseline results for all successful sessions (with correct ambiguity resolution) have also been derived. The difference in the latitude, longitude, height and baseline components relative to the "ground truth" values (derived using the ionosphere-free observables) are illustrated in Figure 3-20 (in a similar fashion to Figure 3-18). To simplify the relative between the different baseline and their standard deviations, also present in box-and-whisker plot (Figure 3-21). The mean values and the standard deviation of the variations are given in Table 3-10. It can be seen that the mean offsets in the latitude, longitude and baseline length components are at the 3-4cm level, and the standard deviation of the variation in these three components are at the 2-3cm level. The maximum bias is less than 10cm (in contrast to 3cm in the case with 'corrections') in the latitude, longitude and baseline length components, and less than 16cm (in contrast to 5cm in the case with 'corrections') for the height component. It can be concluded that the accuracy of the baseline vectors has been significantly improved, in addition to achieving a 100% success rate for ambiguity resolution, by applying the 'correction' terms generated by the multiple reference stations.

Table 3-9. The number of sessions with correct ambiguity resolution.

Time Span / Baseline	1-hour Session (48 in total)		40-minute Session (72 in total)	
	With correction	Without correction	With correction	Without correction
0478-0479(23km)	48	40	72	58
0466-0478(32km)	48	38	72	64
0466-0479(55km)	48	34	72	23
0465-0479(77km)	48	16	72	10

Table 3-10. The mean offsets (in mm) and standard deviation (in mm) of variations for each session's (40min) results (without 'corrections' applied, compare with Table 3-8).

Baseline / Comp.	0478-0479 (23km)		0466-0478 (32km)		0466-0479 (55km)		0465-0479 (77km)	
	Mean	StD	Mean	StD	Mean	StD	Mean	StD
Latitude	5.0	10.9	15.3	14.5	18.9	25.70	37.1	22.5
Longitude	-1.7	6.7	-3.7	7.6	-3.5	12.7	-15.4	18.0
Height	6.0	17.8	8.2	34.1	17.3	59.0	64.1	35.4
Length	-5.1	10.6	-15.6	14.8	-19.0	26.2	-38.7	24.9

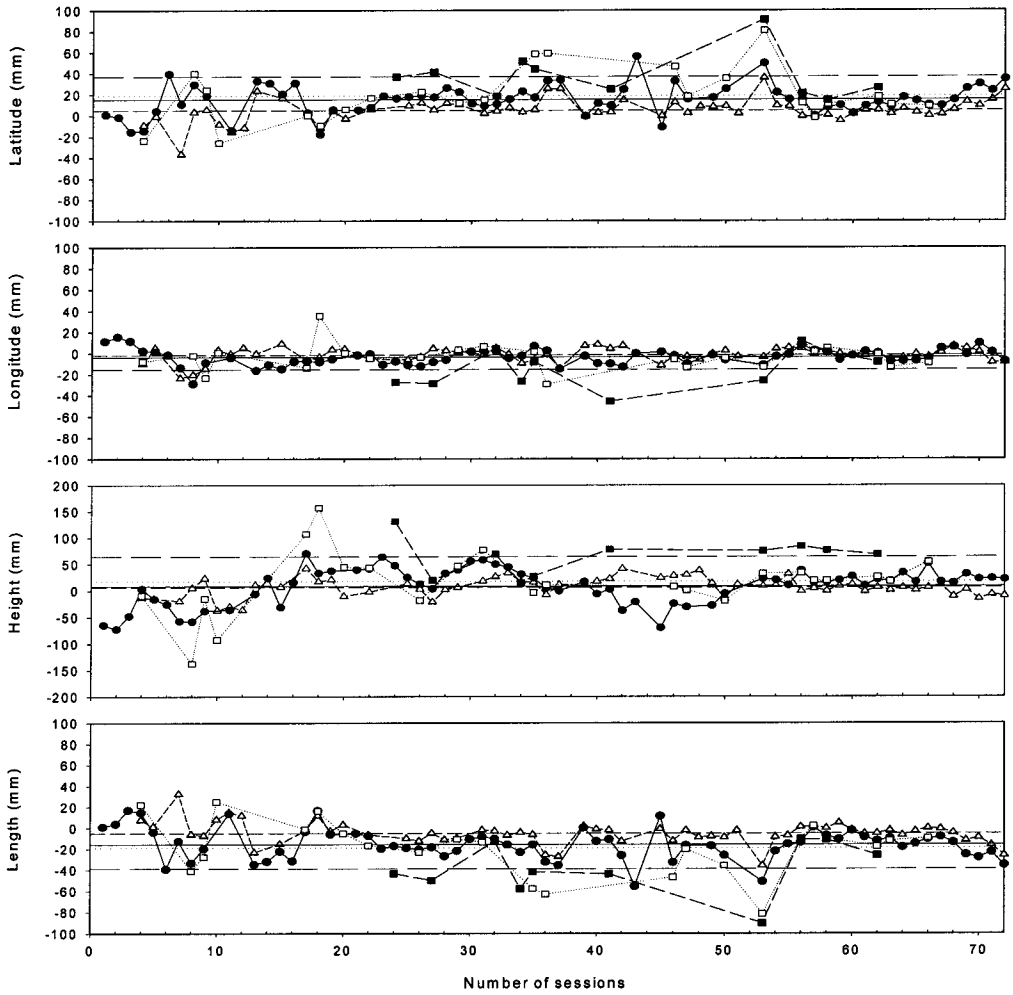

Figure 3-20. The conventional baseline solutions, i.e. without applying 'corrections' (top to bottom): latitude, longitude, height, baseline length) after subtraction of the "true" value. The x-axis represents the session number (40 minute sessions), and the y-axis are in linear units of mm. For each plot the four baseline are represented by white triangles (23km baseline, mean short dash line), solid circles (32km, mean: solid line), white squares (55km, mean: dotted line), and solid squares (77km, mean: long dash).

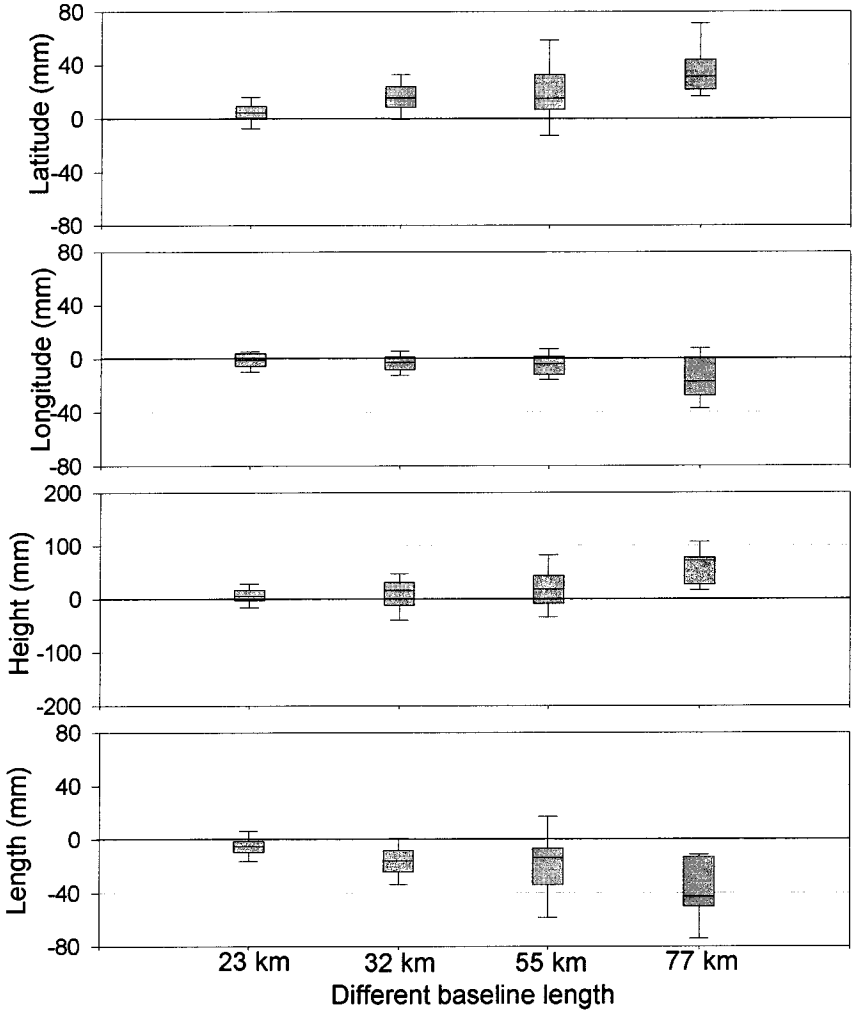

Figure 3-21. The conventional baseline solutions, i.e. without applying 'corrections' (top to bottom): latitude, longitude, height, baseline length) after subtraction of the "true" value. The x-axis represents the different baseline length, and the y-axis are in linear units of mm.

3.7 Concluding Remarks

Although multiple reference station techniques have been proposed and tested by several researchers, most of the applications that were investigated were limited to dual-frequency users or kinematic applications. This chapter has demonstrated the potential for a low-cost, single-frequency precise application based on the 'rapid static' mode of positioning. Some concluding comments can be made:

1. An extended functional model (Equation (3-25)) has been proposed and tested for cases where there are more than one user station (Chen et al., 1999). This functional model does not need the full set of observations from reference stations. Between the user stations precise position results can be obtained only using the approximate coordinates

of the user stations and the 'corrections' generated from the centralised processing reference station data.

2. Two types of correction weights have been analysed for different baselines (Figure 3-6). Using different α values computed in either the Gaussian plane coordinate system or the geocentric coordinate system, there is only a 2mm difference in offset variation due to the different sets of computed α values

3. The effect of different numbers of reference stations on position accuracy has been analysed (Table 3-6). There is no obvious difference in the offset values and standard deviations in the single-frequency hourly results using different combinations of reference stations (only 1~2mm difference).

4. A variety of data from GPS stations with different inter-station distances, geographical regions and seasons of the year were analysed in order to study the performance of the linear combination model for medium-range, 'rapid static' GPS positioning using single-frequency receivers. The positioning results appear to be stable and reliable. Hence it is feasible to achieve 1cm accuracy in the horizontal components, and 3-5cm accuracy in the height component under most conditions.

Chapter 4

ATMOSPHERIC BIAS PREDICTION FOR RESOLVING AMBIGUITIES BETWEEN REFERENCE STATIONS

4.1 Introductory Remarks

Regional-scale permanent GPS station network have been established to support many carrier phase-based positioning applications. As already discussed, various network-based techniques designed to support user applications (especially the real-time versions) use some form of 'correction meassges' generated by the reference station network. In such configurations the major challenge is the resolution of ambiguities during the continuous processing of reference station data. Due to the presence of distance-dependent biases such as ionospheric and tropospheric delays, the ambiguities are difficult to resolve instantaneously (i.e. with a single epoch of data) when the distance between the reference stations is many tens of kilometres.

In practice, the ambiguities among the reference stations can be correctly resolved during an initialization procedure, but the main challenge is to continuously resolve the new ambiguities that result when the tracked satellite experiences cycle slips, or after any long data gap, or when a new satellite rises. In this chapter a three-step methodology is proposed which can be implemented in real-time. Firstly, the high correlation of the atmospheric delay between adjacent epochs is used to assist cycle-slip recovery and ambiguity resolution. Then these atmospheric biases are predicted for double-differenced observations on an epoch-by-epoch and satellite-by-satellite basis. Finally these predicted atmospheric biases are applied to an algorithm that can fix the new ambiguities after a long data gap or when a new satellite rises.

Data from a set of reference stations spaced 80km apart were used to test the effectiveness of the algorithm. The results indicate that the proposed methodology can provide reliable integer ambiguities for reference stations spaced many tens of kilometres apart.

4.2 Aiding Ambiguity Resolution

4.2.1 General description

The receivers used in network-based applications fall into two categories; receivers deployed at the reference stations, or those employed by user. For high accuracy real-time, or near real-time, applications, the reference station network is required to generate and transmit the 'correction messages' continuously, and the user stations make use of this transmitted data to fix the integer ambiguities as quickly as possible. Hence, there are two major challenges: how to maintain *the operation of the reference station network,* and how to use the transmitted 'correction messages' *at the user stations* to support carrier phase-based positioning.

In the case of medium-range multiple reference station networks (defined here rather arbitrarily as those networks in which the inter-receiver separations are up to 100km), the ambiguity resolution process is affected by residual atmospheric biases. Therefore to reliably resolve the ambiguities, in real-time or near real-time, at the reference stations is a significant challenge. To successfully provide a real-time service it is necessary to rapidly (ideally instantaneously) fix the integer ambiguities. Li & Gao (1998) and Rabah & Leinen (1999) have proposed algorithms for resolving the ambiguities in the case of medium-range GPS baselines.

At the user stations, because the biases can be (to some extent) mitigated between the user and reference stations, then the task of resolving the ambiguities is easier. Wübbena et al. (1996), Han & Rizos (1997b) and Wanninger (1997) have investigated how user stations can use 'corrections' generated by a reference station network to assure reliable, high accuracy positioning.

Although the integer ambiguities with the multiple reference station network can be resolved at the beginning of their operation by using data collected over several hours, ambiguities have to be resolved again and again when any tracked satellite suffers from a cycle slip, or after the occurrence of a long data gap, or a new satellite rises.

The objectives of the research described in this chapter are:

1. Investigate the prediction of ionospheric and tropospheric delays for tracked satellites at the reference stations using previous measurements. After tracking of satellite is disrupted, the atmospheric delay could be predicted in order to aid in the resolution of the new integer ambiguities.

2. Investigate the prediction of tropospheric delay for a newly-risen satellite at the reference stations using an empirical model derived from data to other tracked satellites. This prediction of the tropospheric delay for a newly-risen satellite could aid the process of ambiguity resolution.

4.2.2 Correlations between prior information

The reference station integer ambiguities can be initialised during the network set up stage. If a cycle slip or data gap of up to a few minutes occurs, an "ambiguity recovery" technique can be used (Han 1997). However, after a long data gap or when a new satellite rises, new ambiguities have to be estimated, and the whole process is complicated due to the residual ionosphere delay and troposphere delay over medium-range baselines.

Ionospheric delay

According to Equations (3-26) and (3-28), the expression for the ionosphere delay is:

$$\Delta\nabla I = \left(\frac{f_2^2}{f_1^2 - f_2^2}\right)\left[(\Delta\nabla L_1 - \Delta\nabla N_1)\lambda_1\right] - \left(\frac{f_2^2}{f_1^2 - f_2^2}\right)\left[(\Delta\nabla L_2 - \Delta\nabla N_2)\lambda_2\right] \qquad (4\text{-}1)$$

where L_1, L_2: the carrier phase observations on the two frequencies,

f_1, f_2: the frequencies of L_1 and L_2 (f_1=1575.42MHz, f_2=1227.60MHz),

N_1, N_2: the integer ambiguities for L_1, L_2,

λ_1, λ_2: the corresponding wavelengths ($\lambda_1 \cong 19\text{cm}, \lambda_2 \cong 24\text{cm}$).

If the integer ambiguity can be resolved, the double-differenced ionospheric delay can be derived using Equation (4-1). Figure 4-1 displays the double-differenced ionospheric delay, as derived from Equation (4-1), for the satellite pair 24 and 04, on two successive days. The x-axis represents the epoch number (from epoch 136 to 240 (UTC $1^h{:}08^m{:}00^s$~$02^h{:}00^m{:}00^s$)). The left-hand side of the y-axis denotes the double-differenced ionospheric delay (units of mm), while the right-hand side shows the satellite elevations (in degrees). The elevation of satellite number 24 rises from 63° to 77 °, and in the case of satellite number 04 falls from 57° to 42°. During this observation period the maximum difference in the double-differenced ionospheric delay is only 3cm, on two successive days, for this high elevation satellite pair.

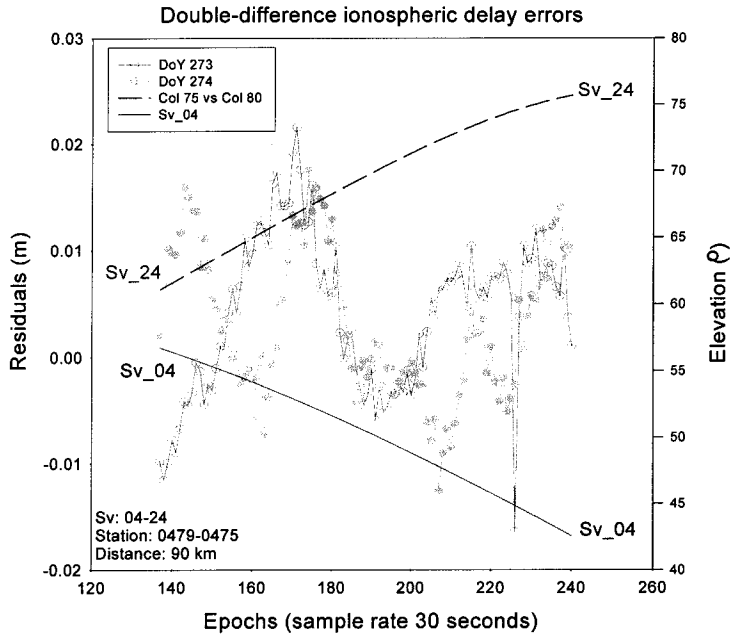

Figure 4-1. Double-differenced ionospheric delay for high elevation satellite pair (24 and 04), from epoch 136 to 240 (UTC 1^h:08^m:00^s~02^h:00^m:00^s + 0900), for DoY 273 and 274 (1997), observed at Kyushu, Japan.

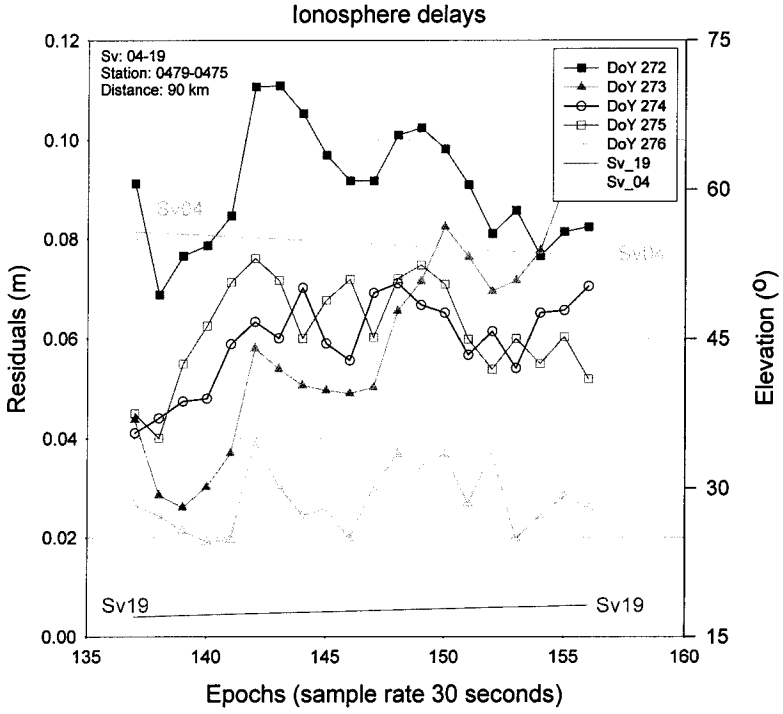

Figure 4-2. Double-differenced ionospheric delay on 5 successive days for a low elevation satellite pair (19 and 04), from epoch 137 to 156 (UTC 1^h:08^m:30^s~01^h:18^m:00^s + 0900), for DoY 272, 273, 274, 275 and 276 (1997), observed at Kyushu, Japan.

Figure 4-2 displays the double-differenced ionospheric delay, as derived from Equation (4-1) for the satellite pair 04 and 19, on five successive days. Satellite 19 is the rising satellite. As in Figure 4-1, the x-axis represents the epoch number. The left-hand side of the y-axis denotes the double-differenced ionospheric delay (units of mm) while the right-hand side shows the satellite elevation (in degrees). The elevation of satellite 19 rises from 17 ° to 18 °, and satellite 04 falls from 57 ° to 53 °. During this observation period the maximum difference in the double-differenced ionospheric delay is 7cm, for any two successive days, for this low elevation satellite pair.

Figure 4-3 shows the cross-correlation value for the low elevation satellite (newly rising satellite 19) of the double-differenced ionospheric delay value for 5 successive days at stations 0479-0475 (90km baseline), Kyushu, Japan with respect to satellite 04. There are 20 epochs (from epoch 137 to 157) during which the newly risen satellite in this cross-correlation test results in a normalised cross-correlation value of 0.78.

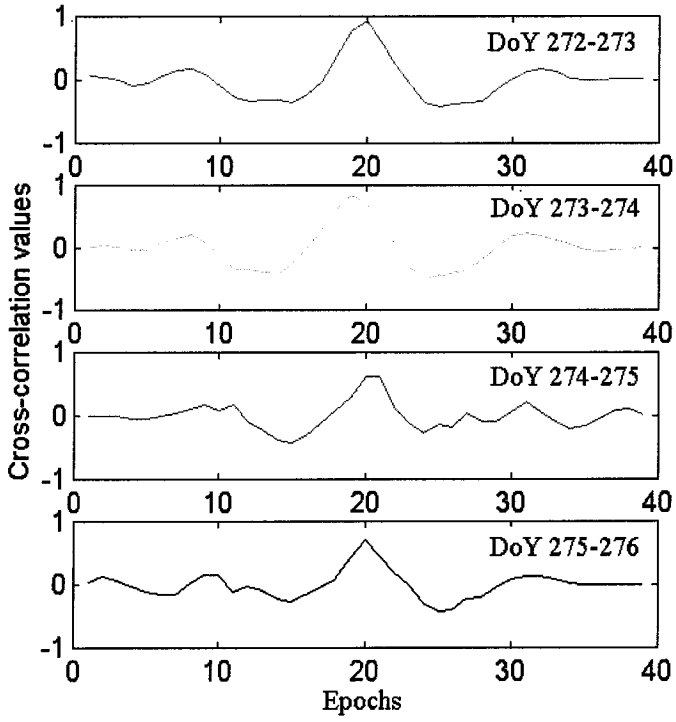

Figure 4-3. Cross-correlation value across 5 successive days (for a 90km baseline) for DoY 272, 273, 274, 275, 276 (1997), satellites 04 and 19, observed at Kyushu, Japan.

Tropospheric delay

The tropospheric delay also has some similarity between successive days, and the tropospheric delay of the currently tracked satellites could be estimated by (ignoring the multipath and observation error):

$$\Delta\nabla\mathrm{Trop} = \left(\frac{f_1^2}{f_1^2 - f_2^2}\right)\left((\Delta\nabla L_1 - \Delta\nabla N_1)\lambda_1\right) - \left(\frac{f_2^2}{f_1^2 - f_2^2}\right)(\Delta\nabla L_2 - \Delta\nabla N_2)\lambda_2 + \Delta\nabla\rho \qquad (4\text{-}2)$$

Figure 4-4 displays the double-differenced tropospheric delay on satellite pair 10 and 04 on successive days, using Equation (4-2). The x-axis represents the epoch number (from epoch 98 to 305). The left-hand side of y-axis denotes the double-differenced tropospheric delay (units of mm) and the right-hand side shows the satellite elevation (in degrees). Figure 4-5 shows the simplification of the residuals for the satellite number 04-10 at different day. The elevation of satellite 10 rose from 51° to 59 °, and satellite 04 fell from 58 ° to 26 °. During this observation period the maximum difference in the double-differenced tropospheric delay is only 7cm between two successive days, for this high elevation satellite pair.

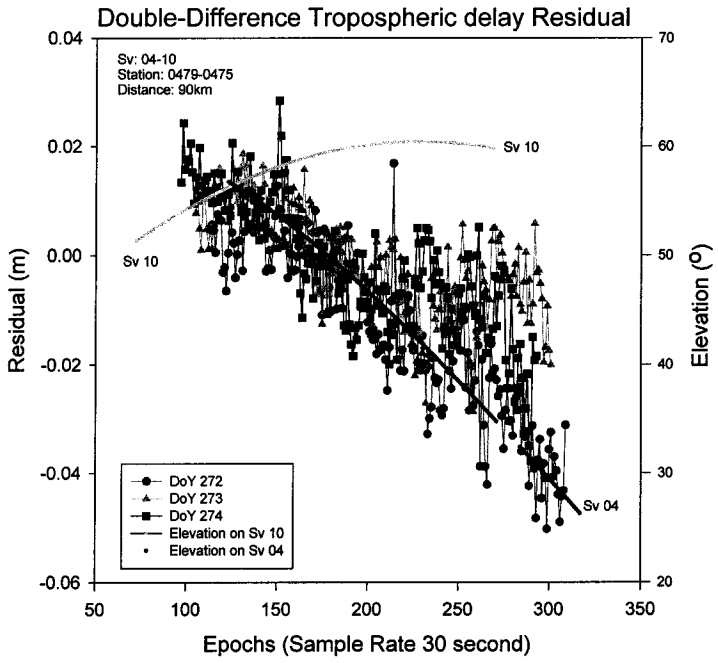

Figure 4-4. Double-differenced troposphere delay for a low satellite elevation pair (04 and 10), on 3 successive days, DoY 272, 273 and 274 (1997), observed at Kyushu, Japan.

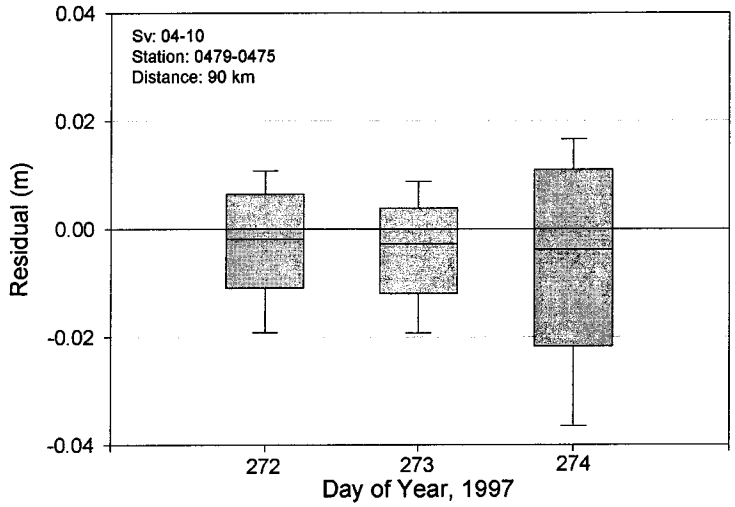

Figure 4-5. Using the box-and-whisker plot to represent the double-differenced troposphere delay for a low satellite elevation pair (04 and 10), on 3 successive days, DoY 272, 273 and 274 (1997), observed at Kyushu, Japan.

Figure 4-6 displays the double-differenced tropospheric delay, derived using Equation (4-2), for satellite pair 04 and 19, on five successive days. Satellite 19 is the rising satellite. As before, the x-axis represents the epoch number. The left-hand side of the y-axis denotes the double-differenced tropospheric delay (units of mm) and the right-hand side shows the satellite elevation (in degrees). Figure 4-7 shows the simplification of the residuals for the satellite number 04-19 at different day. The elevation of satellite 19 rises from 17 ° to 18 °, and satellite 04 falls from 57 ° to 53 °. During this observation period the maximum difference in the double-differenced tropospheric delay for this low elevation satellite pair is 8cm, for two successive days.

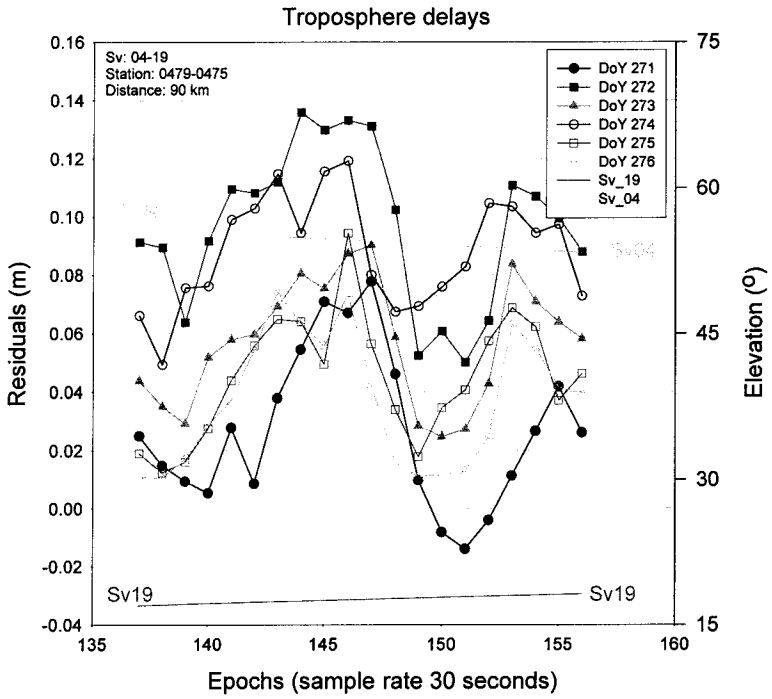

Figure 4-6. Double-differenced tropospheric delay in 6 successive days of a low elevation satellite pair (19-04), for DoY 271, 272, 273, 274, 275 and 276 (1997), observed at Kyushu, Japan.

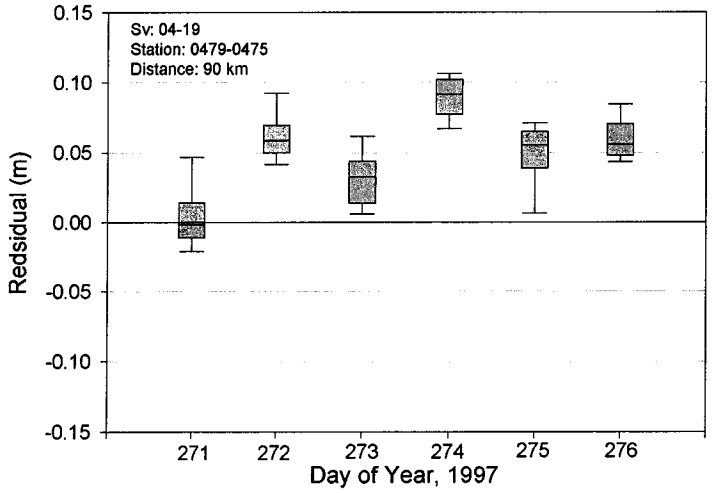

Figure 4-7. Using the box-and whisker plot to show the double-differenced tropospheric delay in 6 successive days of a low elevation satellite pair (19-04), for DoY 271, 272, 273, 274, 275 and 276 (1997), observed at Kyushu, Japan.

Figure 4-8 shows the tropospheric delay similarity and cross-correlation values of the double-differenced tropospheric delay on successive days (for a 90km baseline), for DoY 271, 272, 273, 274, 275, 276 (1997), observed at Kyushu, Japan. The normalised cross-correction values are at the 0.9 level.

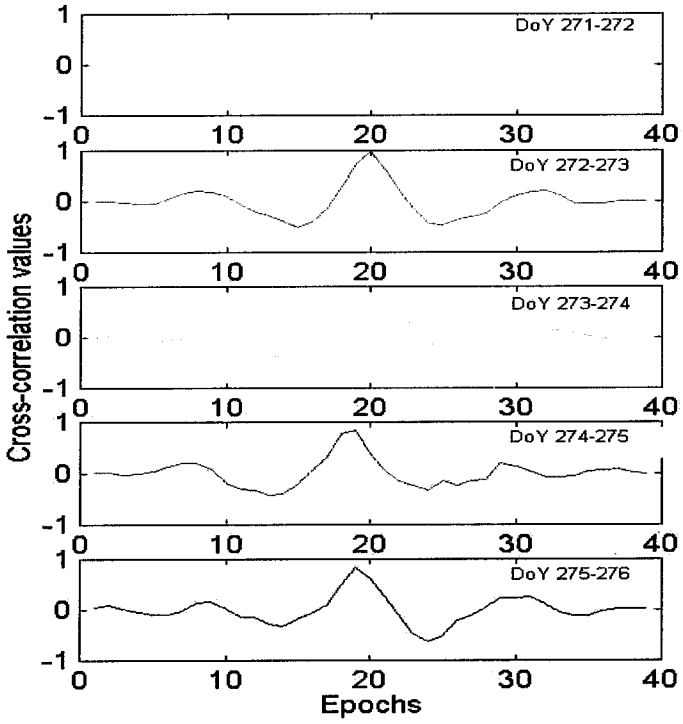

Figure 4-8. Cross-correlation value across 6 successive days (for a 90km baseline) for DoY 271, 272, 273, 274, 275, 276 (1997), satellites 04 and 19, observed at Kyushu, Japan.

It is evident that double-differenced ionospheric and tropospheric biases have a high correlation between successive days, as indicated by the results shown in Figures 4-2 and 4-6. Therefore, in the case of the rise of a new satellite, a linear polynomial function model between successive days and previous epochs can be determined, and a double-differenced ionospheric and tropospheric delay values for the new satellite can, in principle, be predicted.

4.2.3 Experimental results

An experiment was carried out to investigate the ability of the polynomial function model to predict the atmospheric delay when a new satellite rises, or after a long data gap occurs at any reference station. Figure 4-9 shows part of GSI's permanent GPS network in Kyushu, Japan. All stations host dual-frequency GPS receivers. All reference station coordinates have been computed using the ionosphere-free data combination, and the results are considered as 'ground truth' for comparison purposes.

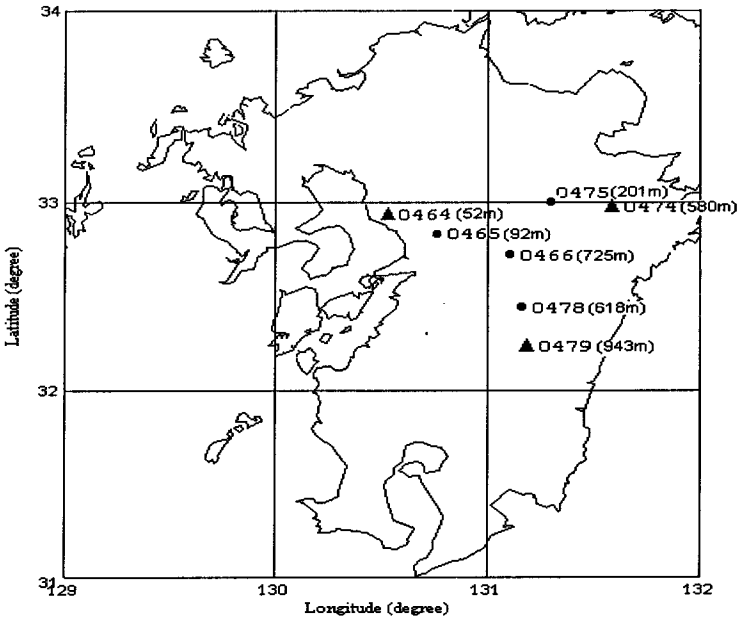

Figure 4-9. Stations of GSI's Kyushu GPS network, Japan, that were used in investigations.

Forty satellite-rising events occurred at stations 0479 and 0475 (90km baseline) on DoY 272, 1997. The similarity of the double-differenced ionospheric and tropospheric delays between successive days and previous data epochs was used in the ambiguity resolution process, in the manner outlined above. The results are shown in Figure 4-10. The x-axis is the (newly risen) satellite numbers, and the y-axis is the epoch number when correct ambiguity resolution was achieved. Applying the proposed polynomial model for ambiguity resolution, the estimation time can be reduced and the success rate can be increased most of the time (as indicated by the black colour, compared to not using any aiding information).

The ambiguity resolution success rate is 70% using the predicted atmospheric bias information from the previous day, and 50% if not used (Figure 4-10). In most cases the number of epochs required to fix the integer ambiguities was reduced, except satellite numbers 10, 15 and 31, for which the integer ambiguities could not be resolved. For satellite numbers 2, 9, 19, 21 and 27 the correct integer ambiguities could not be estimated at all.

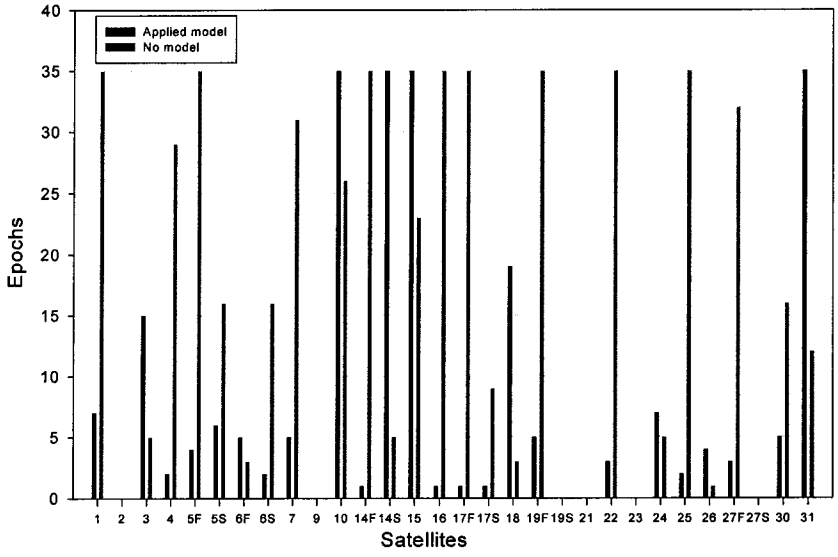

Figure 4-10. Number of epochs needed for ambiguity resolution for newly-risen satellites, on DoY 272 (1997), observed at Kyushu, Japan, with (in black) and without (in blue) predicted ionospheric and tropospheric delay models applied.

4.3 Estimating the Atmospheric Bias

4.3.1 Computing the atmospheric delay

Equations (4-1) and (4-2) can be rewritten as:

$$\Delta\nabla I = \left(\frac{f_2^2}{f_1^2 - f_2^2}\right)[(\Delta\nabla\phi_1 - \Delta\nabla\phi_2) - (\lambda_1\Delta\nabla n_1 - \lambda_2\Delta\nabla n_2) - (\varepsilon_{\Delta\nabla\phi_1} - \varepsilon_{\Delta\nabla\phi_2})] \tag{4-3}$$

$$\Delta\nabla T = \left(\frac{f_1^2}{f_1^2 - f_2^2}\right)\left[(\Delta\nabla\phi_1 - \lambda_1\Delta\nabla n_1 - \varepsilon_{\Delta\nabla\phi_1})\right] - \left(\frac{f_2^2}{f_1^2 - f_2^2}\right)\left[(\Delta\nabla\phi_2 - \lambda_2\Delta\nabla n_2 - \varepsilon_{\Delta\nabla\phi_2})\right] - (\Delta\nabla\rho + \Delta\nabla d\rho + \Delta\nabla M) \tag{4-4}$$

where ϕ_1, ϕ_2: the carrier phase observations on the two frequencies,

f_1, f_2: the frequencies of ϕ_1 and ϕ_2 (f_1=1575.42MHz, f_2=1227.60MHz),

n_1, n_2: the integer ambiguities for ϕ_1, ϕ_2,

λ_1, λ_2: the corresponding wavelengths ($\lambda_1 \cong 19\text{cm}, \lambda_2 \cong 24\text{cm}$),

$\Delta\nabla\rho$: the double-differenced geometric errors,

$\Delta\nabla d\rho$: the double-differenced orbit error, and

$\Delta\nabla M$: the double-differenced multipath error.

Equation (4-3) is not affected by station coordinate errors. As the ambiguities have been fixed, the ionospheric delay can be estimated on an epoch-by-epoch and satellite-by-satellite basis. The high correlation of the ionospheric delay between epochs can be used to assist cycle slip recovery and ambiguity resolution.

For the reference stations, the coordinates can be precisely estimated in the static mode. After careful selection of the reference stations, and using both hardware and software multipath error reduction techniques, multipath error can be assumed to have been reduced. Therefore the accuracy of the tropospheric delay is slightly limited by the station coordinate error, orbit error and multipath, as indicated in Equation (4-4).

Figures 4-11 and 4-12 show the ionospheric delay and tropospheric delay (after applying the standard tropospheric model) derived from Equations (4-3) and (4-4) respectively. Satellite 27 is a newly-risen satellite. The ionospheric delay value has more than 10cm change during the first 20 minutes, but the difference between consecutive epochs is less than 2cm. The variation of the tropospheric delay (Figure 4-12) is up to 1.5cm when satellite 27 is at a low elevation.

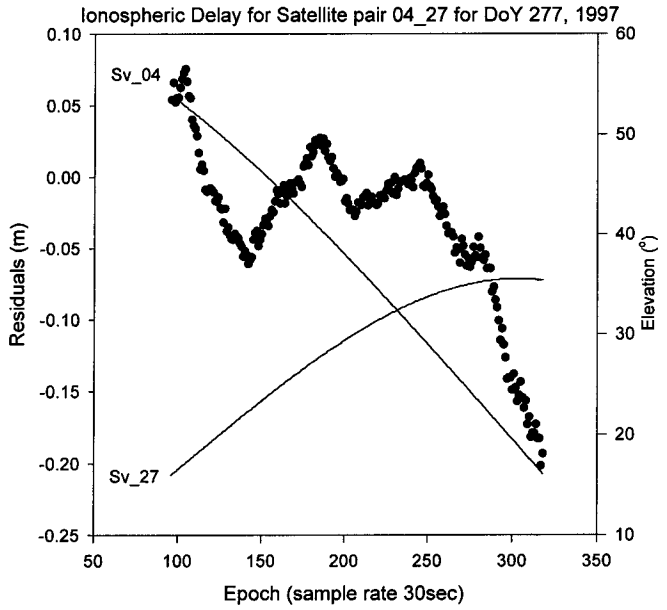

Figure 4-11. Double-differenced ionospheric delay for satellite pair 04 and 27, on DoY 277 (1997), observed in north Japan. The baseline length is 100km. The x-axis represents the epoch number (start at UTC: 00:47:00 and end at 02:38:30 + 0900). The left-hand y-axis denotes the double-differenced ionospheric delay values (in metres), and the right-hand side shows the satellite elevation (in degrees).

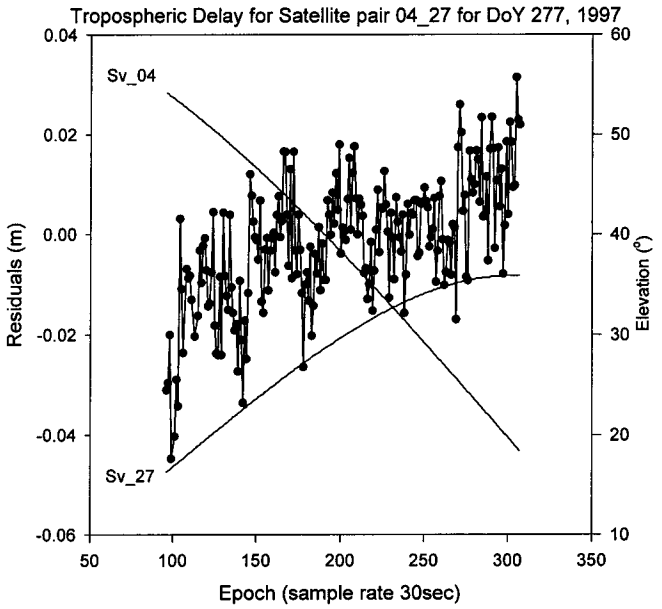

Figure 4-12. Double-differenced tropospheric delay on satellite pair 04 and 27, for DoY 277 (1997), observed in north Japan. The baseline length is 100km. The x-axis represents the epoch number (start at UTC: 00:47:00; end 02:38:30 + 0900). The left-hand y-axis denotes the double-differenced tonospheric delay values (in metres), and the right-hand side shows the satellite elevation (in degrees).

4.4 Ambiguity Resolution for Medium-Range Reference Station Network

For medium-range carrier phase ambiguity resolution, several algorithms have been proposed (for example, Han, 1997; Li & Gao, 1997; Rabah & Leinen, 1999; and Sun et al., 1999). The general characteristics of these algorithms is to form the linear data combinations of L1+L2 observations with comparatively long wavelength and low noise.

At the beginning of receiver station network operations, the integer ambiguities can be determined for the reference stations using known coordinates. Hence, the double-differenced ionospheric and tropospheric delays can be estimated and then used to assist ambiguity resolution for the next epoch, if necessary. The linear combinations commonly used for medium-range, carrier phase ambiguity resolution are the widelane, the L1 or the ionospheric-free linear combinations.

4.4.1 Widelane ambiguity resolution

The double-differenced widelane linear data combination can be written as:

$$\Delta\nabla\phi_{WL} = \frac{f_1}{f_1 - f_2}\Delta\nabla\phi_1 - \frac{f_2}{f_1 - f_2}\Delta\nabla\phi_2$$

$$= \Delta\nabla\rho + \Delta\nabla d\rho + \Delta\nabla T + \Delta\nabla M + \frac{f_1}{f_2}\Delta\nabla I + \frac{c}{f_1 - f_2}(\Delta\nabla n_1 - \Delta\nabla n_2) + \Delta\nabla\varepsilon_{\Delta\nabla\phi_{WL}} \quad (4\text{-}5)$$

where ϕ_1, ϕ_2: the carrier phase observations,

f_1, f_2: the frequencies of ϕ_1 and ϕ_2 (f_1=1575.42MHz, f_2=1227.60MHz),

n_1, n_2: the integer ambiguities for ϕ_1, ϕ_2,

λ_1, λ_2: the corresponding wavelengths ($\lambda_1 \cong 19\text{cm}, \lambda_2 \cong 24\text{cm}$),

$\Delta\nabla\rho$: the double-differenced geometric errors,

$\Delta\nabla d\rho$: the double-differenced orbit error,

$\Delta\nabla M$: the double-differenced multipath error,

c: the speed of light,

$\lambda_{WL} = \frac{c}{f_1 - f_2}$: widelane wavelength, 86.2cm, and

$\Delta\nabla n_{WL,FLOAT} = (\Delta\nabla n_1 - \Delta\nabla n_2)$: widelane integer ambiguity.

Hence

$$\Delta\nabla n_{WL,FLOAT} = \frac{1}{\lambda_{WL}}(\Delta\nabla\phi_{WL} - \Delta\nabla\rho - \Delta\nabla d\rho - \Delta\nabla T - \Delta\nabla M - \frac{f_1}{f_2}\Delta\nabla I - \Delta\nabla\varepsilon_{\Delta\nabla\phi_{WL}}) \quad (4\text{-}6)$$

Equation (4-6) can be used to resolve the widelane ambiguity. The geometric errors and multipath can be assumed to have been mitigated at reference stations (by careful selection station sites and the use of the IGS predicted orbit). Although the noise and ionospheric delay relative to L1 are up to 6 and 1.3 times respectively, the integer ambiguity can be fixed using the predicted atmospheric delay from previous data epochs and the long wavelength characteristics of this combination.

4.4.2 Ionosphere-free linear combination

The ionosphere-free linear data combination can be expressed as:

$$\Delta\nabla\phi_{IONO-FREE} = \frac{f_1^2}{f_1^2 - f_2^2}\Delta\nabla\phi_1 - \frac{f_2^2}{f_1^2 - f_2^2}\Delta\nabla\phi_2$$

$$= \Delta\nabla\rho + \Delta\nabla d\rho + \Delta\nabla T + \Delta\nabla M + \varepsilon_{\Delta\nabla\phi_{IONO-Free}} + \frac{f_1^2}{f_1^2 - f_2^2}\lambda_1\Delta\nabla n_1 - \frac{f_2^2}{f_1^2 - f_2^2}\lambda_2\Delta\nabla n_2 \quad (4\text{-}7)$$

The ionospheric refraction bias can be eliminated by constructing a ionosphere-free phase or pseudorange observable from the ϕ_1 and ϕ_2 data.

The last term in Equation (4-7) can be rewritten as:

$$\begin{aligned}\text{Bias}_{\text{IONO-FREE}} &= \frac{f_1^2}{f_1^2 - f_2^2}\lambda_1 \Delta\nabla n_1 - \frac{f_2^2}{f_1^2 - f_2^2}\lambda_2 \Delta\nabla n_2 \\ &= \frac{c \cdot f_2}{f_1^2 - f_2^2}\Delta\nabla n_{WL} + \frac{c}{f_1 + f_2}\Delta\nabla n_1 \\ &= \frac{f_2 \cdot \lambda_{NL}}{f_1 - f_2}\Delta\nabla n_{WL} + \lambda_{NL}\Delta\nabla n_1 \end{aligned} \quad (4\text{-}8)$$

Therefore, Equation (4-8) becomes:

$$\begin{aligned}\Delta\nabla n_{1,\text{FLOAT}} = \frac{1}{\lambda_{NL}}(\Delta\nabla\phi_{\text{IONO-FREE}} - \Delta\nabla\rho - \Delta\nabla d\rho - \Delta\nabla T - \Delta\nabla M - \Delta\nabla\varepsilon_{\Delta\nabla\phi_{\text{IONO-FREE}}}) \\ - \frac{f_2}{f_1 - f_2}\Delta\nabla n_{WL}\end{aligned} \quad (4\text{-}9)$$

In Equation (4-9), the last term on the right-hand side is the widelane ambiguity. If the widelane ambiguity can be resolved to its integer value, in subsequent processing the wavelength $\lambda_{\text{IONO-FREE}}$ is only 10.7cm.

Due to the fact that geometric errors and multipath can be mitigated at the reference stations, the most significant error in the determination of the $\Delta\nabla n_1$ ambiguity is the double-differenced tropospheric delay that remains after applying the standard tropospheric model.

4.4.3 Real-time precise ionospheric determination

To use Equations (4-6) and (4-9) for real-time ambiguity resolution, the main task is to predict the ionospheric delay as precisely as possible because the widelane ionospheric delay effect is 1.3 times that of the L1 observations. If the ionospheric delay has more than 2 cycle biases in L1 wavelength for newly risen satellites, or after long data gaps, the widelane ambiguity resolution will fail, even though the coordinate of the reference stations are known. There are two options for estimating the correct widelane ambiguities. One option is to predict the ionospheric delay as precisely as possible (see, for example, Schaer et al., 1998, 1999; Hernández-Pajares et al., 1998, 1999, Colombo et al., 1999), or to form an ionosphere-free linear combination to eliminate the effect of ionospheric delay (when the accuracy of the pseudorange observations is better than 30cm.)

Predicting the ionospheric delay

For local or regional-scale precise ionospheric determination, utilisation of an ionospheric delay model has been shown to increase the success rate of the widelane ambiguity resolution (Wild, 1993; Hernández-Pajares et al., 1999). As the ionosphere is at the upper part of the atmosphere (approximately between 70 to 1000 kilometres above the Earth), the

signal propagation is mainly affected by free charged particles (Rotacher et al., 1996). The ionosphere can be modelled as a single-thin layer at 350 to 400 kilometre height (Schaer et al., 1995, 1996), or in two layers with boundaries at 60-740-1420 kilometres (Hernández-Pajares et al., 1998).

Hernández-Pajares et al. (1999) and Colombo et al. (1999) have proposed a two layer ionosphere model, and demonstrated the feasibility of predicting ionospheric delay for real-time ambiguity resolution at reference stations. They have suggested that a tomographic model of a two layer ionosphere model can provide sufficient accuracy (better than 10 centimetres) in the double-difference of the STEC (Slant Total Electron Content), and hence allow for successful on-the-fly widelane ambiguity resolution. Figure 4-13 shows the result from Hernández-Pajares et al. (1999).

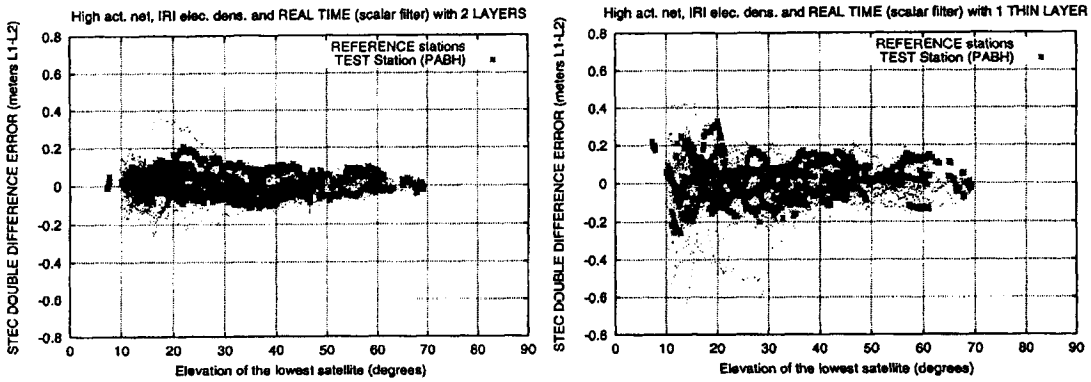

Figure 4-13. Errors (metres of L1-L2 delay) in the double-differenced Slant Total Electron Content (STEC), using the two layer model (left-hand graph) and the single thin layer model (right-hand graph) on 3 May 1998, for the USA. The bias and RMS values are 0.01m and 0.06m, and 0.02m and 0.09m, for the two layer and single layer model respectively.

Ionosphere-free linear combination (applying the pseudorange observables)

According to Equations (3-26)~(3-29), the carrier phase combination (i, j) can be written as (Rizos, 1996):

$$\nabla\Delta\phi_{i,j} = i\nabla\Delta\phi_1 + j\nabla\Delta\phi_2 \tag{4-10}$$

where i and j are integer constants.

The integer ambiguity is:

$$\nabla\Delta n_{i,j} = i\nabla\Delta n_1 + j\nabla\Delta n_2 \tag{4-11}$$

The effective wavelength is:

$$\lambda_{i,j} = c/(if_1 + jf_2) \tag{4-12}$$

where c is the speed of light.

The geometry-free and ionosphere-free combination of pseudorange observations can be generated (Equations (3-27) & (3-29)). The geometry-free observable is:

$$\nabla\Delta I = \frac{f_2^2}{f_1^2 - f_2^2}(\nabla\Delta P_1 - \nabla\Delta P_2) \tag{4-13}$$

The ionosphere-free observable is (ignoring the orbit bias, tropospheris delay, and multipath):

$$\nabla\Delta\rho = \frac{f_1^2\nabla\Delta P_1 - f_2^2\nabla\Delta P_2}{f_1^2 - f_2^2} \tag{4-14}$$

Equation (4-10) can be expressed as:

$$\nabla\Delta\phi_{i,j} = i\nabla\Delta\phi_1 + j\nabla\Delta\phi_2 = \frac{1}{\lambda_{i,j}}\cdot\nabla\Delta\rho - \left(\frac{i}{\lambda_1} + \frac{j}{\lambda_2}\cdot\frac{f_1^2}{f_2^2}\right)\cdot\nabla\Delta I + \nabla\Delta n_{i,j} \tag{4-15}$$

Substituting Equations (4-13) and (4-14) into (4-15), then the ambiguity term can be represented as:

$$\nabla\Delta n_{i,j} = \nabla\Delta\phi_{i,j} + c_1\cdot\nabla\Delta P_1 + c_2\cdot\nabla\Delta P_2 \tag{4-16}$$

where

$$c_1 = -\left(i\cdot\frac{f_1^2 + f_2^2}{f_1^2 - f_2^2} + j\cdot\frac{2f_1f_2}{f_1^2 - f_2^2}\right)\frac{1}{\lambda_1} \tag{4-17}$$

$$c_2 = -\left(i\cdot\frac{2f_1f_2}{f_1^2 - f_2^2} + j\cdot\frac{f_1^2 + f_2^2}{f_1^2 - f_2^2}\right)\frac{1}{\lambda_2} \tag{4-18}$$

The standard deviation of the computed ambiguities is (Equation (4-16)):

$$m_{\nabla\Delta n_{i,j}} = \sqrt{i^2\cdot m_{\nabla\Delta\phi_1}^2 + j^2\cdot m_{\nabla\Delta\phi_2}^2 + c_1^2\cdot m_{\nabla\Delta P_1}^2 + c_2^2\cdot m_{\nabla\Delta P_2}^2} \tag{4-19}$$

Assuming that $m_{\nabla\Delta\phi_1} = m_{\nabla\Delta\phi_2} = 0.01$ cycle, and $m_{\nabla\Delta P_1} = m_{\nabla\Delta P_2} = 0.30$ metre, then for the widelane linear combination, i = 1, j = -1, the effective wavelength is 0.862m and its standard deviation is 0.248m (Han & Rizos, 1996b).

Hence, using the known coordinates of the reference stations and accumulating the widelane observables to decrease the standard deviation (Equation (4-19)), ambiguity resolution for newly-risen satellites can be easily performed.

4.5 Estimating the Relative Tropospheric Zenith Delay

Zhang (1999) discussed the estimation of the residual tropospheric delay for a rising satellite, using a network of reference stations. Schaer et al. (1999) claimed that the model of tropospheric refraction using one zenith path delay parameter per hour, and the corrections from the linear models of tropospheric zenith delay, can be generated at reference stations at time intervals of 30 minutes, as a function of latitute, longitude and height of user stations. Hence, the prediction of tropospheric zenith delay at the reference stations, using a few epochs of tropospheric delay information (derived from Equation (4-4) or (4-9)), can not only mitigate the observation noise but also increases the accuracy of the tropospheric zenith delay prediction.

After fixing the integer ambiguities, the tropospheric delay can be estimated using the ionosphere-free linear data combination (Equation (4-9)). The double-differenced tropospheric delay $\Delta\nabla T$ can be written as (Zhang, 1999):

$$\Delta\nabla T \cong (T_{az} - T_{bz})[MF(\varepsilon^x) - MF(\varepsilon^y)] \qquad (4\text{-}20)$$

where T_{az}, T_{bz}: the tropospheric zenith delays at receiver a and b,

$RTZD = (T_{az} - T_{bz})$: the relative tropospheric zenith delay,

MF: the mapping function, and

$\varepsilon^x, \varepsilon^y$: the average elevation angles at the receivers a and b for satellites x and y respectively.

Before the estimation of the tropospheric zenith delay model, the tropospheric delay has been computed because the integer ambiguities can be fixed in Equation (4-9).

Figures 4-14 and 4-15 display 7 days of tropospheric delay with different satellite elevation pairs for the period DoY 271-277 (1997), observed in northern Japan, for a baseline length of 100km. The right-hand side of the graphs displays the relative offset and variation of the tropospheric delays. In order to display the behaviour of the tropospheric delay (after

applying the standard troposphere model) for the high elevation satellite pair and newly-risen satellites pair (cut off angle 15°), the testing epoch number is chosen as 20 epochs (i.e. 10 minutes for 30second sample rate) for specific satellite pair. For the high elevation pair (Figure 4-14) the variation is 4.2mm, but is 11.7mm for the low elevation pair (Figure 4-15).

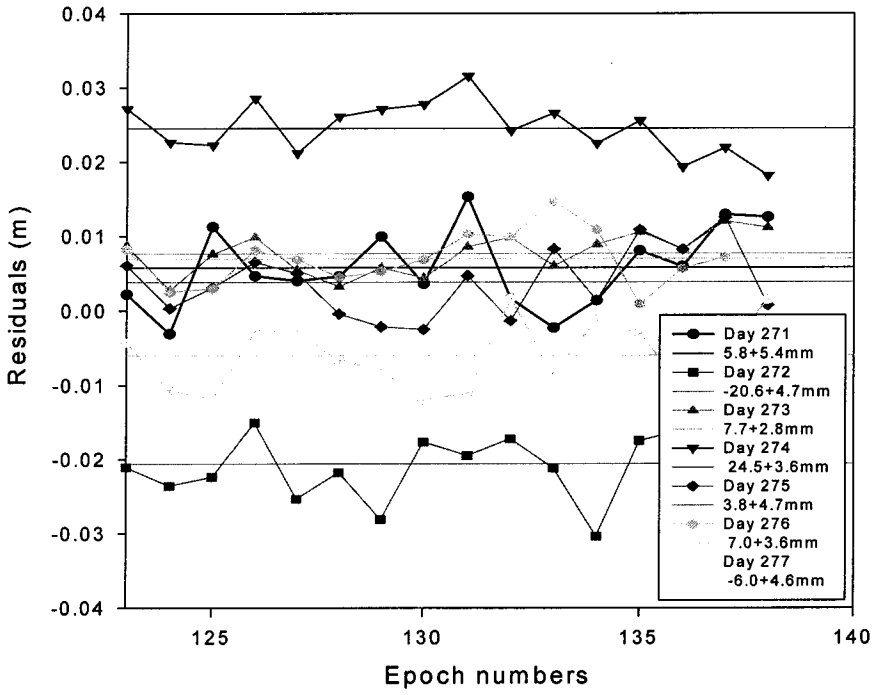

Figure 4-14. Double-differenced tropospheric delay for a high elevation satellite pair 04 and 10 (elevations 57° and 51°). All data sets are referred to DoY 271 (1997). For the high elevation satellite pair, the tropospheric delay variation is only 4.2mm in these 7 testing days.

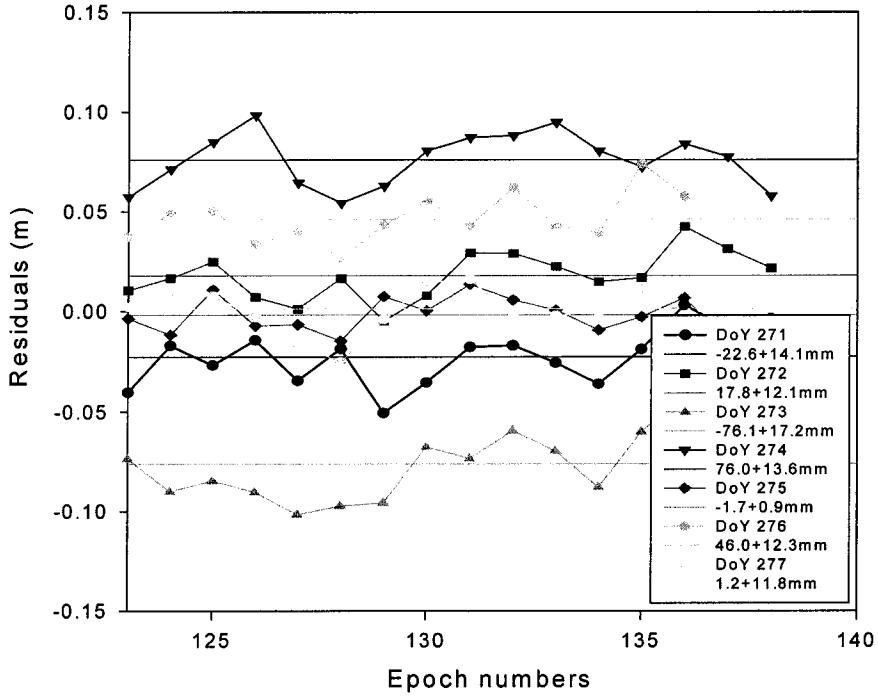

Figure 4-15. Double-differenced tropospheric delay for low elevation satellite pair 04 and 19 (elevations are 57° and 16°). All data sets are referred to DoY 271. For the low elevation satellite pair, the tropospheric delay variation reaches 11.7mm in these 7 testing days.

Applying Equation (4-20) to predict the tropospheric delay for a newly-risen satellite (05), the difference between the predicted and computed value is 2.2cm (Figure 4-16), which is approximately a 0.2 cycle bias in the narrowlane ambiguity.

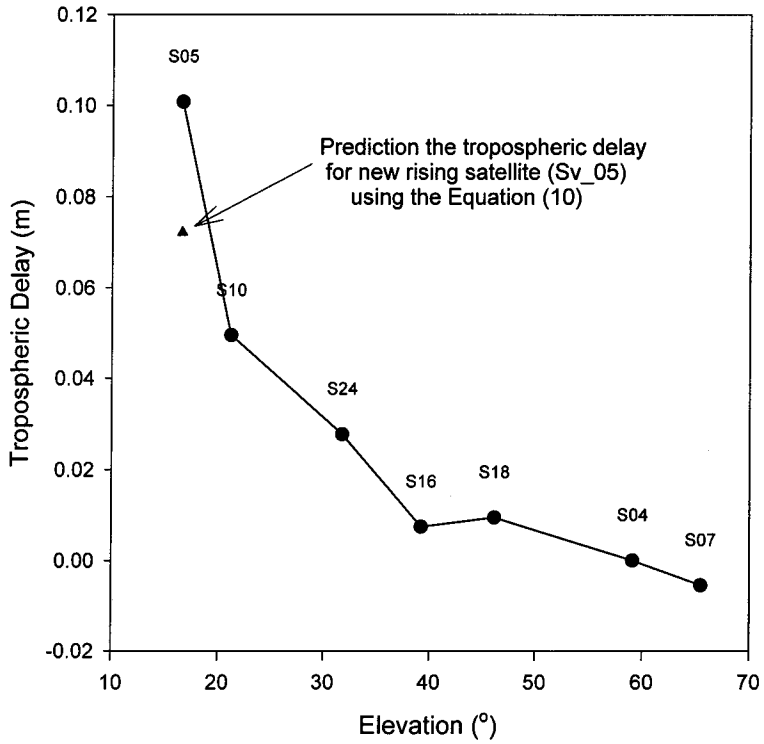

Figure 4-16. The predicted and computed tropospheric delay value at time 23:14:39 UTC (DoY 271, 1997, northern Japan, baseline length 100km), using Equation (4-20).

4.5.1 Summarising the procedure for data processing

The proposed data processing procedure can be divided into four steps, as indicated in Figure 4-17:

1. At the beginning of the network operation, the coordinates and the ambiguities need to be determined for the reference stations.

2. After resolving the ambiguities for the reference stations, the ionospheric and tropospheric delays can be estimated using Equations (4-3) and (4-4). Although the RTZD (Relative Tropospheric Zenith Delay) can be computed at every epoch in Step 1, the variation in RTZD value still can be up to a few centimetres because of the observation noise and tropospheric delay residuals. It is therefore recommanded that the RTZD values be computed every 5minutes.

3. For the next epoch, the observations can be corrected for the ionospheric and tropospheric delay values estimated from the previous epoch. This helps resolve the current ambiguities using the ionosphere-free linear data combination (first fixing the widelane integer ambiguity, then the L1 integer ambiguity). If there is a long data gap, or a new satellite has risen, the tropospheric delay can be predicted from the RTZD

value. At the reference stations, although the coordinates are known, the orbit error will only slightly affect ambiguity resolution (when the predicted IGS orbit is used). The multipath error can be reduced by various hardware and software techniques. Therefore the main error source in Equation (4-9) is the tropospheric delay.

4. Using the ionosphere-free linear data combination, after fixing the widelane integer ambiguities, try to resolve the L1 integer ambiguities. However, the effective wavelength of L1 is only 10.7cm, and the observation noise combined with the tropospheric delay do have a large variation (Figures 4-15 and 4-16), hence accumulating the observations to low elevation satellites is necessary.

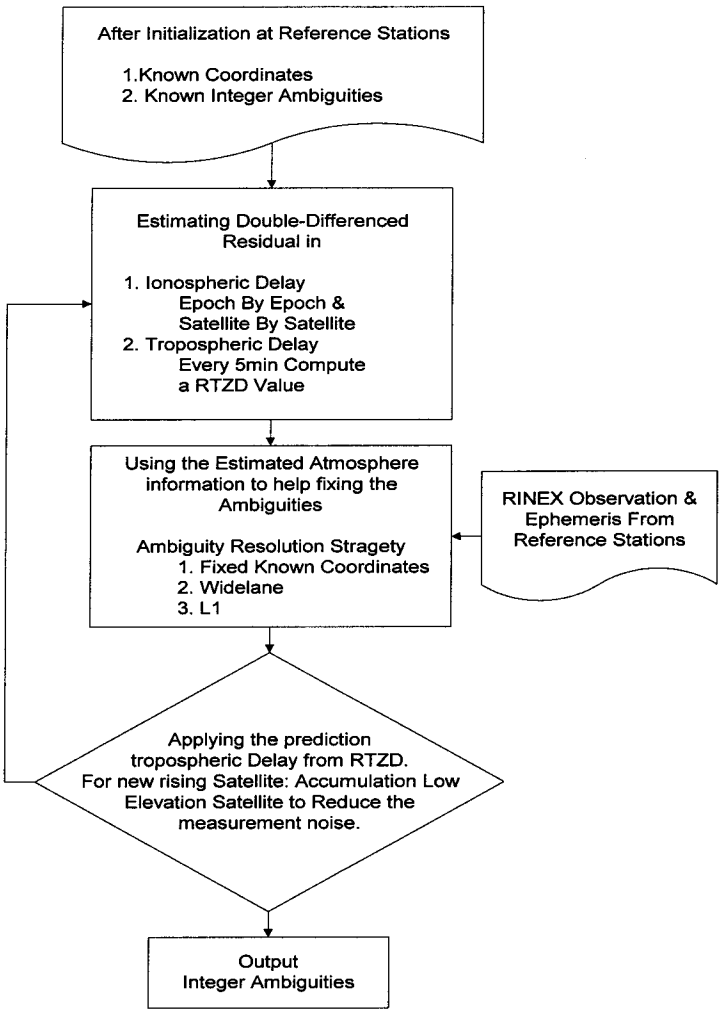

Figure 4-17. Flow chart for the proposed data processing steps in a medium-range reference station network.

4.5.2 Predicting tropospheric delay to aid ambiguity

The challenge is to estimate the tropospheric delay for a satellite from the tracking of other satellites, and to determine a relative tropospheric zenith delay model, in order to help

resolve the integer ambiguities for a newly-risen satellite or after a long data gap. Two different experimental results will be discussed. For a newly-risen satellite, testing for correct ambiguity resolution will concentrate on the first few data epochs. After a long data gap, testing for correct ambiguity resolution will involve the whole tracking period.

Data were collected from one part of the Geographical Survey Institute's (GSI) permanent GPS network in Kyushu, Japan (Figure 4-18). The experiment period was 28-29 September 1997 (DoY 272 to 273).

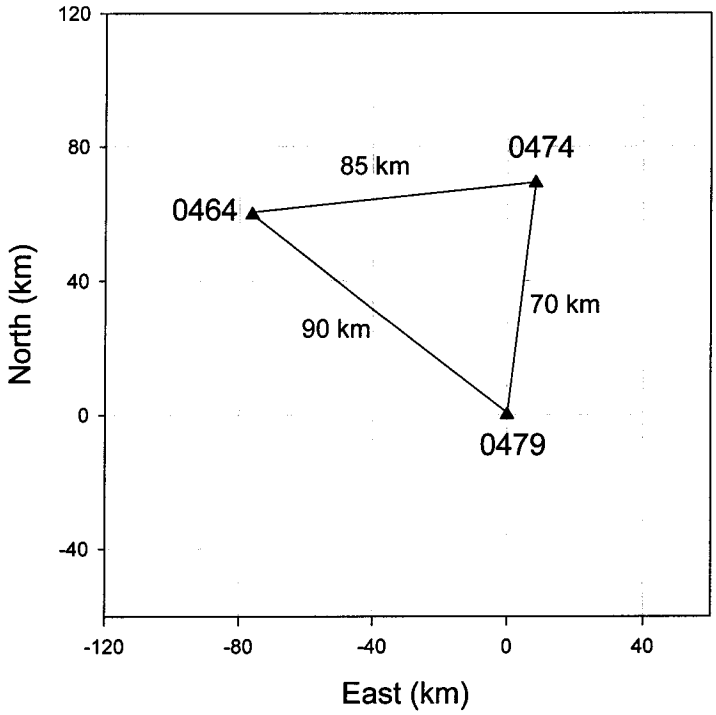

Figure 4-18. Some stations of GSI's Kyushu permanent GPS network. The approximate distances between reference stations is 85, 70 and 97km, for 0464-0474, 0474-0479 and 0479-0464 respectively.

Using the procedure described earlier, the observational data (ionosphere-free linear data combination) were processed to determine the precise coordinates and ambiguities, using the whole day's data. Then the coordinates and resolved integer ambiguities were held fixed to generate the ionospheric and tropospheric delay values on an epoch- by-epoch and satellite-by-satellite basis.

4.5.3 Analysis for a newly-risen satellite

In order to test the algorithm performance in the case of a newly-risen satellite, data for every newly-risen satellite for that period when the satellite elevation angle was between 15 to 20° (around 10 epochs) was considered. Table 4-1 shows the results obtained with,

and without predict tropospheric delay model (Equation 4-20), using the proposed algorithm for ambiguity resolution for every satellite.

Table 4-1. Single epoch ambiguity resolution results for the baseline 0479-0474 (70km), DoY 272 and 273 (1997).

Sat. \ Rising Epoch	Rising Epoch	Without		With	
		272	273	272	273
		Fail in the number of Ambiguity Resolution			
S19_1	113	5	0	0	0
S27_1	134	2	0	0	0
S26	191	0	0	0	0
S06_1	206	1	2	0	0
S17_1	418	5	0	0	0
S09	448	0	7	0	0
S23	552	5	0	0	0
S05_1	712	0	2	0	2
S21	750	0	0	0	0
S30	849	0	3	0	0
S01	889	0	0	0	0
S25	1027	0	0	0	0
S06_2	1145	0	1	0	0
S22	1272	0	0	0	0
S14_1	1381	0	0	0	0
S03	1477	0	0	0	2
S17_2	1604	0	0	0	0
S31	1641	0	0	0	0
S18_1	1672	0	0	0	0
S19_2	1813	0	0	0	0
S15	1907	0	0	0	0
S27_2	2007	0	0	0	0
S02	2163	0	5	0	0
S14_2	2194	0	0	0	0
S07	2301	0	0	0	0
S16	2306	0	0	0	0
S04	2428	0	0	0	0
S18	2574	0	0	0	0
S24	2671	0	7	0	0
S10	2759	0	10	0	0
S05_2	2777	0	10	0	0
Total Fail number in AR		18	47	0	4

From left to right column of the Table 4-1, the column 'Sat.' represents the satellite PRN number and the symbols '_1' or '_2' denote the rising times of the satellites. The column 'Rising Epoch' represents the testing satellites of the rising epoch (cut off angle 15°) and the counting number is starting from UTC 00h 00m 00s. The column 'Without' and 'With' denotes without or with using the proposed algorithm for single epoch ambiguity resolution for every satellite respectively.

When not applying the predicted tropospheric delay model there are 5 newly-risen satellite events (S19_1, S27_1, S06_1, S17_1 and S23) for which the correct ambiguities on DoY 272 cannot be resolve. There are 9 such cases for DoY 273 (S06_1, S09, S05_1, S30, S06_2, S02, S24, S10, and S05_2). This means that about 20~30% will fail single epoch ambiguity resolution.

After applying the predicted tropospheric delay model there are only 2 cases of newly-risen satellites for which the correct ambiguities cannot be resolved on DoY 273, but none on DoY 272. Therefore, the predicted tropospheric delay model is effective in aiding ambiguity resolution for newly-risen satellites.

For the baseline 0479-0464 similar results to Table 4-1 are obtained. That is, when the predicted tropospheric delay model is applied, the correct single epoch ambiguity resolution rate is higher than when it is not applied (Figure 4-19).

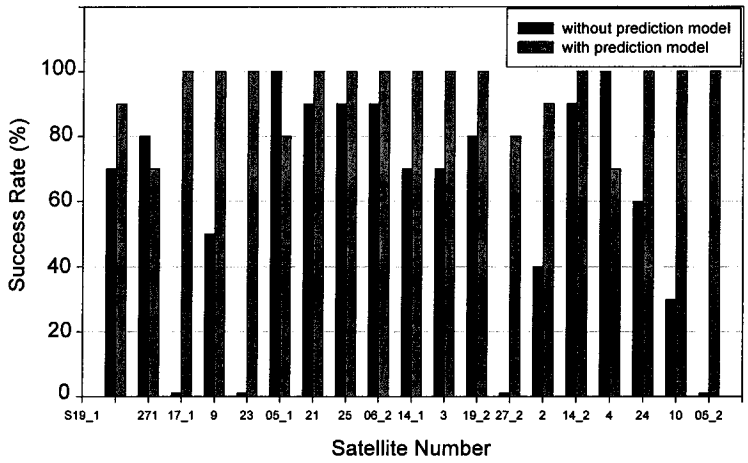

Figure 4-19. Single epoch ambiguity resolution results, with and without the use of the predicted tropospheric delay model for newly-risen satellites, for baseline 0479-0464 (97km), DoY 273 (1997). The x-axis represents satellite number and y-axis denotes the ambiguity resolution success rate in this testing period (10 epochs)

Finally, in the case of the baseline 0479-0464, the average ambiguity resolution success rate is improved from 58% to 93% after applying the predicted tropospheric delay model.

4.5.4 Analysis for the case of a long data gap

In order to investigate the performance of the proposed algorithm when there is a long data gap, the testing data was divided into 31 different time spans, one for each of the satellites.

Table 4-2. Single epoch ambiguity resolution results for the baseline 0479-0474 (70km), on DoY 272 and 273 (1997).

Sat.	Rising Epoch	Testing Epoch	Without		With	
			272	273	272	273
			Fail in the number of Ambiguity Resolution			
S19_1	113	191	33	8	6	5
S27_1	134	363	3	0	0	3
S26	191	541	7	3	4	1
S06_1	206	297	8	9	3	2
S17_1	418	491	15	6	9	3
S09	448	604	2	19	1	2
S23	552	613	9	1	6	1
S05_1	712	511	0	30	4	8
S21	750	537	0	2	0	1
S30	849	568	0	24	0	3
S01	889	600	0	21	0	7
S25	1027	601	1	2	0	1
S06_2	1145	430	0	1	0	0
S22	1272	560	1	10	0	6
S14_1	1381	74	0	0	0	0
S03	1477	617	1	12	2	10
S17_2	1604	169	1	1	1	1
S31	1641	486	0	6	0	6
S18_1	1672	248	1	0	1	0
S19_2	1813	479	1	0	1	0
S15	1907	601	0	19	0	7
S27_2	2007	371	0	0	0	0
S02	2163	538	0	31	0	0
S14_2	2194	512	0	33	0	1
S07	2301	437	0	6	0	0
S16	2306	443	1	32	1	0
S04	2428	421	0	0	0	18
S18	2574	289	0	2	0	0
S24	2671	191	0	56	0	4
S10	2759	107	0	46	0	0
S05_2	2777	90	0	90	0	12
Total Fail Number in AR			84	470	39	102

Table 4-2 lists the failure epochs for ambiguity resolution for each satellite. The number of failed single epoch ambiguity resolution attempts is reduced from 84 to 39 on DoY272, and from 470 to 102 on DoY 273, after applying the tropospheric delay model for the whole tracking period. Hence, when using the widelane / narrowlane (ionosphere-free) linear data combination to resolve the integer ambiguity in a single epoch, the success rate is very dependent on the accuracy of the predicted tropospheric delay values. Compared with the failure rate in the case of not applying prediction model, only 3 epoch/satellite

(there are 31 satellites in this testing data and 84 epochs fail in ambiguity resolution) for DoY 272 but almost 15 epoch/satellite (there are 31 satellites in this testing data and 470 epochs fail in ambiguity resolution) for DoY 273 and in with the prediction model, only 1 epoch/satellite for DoY 272 (there are 31 satellites in this testing data and 39 epochs fail in ambiguity resolution) but almost 3 epoch/satellite (there are 31 satellites in this testing data and 102 epochs fail in ambiguity resolution) for DoY 273.

The tropospheric delay values have large differences for consecutive days (DoY 272 and 273), which affects the ambiguity resolution success rate. This is especially the case for satellites 24, 10 and 05_2, where the success rate is reduced from 100% to 73%, 57%, and 0% respectively. For some of the satellites (27_1 and 04), the correct integer ambiguity rate after applying the prediction model is decreased on DoY 273, because the tropospheric delay residuals have a dramatic change, similar to Figure 4-21.

From left to right column of the Table 4-2, the column 'Sat.' represents the satellite PRN number and the symbols '_1' or '_2' denote the rising times of the satellites. The column 'Rising Epoch' represents the testing satellites of the rising epoch (cut off angle 15°) and the counting number is starting from UTC 00h 00m 00s. The column 'Testing Epoch' represents the whole computing epoch for the ambiguity resolution of the testing satellites. The column 'Without' and 'With' denotes without or with using the proposed algorithm for single epoch ambiguity resolution for every satellite respectively.

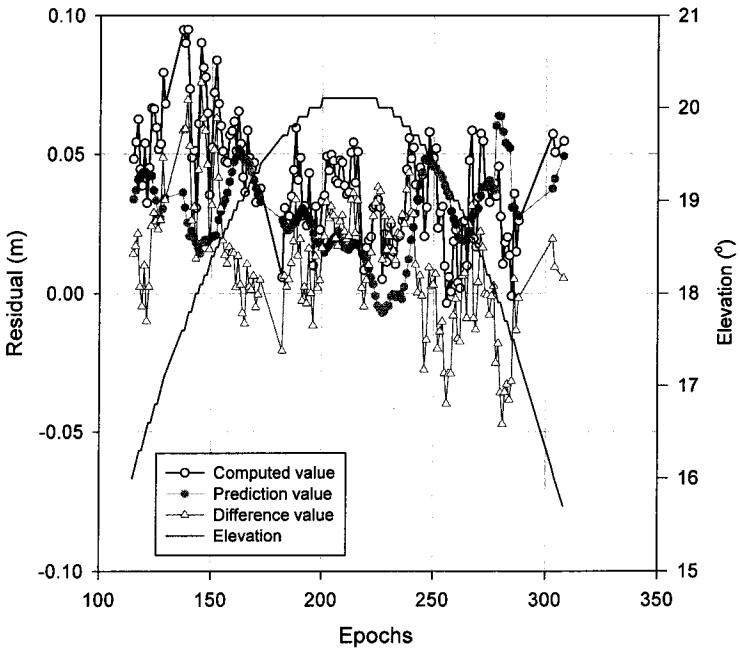

Figure 4-20. Tropospheric delay residuals for satellite pair 04-19, DoY 272, 1997 (baseline: 0479-0474). The open circle denotes the computed tropospheric delay, the open triangle represents the predicted value, and the filled circle represents the difference (computed minus predicted values). The centre curve is the satellite elevation. The x-axis is epoch number, and the y-axis is the residuals (computed from Equation (4-9)).

Figure 4-20 shows the computed, predicted, and the difference (computed minus predicted) tropospheric delay values for the satellite pair 04-19 on DoY 272, 1997. The number of failed single epoch ambiguity resolution attempts is reduced from 33 to 6 when the prediction model is applied.

Table 4-3. Single epoch ambiguity resolution results of the baseline 0479-0464, 97km, DoY 272, 1997.

Sat.	Rising Epoch	Testing Epoch	Without 272	With 272
S19_1	113	191	23	6
S27_1	134	363	5	4
S26	191	541	75	2
S06_1	206	297	3	0
S17_1	418	491	86	1
S09	448	604	26	3
S23	552	613	53	0
S05_1	712	511	0	2
S21	750	537	0	0
S30	849	568	7	0
S01	889	600	14	0
S25	1027	601	4	0
S06_2	1145	430	10	0
S22	1272	560	0	0
S14_1	1381	74	14	0
S03	1477	617	7	0
S17_2	1604	169	0	0
S31	1641	486	1	0
S18_1	1672	248	1	2
S19_2	1813	479	3	2
S15	1907	601	8	5
S27_2	2007	371	21	2
S02	2163	538	32	7
S14_2	2194	512	28	4
S07	2301	437	7	2
S16	2306	443	9	5
S04	2428	421	2	8
S18	2574	289	1	0
S24	2671	191	17	1
S10	2759	107	26	1
S05_2	2777	90	36	6
Total Fail Number in AR			513	63

Table 4-3 shows the single epoch ambiguity resolution results for baseline 0479-0464 on DoY 272. Applying the predicted tropospheric delay model has effectively reduced the

number of epochs of failed ambiguity resolution from 519 to 63. When there is a long data gap, utilizing the predicted tropospheric delay model can increase the correct ambiguity resolution rate. Figure 4-21 shows the largest improvement (for satellite pair 04-17) when the prediction model is used.

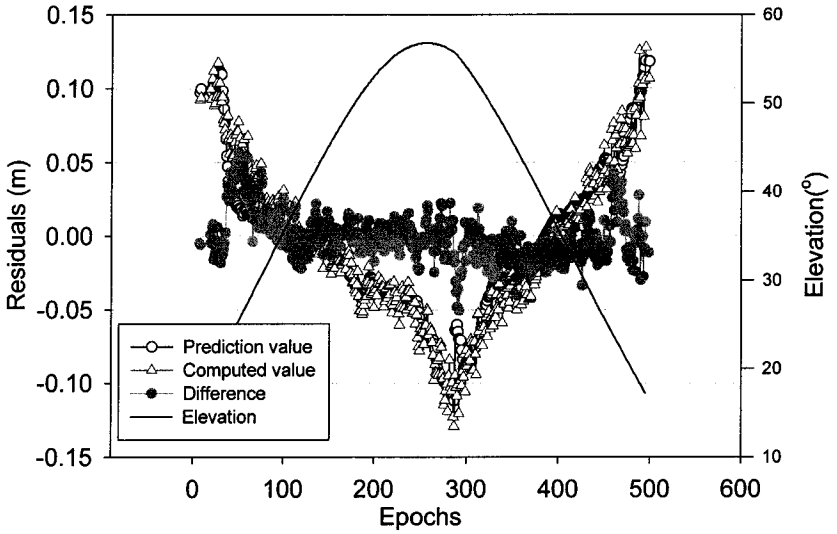

Figure 4-21. Tropospheric delay residual for satellite pair 04-17, DoY 272, 1997 (baseline: 0479-0464). The open circle denotes the computed tropospheric delay, the open triangle represents the predicted value, and the filled circle represents the difference (computed minus predicted values). The centre curve is the satellite elevation. The x-axis is epoch number, and the y-axis is the residual (computed from Equation (4-9)).

4.6 Concluding Remarks

Although the precise coordinates are known for reference stations within a permanent GPS network, it is still a challenge to correctly resolve, in real-time, the integer ambiguity values between the reference stations when a new satellite rises, or when there is a cycle slip, or after a long data gap.

This chapter describes the data processing methodology for the reference stations using the widelane and narrowlane linear data combination model (ionosphere-free), and the predicted tropospheric delay model (after applying the standard troposphere model). The proposed procedure can improve the success rate for single epoch ambiguity resolution. From the tests carried out the following conclusions can be drawn:

1. The results obtained, by applying a predicted tropospheric delay model derived from data to other tracked satellites, can improve the success rate for ambiguity resolution by up to 90% when a new satellite rises.

2. When there is a long data gap, the proposed algorithm can provide more reliable ambiguity resolution, especially when the tropospheric delay values are larger than 0.5 cycle in the narrowlane combination.
3. The ability to predict the tropospheric delay value is dependent on how smooth the real tropospheric delay for each satellite is.
4. The proposed algorithm can be implemented for real-time, or near real-time, applications.

Chapter 5

AMBIGUITY RECOVERY USING TRIPLE-DIFFERENCED-TYPE APPROACH FOR LONG-RANGE GPS KINEMATIC POSITIONING

5.1 General Description

For medium or long-range precise kinematic GPS positioning, the main requirement is that carrier phase ambiguities be resolved correctly. In the case of short baseline techniques, the residual effect due to atmospheric delay and orbit bias can be ignored. However, this is hardly the case for medium or long-range precise kinematic GPS positioning. Several ambiguity resolution algorithms have been proposed for such scenarios. Hernández-Pajares et al. (1999, 2000) and Colombo et al. (1999) have proposed a two-layer ionosphere model to generate ionospheric corrections from the reference station data, and then an interpolation method to estimate the ionospheric delay between the reference and rover stations. The results indicate that the widelane ambiguities could be fixed with a success rate of nearly 100% for satellite elevations above 20°, and the resolution of the ϕ_1 & ϕ_2 ambiguities is possible with a success rate of more than 80% for baseline lengths up to few hundred kilometres. Li & Gao (1998) extend the Gao et al. (1997) ambiguity resolution approach, applying day-to-day correlations of the orbit error, atmosphere bias and multipath to improve the network ambiguity resolution (for baseline lengths ranging from 160-400km). Rabah & Leinen (1999) have suggested a widelane/narrowlane ambiguity resolution algorithm for kinematic positioning for baseline lengths in the range of 30-120km, however the ambiguity resolution success rate is dependent on the magnitude and variability of atmospheric delay across the test area. The algorithms referred to above were tested for static GPS stations, but not in the kinematic mode. However, for long-range kinematic positioning, the challenge of ambiguity resolution is not to determine the 'absolute' ambiguities "on-the-fly", but rather to estimate the 'relative' ambiguities (equivalent to cycle slip detection and repair).

Precise, long-range GPS kinematic positioning to centimetre accuracy requires the carrier phase ambiguities be resolved correctly during initialisation and to then 'recover' the 'lost' ambiguities in the event of a cycle slip. Furthermore, to maximise navigational efficiency,

ambiguity resolution and carrier phase-based positioning need to be carried out in 'real-time'. Due to the presence of the ionospheric signal delay, satellite orbit errors and the tropospheric delay, so-called 'absolute' ambiguity resolution "on-the-fly" for long-range applications becomes very difficult, and largely impossible. However, all of these errors exhibit a high degree of spatial and temporal correlation. In the case of short-range ambiguity resolution, because of the high spatial correlation, their effect can be neglected, but their influence will dramatically increase as the baseline length increases. On the other hand, between discrete trajectory epochs they will still exhibit a large degree of similarity for short time spans. In this chapter, a method is described in which similar triple-differenced observables formed between one epoch with unknown ambiguities and another epoch with fixed ambiguities can be used to derive 'relative' ambiguity values, which are ordinarily equal to zero (or to the number of cycles that have 'slipped' when loss-of-lock occurred). Because of the temporal correlation characteristics of the error sources, the cycle slips can be recovered using the proposed methodology. In order to test the performance of the proposed algorithm an experiment involving the precise positioning of an aircraft, over distances ranging from a few hundred metres up to 700 kilometres, was carried out in October 1999. The results indicate that the proposed technique can successfully resolve 'relative' ambiguities (or cycle slips) over long distances in an efficient manner that can be implemented in 'real-time' (Liwen et al., 2000).

5.1.1 The evolution of carrier phase-based kinematic GPS positioning

Carrier phase-based kinematic positioning is one of the most difficult engineering challenges for GPS system developers. Over the past decade or so several developments have occurred which deliver high accuracy performance in "real-time" – that is, in the field, immediately after making the measurements (but after the data from the reference receiver has been transmitted to the user receiver's computer for processing). Real-time positioning is even possible when the GPS receiver is in motion (with ambiguity resolution being carried out using a so-called "on-the-fly", or OTF, algorithm). These systems are commonly referred to as RTK systems ("real-time-kinematic"), and for the first time make *feasible* the use of GPS for time-critical applications such as machine control, GPS-guided earthworks/excavations, automated container port operations, etc. Although RTK systems represent the "state-of-the-art" in GPS technology, there are several conditions (or constraints) that must be fulfilled. These constraints may be so restrictive that they prevent the widespread adoption of precise GPS technology for both engineering surveys (a traditional application of carrier phase-based GPS techniques), as well as for new applications such as precise navigation in support of autonomous robot vehicle operation (identified by many as one of the new "frontier" applications of GPS).

If GPS signals were continuously tracked and loss-of-signal-lock never occurred, the integer ambiguities determined at the beginning of a survey would be valid for the whole

period that GPS was being used, whether the antenna was stationary ("static" positioning) or moving ("kinematic" positioning). However, the GPS satellite signals can be shaded (e.g., due to buildings in 'urban canyon' environments, or when the receiver passes under a bridge or through a tunnel), in which case the ambiguity values are 'lost' and must be redetermined. *This process can take from several tens of seconds up to a few minutes with present GPS commercial-off-the-shelf (COTS) systems, but only when the reference-to-rover receiver distance is less than about 10-15km,* although recent developments suggest that this constraint has been relaxed out to 30km or so. During this 're-initialisation' period centimetre accuracy positioning is not possible, and hence there is "dead" time until sufficient data has been collected to "resolve the ambiguities". If interruptions to the GPS signals occur repeatedly, then ambiguity re-initialisation is at the very least an irritation, and at worse a significant weakness of GPS COTS carrier phase-based systems. In addition, the longer the period of tracking required to ensure reliable on-the-fly ambiguity resolution (OTF-AR), the greater the risk that cycle slips will occur during this crucial (re-) initialisation period. These shortcomings are also present in any system based on data post-processing as well.

Over the last few years several important developments have occurred that appear to have overcome some of the constraints for carrier phase-based kinematic GPS positioning:

- Under certain conditions decimetre level positioning accuracy has been possible even when the baseline lengths have been from a few tens up to hundreds of kilometres in length (Han & Rizos, 1997b; Han et al., 1998).

- Reliable OTF-AR in the shortest period of time possible, even with just one measurement epoch, has been demonstrated (Han, 1997a; 1997b). Given very short periods of "time-to-AR" the notion of cycle slips, or having to re-initialise the ambiguities, has no meaning because so-called *instantaneous* OTF (IOTF) becomes the normal mode of kinematic positioning for *all epochs*.

The most significant algorithm improvements therefore have been in: (a) shortening the "time-to-AR" to just one epoch of data, and (b) overcoming the baseline length constraint. Together with advances in GPS hardware (principally the availability of dual-frequency receivers capable of making carrier phase and precise pseudo-range measurements on both the L1 and L2 frequencies), developments in fast ambiguity resolution algorithms and validation criteria procedures, improvements in the observation stochastic modelling and the application of careful quality control procedures, have generally been responsible for this increased level of AR performance. However, using a single reference GPS receiver still typically requires that the baseline lengths be less than about 10-20km, a significant constraint for many high precision kinematic positioning applications. Although carrier phase-based, *medium-range* GPS kinematic positioning has been reported for baselines many tens of kilometres in length (see, e.g., Wübbena et al., 1996; Han, 1997a; Han &

Rizos, 1997b), such exceptional positioning performance requires the use of multiple reference stations in order to mitigate the effect of satellite orbit bias, as well as the ionospheric and tropospheric biases, multipath and observation noise.

5.2 The Functional Model of the Triple-Differenced-Type of Observable

The distance-dependent biases can be ignored for short-range kinematic or static ambiguity resolution, and the integer ambiguities can easily be resolved. As the baseline length increases, the distance dependent biases will gradually affect not only the positioning accuracy but also the ambiguity resolution process.

From the computational point of view, the distance dependent biases have a high temporal correlation. This means that between two consecutive observation epochs the GPS signals have been affected by almost the same atmospheric propagation conditions. Hence, the triple-differenced observables are similarly affected. They can be used to 'link' one epoch with unknown ambiguities to another epoch with fixed ambiguities, in order to derive the 'relative' ambiguity values. They are ordinarily equal to zero (or to the number of cycles that have 'slipped' when loss-of-lock occurred).

5.2.1 Functional model

The double-differenced GPS observables can be written as (after Equations 3-26~3-29).

$$\Delta\nabla\phi_1 = \Delta\nabla\rho + \Delta\nabla d\rho - \Delta\nabla I + \Delta\nabla T + \Delta\nabla M + \lambda_1\Delta\nabla n_1 + \Delta\nabla\varepsilon_{\phi_1} \tag{5-1}$$

$$\Delta\nabla P_1 = \Delta\nabla\rho + \Delta\nabla d\rho + \Delta\nabla I + \Delta\nabla T + \Delta\nabla M + \Delta\nabla\varepsilon_{P_1} \tag{5-2}$$

$$\Delta\nabla\phi_2 = \Delta\nabla\rho + \Delta\nabla d\rho - \frac{f_1^2}{f_2^2}\Delta\nabla I + \Delta\nabla T + \Delta\nabla M + \lambda_2\Delta\nabla n_2 + \Delta\nabla\varepsilon_{\phi_2} \tag{5-3}$$

$$\Delta\nabla P_2 = \Delta\nabla\rho + \Delta\nabla d\rho + \frac{f_1^2}{f_2^2}\Delta\nabla I + \Delta\nabla T + \Delta\nabla M + \Delta\nabla\varepsilon_{P_2} \tag{5-4}$$

where for either the L_1 or L_2 signals (designated by the subscript):

$\Delta\nabla\phi$: double-differenced carrier phase measurements;

$\Delta\nabla P$: double-differenced pseudo-range measurements;

$\Delta\nabla\rho$: double-differenced geometric range;

$\Delta\nabla d\rho$: double-differenced orbit error;

$\Delta\nabla I$: double-differenced ionospheric delay;

$\Delta\nabla M$: double-differenced multipath error;

$\Delta\nabla T$: double-differenced tropospheric delay;
λ: wavelength;
f: frequency;
$\Delta\nabla n$: double-differenced phase ambiguity; and
$\Delta\nabla\varepsilon$: double-differenced carrier phase noise.

For epochs t and t + 1 the L1 carrier-phase observables can be represented as:

$$\Delta\nabla\phi(t) = \Delta\nabla\rho(t) + \lambda\Delta\nabla n_t + (\Delta\nabla d\rho - \Delta\nabla I + \Delta\nabla T + \Delta\nabla M)_{(t)} + \Delta\nabla\varepsilon_\phi(t) \quad (5\text{-}5)$$

$$\Delta\nabla\phi(t+1) = \Delta\nabla\rho(t+1) + \lambda\Delta\nabla N_{t+1} + (\Delta\nabla d\rho - \Delta\nabla I + \Delta\nabla T + \Delta\nabla M)_{(t+1)} + \Delta\nabla\varepsilon_\phi(t+1) \quad (5\text{-}6)$$

The triple-differenced combination can then be formed as:

$$\begin{aligned}\Delta\nabla\phi(t+1) - \Delta\nabla\phi(t) = {} & (\Delta\nabla\rho(t+1) - \Delta\nabla\rho(t)) + \lambda(\Delta\nabla N_{t+1} - \Delta\nabla N_t) \\ & + (\Delta\nabla d\rho - \Delta\nabla I + \Delta\nabla T + \Delta\nabla M)_{(t+1)} - (\Delta\nabla d\rho - \Delta\nabla I + \Delta\nabla T + \Delta\nabla M)_{(t)} \\ & + (\Delta\nabla\varepsilon_\phi(t+1) - \Delta\nabla\varepsilon_\phi(t))\end{aligned} \quad (5\text{-}7)$$

$$\begin{aligned}\cong {} & (\Delta\nabla\rho(t+1) - \Delta\nabla\rho(t)) + \lambda(\Delta\nabla N_{t+1} - \Delta\nabla N_t) + \\ & (\Delta\nabla M_{(t+1)} - \Delta\nabla M)_{(t)} + (\Delta\nabla\varepsilon_\phi(t+1) - \Delta\nabla\varepsilon_\phi(t))\end{aligned} \quad (5\text{-}8)$$

For epochs t and t + 1 the L1 pseudo-range observables can be represented:

$$\Delta\nabla P\ (t) = \Delta\nabla\rho(t) + (\Delta\nabla d\rho + \Delta\nabla I + \Delta\nabla T + \Delta\nabla M)_{(t)} + \Delta\nabla\varepsilon_P(t) \quad (5\text{-}9)$$

$$\Delta\nabla P\ (t+1) = \Delta\nabla\rho(t+1) + (\Delta\nabla d\rho + \Delta\nabla I + \Delta\nabla T + \Delta\nabla M)_{(t+1)} + \Delta\nabla\varepsilon_P(t+1) \quad (5\text{-}10)$$

$$\begin{aligned}\Delta\nabla P(t+1) - \Delta\nabla P(t) = {} & (\Delta\nabla\rho(t+1) - \Delta\nabla\rho(t)) \\ & + (\Delta\nabla d\rho + \Delta\nabla I + \Delta\nabla T + \Delta\nabla M)_{(t+1)} \\ & - (\Delta\nabla d\rho + \Delta\nabla I + \Delta\nabla T + \Delta\nabla M)_{(t)} \\ & + (\Delta\nabla\varepsilon_P(t+1) - \Delta\nabla\varepsilon_P(t))\end{aligned} \quad (5\text{-}11)$$

$$\cong (\Delta\nabla\rho(t+1) - \Delta\nabla\rho(t)) + (\Delta\nabla M_{(t+1)} - \Delta\nabla M)_{(t)} + (\Delta\nabla\varepsilon(t_{k+1}) - \Delta\nabla\varepsilon(t)) \quad (5\text{-}12)$$

Where the term $\Delta\nabla N_{t+1} - \Delta\nabla N_t$ is the 'relative' ambiguity (or cycle slip) and $\Delta\nabla\rho(t)$ can be computed using the previous epoch. Because of the temporal correlation, the main biases due to ionospheric delay, the satellite orbit bias and the tropospheric delay can be largely mitigated after between-epoch differencing. Therefore standard ambiguity resolution techniques can still be used to resolve $\Delta\nabla N_{t+1} - \Delta\nabla N_t$ in Equation (5-8).

Assuming the ambiguities and the station coordinates have been fixed at epoch t, then Equation (5-5) can be written as:

$$\begin{aligned} v(t) &= \Delta\nabla\phi(t) - \Delta\nabla\rho(t) + \lambda\Delta\nabla n_t \\ &= (\Delta\nabla d\rho - \Delta\nabla I + \Delta\nabla T + \Delta\nabla M)_{(t)} + \Delta\nabla\varepsilon_\phi(t) \end{aligned} \tag{5-13}$$

Introducing Equation (5-13) into Equation (5-6), and considering the spatial correlation of the atmospheric effects, epoch t + 1 can be derived:

$$\begin{aligned} \Delta\nabla\phi(t+1) = \Delta\nabla\rho(t+1) + \lambda\Delta\nabla N_{t+1} + (\Delta\nabla M_{(t+1)} - \Delta\nabla M_{(t)} \\ + (\Delta\nabla\varepsilon_\phi(t+1) - \Delta\nabla\varepsilon_\phi(t)) - v(t) \end{aligned} \tag{5-14}$$

Hence, according to Equation (5-14), ambiguity resolution is only affected by relative multipath and observation noise. Compared with Equation (5-12), Equation (5-14) is easier to use in the ambiguity resolution procedure. If the orbit bias and atmospheric delay can be ignored for consecutive epochs, the integer ambiguity can be fixed.

After estimating the integer ambiguities, the ionospheric and tropospheric delay can been computed using the Equations (5-15) and (5-16), then the coordinates can be determined. For kinematic applications the multipath bias cannot be ignored in Equation (5-16), hence the tropospheric delay cannot be estimated precisely. However, because of the temporal correlation between epochs, the multipath bias and observation bias can be assumed to have only a minor influence on ambiguity resolution. Hence:

$$\Delta\nabla I = \left(\frac{f_2^2}{f_1^2 - f_2^2}\right)[(\Delta\nabla\phi_1 - \Delta\nabla\phi_2) - (\lambda_1\Delta\nabla n_1 - \lambda_2\Delta\nabla n_2) - (\Delta\nabla\varepsilon_{\phi_1} - \Delta\nabla\varepsilon_{\phi_2})] \tag{5-15}$$

$$\begin{aligned} \Delta\nabla T = \left(\frac{f_1^2}{f_1^2 - f_2^2}\right)[(\Delta\nabla\phi_1 - \lambda_1\Delta\nabla n_1 - \Delta\nabla\varepsilon_{\phi_1})] - \left(\frac{f_2^2}{f_1^2 - f_2^2}\right)[(\Delta\nabla\phi_2 - \lambda_2\Delta\nabla n_2 - \Delta\nabla\varepsilon_{\phi_2})] - \\ (\Delta\nabla\rho + \Delta\nabla d\rho + \Delta\nabla M) \end{aligned} \tag{5-16}$$

5.3 Ambiguity Recovery Using Triple-Differenced Approach

The triple-differenced approach for 'ambiguity recovery' can be used in any kind of linear combination to determine the 'relative' integer ambiguities. The remained biases still have a significant effect, hence some strategies for implementing the 'ambiguity recovery' technique should be developed to improve the success rate of ambiguity resolution.

If ambiguity resolution fails, the initialisation procedure needs to be carried out again. However, this will seriously limit the long-range kinematic applications. One option is to use some useful linear combinations to detect the cycle slips. If no cycle slips for some satellite pairs have been detected, the search procedure doesn't need to be applied to these satellite pairs, which can dramatically reduce the number of satellite pairs to be searched. If cycle slips occur, the search space can be determined using the former linear combinations, which will significantly reduce the search space. These strategies can contribute to improving the success rate of ambiguity resolution.

5.3.1 Basic linear combination for 'ambiguity recovery'

According to Equations (5-1) to (5-4), the carrier phase combination (i, j), integer ambiguity and wavelength can be represented as (Han & Rizos, 1996):

$$\phi_{i,j} = i \cdot \phi_1 + j \cdot \phi_2 \tag{5-17}$$

$$n_{i,j} = i \cdot n_1 + j \cdot n_2 \tag{5-18}$$

$$\lambda_{i,j} = c/(i \cdot f_1 + j \cdot f_2) \tag{5-19}$$

where:
i, j are arbitrary integer numbers, and
c is the speed of light in the vacuum.

Combining the pseudo-range and carrier phase observations (Equations (5-1) - (5-4)), the ionosphere-free linear combination can be written as:

$$n_{i,j} = \phi_{i,j} - \frac{9240(i+j)+289i}{2329 \cdot \lambda_1} \cdot P_1 + \frac{9240(i+j)+289j}{2329 \cdot \lambda_2} \cdot P_2 \tag{5-20}$$

$$m_{n_{i,j}} = \sqrt{i^2 \cdot m^2_{\varphi_1(cy)} + j^2 \cdot m^2_{\varphi_2(cy)} + a^2 \cdot m^2_{P_1} + b^2 \cdot m^2_{P_2}} \tag{5-21}$$

Setting i, j to 1, -1 respectively, the double-differenced widelane ambiguity can be represented as:

$$\Delta\nabla n_{1,-1} = \Delta\nabla\phi_{1,-1} - \frac{17}{137\cdot\lambda_1}\Delta\nabla P_1 - \frac{17}{137\cdot\lambda_2}\Delta\nabla P_2 \qquad (5\text{-}22)$$

In the case of medium-range 'ambiguity recovery on-the-fly, investigators use linear combinations of GPS observations (pseudo-range and carrier phase) in Equations (5-1) - (5-4) to achieve longer wavelength and lower noise. Several linear combinations can be formed, but only a few of them are suitable. The widelane $(\varphi_1 - \varphi_2)$ linear combination is a good candidate because it has a 86.2cm wavelength, and the standard deviation of the estimated ambiguities is only 0.248 cycles. However, using only the widelane linear combination is not enough to solve for the n_1, n_2 ambiguities.

Han (1997a) proposed a two-step ambiguity resolution procedure. The first step is to use the widelane carrier phase observable, together with the combined observation $(-7\varphi_1 + 9\varphi_2)$ and the precise pseudo-ranges, to detect and correct for cycle slips. The main linear combination and standard deviation of the real-valued ionosphere-biased ambiguities are:

$$n_{i,j} = \varphi_{i,j} - \frac{P}{\lambda_{i,j}} + \gamma_{i,j}\frac{I}{f_1^2} \qquad (5\text{-}23)$$

$$m_{n_{i,j}} = \sqrt{i^2\cdot m^2_{\varphi_1(cy)} + j^2\cdot m^2_{\varphi_2(cy)} + \frac{1}{\lambda^2_{i,j}}\cdot m_P^2 + \gamma^2_{i,j} m^2_{I/f_1^2}} \qquad (5\text{-}24)$$

where $\gamma_{i,j} = \left(\frac{i}{\lambda_1} + \frac{j}{\lambda_2}\cdot\frac{f_1^2}{f_2^2}\right) + \frac{\alpha}{\lambda_{i,j}}$ (5-25)

$\alpha = 1$ for $P = P_1$;

$\alpha = 1.647$ for $P = P_2$; and

$\alpha = 1.323$ for $P = (P_1 + P_2)/2$.

Compared with Equation (5-21), Equation (5-24) is affected by ionospheric delay, but not affected much by the (in)accuracy of the pseudo-range observation.

The second step uses two carrier phase combinations ($\varphi_1 - \varphi_2$ and $-3\varphi_1 + 4\varphi_2$) and the predicted roving receiver position to detect and correct cycle slips using a Kalman filter.

Han (1997a) derived the standard derivations (STD) of various real-valued ionosphere-biased ambiguities (Table 5-1), suitable for long-range ambiguity recovery techniques, using Equation (5-24). It should be pointed out that the standard deviations of these linear combinations are 0.247 cycle for $n_{1,-1}$, 0.140 cycle for $n_{-3,4}$ and 0.115 cycle for $n_{-7,9}$ after neglecting the error of the predicted ionospheric delay. However, a one centimetre error in the predicted ionospheric delay will bias by 0.24 cycles the $(-7\varphi_1 + 9\varphi_2)$ combination, and bias by 0.12 cycles the widelane combination (Equation (5-24)). This is because the γ values are 12.024 for the widelane, and 24.001 for the $(-7\varphi_1 + 9\varphi_2)$ combination. In practice, a few centimetres accuracy in the predicted ionosphere delay may be normal for highly kinematic positioning, especially when data gaps occur. On the other hand, this technique uses the precise pseudo-range observations.

Table 5-1. STD of real-valued ionosphere-biased ambiguities.

	$n_{1,-1}$		$n_{-3,4}$		$n_{-7,9}$	
P	$m_{n_{i,j}}$	γ	$m_{n_{i,j}}$	γ	$m_{n_{i,j}}$	γ
P_1	0.348	-0.329	0.191	11.825	0.116	23.979
P_2	0.348	0.422	0.191	12.222	0.116	24.023
Mean	0.247	0.047	0.140	12.024	0.115	24.001

Note to column $m_{n_{i,j}}$: assume that $m_{\varphi_1(cy)} = m_{\varphi_2(cy)} = 0.01$ cycle and $m_{P_1} = m_{P_2} = 0.3$ metres.

5.3.2 Methodology for ambiguity recovery using Triple-Differenced approach

After initialisation of reference network operations, the ambiguities and coordinates are known, and the residuals of the ϕ_1, ϕ_2 carrier phase can be computed on an epoch-by-epoch and satellite-by-satellite basis (Equation (5-13)). Considering the long wavelength factor, the linear combination of widelane (Equation (5-22)) and the 'monster' widelane $(-7\phi_1 + 9\phi_2)$ can be derived for the current epoch.

At the next epoch (t + 1), the cycle slip detection procedure uses the between-epoch widelane and 'monster' widelane linear combinations. This can be expressed as:

$$\begin{aligned} &\left|CS_{1,-1} = N_{1,-1}(t+1) - N_{1,-1}(t)\right| < 0.5 \text{ (cycle)} \\ &\left|CS_{-7,9} = N_{-7,9}(t+1) - N_{-7,9}(t)\right| < 0.5 \text{ (cycle)} \end{aligned} \tag{5-26}$$

where CS is the cycle slip.

Because the two combinations have an odd-even relationship, if one combination has been resolved therefore the other combination's wavelength is doubled:

If $CS_{1,-1}$ is even, $CS_{-7,9}$ has to be even

If $CS_{1,-1}$ is odd, $CS_{-7,9}$ has to be odd (5-27)

The noise of the widelane linear combination is around 0.25 cycles (assuming $m_{\varphi_1(cy)} = m_{\varphi_2(cy)} = 0.01$ cycles and $m_{P_1} = m_{P_2} = 0.3$ metres), as derived from Equation (5-21) or (5-24). The noise of the 'monster' widelane linear combination is 15.74 cycles using Equation (5-21). However, applying Equation (5-24) the noise is only 0.115 cycles (Table 5-1) if the ionospheric delay can be ignored. The prediction of the ionospheric delay needs to be as good as 2cm (the noise of the 'monster' widelane $-7\phi_1 + 9\phi_2$ is 0.48 cycles), if the baseline length is short or under low solar activity conditions.

Hence, Equations (5-26) and (5-27) can reduce the computation time, if the predicted ionospheric delay is precise enough and no cycle slips occur. The coordinates can be estimated, using the ionosphere-free linear combination $(77\phi_1 - 60\phi_2)$, and the residual of the ϕ_1 and ϕ_2 double-differenced observation can be computed.

If epoch t + 1 cannot satisfy Equations (5-26) & (5-27), this means that there is a cycle slip present, or the between-epoch ionospheric delay is larger than 2cm. Following Equation (5-14), the triple-differenced-type algorithm then can be used to reduce the residual of the observation. Next, according to Equations (5-26) & (5-27), the ϕ_1 and ϕ_2 search space is determined, and then the ambiguity resolution carried out.

For real-time cycle clip determination, there are three steps that need to be followed:

1. Search Range Determination

$$DN_{1,-1} - 3m_{1,-1} < CS_{1,-1} < DN_{1,-1} + 3m_{1,-1} \quad \text{and}$$
$$DN_{-7,9} - 3m_{-7,9} < CS_{-7,9} < DN_{-7,9} + 3m_{-7,9} \qquad (5\text{-}28)$$

where: $DN_{1,-1} = N_{1,-1}(t+1) - N_{1,-1}(t)$ and $DN_{-7,9} = N_{-7,9}(t+1) - N_{-7,9}(t)$.

The $m_{1,-1}$ and $m_{-7,9}$ are the standard deviations of the widelane and 'monster' widelane, and they can be derived from the linear combination model.

2. L1 and L2 Search Range Determination

$$CS_1 = \frac{1}{2}(CS_{-7,9} + 9 \cdot CS_{1,-1})$$

$$CS_2 = \frac{1}{2}(CS_{-7,9} + 7 \cdot CS_{1,-1}) \qquad (5\text{-}29)$$

The cycle slips (or 'relative' ambiguities) on ϕ_1 and ϕ_2 can be determined from Equation (5-29).

3. Validation Criteria for Decision

$$\frac{(QF)_i}{(QF)_{min}} < \xi_{F_{m,m};1-\alpha} \qquad (5\text{-}30)$$

where: QF is the quadratic form of the residuals, with respect to a cycle slip candidate set.

It is also possible to use two linear combinations to determine the search range for the cycle slips. After that, the ϕ_1 and ϕ_2 cycle slips can be derived from the two linear combinations. Finally, use the criteria of Equation (5-30) for cycle slip validation.

The 'ambiguity recovery algorithm' is summarised in Figure 5-1.

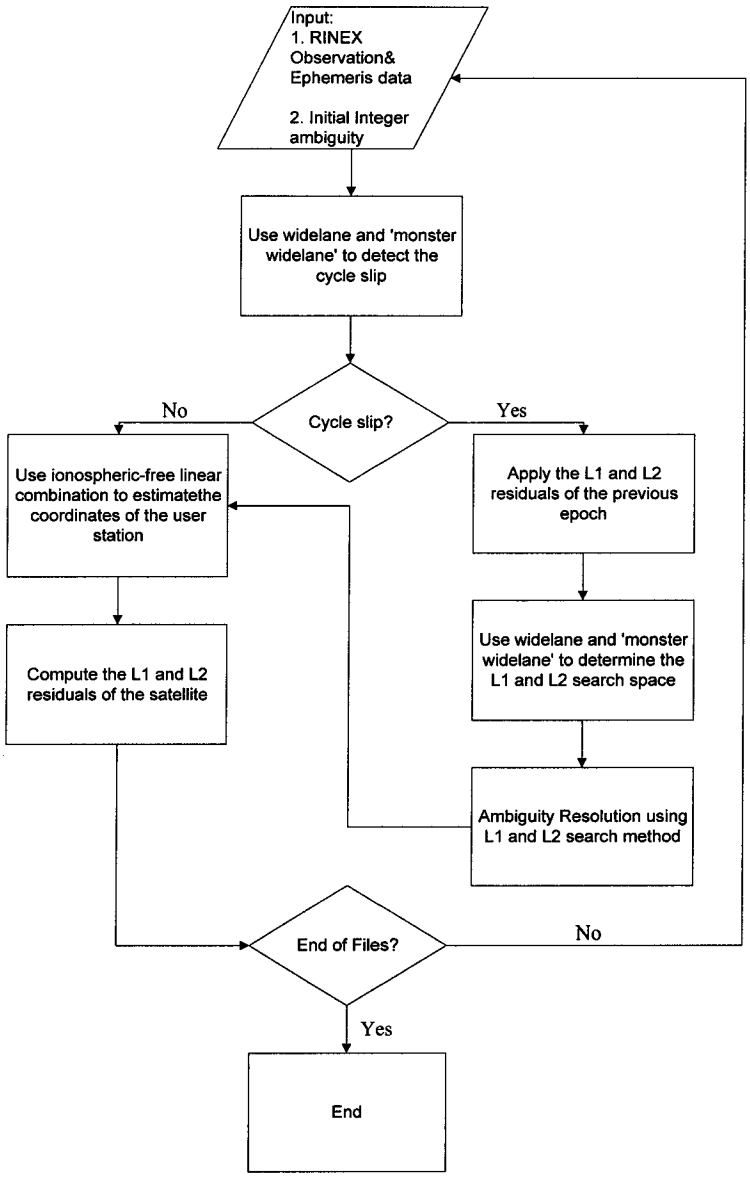

Figure 5-1. Flow chart of the Triple-difference-type algorithm for 'ambiguity recovery'.

5.3.3 The advantage for medium range positioning of Triple-Differenced approach

According to Equation (5-8), 'relative' ambiguities can be solved for if the observations are only affected by multipath bias and observation noise. For medium or long-range positioning, the ionospheric delay is the most significant bias impacting on ambiguity resolution. The double-differenced ionospheric delay is dependent on geographic location, geomagnetic longitude, the level of solar activity and the baseline length. Figure 5-2 displays the double-differenced ionospheric delay for a 38km baseline, during comparatively active ionospheric conditions.

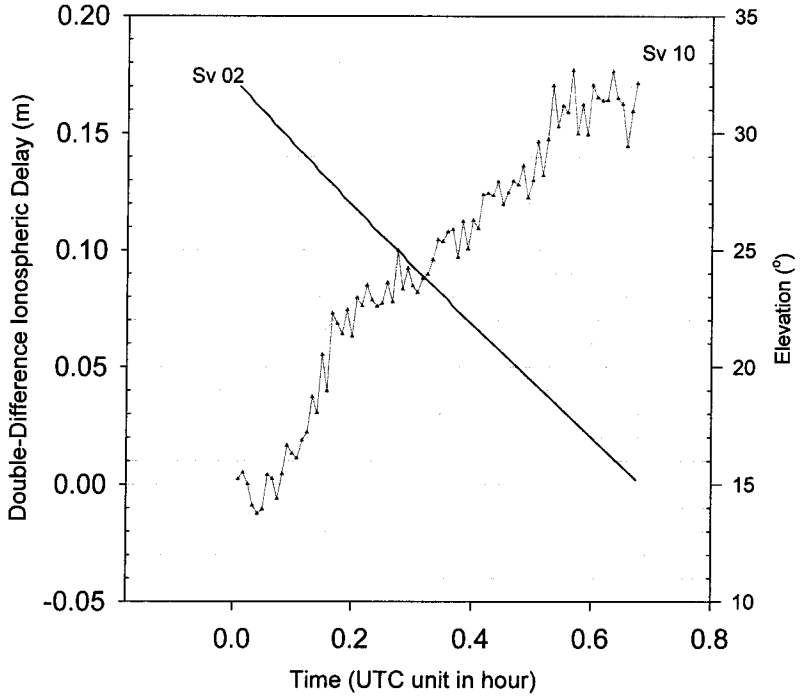

Figure 5-2. Double-differenced ionospheric delay for a 38km baseline, satellite pair 2 and 10, Chukuo, Taiwan, on Doy 223, 1999.

Although the baseline length is only 38km, the double-differenced ionospheric delay varies more than 1cm between epochs. Hence, it will cause 0.25 cycles noise when the 'monster' widelane $(-7\phi_1 + 9\phi_2)$ linear combination is formed. However, if ambiguity resolution is carried out using the triple-differenced-type 'ambiguity recovery' algorithm (Equation (5-14)), and searching in the ϕ_1 & ϕ_2 space, the 1cm variation of the double-differenced ionospheric delay only causes less than 0.1 cycle noise in the ϕ_1 carrier phase.

Hence, this algorithm for 'relative' ambiguity recovery, or cycle slip detection, has several advantages:

- The functional model is only slightly affected by the variability of the ionospheric delay.
- The functional model is independent of the baseline length.
- Easy to implement.
- Effective.
- Good performance for determining relative ambiguities in real-time.

5.3.4 Using the Triple-Differenced approach

For medium-range monitoring systems, the proposed triple-differenced approach has two main applications. The first one is in real-time ambiguity resolution for the multiple

reference station data processing. The second application is in detecting the deformation of the medium-range monitoring system.

To generate 'correction messages', the integer ambiguities need to be resolved for the reference station data. Using the triple-differenced-type 'ambiguity recovery' technique, once the initialisation has been carried, cycle slips can be detected and repaired, ensuring that the corrections can be generated reliably on a continuous basis.

From the deformation monitoring point of view, the triple-differenced-type 'ambiguity recovery' technique can be used to estimate the changes in the coordinates, under the assumption that the station coordinates do not change over a certain time period. This monitoring concept is the same as the quasi-kinematic positioning technique, which assumes that the receiver, for a short period of time, is stationary.

5.4 Experimental Results

In order to test these proposals, two sets of data were collected and analysed. The first was static data for an approximately 100km long baseline collected in April 1999, in Sydney, Australia. The second data set was collected for the precise positioning of an aircraft, over distances ranging from a few hundred metres up to 700 kilometres, in October 1999, flying out of Cairns, in northern Australia.

5.4.1 Static positioning

This experiment was carried out on 29 April 1999, using two dual-frequency Leica GPS receivers with choke ring antennas. One of the stations was located at Wollongong and the other station was located at Bilpin. Figure 5-3 shows the double- and triple-differenced residuals for a low elevation difference satellite pair (01-25). The first and third plots show the double-differenced residuals. The second and last plots (represented by dots) are the triple-differenced residuals for L1 and L2 respectively. From this figure it can be seen that the size of the double-differenced residuals are large (of the order of 1 cycle). Fortunately, the triple-differenced residuals are quite small (less than 0.05 cycles). Figure 5-4 shows the double- and triple-differenced residuals for a high elevation difference satellite pair (14-25), hence the residuals are much smaller than those in Figure 5-3.

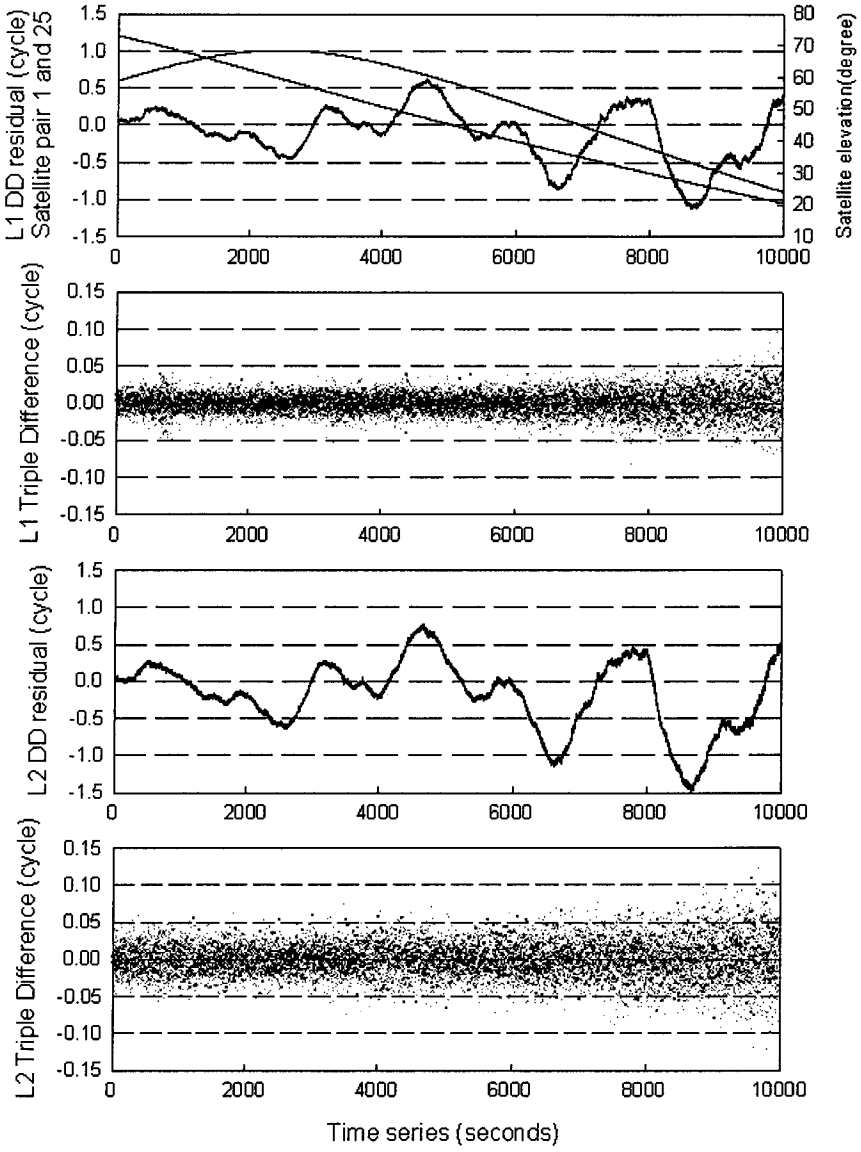

Figure 5-3. L1 and L2 residuals for a low elevation satellite pair 01-25. The x-axis denotes the time in seconds and the y-axis represents the residuals in cycles. From top to bottom the plots are: L1 double-differenced residuals, L1 triple-differenced residuals, L2 double-differenced residuals and L2 triple-differenced residuals.

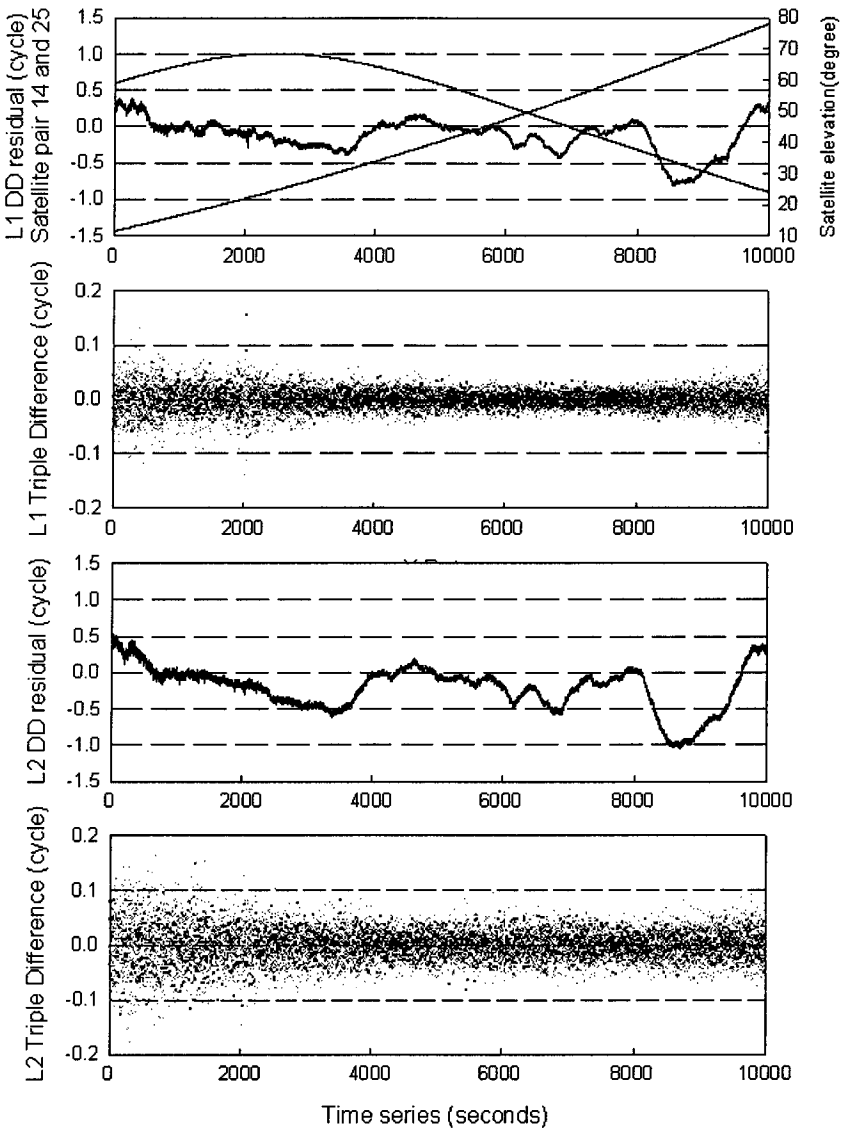

Figure 5-4. L1 and L2 residuals for a high elevation satellite pair 14-25. The x-axis denotes the time in seconds and the y-axis represents the residuals in cycles. From top to bottom the plots are: L1 double-differenced residuals, L1 triple-differenced residuals, L2 double-differenced residuals and L2 triple-differenced residuals.

In order to test the capability of this procedure, a one minute and five minute data gap after every epoch was simulated (Figure 5-5). It can be seen that the noise for the triple-differenced observables using a one minute data gap does not change much (it is still less than 0.1 cycles). The search method therefore still is powerful. For the 5 minute data gaps, the search becomes more difficult because the remaining errors are now quite large (of the order of 0.2 cycles). The main explanation is that the temporal correlation becomes weaker as the size of the data gap increases. In the kinematic case, the spatial correlation becomes weaker as well.

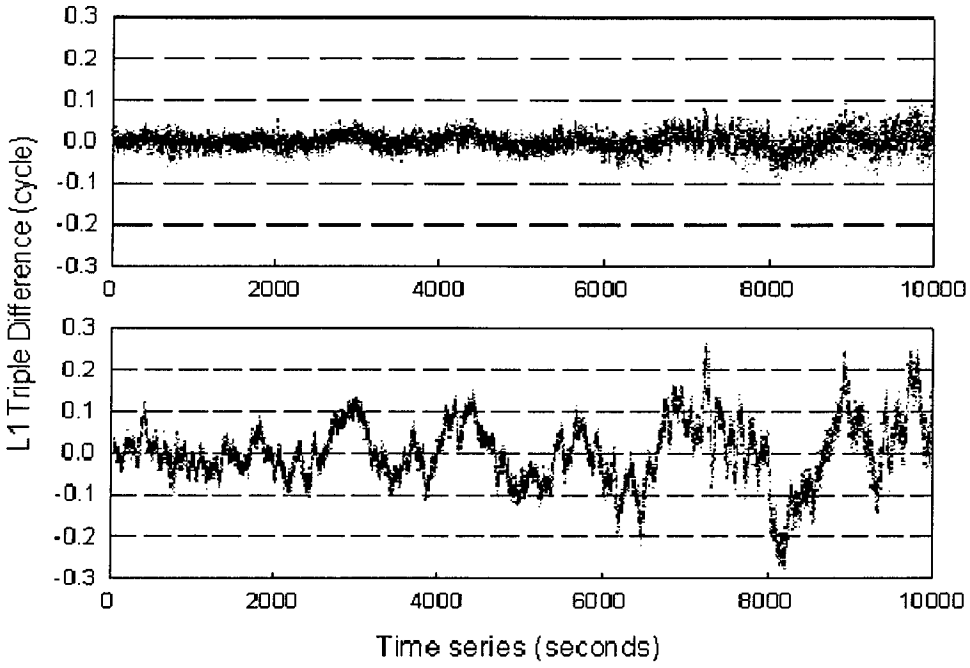

Figure 5-5. 'Ambiguity recovery' with simulated data gaps. The upper plot is for a one minute simulated data gap, and the lower plot is for 5 minute simulated data gap.

5.4.2 Kinematic positioning

An airborne kinematic experiment was carried out in north-east Australia in October 1999. The base station was set up at the airport in the city of Cairns. The aircraft flew from Cairns to Thursday Island (at the tip of Cape York), and back. Trimble 4700 and Ashtech GPS receivers were used, with a sampling rate of 1 second. One Trimble receiver was used at the base station. Another Trimble and one Ashtech receiver were mounted on the wing of the aircraft as mobile receivers (Figure 5-6). The constant distance between the two rover receivers could be used to check whether the kinematic results were correct.

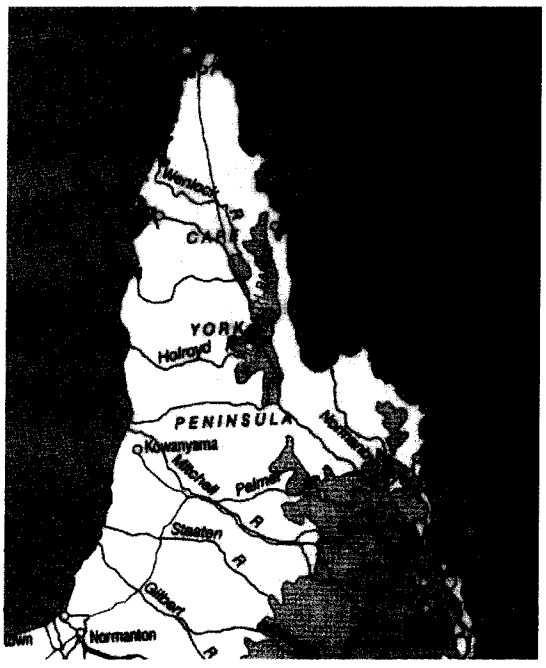

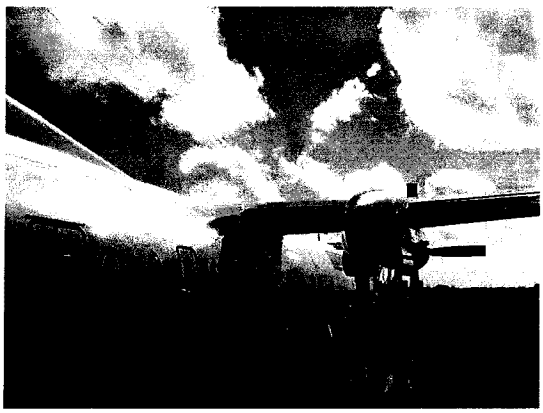

Figure 5-6. The left-hand graph shows the general topography of north-east Australia.

The flight line was from Cairns (near bottom of map) to Thursday Island (tip of Cape York), and back. The right-hand graph shows the airplane and one GPS antenna on the top of the wing.

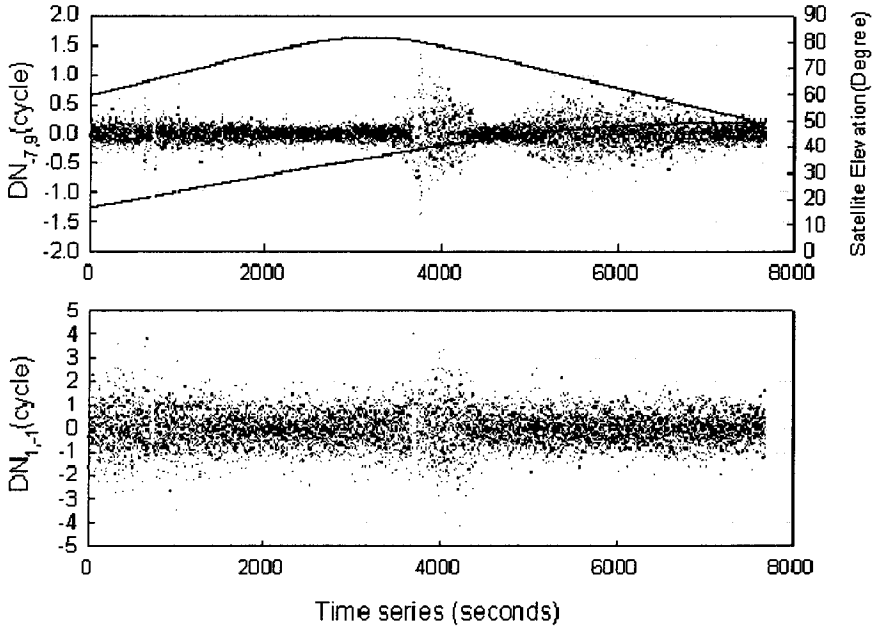

Figure 5-7. From top to bottom: double-differenced residuals of the (–7, 9) and widelane linear combinations. The x-axis denotes the time and the y-axis the residuals (in cycles) for satellite pair 8-24, for data collected in October 1999, Cairns experiment, Australia.

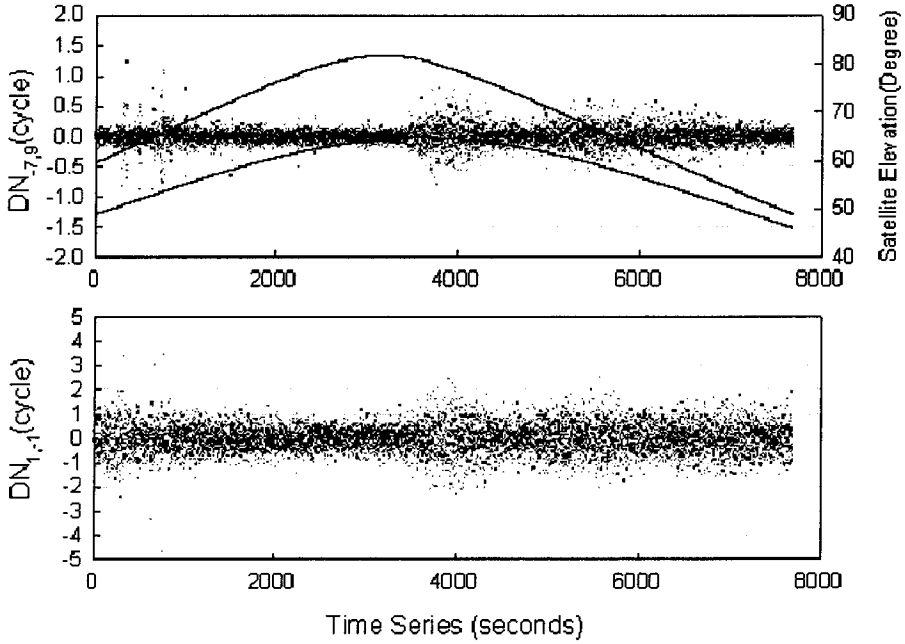

Figure 5-8. From top to bottom: double-differenced residuals of the (–7, 9) and widelane linear combinations. The x-axis denotes the time and the y-axis the residuals (in cycles) for satellite pair 9-24, for data collected in October 1999, Cairns experiment, Australia.

From Figure 5-7, most of the (–7, 9) combination residuals are less than half a cycle, although the widelane errors are quite large. However, when using the odd-even relationship, the wavelength of the widelane combination is doubled. At epoch 3800 the double-differenced residuals are up to 1.5 cycles in size because a data gap has occurred. Figure 5-8 shows the widelane and (-7, 9) linear combination residuals for a high elevation satellite pair (9-24). Note that the double-differenced residuals are much smaller than in Figure 5-7.

If the residuals are larger than a quarter of a cycle, ambiguity resolution will become difficult. Figures 5-9 and 5-10 show the double-differenced TEC values and their change with time, for a low elevation satellite pair (8-24), and a high elevation satellite pair (9-24). As expected the residual ionospheric delay becomes larger with increasing baseline length. But the triple-differenced values remain quite small (less than 1cm). At epoch 3800, the double-differenced residuals are as large as 1.5 cycles, because a data gap has occurred.

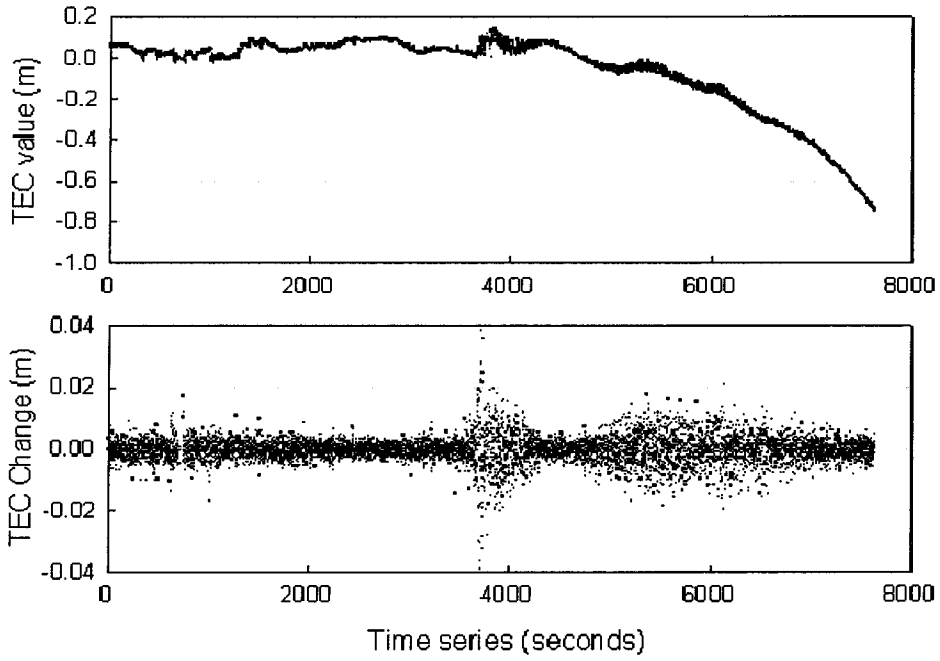

Figure 5-9. Double-differenced TEC values (ionospheric delay), using the geometry-free linear combination. From top to bottom: double-differenced ionospheric delay and the change in the double-differenced ionospheric delay. The x-axis denotes the time, and the y-axis represents the residuals (in cycles) for satellite pair 8-24, for data collected in October 1999, Cairns experiment, Australia.

In Figure 5-10, after epoch 4000, the double-differenced ionospheric delay (upper plot) is larger than 0.2 cycles, and up to 0.8 cycles at epoch 8000. It can affect the L1 observable by from 0.3 to 1.2 cycles. From the lower graph, the change in the double-differenced ionospheric delay is always under 0.2 cycles, except at epoch 3800 seconds (due to a data gap).

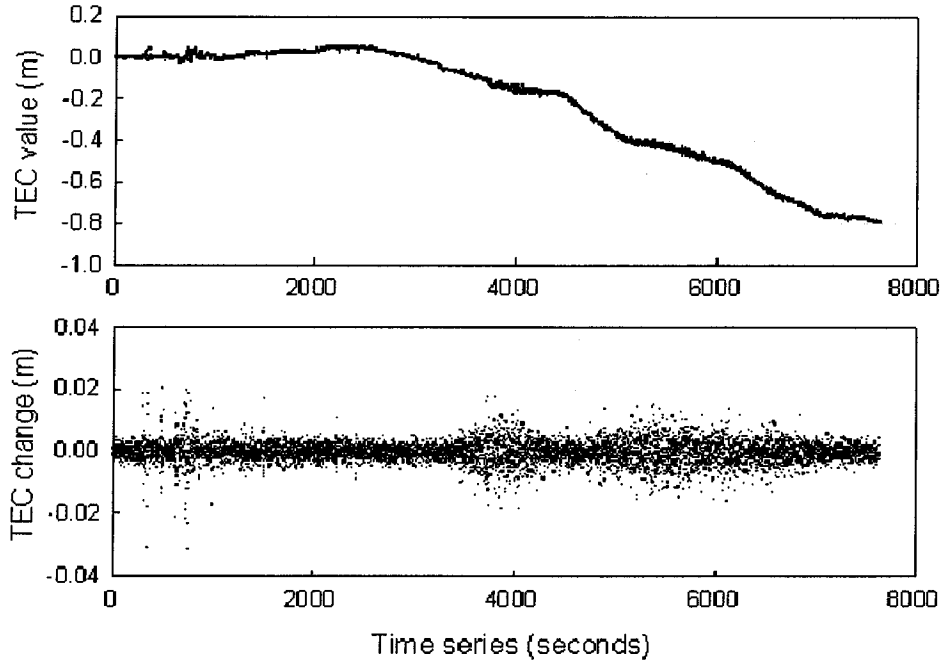

Figure 5-10. Double-differenced TEC values (ionospheric delay), using the geometry-free linear combination. From top to bottom: double-differenced ionospheric delay and the change in the double-differenced ionospheric delay. The x-axis denotes the time, and the y-axis represents the residuals (in cycles) for satellite pair 9-24, for data collected in October 1999, Cairns experiment, Australia.

5.5 Concluding Remarks

The triple-difference-type 'ambiguity recovery' technique has good performance for long-range 'ambiguity recovery'. From these experiments some conclusions can be drawn:

1. The proposed 'ambiguity recovery' procedure can process data without the need for precise pseudo-range data and with no distance limitations.
2. The results indicate that the proposed technique can successfully recover cycle slips over long distances, in an efficient manner such that it can be implemented in real-time.
3. Conditions such as, long data gaps, new satellites rising and long data sampling interval, are still the main obstacles for 'ambiguity recovery'.

Chapter 6

MEDIUM-RANGE NETWORK-BASED GEODETIC MONITORING SYSTEMS

6.1 Introduction

Many permanent GPS reference station network have been established in order to satisfy a variety of crustal deformation monitoring applications in the USA, Japan, Europe, as well as in many other regions. GPS is the most effective tool for determining the deformation caused by an active fault, the surface displacement before/during/after an earthquake, and the relative motion between tectonic plates. Hence one of the tasks of geodesists is to develop techniques for data processing that ensure reliable and high accuracy positioning results can be obtained using the shortest possible observation sessions. For such geodetic applications, typically the data from permanent GPS stations are collected on a daily basis. Then, using carrier phase data processing techniques that have been refined over many years, relative positioning accuracies up to a few parts-per-billion (ppb) can be obtained using so-called 'scientific' GPS software packages.

The design of a permanent GPS reference station network is dependent upon many factors, including the topography and geological characteristics of the region (in particular the location of tectonic faults). Therefore the inter-station distances may vary considerably. In the case of monitoring the pre-seismic or post-seismic displacement of a fault, sub-kilometre resolution may be required (Rizos et al., 2000). Due to the high cost of permanent GPS receiver installations, typically they cannot be established in a dense enough configuration to satisfy such requirements. One possible solution is to use a sub-network of single-frequency receivers to 'in-fill' the network of standard permanent GPS stations, and to then use special data processing strategies to ensure that sub-part-per-million (ppm) relative accuracy can be achieved.

Single-frequency GPS measurements are affected by ionospheric biases which cannot be eliminated in double-differencing or through linear combinations. Because their impact on double-differenced observations is dependent on the inter-station distance, the application of single-frequency techniques is generally limited to short baselines (<10-20km). However, when dual-frequency receivers are also used, there is so much benefit. A linear combination model has been proposed by Han & Rizos (1997b) which is designed for

medium-range GPS positioning. This data processing strategy can account for orbit and ionospheric delay, as well as reducing tropospheric delay, multipath and measurement noise across a GPS receiver network. This data processing strategy permits high relative positioning accuracy, using data from single-frequency receivers installed within a sparse permanent network of dual-frequency receivers, even if the baseline lengths are of the order of a few tens of kilometres or more.

In this chapter various scenarios of the multi-reference station methodology for sub-ppm, single-frequency receiver positioning, will be discussed. Three data sets have been analysed: (a) simulated single-frequency data (derived from dual-frequency receivers but using only the L1 observations), (b) data for comparatively short observation spans, and (c) data collected in operational environments (combining several single-frequency and dual-frequency receivers which occupy the same stations within a sparse permanent network). The data sets are selected in order that the integrated, dual-mode networks are:

- located at different latitudes and longitudes,
- exhibiting large elevation changes,
- involving data collected during different seasons,
- employing single-frequency receivers of different makes, and
- involving baselines of different lengths, so that the performance of the methodology can be tested.

The results do confirm that sub-ppm relative accuracy, even for baselines up to 100km in length, can be achieved in all of the abovementioned test environments.

6.2 Experiments and Results

In the first experiment, data from 16 stations (consisting of two sub-nets of the GEONET network in Japan), at four different times of the year (for day-of-year 001-007, 091-097, 181-187 and 271-277, in the year 1997) were considered. All stations were equipped with dual-frequency receivers, generating 24hr data files with a sampling rate of 30seconds, and involved baseline lengths ranging from 20 to 100km. This is referred to as the *simulated data set.*

In the second experiment, data collected by 8 stations consisting of 3 dual-frequency and 5 single-frequency receivers (day-of-year 119, 1999), logged at 1Hz, over a period of three hours was used. The baseline length was 50km. This is referred to as the *different receiver data set.*

In the third experiment, 10 stations were occupied by 10 dual-frequency and 4 single-frequency receivers (day-of-year 214-224, 1999), and 24hr data files at a sampling rate of

30 seconds were collected. The baseline lengths varied from 15 to 30km. This is the so-called *practical data set.*

6.2.1 The simulated data set: GEONET (Japan) – 1997

The GEONET data was processed using the procedure described previously (Chapter 3), based on the double-differenced carrier phase observations between user station and multiple reference receiver (or between multiple user stations). The 'correction terms' for the L1 carrier phase measurements were derived for the user stations. A variety of inter-receiver distances, network locations in Japan, and seasons of the year were chosen to test the proposed methodology. Interest was principally in the resultant coordinate accuracy and repeatability for the different data sets linking the same receiver stations.

Three different sub-nets, located in Hokkaido (144E 43N), Tokai (139E 35N) and Kyushu (131E 33N), were used to simulate an experimental network (Figure 6-1).

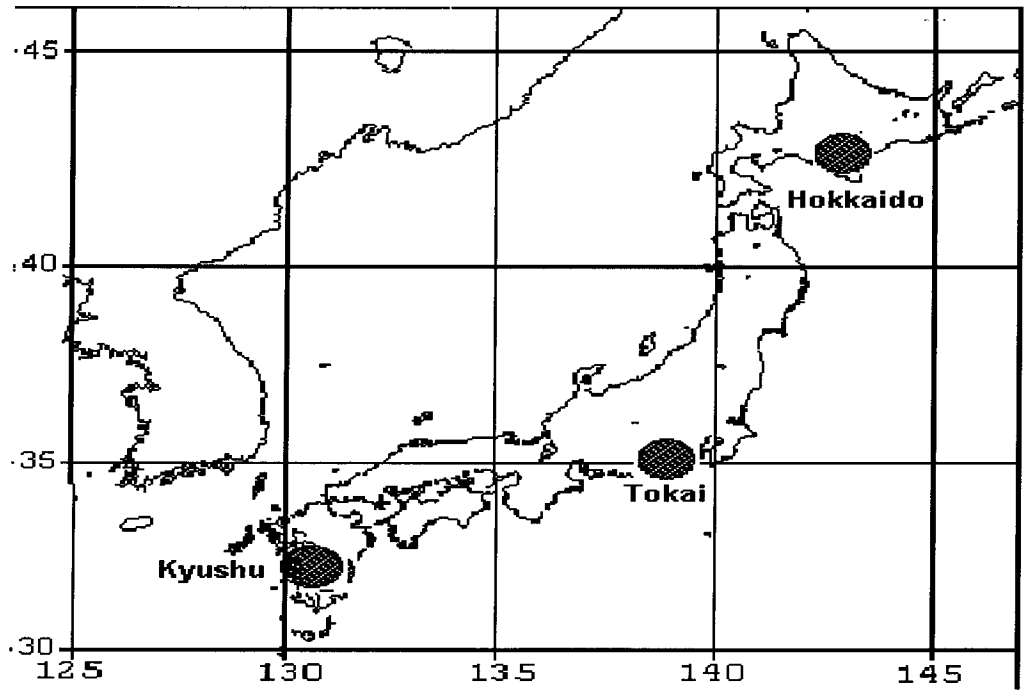

Figure 6-1. The three areas of the GEONET that provided data for investigations are denoted by dark circles.

Daily data processing was carried out for the four different periods (corresponding to each season of the year) using the ionosphere-free linear data combination with the Bernese Software. Table 6-1 lists the standard deviations for the resulting three coordinate components. For the horizontal components (latitude and longitude) the values for the seven daily solutions, for each season, for the three test areas considered, are all below **5mm**, and in the case of the vertical component (height) the standard deviations are all

below **18mm**. These results (for receiver coordinates and associated ambiguities) were compared with the single-frequency results generated from processing the multi-reference station data with the 'correction terms' applied.

In order to test the efficiency of bias elimination in this scenario, the experiment was separated into two parts: (a) the daily result (derived from 24hr data files), and (b) a 'fast static' solution (by varying observation session length). (Note 'fast static' here refers to data sets only a few hours in length, which is comparatively short, against the norm for GPS geodesy, which is the 24hr data file.)

Table 6-1. The standard deviations (units in mm) of the daily results for the latitude, longitude and height components, for each of the three GPS networks in Japan, for the four seasonal periods.

Day of the year	Hokkaido			Tokai			Kyushu		
	Standard deviations of the coordinate components (mm)								
	σ_φ	σ_λ	σ_h	σ_φ	σ_λ	σ_h	σ_φ	σ_λ	σ_h
001-007	1.2	1.1	6.6	2.8	4.4	12.2	1.6	2.4	5.7
091-097	1.3	1.6	7.5	3.0	2.9	11.5	2.0	1.4	6.1
181-187	2.3	1.7	6.7	4.0	4.0	17.2	2.5	1.8	8.7
271-277	1.2	1.6	6.6	1.8	1.4	7.1	1.9	1.3	5.8

Daily Result from the Hokkaido Network

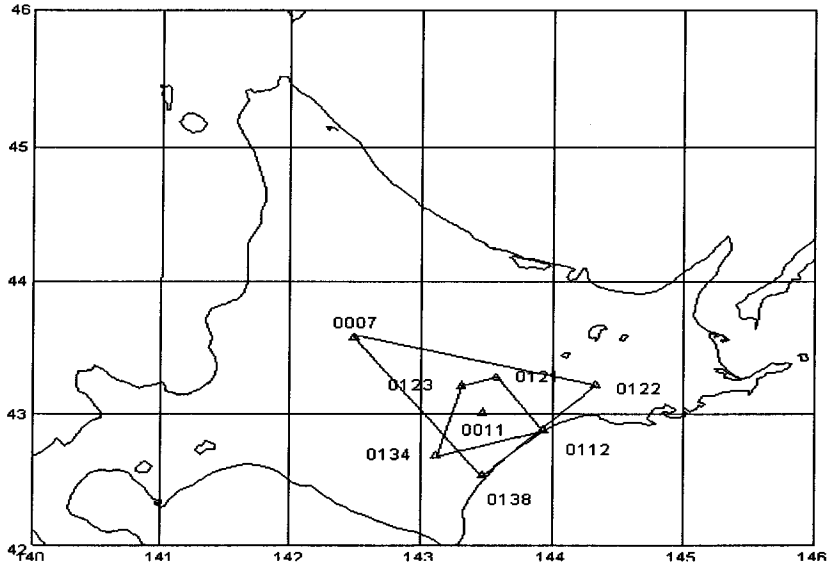

Figure 6-2. Hokkaido GPS network, stations numbered 0112, 0134, 0123 and 0121 are the reference stations for sub-net 1, and 0007, 0138 and 0122 are the reference stations for sub-net 2. The user receivers are assumed to be at stations 0121, 0123 and 0011.

The Hokkaido GPS network comprises 8 stations (Figure 6-2), grouped into two test arrays with user-reference baseline lengths of 41km (0112-0011; in sub-net 1) and 100km (0007-

0011; in sub-net2) respectively. Sub-net 1 consists of both a 3 reference station (0112-0123-0134) or 4 reference station (0112-0121-0123-0134) test network configuration. (Both the 3 and 4 reference station configurations were tested in order to determine if there was any impact on the baseline accuracy.) Sub-net 2 consists of a 3 reference station (0007-0138-0122) test network.

Two sets of results were obtained from the analysis of the Hokkaido network data. The first set compares the difference between the daily computed (dual-frequency, ionosphere-free) solution to the single-frequency results. The second set focuses on the 'fast static' results and how they vary from season to season.

The single-frequency results with 'correction terms' are listed in Table 6-2, using 28 days of data (DoY 001-007, 091-097, 181-187 and 271-277, in year 1997) to compute the offset (and standard deviations) of the latitude, longitude, height and baseline length components against the 'known' dual-frequency results for the three baselines 0007-0123, 0007-0121 and 0007-0011.

Table 6-2. Hokkaido GPS test: a comparison of the 'true' dual-frequency (ionosphere-free) results and the single-frequency results (with 'correction terms') for three different baselines.

Base-line / DoY	0007-0123 (77km)	0007-0121 (93km)	0007-0011 (100km)
001-007	-5.1±2.1$^{\alpha}$	-3.8±0.9	8.5±1.6
	-1.5±1.6$^{\beta}$	0.3±0.7	-5.9±0.8
	-6.1±10.0$^{\chi}$	-14.7±9.0	-0.2±6.7
	-3.9±2.0$^{\delta}$	1.7±0.7	-10.0±0.8
091-097	-5.1±2.1	-3.8±0.9	9.7±2.5
	-1.5±1.6	0.3±0.7	-6.8±1.3
	-6.1±10.0	-14.7±9.0	-2.4±11.0
	-3.9±2.0	1.7±0.7	-11.4±2.2
181-187	-1.7±2.5	0.3±3.2	10.9±3.4
	0.6±1.0	-1.2±2.3	-6.9±1.8
	-10.7±12.8	-0.5±15.4	-2.9±15.0
	-1.3±1.9	-1.2±2.5	-12.3±3.0
271-277	-2.8±1.4	-2.5±0.9	11.2±3.0
	0.6±1.4	-0.2±1.2	-5.9±1.5
	-1.1±7.7	11.3±7.1	-8.0±9.6
	-0.9±1.1	0.8±1.3	-11.6±2.6

Units in mm; α, β, χ and δ represent the offset and variation in latitude, longitude, height and baseline length components against the 'known' dual-frequency results.

Table 6-3 summarises the results for user station 0011 (sub-net 1) when computed using both the 3 and 4 reference station network configurations.

Table 6-3. Hokkaido GPS test: using different number of reference stations to compute 'correction terms' for baseline 0011-0112 (Units in mm).

Base-line / DoY	0011-0112(42km)	
	3 reference stations (0112, 0134, 0123)	4 reference stations (0112, 0134, 0123 and 0121)
001-007	-9.8±0.6 5.4±0.6 2.1±3.9 8.6±0.7	-9.4±0.7 5.2±0.6 6.3±5.8 8.4±0.5
091-097	-9.1±1.0 4.6±0.6 -7.3±4.9 7.6±0.6	-7.9±2.3 4.3±1.2 -5.9±2.4 6.9±1.9
181-187	-8.4±6.1 2.9±2.6 -14.2±11.8 5.7±4.4	-7.9±6.0 3.1±2.8 -9.3±10.0 5.7±4.6
271-277	-9.6±0.7 4.7±0.8 -9.4±3.5 7.7±0.9	-9.2±0.6 4.6±0.8 -6.4±4.1 7.6±0.8

From Tables 6-2 and 6-3, the following comments can be made:

- Using the proposed algorithm for integrated single- and dual-frequency receiver processing, the results for the horizontal components (latitude, longitude, baseline length) are less than **12mm** different to those obtained using the standard dual-frequency processing algorithm, while the difference in the results for the height component is less than **15mm**, even when the baseline length is up to 100km.
- There is no obvious difference in the quality of the results obtained using 3 or 4 reference stations (Table 6-3). For example, in the case of the first result (DoY 001-007), the offsets of the horizontal components are –9.8, 5.4, 8.6mm using of 3 reference station processing, and –9.2, 5.4, 8.4mm using 4 reference station processing method.

'Fast Static' Results from the Hokkaido Network

The objective of the 'fast static' experiment was to test the performance of the proposed methodology for medium-range rapid GPS positioning using single-frequency receivers. All of the Hokkaido GPS data were split into 240 epochs per file, resulting in 12 files per day. These were processed one at a time to gauge the repeatability of the user station coordinates derived using these comparatively short observation spans (2 hours). In Figure 6-3 the 334 positioning results for the user station 0011, comparing 3 (0112, 0134, 0123)

and 4 reference station processing (0112, 0134, 0123 0121), for the periods (day-of-year) 001-007, 091-097,181-187 and 271-277, are shown.

The 'fast static' results indicate no obvious difference in using the 3 or 4 reference station configurations (confirming the results of Table 6-3). However, the DoY 181-187 results exhibit larger variations compared to the other seasons.

Comparing the daily (Table 6-3) and 'fast static' results (Figure 6-3), the variation is less than 3 mm in the horizontal components and 1cm in the height component, but the offset is almost the same. As expected, the longer the observation session, the smaller is the solution variation.

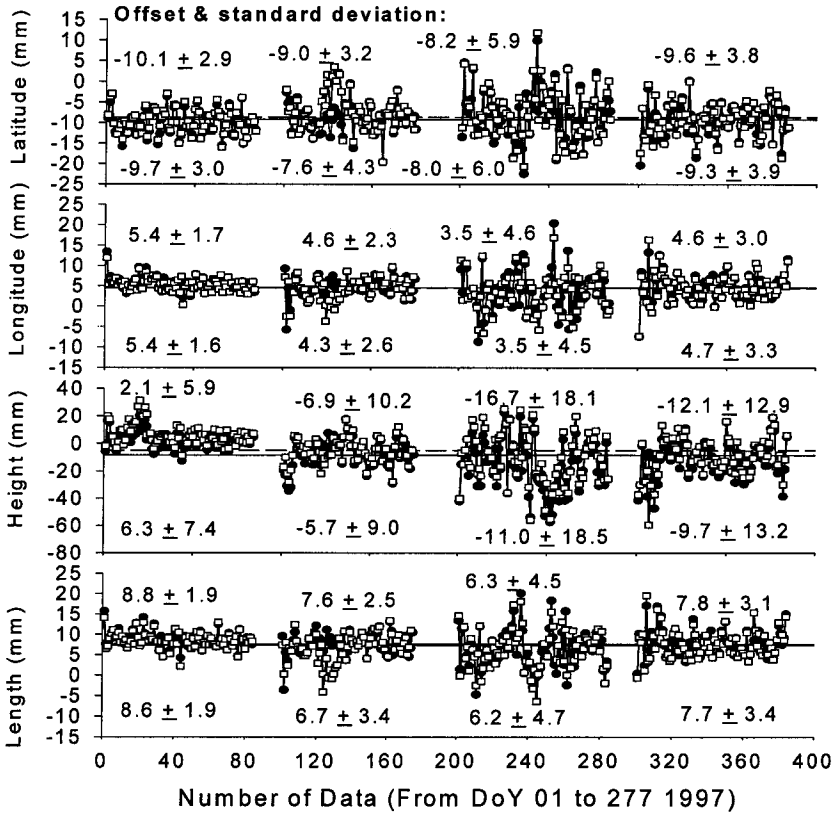

Figure 6-3. The offset and variability of the three baseline components and the baseline length. The upper values refer to the positioning result using 3 reference station processing, while the lower values refer to the positioning result using 4 reference station processing.

Daily Result from the Tokai Network

The Tokai GPS network consists of 7 stations (Figure 6-4). This area has significant height differences, for example from the west (3072) of the network to the east (3034) the elevation change is 1450m in just 63km of distance. Two sub-nets were considered,

reference stations 0264-3053-3032 and 3072-3053-3032. The coordinate repeatability for user stations 3066, 3034 and 5105 was studied.

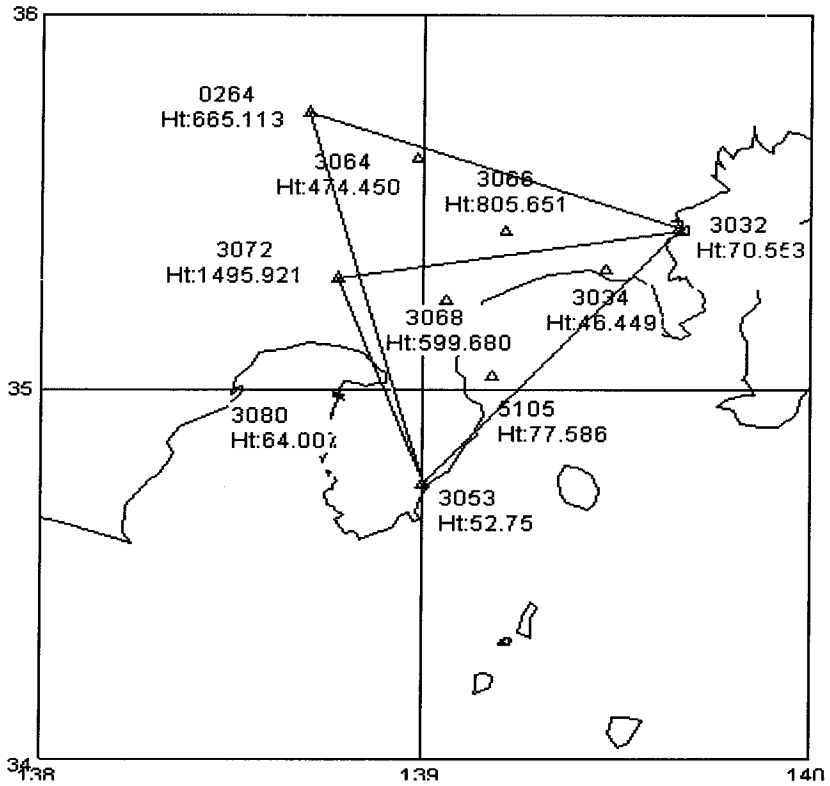

Figure 6-4. The Tokai GPS network traverses two distinct terrains. From point number 3034 along the coastline to 3080 the average station elevation is only 65m, while the western side is mountainous and the average station elevation there is nearly 800m.

Tables 6-4 and 6-5 show the positioning results for the 3 user stations from two different reference stations (Table 6-4 & 6-5 are arranged in a similar format to Table 6-2). The approximate distance from reference station 3072 to the user stations 3066, 5105 and 3034 is 41km, 47km and 63km respectively (Table 6-4), and from reference station 0264 to the user stations 3066, 3034 and 5105 the distances are 58km, 84km and 89km respectively (Table 6-5).

Table 6-4. Tokai GPS test: a comparison of the 'true' solutions based on dual-frequency (ionosphere-free) processing and single-frequency processing (with 'correction terms' generated using 3072-3032-3053 as reference stations) (Units in mm).

Baseline / DoY	3072-3066 (41km)	3072-5105 (47km)	3072-3034 (63km)
001-007	0.2±1.7	-1.7±3.2	-0.7±2.0
	3.5±3.3	3.6±2.1	2.4±2.0
	-7.7±6.9	0.7±11.0	-4.6±10.8
	3.2±3.4	3.8±1.7	2.4±2.1
091-097	-0.6±1.0	-2.6±2.7	-1.4±1.4
	-2.0±5.0	2.8±5.1	2.0±6.0
	-16.5±5.8	5.2±10.5	-2.5±6.0
	1.5±5.0	3.7±3.1	1.9±6.1
181-187	0.0±1.4	-0.2±6.7	0.1±2.6
	1.3±4.1	1.9±3.9	0.5±2.5
	7.2±12.0	-13.0±11.1	-14.0±6.8
	1.2±3.9	2.0±6.7	0.8±2.5
271-277	-1.2±1.3	-1.7±1.3	-1.6±1.4
	-0.5±2.2	-0.6±2.7	0.6±1.9
	10.9±9.1	-1.2±8.7	-4.9±12.0
	-0.9±2.4	1.6±2.8	0.6±2.0

Table 6-5. Tokai GPS test: a comparison of the 'true' solutions based on dual-frequency (ionosphere-free) processing and single-frequency processing (with 'correction terms' generated from the larger reference network 0264-3032-3053) (Units in mm).

Baseline / DoY	0264-3066 (58km)	0264-5105 (89km)	0264-3034 (84km)
001-007	-5.0±2.7	-6.4±2.4	-8.4±2.9
	-4.9±3.7	-6.4±3.3	-8.1±2.7
	30.5±13.7	-19.0±12.7	-16.8±10.1
	-0.7±2.1	-2.5±1.7	-2.1±2.4
091-097	-5.6±3.5	-9.7±2.8	-9.6±0.9
	-10.0±1.1	-11.0±1.2	-11.6±1.4
	31.6±9.6	-11.6±17.3	-19.1±9.2
	-4.4±0.9	-3.1±2.8	-4.3±1.2
181-187	-3.8±3.5	0.7±6.2	1.0±4.0
	-0.7±4.1	0.2±3.6	-0.7±1.9
	31.0±15.3	-9.1±15.4	-13.1±11.1
	-2.6±3.9	-0.5±6.9	-1.1±2.2
271-277	-1.6±0.9	-4.5±1.3	-5.0±1.6
	-9.4±1.5	-10.3±0.9	-10.4±1.7
	32.6±8.8	-8.4±10.4	-14.7±10.4
	-6.3±1.5	-1.0±1.2	-5.8±1.4

Comparing the results of Tables 6-4 and 6-5, it is evident that the results obtained from the less extensive network (Table 6-4) are significantly better than those obtained using the more extensive network (Table 6-5). In the case of the smaller network, an accuracy of 3mm in the horizontal components and 15mm in the height component was obtained, while the corresponding results from the larger network are 15mm in horizontal and 33mm in height.

'Fast Static' Results from the Tokai Network

Two hours of single-frequency data were used for these experiments. There are almost 1000 data files (28days*12files*3stations) to be processed, and results can be compared with the known coordinate values for the user stations 3066, 5105 and 3034. The results are summarised in Table 6-6 (this table is arranged in a similar format to Table 6-2).

Table 6-6. The 'fast static' results for the three user stations compared to the 'true' results (same format as Tables 6-4 and 6-5) (Units in mm).

Base-line / DoY	0264-3066 (58km)	0264-5105 (89km)	0264-3034 (84km)
001-007	-5.1±4.3	-6.6±4.4	-8.7±5.1
	-4.7±4.6	-6.2±4.1	-7.8±4.8
	28.5±22.2	-18.3±21.7	-16.3±20.1
	-0.8±4.2	-2.5±1.7	-2.4±4.1
091-097	-5.8±4.4	-6.5±3.5	-9.8±4.2
	-1.0±4.0	-12.6±3.5	-10.8±4.4
	31.9±19.8	-18.8±17.5	-19.0±19.1
	-4.3±5.0	-0.4±3.9	-4.2±4.2
181-187	-3.4±7.0	1.6±8.0	1.0±6.9
	-0.1±6.3	-0.4±8.0	-0.9±6.2
	32.7±32.1	-9.0±34.8	-6.8±23.7
	-1.7±6.3	-1.7±7.8	-1.4±6.0
271-277	-1.7±4.6	-4.9±4.3	-5.3±4.9
	-9.5±4.0	-10.5±4.0	-10.5±4.0
	28.3±22.9	-8.9±18.0	-15.6±18.6
	-6.3±4.7	-0.9±4.3	-5.8±4.5

Comparing the daily result (Table 6-5) and the 'fast static' result (Table 6-6), the variation in the horizontal components is less than 3mm, and less than 2cm for the height component. The offset is similar. For example, for the first result (DoY 001-007), the offsets of the latitude, longitude, height and baseline length components are –5.0, -4.9, 30.5 and -0.7mm in the daily result, and –5.1, -4.7, 28.5 and –0.8mm for the 'fast static' results. The variability of the latitude, longitude, height and baseline length components is 2.7, 3.7,

13.7 and 2.1mm in the daily result, and 4.3, 4.6, 22.2 and 4.2 in the 'fast static' result respectively. These results are similar to those presented in section 3.1.1.

Daily Result from the Kyushu Network

The Kyushu GPS network is composed of 7 stations (Figure 6-5). This area has provided the best positioning results from these GEONET tests. The offset and variation of the residual vectors are smaller than the other networks in the case of daily processing (Table 6-7). Data at station 0466 in the DoY 001-007 session was missing. The reference stations were defined by stations 0479-0464-0474, and these were then used to determined the position of the user stations 0478, 0466, 0465 and 0475 with respect to reference station 0479. From Table 6-7, the largest offset in the horizontal components is only 3.4mm, and 16.3mm in the case of the height component. The largest variation in the horizontal components is 5.3mm, and 12.0mm in the height component.

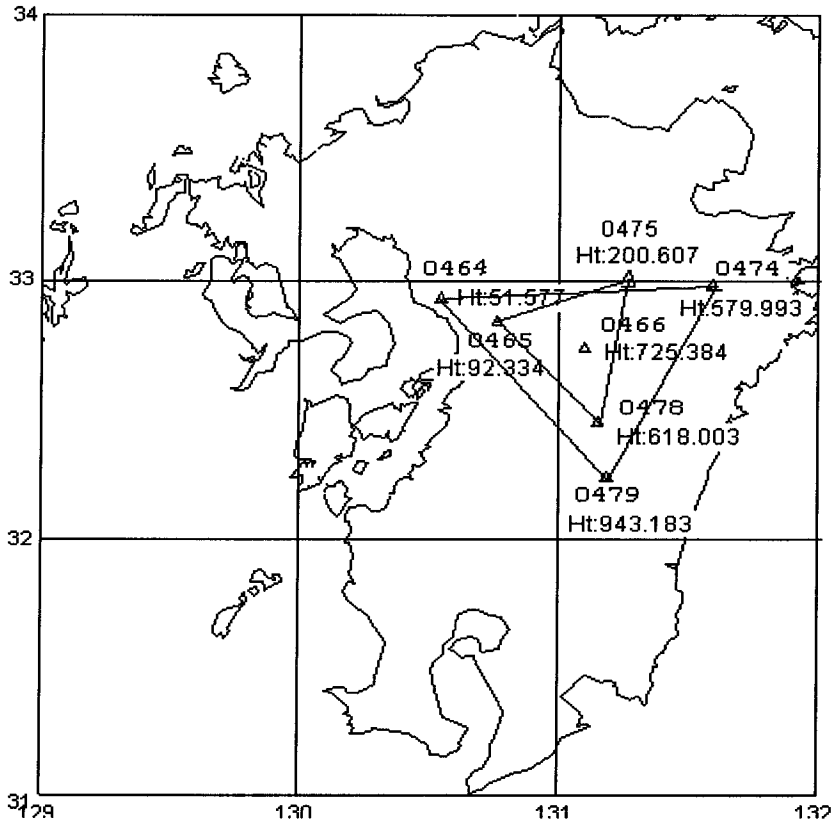

Figure 6-5. Kyushu GPS network. The points numbered 0479-0464-0474 were assumed to be the reference stations for the tests.

Table 6-7. Kyushu GPS test: a comparison of the 'true' dual-frequency (ionosphere-free) and the single-frequency (with 'correction terms') results, various baselines (Units in mm).

Base-line / DoY	0479-0478 (23km)	0479-0466 (55km)	0479-0465 (77km)	0479-0475 (90km)
001-007	-2.2±1.7 -0.2±2.9 -0.7±5.4 2.1±1.8	*N/A	-1.0±2.4 -0.3±3.3 -4.3±7.1 0.8±3.4	3.3±1.5 0.9±3.0 -16.3±10.0 -3.4±0.9
091-097	-1.1±0.4 -0.4±0.9 -5.2±8.6 1.0±0.5	-0.2±2.5 -0.4±1.5 -0.6±7.9 0.3±2.5	0.1±4.0 -1.4±2.9 -0.5±12.7 -0.9±4.8	-0.1±2.9 -0.8±2.7 -1.6±12.0 -0.4±2.6
181-187	-1.3±1.6 -0.4±1.8 -5.1±5.7 1.2±1.5	-1.0±2.2 1.0±1.9 -3.1±3.4 -0.9±2.9	0.8±1.8 -0.4±1.7 -8.7±8.3 -1.1±1.9	1.7±2.3 1.4±5.3 6.9±10.6 0.9±2.6
271-277	-0.9±1.7 -0.5±2.0 -0.9±7.7 0.8±1.9	-0.3±3.6 -0.6±1.8 -10.1±2.4 0.3±3.6	-0.6±2.5 -1.7±1.6 3.0±8.0 -0.3±2.5	0.3±3.3 -0.8±2.8 -13.1±10.3 0.9±3.4

*N/A: There are no data at station 0466, for the day of year 001-007, 1999

'Fast Static' Results from the Kyushu Network

All of the Kyushu GPS data sets were split into 240 epochs per file (corresponding to 2hr spans, resulting in 12 files per day). They were processed one at a time to gauge the repeatability of the user station coordinates derived using comparatively short observation spans. Two sub-nets were considered (Figure 6-5): reference stations 0479-0464-0474 ('outer'), and 0478-0465-0475 ('inner'). The coordinate repeatability for user station 0466 was studied. A summary of the positioning result is provided in Tables 6-8 and 6-9.

Table 6-8. Kyushu GPS test: user coordinate solutions (compared to 'true' values) using different reference station configurations to compute 'correction terms' (Units in mm).

Base-line / DoY	0466 (From 0478 inner network) (32km)	0466 (From 0479 outer network) (55km)
181-187	0.2±5.7 0.9±3.6 7.3±20.6 -0.1±5.7	1.1±6.0 1.4±4.5 2.3±18.6 -0.8±6.0
271-277	-2.3±4.5 0.5±2.8 2.2±16.0 2.3±4.5	1.5±5.7 0.5±3.2 5.6±15.8 -1.5±5.6

Table 6-9. Kyushu GPS test: a comparison of the dual-frequency (ionosphere-free) results and single-frequency (with 'correction terms') results (different baseline lengths) (Units in mm).

Base-line / DoY	0479-0478 (23km)	0479-0466 (55km)	0479-0465 (77km)
001-007	-2.0±0.6 4.1±5.4 -6.4±15.5 2.0±4.2	*N/A	-0.9±4.4 0.2±4.0 -4.8±17.0 0.7±5.1
091-097	-2.4±3.5 -0.2±3.1 -7.4±15.6 2.3±3.5	-0.7±4.7 -0.5±4.3 1.3±19.0 0.8±4.9	0.1±5.3 -1.7±5.0 -1.2±20.6 -0.8±6.1
181-187	-0.4±6.3 0.4±4.1 -4.8±24.9 0.5±6.2	1.1±6.0 1.4±4.5 2.3±18.6 -0.8±6.0	0.8±5.7 -0.5±4.8 -8.8±21.0 -1.0±5.8
271-277	-2.0±5.2 -0.5±3.6 -5.2±15.7 1.9±5.2	1.5±5.7 0.5±3.2 5.6±15.8 -1.5±5.6	-0.6±4.3 -1.7±3.5 5.2±13.1 -0.3±4.8

*N/A: There are no data at station 0466, for the day of year 001-007, 1999

6.2.2 The different receiver data set: Sydney, Australia

Eight stations were occupied by four dual-frequency and four single-frequency receivers, Day-of-Year 119 (1999), logging data at 1Hz, for a 2 hour observation period. Three Leica CRS1000 dual-frequency receivers were set up at the reference stations, one Leica SR399 dual-frequency receiver was set up near the station BASE, and four single-frequency GPS systems occupied the user stations (three Canadian Marconi GPS receivers, and one Ashtech GG24 receiver), as shown in Figure 6-6.

Data processing was divided into two parts. First, use the modified Bernese GPS software to compute the relative positions of the reference receivers and station BASA (all occupied by dual-frequency receivers). Then generate the 'correction terms', to be applied to the single-frequency receivers (BASE, PIL5, SLV1 and SLV2). The station BASA is close to the single-frequency stations (<10km), hence the relative positions of BASE, PIL5, SLV1 and SLV2 can be determined precisely using conventional techniques (i.e. without using 'correction terms'). Second, apply the 'correction terms' in order to compute the coordinates of the single-frequency stations with respect to the reference station 'Wollongong'. Hence, the accuracy of the user stations can be compared, using the conventional (local) positioning method on the one hand, and the reference station network-based algorithm on the other hand.

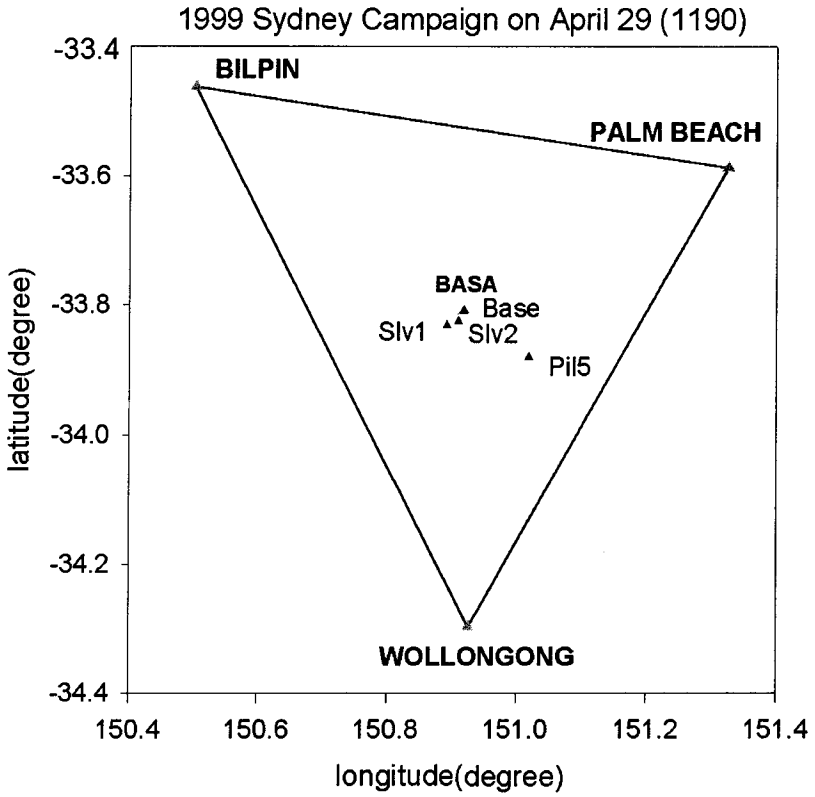

Figure 6-6. Configuration of the reference stations and the user stations.

The results for the 2hr processing are shown in Figure 6-7. The differences in the coordinates of the user stations computed by the two methods is less than 8mm for the horizontal components, and 15mm for the height component.

To test the repeatability of the single-frequency positioning results obtained using the 'correction terms', the data was cut into 20 minute observation sessions. The results for the user stations BASE (bottom plot) and PIL5 (upper plot) are shown in Figure 6-8. The horizontal components (latitude, longitude and baseline length) appear to be accurate at the 8mm level, and the height component difference is less than 3cm from that obtained for the 2hr result. The repeatability refers to two different sets solutions from 20min/session processing for a 47km baseline (Wollongong-PIL5) and a 54km baseline (Wollongong-BASE). The x-axis represents session number, and the y-axis is in linear units of mm. The zero value is computed from the 2hr session result (with 'correction terms').

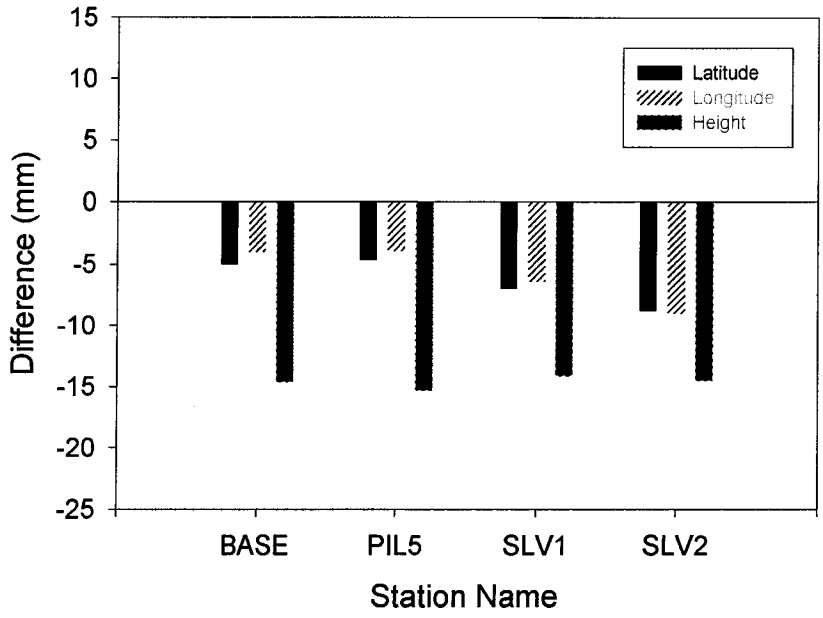

Figure 6-7. Sydney GPS test: comparing the coordinate results for the user stations obtained from single-frequency processing of the 2hr data set with the 'correction terms' generated from the reference stations, and with respect to the new reference station BASA (without 'correction terms').

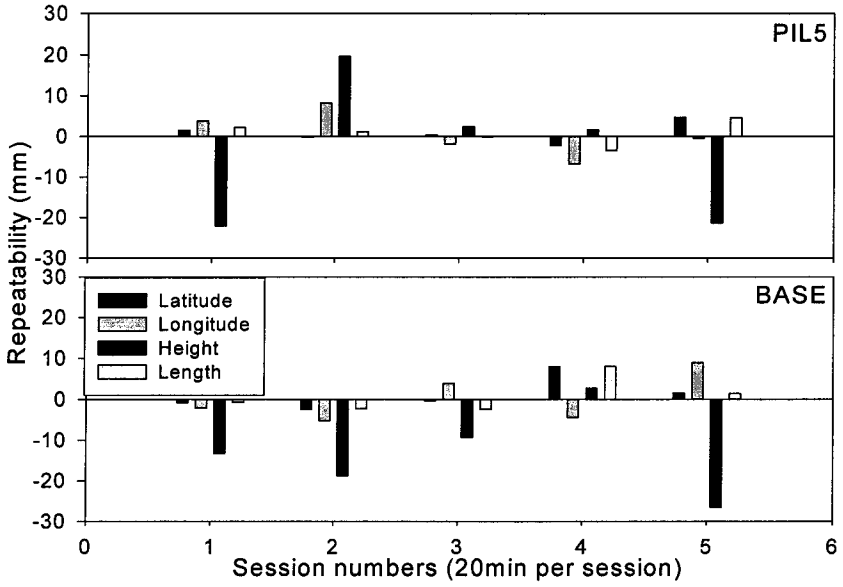

Figure 6-8. Sydney GPS test: comparing the result obtained from single-frequency processing of the 20min data sets at the stations BASE and PIL5, with respect to the 2hr session.

This result indicates that low-cost GPS receivers, using comparatively short observation sessions, when processed with 'correction terms' derived from a multi-reference station network, are capable of producing accurate results, even for baseline lengths up to 50km.

6.2.3 The practical data set: Network in Tsukuba, Japan

The test network consisted of 14 stations (Figure 6-9), six of them were GEONET permanent stations (960582, 93002, 93006, 960584, 93012 and 960583), and the remaining 8 stations were user stations additionally located within this permanent network. Pairs of stations were established for sharing (or swapping) two kinds of receivers: (a) dual-frequency Trimble 4000SSi receivers, and (b) single-frequency Canadian Marconi Corp. (CMC) receivers. Hence, four pairs of stations, all equipped with both CMC and Trimble 4000SSi receivers, with antennas atop two closely spaced tripods, were set up as user stations. The tripods initially occupied by the Trimble antennas are designated YATT, GOKT, HOJT and NIIT. The tripods initially occupied by the CMC antennas are designated YATA, GOKA, HOJO and NIIH.

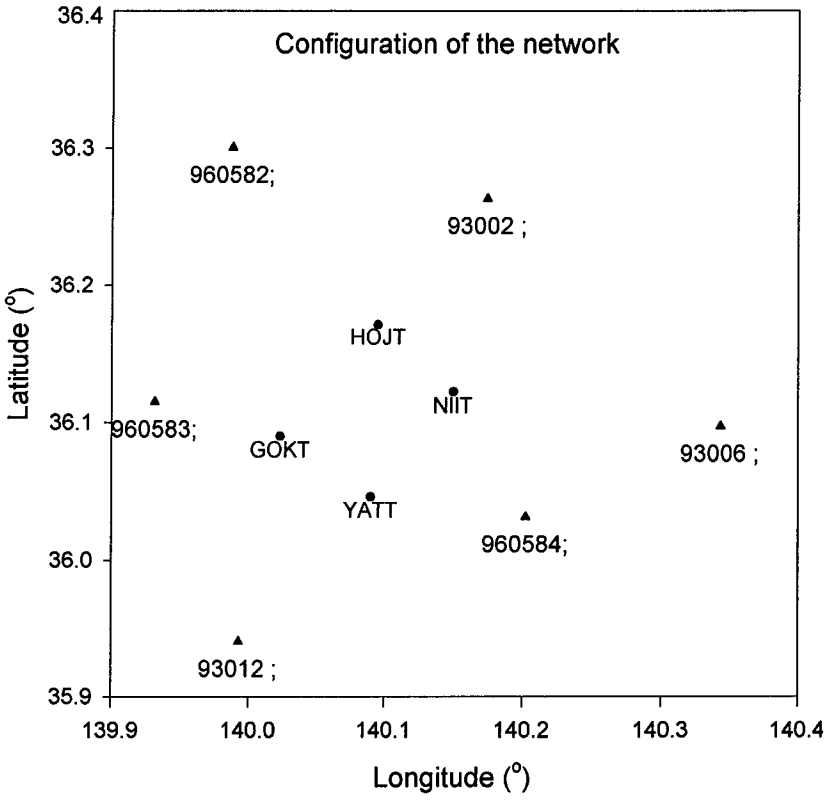

Figure 6-9. Tsukuba GPS test network (GEONET and temporary user stations).

Long Session Results

Table 6-10 shows the mean values and standard deviations for the 8 stations, in the case of the long session result (data files 8hr-24hr in length). The coordinate of station 3012 was held fixed. Table 6-10 is arranged in a similar format to Table 6-2. The 'true' coordinate values were computed from the processing of the data from the whole campaign (DoY 214 to 224, 1999). Some stations were only occupied once, and therefore no standard deviation value is shown.

Comparing the mean values and standard deviations of the dual-frequency processing with those of the single-frequency processing (with 'corrections'), there is no apparent difference in the horizontal components (latitude, longitude and length). However, in the case of the height component there are larger variations for the single-frequency results, most noticeably at station GOKA.

In order to compare the single-frequency and the dual-frequency relative positioning capabilities, three stations (HOJT, GOKT and YATT) were equipped with an antenna splitter device which enabled two receivers to share the same antenna. The results are listed in Table 6-11 (this table is arranged in a similar format to Table 6-2). According to the results in Table 6-11, the horizontal components (latitude, longitude and baseline length) display no obvious difference, but the height component is 9mm worse in the case of the single-frequency processing (with 'corrections').

Table 6-10. Tsukuba GPS test: comparing dual-frequency and single-frequency (with 'corrections') results for 8 user stations (latitude, longitude, height and baseline length components).

Component / Station	Freq.	Obs.	Latitude (mm)	Longitude (mm)	Height (mm)	Length (mm)
YATA (12.9km)	Dual	1	-3.0	3.0	-1.4	-0.7
	Single	5	1.6±5.5	-3.2±2.5	-11.0±5.2	-0.5±5.8
YATT (12.9km)	Dual	4	1.2±0.7	-1.0±1.7	0.9±3.2	0.4±1.5
	Single	2	1.9±0.2	0.1±4.7	-13.4±4.5	1.6±2.8
GOKA (14.4km)	Dual	N/A				
	Single	5	-0.8±1.8	0.0±2.7	-24.3±4.7	-0.8±1.6
GOKT (14.4km)	Dual	4	0.6±2.5	-0.5±1.6	0.4±6.4	0.5±2.4
	Single	2	3.6±0.2	2.1±2.2	-9.6±1.9	3.6±0.4
NIIH (26.1km)	Dual	1	-2.3	1.1	-7.0	-1.3
	Single	2	-3.3±7.9	-2.3±1.6	20.7±4.5	-4.0±7.4
NIIT (26.1km)	Dual	4	1.5±1.2	-0.5±1.1	2.1±10.1	1.1±1.6
	Single	1	-1.6	1.3	13.5	-0.4
HOJO (27.2km)	Dual	N/A				
	Single	4	-5.1±1.8	-6.9±0.8	-1.4±8.3	-7.0±1.8
HOJT (27.2km)	Dual	4	0.6±0.9	-0.4±0.9	0.0±6.5	0.4±1.0
	Single	1	-5.4	-4.9	-4.0	-6.7

Table 6-11 represents the single-frequency results (with 'correction terms') when the antenna splitter was used. Compared with Table 6-10, these splitter results suggest the same accuracy as the dual-frequency results. The offset values and standard derivation have the same characteristic as the dual-frequency results. There is no obvious difference between the dual-frequency and single-frequency results.

Table 6-11. Splitter results for 8 user stations in the Tsukuba test network (latitude, longitude, height and baseline length components) (compare with Table 6-10).

Comp. / Freq.	Latitude (mm)	Longitude (mm)	Height (mm)	Length (mm)
Dual	1.9±2.2	-0.6±1.7	3.1±4.9	1.7±2.1
Single	2.9±1.1	0.3±3.4	-11.9±4.2	2.3±2.3

Hourly Session Results

The original observation files were divided into hourly sessions. For this testing period there were 387 dual-frequency (Trimble 4000SSi) data files and 475 (single-frequency CMC) data files. (The CMC receivers continued to log data during the weekend of 7-8 August 1999, hence there are more single-frequency data files than dual-frequency data files.) Table 6-12 lists the ambiguity success rate and the standard deviations of relative positioning (this table is arranged in a similar format to Table 6-2).

Table 6-12. Hourly results (in terms of standard deviations of components and ambiguity resolution success rates) for both dual-frequency processing and single-frequency processing (with 'corrections').

Comp. / Freq.	Ambiguity success rate	Latitude (mm)	Longitude (mm)	Height (mm)	Length (mm)
Dual	91% (387/35)	0.6±5.5	0.0±6.4	-3.2±22.9	0.5±5.3
Single	99% (475/4)	0.2±5.9	-2.3±5.9	-9.9±18.0	-0.8±5.8

The QIF (Quasi Ionosphere-Free) method was used to fix the integer ambiguities for the dual-frequency receivers, while a search method was used for the single-frequency receiver ambiguity resolution. The results obtained indicate a similar variation in the different components of the single- vis-a-vis dual-frequency processing. However, what is notable is that the processing of single-frequency data resulted in a higher ambiguity success rate than those of the dual-frequency processing. This could be explained by the fact that the dominant distance dependent biases (such as due to the ionosphere, the troposphere and satellite orbit error) have been effectively reduced by the 'correction terms' used in the single-frequency processing.

6.2.4 Concluding remarks

In this section a range of data sets, from different GPS networks, with different geographical locations, traversing large elevation changes, from different seasons of the year, employing different types of receivers, with varying observation session spans, and different baseline lengths, have been processed to investigate the performance of the linear combination model proposed by Han & Rizos (1997b). As a result, the following conclusions can be drawn:

1. The results obtained from long observation spans are similar for the single-frequency data processing (with 'correction terms') and the dual-frequency data processing in the case of the horizontal baseline components. However, there appears to be a 1-2cm discrepancy in the height component.
2. In the 'fast static' experiments, the accuracy in the horizontal components is essentially the same as that obtained from long session processing. However, there appears to be a degradation in the height component accuracy of the order of 2-3cm.
3. There is no significant difference in the results obtained by using more than the minimum of three reference stations to generate the 'correction terms'.
4. The shorter the baseline lengths between reference stations, the better the positioning precision. However, within the same reference station network, the same level of precision can be achieved for all baseline lengths.
5. The brand of user receiver does not appear to have an influence upon the overall quality of the solution obtained using this algorithm.

Finally, it appears that this multi-reference receiver data processing methodology can be successfully implemented under a variety of operational environments.

6.3 Real-Time GPS Medium-Range Experiment Results

Carrier phase-based kinematic positioning is one of the most difficult engineering challenges for GPS system developers. Over the past half decade or so several developments have occurred which deliver high accuracy performance in real-time — that is, in the field, immediately after making the measurements (but after the data from the reference receiver has been transmitted to the user receiver's computer for processing). Real-time positioning is nowadays possible when the GPS receiver is in motion (with AR being carried out using a so-called "on-the-fly", or OTF, algorithm). These systems are commonly referred to as RTK systems ("real-time-kinematic"), and for the first time make *feasible* the use of GPS for time-critical applications such as machine control, GPS-guided earthworks/excavations, automated container port operations, etc. Although RTK systems represent the 'state-of-the-art' in GPS technology, able to deliver centimetre level accuracy in real-time using a pair of GPS receivers, there are several conditions that must be fulfilled. These conditions (or constraints) may be so restrictive that they prevent the widespread adoption of precise GPS technology for both engineering surveys (a traditional application of carrier phase-based GPS techniques), as well as for new applications such as precise navigation in support of autonomous robot vehicle operation (identified by many as one of the new 'high growth' applications of GPS).

The advantages of carrier phase-based, multi-reference station GPS positioning techniques can be summarised as:

(a) Rapid static and kinematic GPS positioning techniques can be used over baselines several tens of kilometres in length.

(b) Instantaneous OTF-AR algorithms can be used for kinematic GPS positioning, at the same time ensuring high accuracy, availability and reliability for critical applications.

Hence the question of "how to improve GPS surveying performance?" is answered in various ways. If the baseline length constraint is the crucial factor impacting on static or kinematic GPS, then overcoming this constraint through using multi-reference receiver techniques results in significant performance improvements. If "improving performance" is related to lowering receiver costs, then a multi-reference receiver network would allow the use of single-frequency GPS receivers instead of expensive dual-frequency receivers for static positioning. If the "time-to-AR" is the critical performance indicator, then a multi-reference receiver system would contribute to faster AR (including single-epoch AR) as well as enhance the reliability of AR, even for baselines several tens of kilometres in length. However, as a user, the implementation of a GPS positioning technique based on data from multiple reference stations is much more complicated than the standard single reference receiver scenario.

6.3.1 Sydney 1999

This experiment was carried out on 29 April 1999, using four dual-frequency Leica GPS receivers as the reference network (Figure 6-10). One of the reference stations was located at Wollongong. The other reference station was located at Palm Beach, the third and the fourth were located at Bilpin and Oakdale respectively. In the case of the kinematic experiment, the mobile receiver was mounted on a car and the experiment started at the side of the Motorway No. 4, being 54.12 km, 45.10 km, 54.41 km and 48.14 km away from the Wollongong receiver, the Palm Beach receiver, the Bilpin receiver and the Oakdale receiver respectively. The local reference station, BASE, was also set up near the starting point of the trajectory receiver. Data was collected in static mode for 15 minutes, after which the car was driven along Motorway No. 4 and the Great Western Highway, finishing the experiment in static mode for another 15 minutes, hence concluding a loop (Figure 6-11). The data was collected in two sessions, in the morning and afternoon, with a total of four loops completed. The data rate was 1Hz and a total of 10,587 epochs were processed. The number of observed satellites is plotted in Figure 6-12.

The coordinates of the reference stations were determined using the traditional long-range static positioning procedure and are referenced to the known coordinates of the TIDB station in Canberra. After the integer ambiguities for the L1 and L2 carrier phase observations were resolved, the ambiguity-fixed solution was determined using the ionosphere-free phase combination and the IGS precise ephemeris (IGS, 2001). As a result, the locations of the reference stations can be considered as known.

The Wollongong station was denoted reference station 3, and the Palm Beach and the Bilpin stations were reference stations 1 and 2 respectively (reference station 4 was not used because it was a backup station). The 'correction terms' for the L1 and L2 carrier phase observations are plotted in Figure 6-13 for the satellite PRN 18 (PRN 14 is the reference satellite). In a similar way, the correction terms for the L1 and L2 pseudorange observations can also be determined.

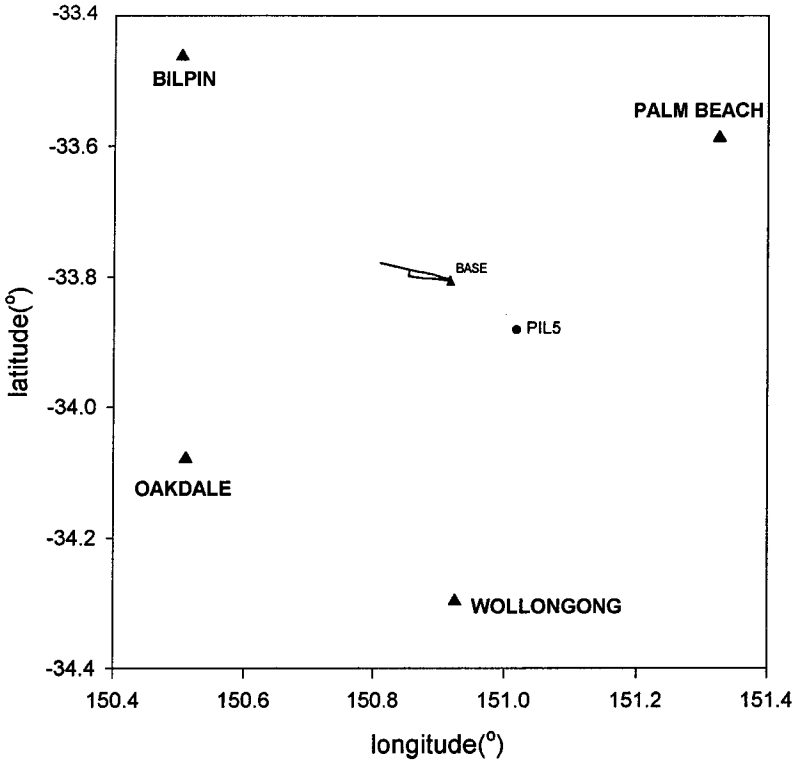

Figure 6-10. Sydney 1999 GPS test: configuration of the reference GPS stations and the mobile receiver trajectory.

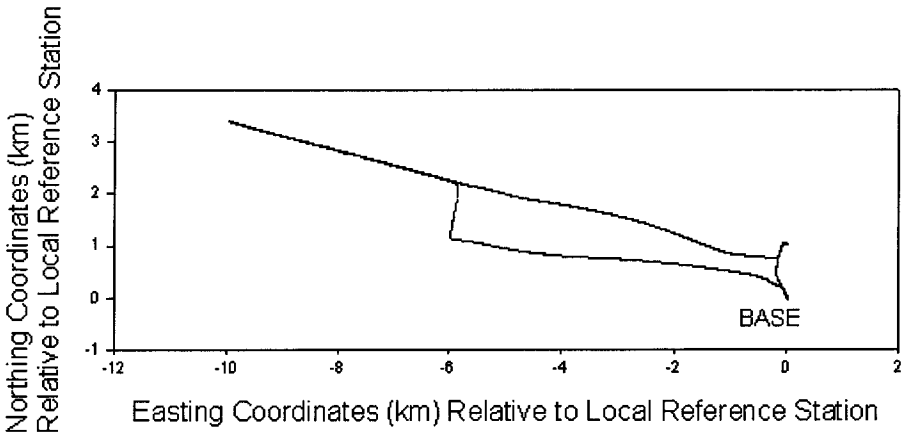

Figure 6-11. Sydney 1999 GPS test: trajectory of the mobile GPS receiver.

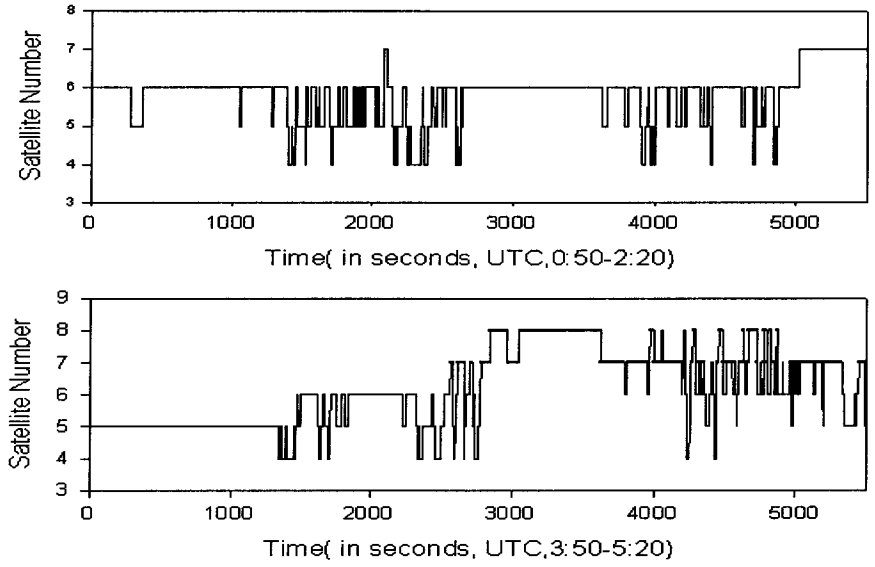

Figure 6-12. The number of observed satellites during the Sydney 1999 GPS experiment.

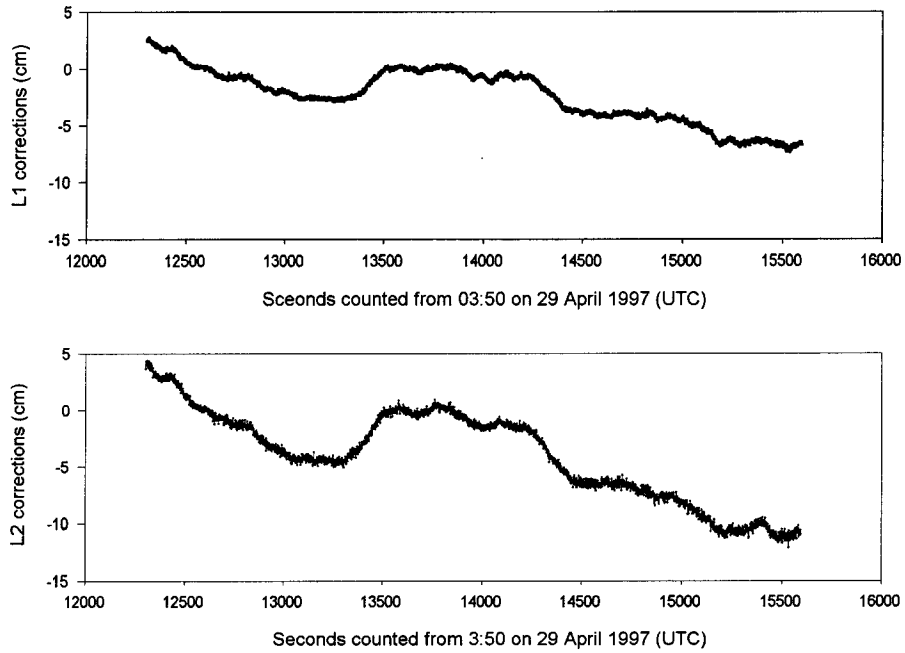

Figure 6-13. Sydney 1999 GPS test: the corrections for double-differenced carrier phase observations for satellite pair PRN 14 and PRN 18.

In the kinematic experiment, in order to compare the performance of multiple reference stations, a set of data was computed using the single-epoch OTF mode, while another set of data was computed by applying the 'correction terms' to the data processing algorithm. A comparison of the results is given in Table 6-13. The 2nd and 4th rows refer to the results obtained from the single-epoch OTF mode (without applying the 'correction terms') from the morning and afternoon sessions respectively. Similarly, the 3rd and 5th rows (bolded)

refer to the results obtained by applying the 'correction terms', for the morning and afternoon sessions respectively.

Table 6-13. Comparison of results in Sydney 1999 GPS kinematic experiment.

Time (UT)	No.of epoch	Correction terms	Correct	Wrong	Reject
0:50-2:20	5273	Yes	5125(97.2%)	0(0.0%)	148(2.8%)
0:50-2:20	5273	No	5037(95.5%)	0(0.0%)	236(4.5%)
3:50-5:20	5314	Yes	5155(97.0%)	0(0.0%)	159(3.0%)
3:50-5:20	5314	No	5075(95.5%)	0(0.0%)	239(4.5%)

6.3.2 Kyushu – 1997

There are two different types of tests of the performance of the multiple reference station algorithm for medium-range single-epoch AR (ie Equation (3-40) and Equation (3-43)). The data was provided by the Kyushu GPS network (Figure 6-14, same as Figure 6-5).

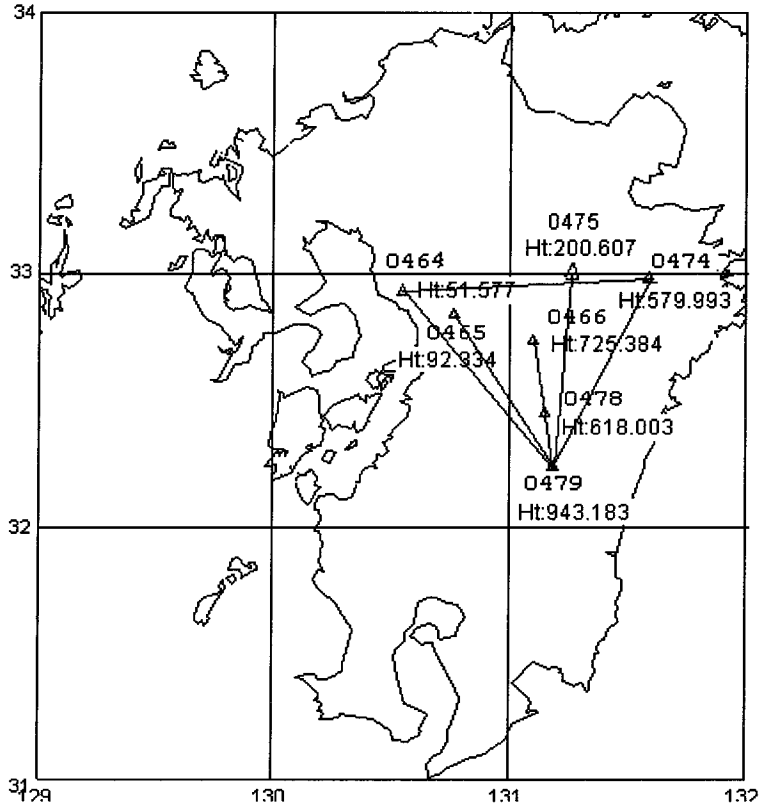

Figure 6-14. Kyushu GPS network consists of 7 stations. The points numbered 0479-0464-0474 are the reference stations, and 0478, 0466, 0465 and 0475 are assumed to be the user stations.

The data was collected on DoY 272, 1997, and all 7 stations were occupied by a Trimble 4000SSI dual-frequency receiver with choke ring antenna. Two different results are based on the same reference stations 0479-0464-0474 (denoted by triangle). The first results used

Equation (3-40), which applied the ambiguity resolution between the user and reference station by a L1& L2 search and used the 'correction terms' from the reference station network. The second results were based on Equation (3-44), which computed the ambiguities between the user and reference station using the ionosphere-free linear combination, after application of the 'corrections' from the reference stations. Figures 6-15, 6-17, 6-19 and 6-21 refer to the first test, and Figures 6-16, 6-18, 6-20 and 6-22 refer to the second test, for the baselines 0479-0478 (23km), 0479-0466(55km), 0479-0465(77km) and 0479-0475(90km) respectively. The daily ionosphere-free linear combination solution is assumed to give the "true" values against which the results are compared.

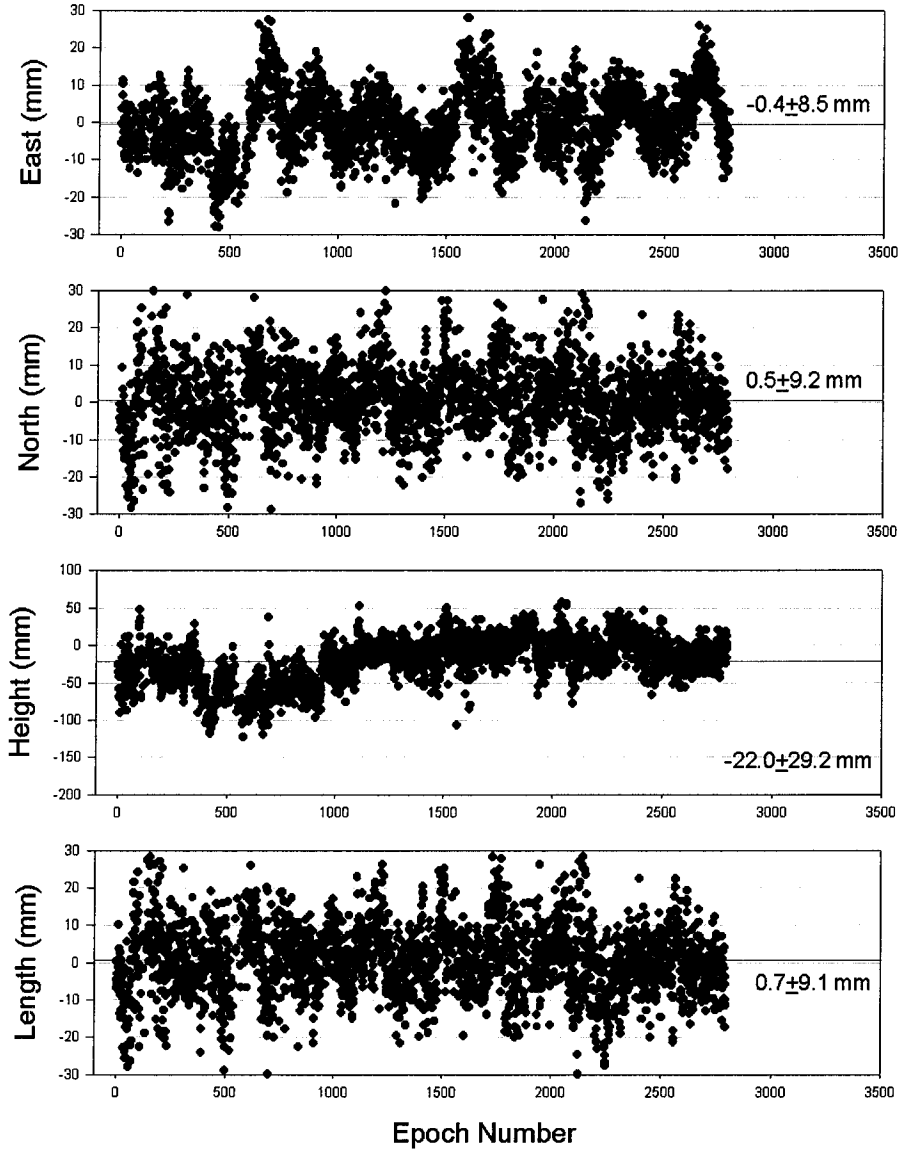

Figure 6-15. Kyushu GPS test: results of single-epoch ambiguity resolution for baseline 0479-0478, using the L1&L2 search. From top to bottom the graphs represent variations in east, north, height and baseline length components, the x-axis denotes the epoch number (data from 00:00:00~23:59:30 29-Sep (272) 1997, 30sec sample rate), and the y-axis represents the difference (between estimated result and true value) in units of mm.

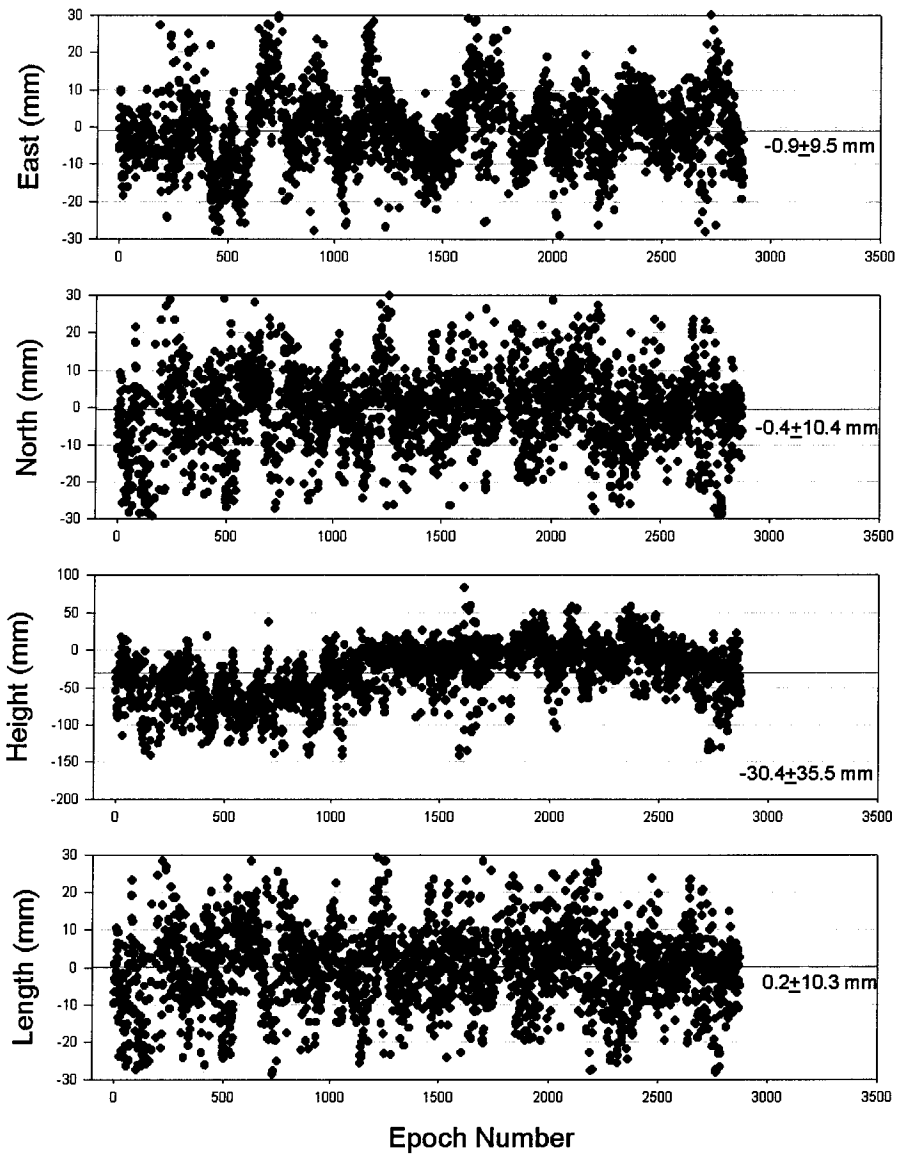

Figure 6-16. Kyushu GPS test: results of the ionosphere-free linear combination for single-epoch ambiguity resolution for baseline 0479-0478. From top to bottom the graphs represent variations in the east, north, height and baseline length components, the x-axis denotes the epoch number (data from 00:00:00~23:59:30 29-Sep (272) 1997, 30sec sample rate), and the y-axis represents the difference (between estimated result and true value) in units of mm.

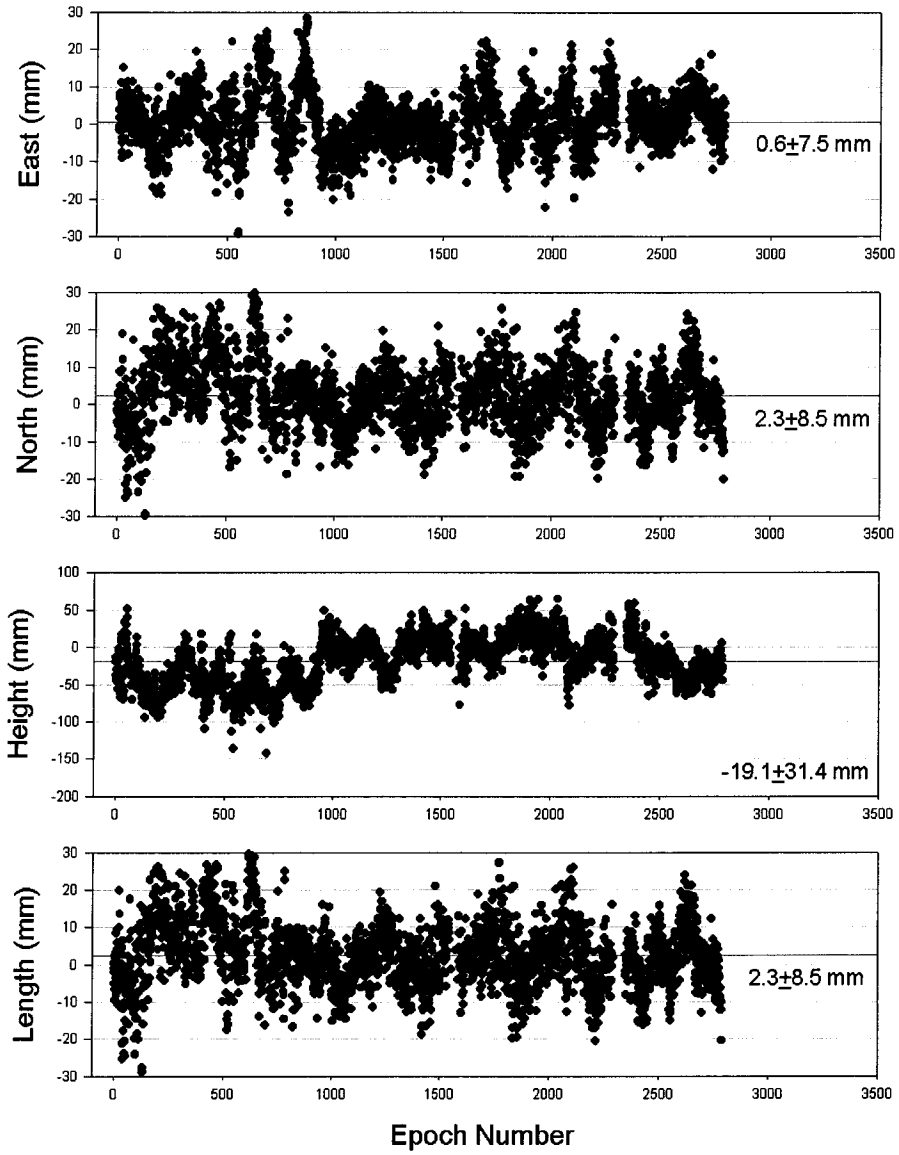

Figure 6-17. Kyushu GPS test: results of single-epoch ambiguity resolution for baseline 0479-0466, using the L1&L2 search. From top to bottom the graphs represent variations in the east, north, height and baseline length components, the x-axis denotes the epoch number (00:00:00~23:59:30 29-Sep (272) 1997, 30sec sample rate), and the y-axis represents the difference (between estimated result and true value) in units of mm.

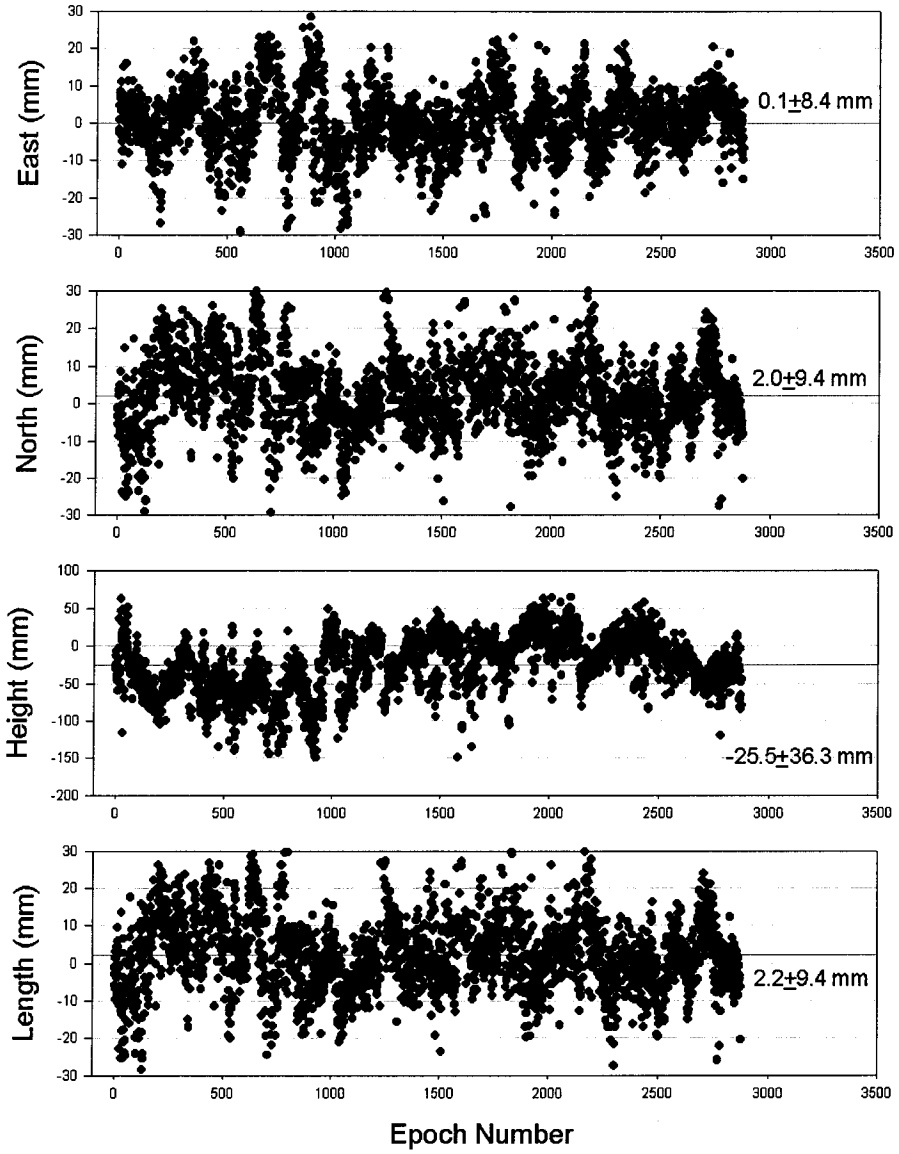

Figure 6-18. Kyushu GPS test: results of the ionosphere-free linear combination for single-epoch ambiguity resolution for baseline 0479-0466. From top to bottom the graphs represent variations in the east, north, height and baseline length components, the x-axis denotes the epoch number (00:00:00~23:59:30 29-Sep (272) 1997, 30sec sample rate), and the y-axis represent the difference (between estimated result and true value) in units of mm.

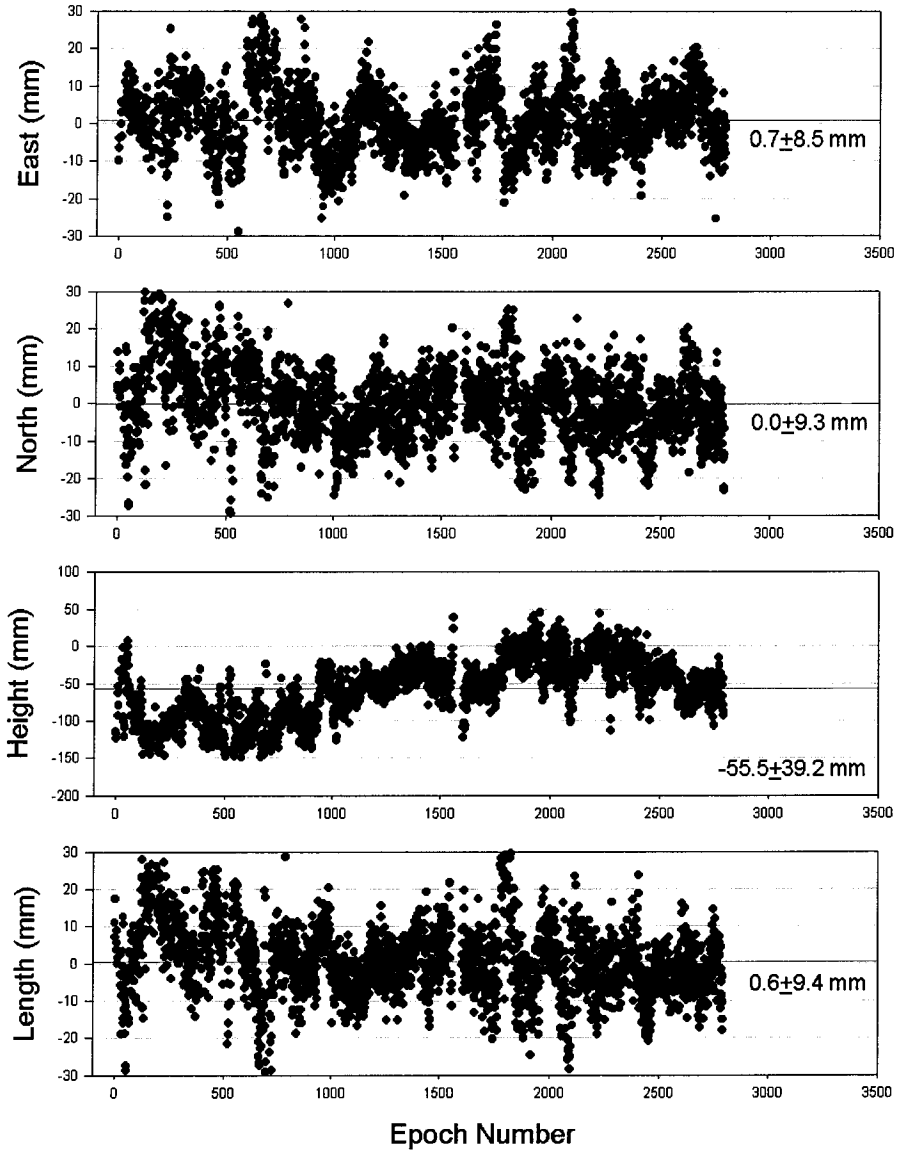

Figure 6-19. Kyushu GPS test: results of single-epoch ambiguity resolution for baseline 0479-0465, using the L1&L2 search. From top to bottom the graphs represent variations in the east, north, height and baseline length components, the x-axis denotes the epoch number (00:00:00~23:59:30 29-Sep (272) 1997, 30sec sample rate), and the y-axis represents the difference (between estimated result and true value) in units of mm.

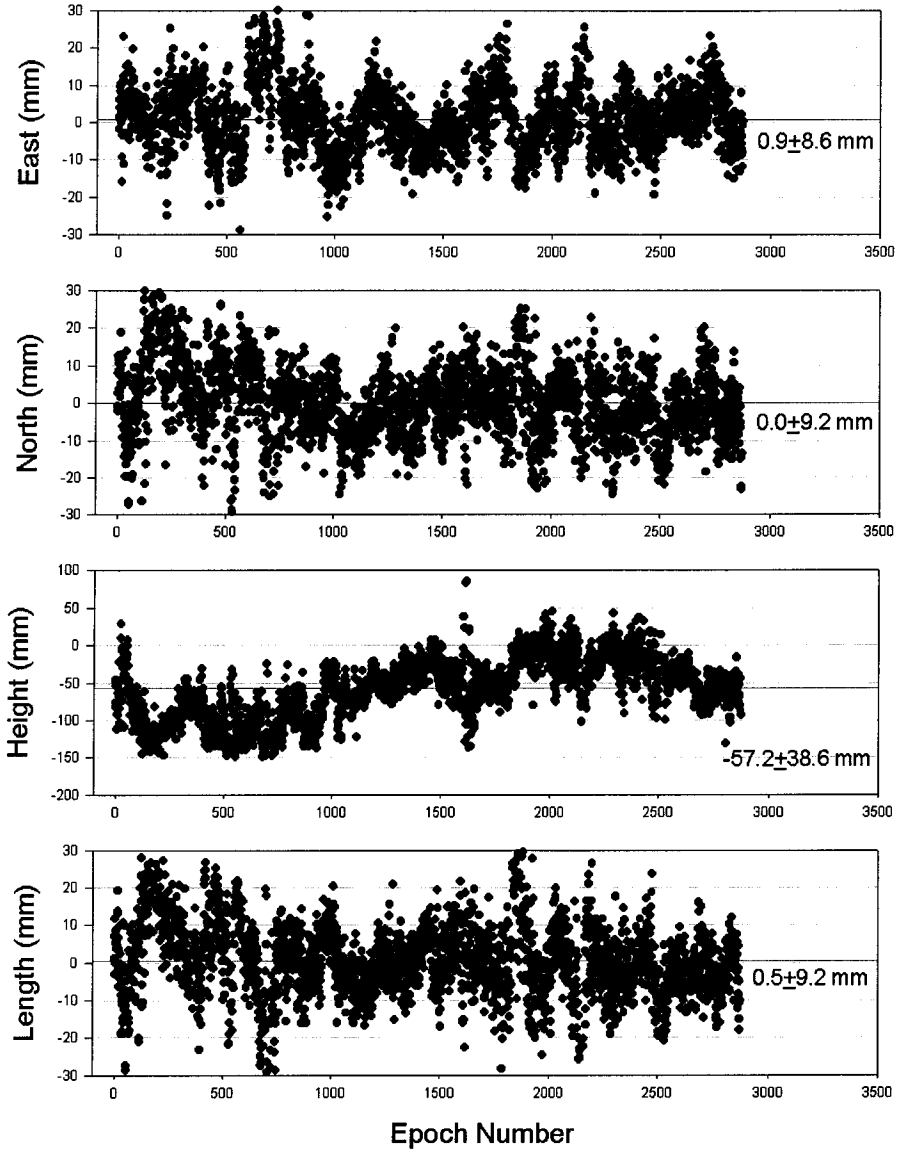

Figure 6-20. Kyushu GPS test: results of the ionosphere-free linear combination for single-epoch ambiguity resolution for baseline 0479-0465. From top to bottom the graphs represent variations in the east, north, height and baseline length components, the x-axis denotes the epoch number (00:00:00~23:59:30 29-Sep (272) 1997, 30sec sample rate), and the y-axis represents the difference (between estimated result and true value) in units of mm.

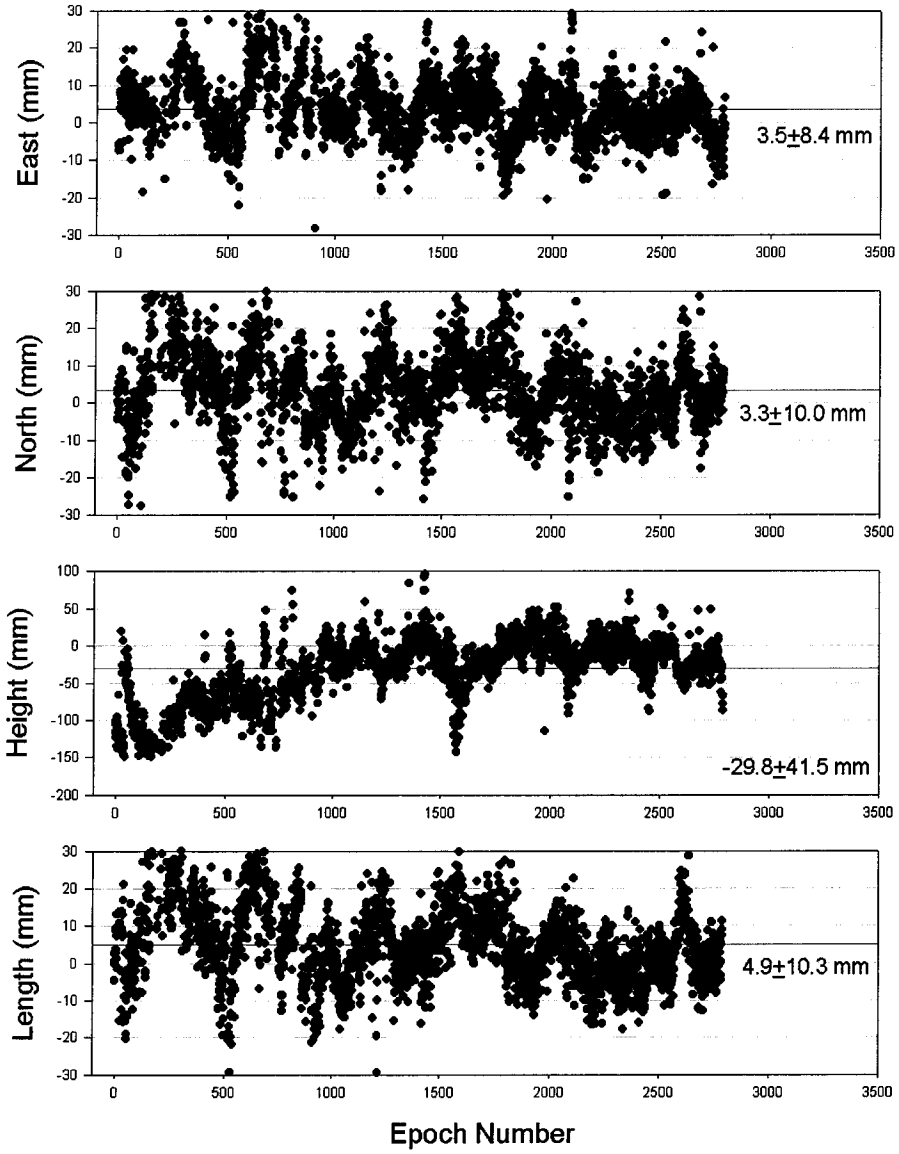

Figure 6-21. Kyushu GPS test: results of single-epoch ambiguity resolution for baseline 0479-0475, using the L1&L2 search. From top to bottom the graphs represent variations in the east, north, height and baseline length components, the x-axis denotes the epoch number (00:00:00~23:59:30 29-Sep (272) 1997, 30sec sample rate), and the y-axis represents the difference (between estimated result and true value) in units of mm.

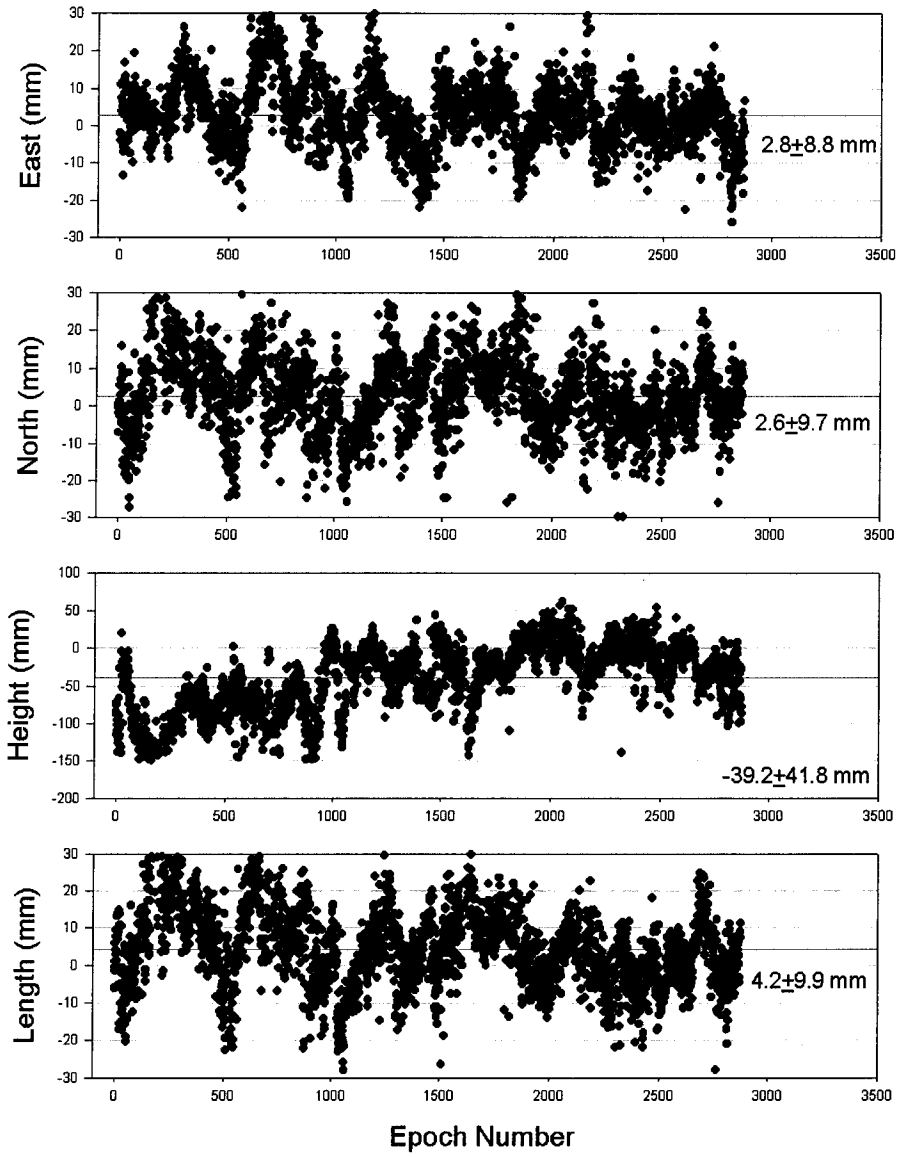

Figure 6-22. Kyushu GPS test: results of the ionosphere-free linear combination for single-epoch ambiguity resolution for baseline 0479-0475. From top to bottom the graphs represent variations in the east, north, height and baseline length components, the x-axis denotes the epoch number (00:00:00~23:59:30 29-Sep (272) 1997, 30sec sample rate), and the y-axis represents the difference (between estimated result and true value) in units of mm.

Comparing the L1&L2 results (Figures 6-15, 6-17, 6-19 and 6-21) and the ionosphere-free linear combination results (Figures 6-16, 6-18, 6-20 and 6-22), the variation is slightly larger in the case of the latter. However, the horizontal component accuracy is less than 1cm even though the baseline length was up to 90km for a single-epoch solution (with corrections from the reference stations).

The offsets and variations of the positioning results are summaried in Table 6-14. The offset is the difference between the estimated result and the "true" value (from the daily

ionosphere-free linear combination result). The variation represents the standard deviation of the positioning results. There was a less than 5mm offset in the horizontal components, even though the baseline length was up to 90 kilometres. For the height component, the values were -57.2mm and -39.2mm using the ionosphere-free linear combination algorithm, and –55.5mm and –29.8mm for the L1&L2 search algorithm for the baselines of length 77km and 90km respectively. This implies that the positioning results have essentially the same accuracy for the horizontal components, but the height accuracy of the component is a function of the baseline length because the tropospheric delay cannot be effectively eliminated. Hence, for the height component, the longer the baseline the lower the accuracy.

Table 6-14. Summary results of Figures 6-15~6-22, comparing the positioning accuracy of two different algorithms.

Method \ Baseline	0479-0478 (23km)	0479-0466 (55km)	0479-0465 (77km)	0479-0475 (90km)
L1 & L2	$0.6\pm7.5^{\alpha}$	-0.4±8.5	0.7±8.5	3.5±8.4
	$2.3\pm8.5^{\beta}$	0.5±9.2	0.0±9.3	3.3±10.0
	$-19.1\pm31.4^{\chi}$	-22.0±29.2	-55.5±39.2	-29.8±41.5
	$2.4\pm8.5^{\delta}$	0.7±9.1	0.6±9.4	4.9±10.3
Ionosphere-free	0.1±8.4	-0.9±9.5	0.9±8.6	2.8±8.5
	2.0±9.4	-0.4±10.4	0.0±9.2	2.6±9.7
	-25.5±36.3	-30.4±35.5	-57.2±38.6	-39.2±41.8
	2.2±9.4	0.2±10.3	0.5±9.2	4.2±9.9

Units in mm; α, β, χ and δ represent the offset and variation in latitude, longitude, height and baseline length components against the 'known' dual-frequency results.

6.3.3 TAIWNET – 1999

In order to test the proposed real-time ambiguity resolution (Chapter 4) and the relative ambiguity estimation algorithms (Chapter 5), data from the Chukuo network was analysed. Figure 6-23 shows the location of the Chukuo GPS stations in Taiwan.

The island of Taiwan is a product of the collision between the Luzon arc and the Chinese continental margin. At present the collision process is still very active, as revealed by the high seismicity and rapid crustal movement in and around the area. During the period from March 1991 to November 1995 stations were surveyed 4-6 times in the Chukuo area, and the results indicated shortening rates from 11.0-27.9 mm/yr. The rates seem to be more or less dependent on the baseline length, implying that the deformation is likely to be distributed across a wide zone and not solely caused by slip along the faults. This means that the crustal strain probably accumulates in this area (Yu et al., 1997). Hence, a permanent GPS monitoring network was set up and has collected data since August 1999. The distance between S011-S106, S011-S012, S011-KULN and S011-CHYN is

approximately 17, 22, 22 and 21km respectively. Figure 6-24 shows the double-differenced geometry-free linear combination residuals. Figure 6-25 displays the double-differenced ionosphere-free linear combination residuals. Figure 6-24 indicates only the ionospheric delay (Equation (4-3)), but multipath, orbit error and tropospheric delay are indicated in Figure 6-25 (Equation (4-4)).

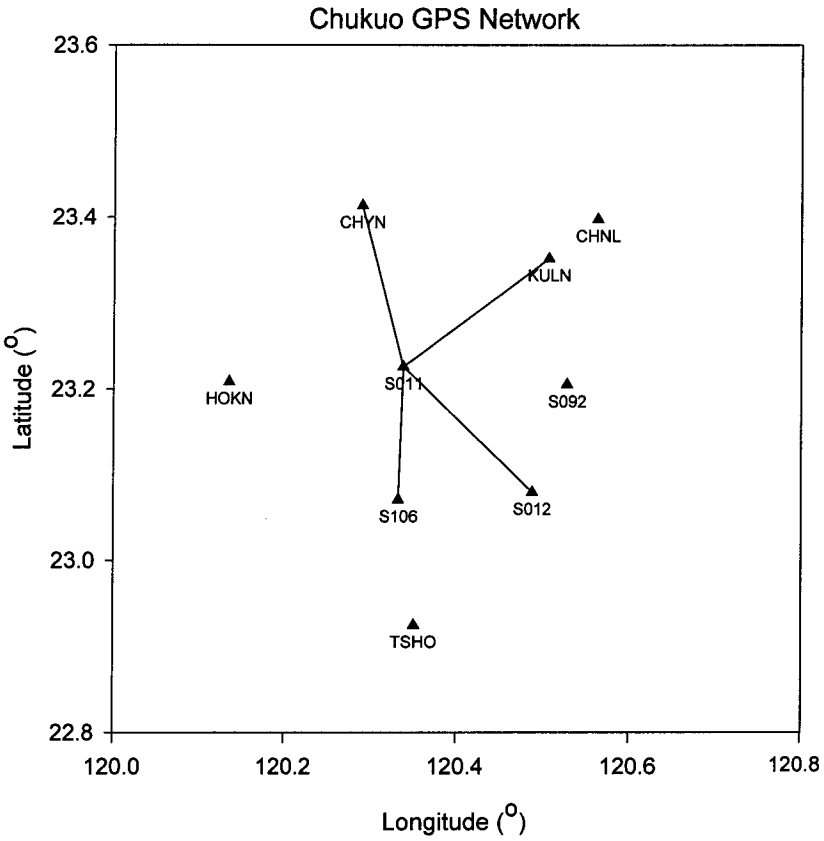

Figure 6-23. GPS network (Chukuo), part of Taiwan's permanent GPS station network.

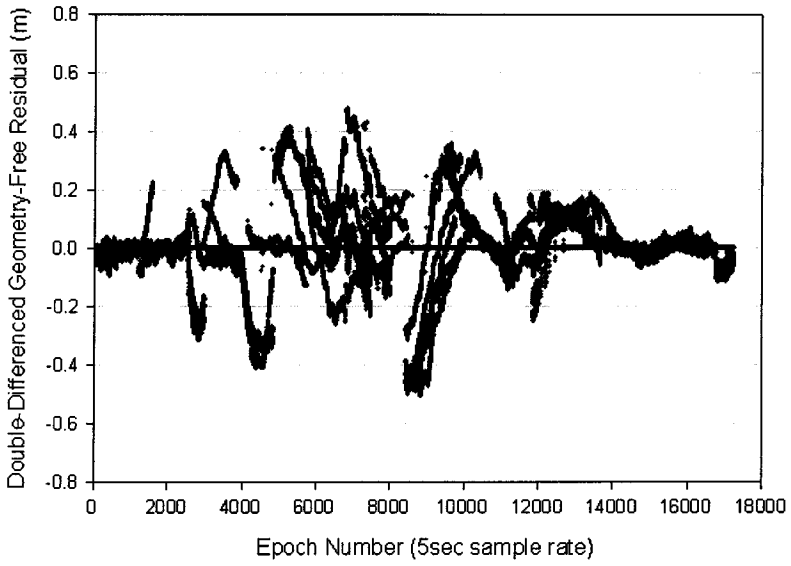

Figure 6-24. Double-differenced geometry-free residual, for baseline (S011-S106) 17km in length, on DoY 335 (1999), Chukuo, Taiwan.

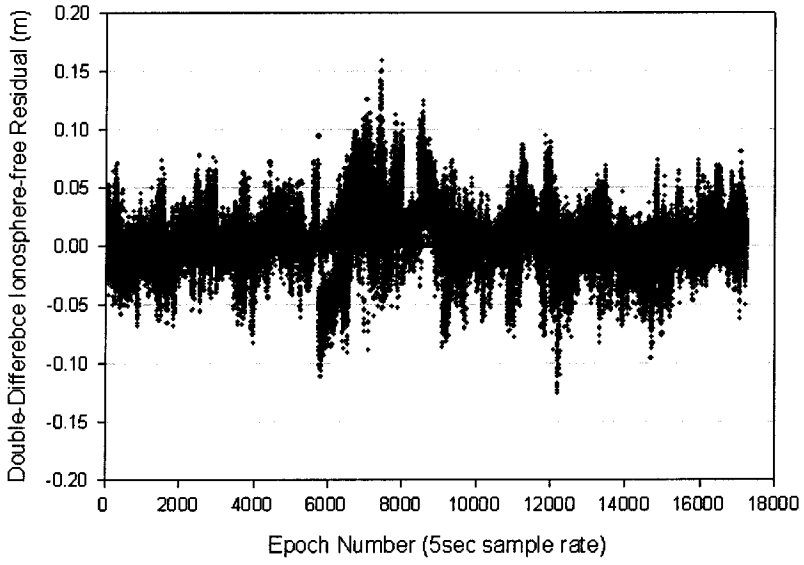

Figure 6-25. Double-differenced ionosphere-free residual, for baseline (S011-S106) 17km in length, on DoY 335 (1999), Chukuo, Taiwan.

The data was collected and computed at a 5sec sample rate. For analysing the ionospheric delay effect, a post-processing algorithm was used to estimate the integer ambiguities using the all of the day's observations. After resolving the integer ambiguities, and forming the double-differenced geometry-free linear combination, the integer ambiguities are used to compute the residuals. According to Equation (4-3), the main residual component represents the ionospheric delay values. The x-axis represents the epoch number (which started in UTC 00h:00m:00s and ended in 23h:58m:55s on DoY 335, 1999), and the y-axis

denotes the residual (units mm). The scatter of the plots are for the double-differenced geometry-free residual for all satellites and all epochs.

For the period defined by epoch number around 0 to 2160 (0h~3h UTC; 8h~11h local time) and 13680 to 17280 (19h~24h UTC; 3h~8h local time), the ionospheric delay value displays only a slight change and the magnitude of the residuals is less than 10cm. This implies that during this period the ionosphere is in an undisturbed condition (StD: 0.03m), compared to when the ionosphere is disturbed (StD: 0.16m). In the latter case, using the L1&L2 observations (Equation (4-1) and (4-2)) to estimate the integer ambiguity is likely to be unsuccessful, because the ionospheric delay effect is more than 1 cycle of the L1 wavelength.

In this experiment, the predicted orbit has been used to replace the broadcast orbit. If it is assumed that the predicted orbit has 20cm accuracy then, applying the well known 'rule-of-thumb', it should only affect the accuracy by 0.2mm for a 20km baseline. After carefully selecting the monitoring station, and using the Dorne Margolin choke ring antennas to reduce the effect of the multipath, the main error in Equation (4-4) is likely to be the tropospheric delay.

The ambiguity resolution algorithm is applied in two steps. The first step is to resolve the widelane ambiguity (using its long wavelength and low noise), and then to fix the L1 ambiguity. The integer ambiguities were resolved using all of the day's observations. Then the double-differenced ionosphere-free linear combination was used to compute the residuals (Figure 6-25). According to Equation (4-4), the main residual component represents the tropospheric delay. The x-axis represents the epoch number (which is the same as Figure 6-24), and the y-axis denotes the residual (units mm).

From epoch number around 5760 to 11520 (8h~16h UTC; 16h~24h local time), the tropospheric delay value is high, and the magnitude of the residuals is more than 10cm. This implies that using the L1&L2 observations to estimate the integer ambiguity will likely be unsuccessful, due to the tropospheric effects being up to 0.5 cycles of the L1 wavelength.

Figure 6-26 shows the result of the L1&L2 search method for single-epoch ambiguity resolution. Because the magnitude of the ionospheric delay is more than 1 cycle (L1 wavelength) from epoch 3000 to 14000 (Figure 6-26), ambiguity resolution has failed. Hence, no solution could be achieved during this period. The x-axis represents the epoch number (same as Figure 6-24), and the y-axis denotes the residual (units mm). From top to bottom is the east-west, north-south, height and length components. The results have had the known value (computed by the ionosphere-free linear combination from a full day's data) subtracted from them.

Figure 6-27 displays the result of the widelane/L1 integer ambiguity resolution method for single-epoch solutions. The ambiguity success rate increases from 42% up to 95% for the L1&L2 search method. Table 6-15 lists the different baselines and different days for the ambiguity resolution tests. To compare the different success rates, the two columns represent the results of the different ambiguity resolution methods. The left hand side of the column denotes the L1&L2 search method, and the right hand side shows the widelane/L1 ambiguity resolution method.

Referring to Table 6-15, there is a lower success rate in DoY 337 than for the other days. Figure 6-28 shows the ionospheric delay for DoY 337, and it can be seen that the magnitude of the ionospheric delay is much higher than for DoY 335 (Figure 6-27). The magnitude of the tropospheric delay on DoY 337 (Figure 6-29) is also larger than that of DoY 335.

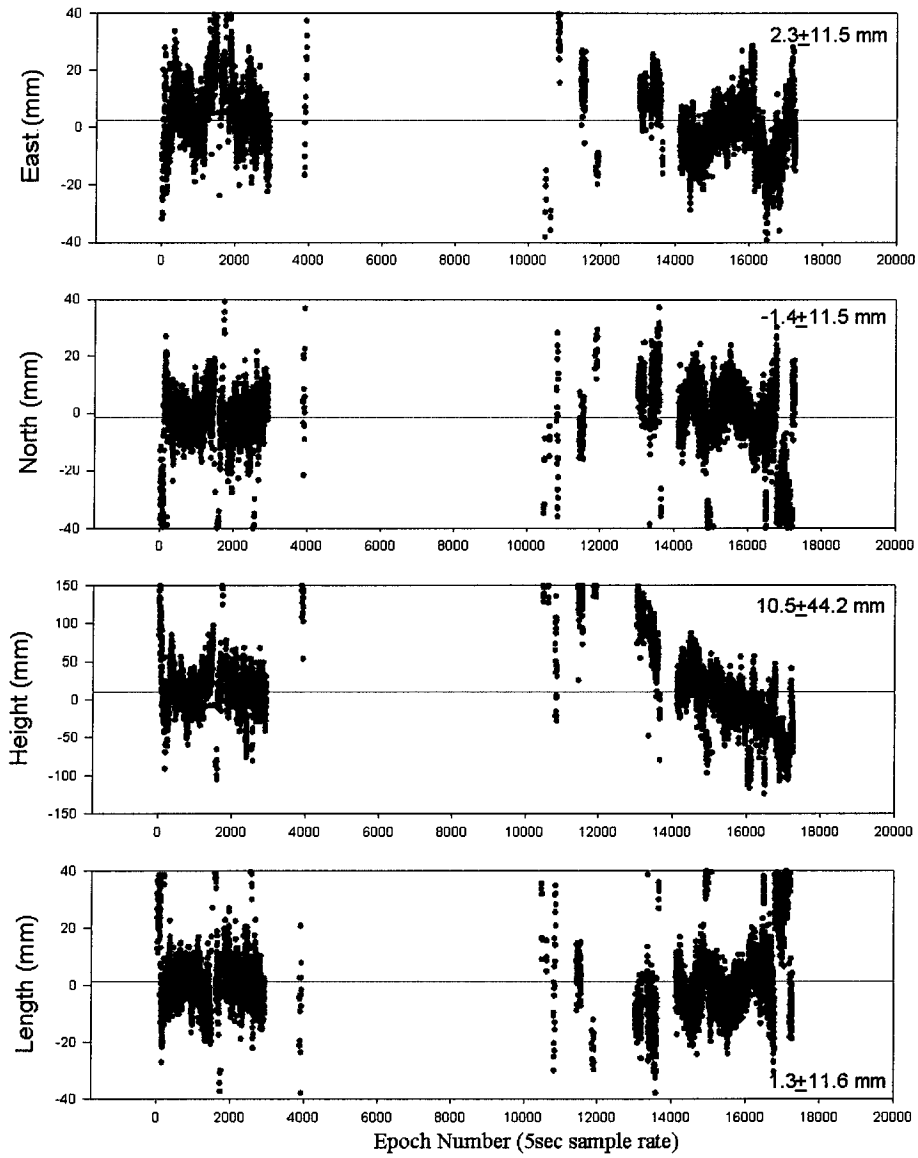

Figure 6-26. Positioning results using the L1&L2 search method for ambiguity resolution, for baseline (S011-S106), 17km in length on DoY 335 (1999), Chukuo, Taiwan.

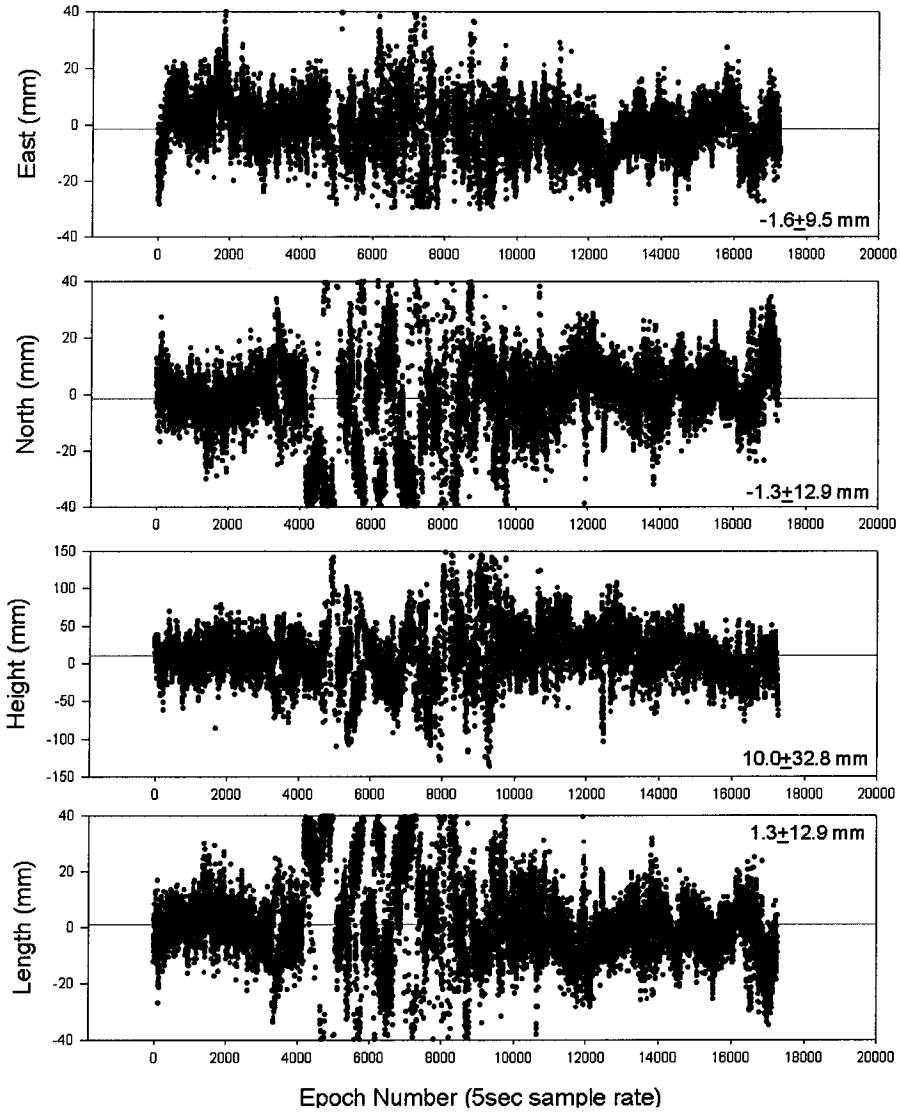

Figure 6-27. Positioning results using the widelane/L1 method for ambiguity resolution for baseline (S011-S106), 17km in length on DoY 335 (1999), Chukuo, Taiwan.

Table 6-15. Comparing the different methodologies for ambiguity resolution on DoY 335~337 (1999), Chukuo, Taiwan.

Baseline / DoY	S011-S106 (17km)		S011-S012 (22km)		S011-KULN (22km)		S011-CHYN (21km)	
	Correctness (%)		Correctness (%)		Correctness (%)		Correctness (%)	
335	42.46	94.78	33.69	97.04	40.55	97.19	32.84	90.51
336	41.62	96.02	33.48	97.74	42.05	95.86	34.87	93.54
337	30.36	96.81	27.53	97.10	26.76	97.06	28.02	96.95
338	44.76	95.60	39.70	96.41	43.41	97.20	38.88	96.89

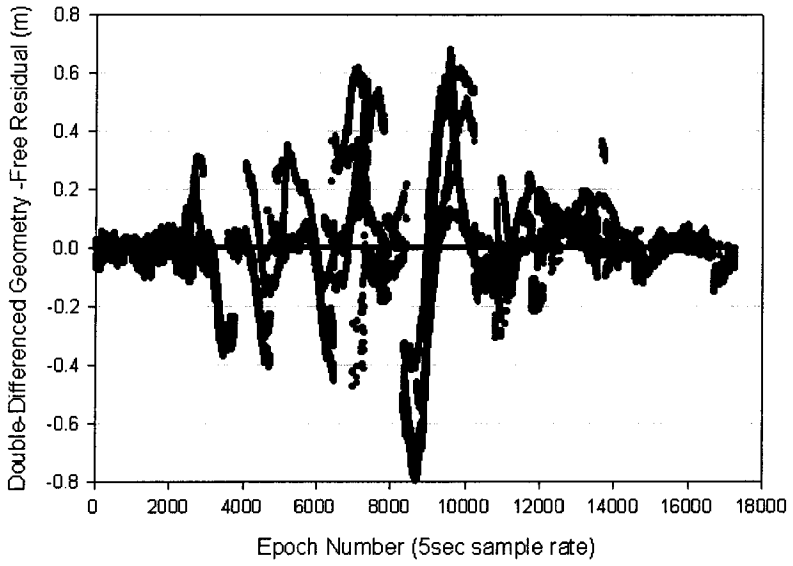

Figure 6-28. Double-differenced geometry-free residual for baseline (S011-S106), 17km in length on DoY 337 (1999), Chukuo, Taiwan.

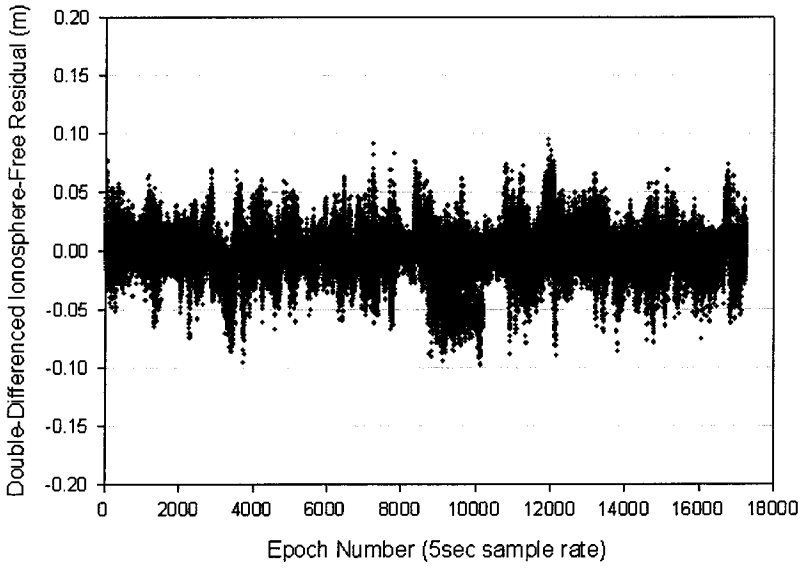

Figure 6-29. Double-differenced ionosphere-free residual for the baseline (S011-S106), 17km in length on DoY 337 (1999), Chukuo, Taiwan.

6.3.4 Concluding Remarks

In the Sydney 1999 kinematic GPS experiment, in order to compare the performance of multiple reference stations, a set of data was computed using single-epoch AR, while another set of data was computed by applying the 'correction terms' to the data processing algorithm. The results are shown in Table 6-13. A higher percentage of correct results can be achieved using the multiple reference station methodology.

In the Kyushu 1997 GPS test, it appears that this multi-reference receiver data processing methodology is feasible for precise medium-range positioning.

From the Chukuo1999 single-epoch AR GPS positioning tests, the widelane/L1 ambiguity resolution method in combination with the relative ambiguity resolution algorithm, can increase the success rate of ambiguity resolution.

Chapter 7
SUMMARY AND RECOMMENDATIONS

7.1 Summary

To implement appropriate data processing algorithms for such multiple reference station systems, three problems need to be addressed:

(1) For precise positioning, such systems can readily support dual-frequency kinematic positioning. The challenge is: How to optimise them for using with single-frequency receivers? How long does the observation period have to be? What is the positioning accuracy?
(2) For kinematic applications, the main challenge of using a multiple reference station system is to continuously resolve ambiguities instantaneously (or with the absolute minimum delay) when tracking a satellite that experiences cycle-slips, or after a long data gap, or when a new satellite rises above the tracking horizon.
(3) For medium- or long-range precise positioning one of the greatest challenges is to resolve the ambiguities in real-time.

To solve these problems, three implement algorithms have been proposed. The first algorithm is to test the medium-range multi-reference station methodology with mixing single-frequency and dual-frequency receivers. The second algorithm is to solve the ambiguities within the permanent GPS receiver network when tracking a satellite that experiences cycle-slips, or after a long data gap, or when a new satellite rises above the tracking horizon. The third algorithm is to apply the triple-differenced-type ambiguity recovery technique in order to resolve the network receiver ambiguities in real-time.

7.1.1 Mixing Single-frequency and Dual-frequency Receivers

Single-frequency GPS measurements contain ionospheric biases which cannot be eliminated using multi-frequency techniques and hence, given that their impact on double-differenced observables is dependent on the inter-receiver distance, their application is generally limited to comparatively short baselines (<10-20km). A linear combination model has been proposed by Han & Rizos (1997b), designed for medium-range GPS

positioning (over baselines of many tens of kilometres), which can account for orbit and ionospheric delay, as well as reduce tropospheric delay, multipath and measurement noise across the GPS reference receiver network. This algorithm makes high relative positioning accuracy possible, using data from single-frequency receiver operating within a sparse continuously operating, dual-frequency GPS reference network, even if the baseline lengths are of the order of a few tens of kilometres or more.

One geodetic implementation is a form of "densification" of a network of dual-frequency GPS receivers in which a permanent array of low-cost, single-frequency GPS receivers can be deployed to increase the spatial resolution of the receiver network. Such an implementation would be beneficial, for example, for deformation monitoring applications. Another implementation allows for the use of cost effective operational procedures based on relatively short station occupation times (as in the "rapid static" GPS surveying technique). The configuration requires two types of GPS receivers: (a) the permanent, continuously operating, dual-frequency reference receivers, and (b) the *mobile*, single-frequency receivers which are used to visit a large number of survey marks for comparatively short periods of time.

To test the performance of the multiple reference station methodology for precise positioning using low-cost, single-frequency GPS receivers, three data sets have been analyzed: (a) simulated single-frequency data (derived from dual-frequency receivers but using only the L1 observations), (b) data for short observation spans, and (c) data collected in operational environments (combining several single-frequency and dual-frequency receivers which occupy the same stations within a sparse permanent network). The data sets were selected so that the integrated, dual-mode networks were located at different latitudes, traverse large elevation changes, involve data collected during different seasons, employ single-frequency receivers of different makes, and involve baselines of different lengths.

In this way the applicability of the multi-reference station methodology could be tested thoroughly. The results do confirm that sub-part-per-million relative accuracy can be achieved in all of the above-mentioned test environments, even for baselines up to 100km in length (Rizos et al., 1998; 2000; Chen et al., 1999 and Chen, 2000).

7.1.2 The Challenge of Resolving Ambiguities within the Permanent GPS Receiver Network

Although precise coordinates are known for the GPS reference stations, it is still a challenge to resolve the integer ambiguities correctly between the reference stations, in real-time, when a new satellite rises, or when a cycle-slip or after a long data gap occurs.

A predicted atmospheric delay algorithm was proposed. Tests have demonstrated how real-time processing of GPS reference station data, using the widelane / narrowlane linear combination model (ionosphere-free), and the predicted tropospheric delay model (residual delay remaining after applying a standard troposphere model), can significantly improve the success rate of ambiguity resolution. Even using only a small number of epochs of data in the case of a newly-risen satellite, or after a cycle-slip, or at the resumption of tracking after a long data gap.

From these results the following conclusions could be drawn:

1. The results obtained indicate that the success rate of integer ambiguity resolution can be improved by up to 90% when a new satellite rises (when processing data for satellite elevations from 15° ~ 20°) by using the predicted troposphere delay model.
2. After a long data gap, the proposed algorithm can provide more reliable ambiguity resolution, especially when the tropospheric delay values are larger than 0.5 cycles of the narrowlane wavelength.
3. The performance of the predicted tropospheric delay model is dependent on how smooth the 'real' tropospheric delay is. For example, although the same algorithm was used on two different days of an experiment (DoY 272 and 273), the day having smooth tropospheric delay values (DoY 272) resulted in a much higher ambiguity resolution success rate.
4. The proposed algorithm is suitable for implementation for real-time (or near real-time) applications.

7.1.3 Triple-Differenced-Type Ambiguity Recovery Technique

GPS carrier phase measurements provide the basis for obtaining the most precise positioning results. Compared with the code (pseudorange) observables, carrier phase measurements have an ambiguity term that needs to be 'resolved' to an integer number. In relative positioning, the distance-dependent biases will grow with increasing baseline length, and hence ambiguity resolution becomes increasingly difficult. Several ambiguity resolution algorithms have been proposed and tested for static positioning, and the positioning accuracy can reach a few ppb, even for inter-receiver distances up to a few thousand kilometres. This is because the orbit error, and residual atmospheric effects, can be effectively mitigated in a number of ways. For precise kinematic positioning, the ambiguities need to be fixed in a very short period of time (ideally, instantaneously, using a single epoch of data). Many researchers have suggested techniques for 'on-the-fly' ambiguity resolution for short-range applications (<20km), where distance-dependent biases can be ignored. This is not the case for medium- or long-range ambiguity resolution. The main challenge is how to resolve the correct integer ambiguity processing

measurements affected by distance-dependent biases. A further challenge is to do so in real time.

Han (1995) has categorised these ambiguity resolution algorithms into three groups: search techniques in the 'measurement domain', search techniques in the 'coordinate domain' and search techniques in the 'estimated ambiguity domain'. The measurement domain techniques are assisted by precise pseudorange observations. The main obstacle in their use for long-range kinematic positioning is that they are limited by the accuracy of the pseudorange measurements and the residual atmospheric biases. The coordinate domain techniques are mainly represented by the Ambiguity Function Method, which requires good approximate initial coordinates. For long-range kinematic applications, the main disadvantage is the magnitude of the residual ionospheric delay. The estimated ambiguity domain techniques are commonly used for short-range applications. For long-range ambiguity estimation applications, the comparatively short wavelength will result in a larger search space, and the ambiguity search will become difficult. Therefore, the optimal algorithm for long-range ambiguity resolution is not to resolve the ambiguities directly, but to estimate them somehow (by any of a variety of techniques appropriate for the particular application) and to the monitor whether the ambiguities have changed. In other words, the challenge becomes to detect and repair cycle slips 'on-the-fly', and in the process to determine the 'relative ambiguity'.

A triple-difference-type ambiguity recovery technique has been proposed and tested that could be used for long-range applications. Between discrete kinematic tracking epochs the distance-dependent biases exhibit a large degree of similarity for short time spans, and hence they can be mostly eliminated by applying the residuals from the previous epoch, when the ambiguity had been fixed. This technique can exhibit good performance during active ionosphere conditions. The proposed ambiguity recovery procedure can process data without precise code measurements and without any distance limitations. Furthermore, the proposed algorithm can be optimised for processing stationary data, especially in the case of medium-range reference station networks, in order to resolve the network receiver ambiguities in real-time.

7.2 Recommendations

In this thesis several algorithms have been proposed to address some of the challenging problems related to implementing real-time, medium-range, carrier phase-based, multiple reference station techniques for kinematic and static positioning applications. A wide range of data sets were analysed to test the proposed algorithms. Based on the test results, conclusions were drawn in the previous section. The distance-dependent biases (orbit error, residual ionospheric and tropospheric delays) are the most important factors impacting on such techniques.

Although the IGS service can already provide 20cm accuracy predicted orbits for real-time users, the ionosphere is disturbed during solar maximum conditions (as at present). After applying the standard model for the tropospheric delay, the residual tropospheric delay can be predicted using multiple reference stations, and the relative zenith tropospheric delay can be used for newly-risen satellites to aid ambiguity resolution. This algorithm needs further testing, in different locations and during different seasons.

For 'fast-static', single-frequency applications, the positioning accuracy has been demonstrated as being as high as that obtained using dual-frequency GPS receivers, if the multiple reference station algorithm is applied. Therefore using single-frequency receivers to "densify" an area of interest for, for example deformation monitoring, can reduce the cost of hardware, without sacrificing positional accuracy in the daily or hourly solutions.

For medium-range kinematic positioning, the single-epoch solution is possible, if the multiple reference station algorithm is used to mitigate the distance-dependent biases. If the distance-dependent biases are of larger scale structure than the inter-station distances, then multiple reference stations can be very successfully used for this purpose (Wanninger, 1999). Hence, the optimal size of the multiple reference station network is dependent on whether the distance-dependent biases can be realistically modelled with the proposed network configuration. This means that in different locations, reference station network may have to have different sizes and receiver densities. The initialisation of the reference station processing is a necessary procedure to resolve the integer ambiguities at the beginning of operations, then the triple-difference-type ambiguity recovery technique can be used to estimate the 'relative ambiguities'. The Sydney test results (May 1999) indicate that if the data gap is shorter than about 5 minutes, ambiguity recovery techniques can easily estimate the correct 'relative ambiguity'.

Some recommendations for further research:

1. Multiple reference stations have great potential for many applications, including deformation monitoring, to support precise farming practices, for precise navigation systems, GPS surveying, etc. If the observations of the Galileo satellites can be acquired, and then combined with GPS and GLONASS, the volume of observations will be increased and this will enhance the reliability of the multiple reference station applications.

2. For real-time applications, the problem of data latency needs to be considered, which includes the receiver data download and transfer delay, data link delay, and baseline or network computation delay. Hence, for real-time users, the issue of data latency still needs to be addressed, and better extrapolation algorithms need to be developed.

3. Although the algorithm to predict the tropospheric delay for newly-risen satellites, or after long data gaps, has exhibited good performance for tests in the southern part of Japan in 1997, this algorithm still needs to be tested in different locations because the troposphere is highly variable across seasons and regions.

4. The triple-difference-type ambiguity recovery technique can be successfully used at the stationary reference stations. Further research should focus on its performance under maximum solar activity conditions.

5. For medium-range kinematic positioning, successful ambiguity resolution is the key requirement for precise applications, hence the reliability of ambiguity resolution needs to be studied further.

REFERENCES

Abidin H.Z. (1993). On the construction of the ambiguity searching space for on-the-fly ambiguity resolution, *Navigation*, 40(3), 321-338.

Australian Surveying & Land Information Group, 2000, web page http://www.auslig.gov.au/geodesy/newhome.htm.

Bock Y., et al. (1997). Southern California Permanent GPS Geodetic Array: continuous measurements of regional crustal deformation between the 1992 Landers and 1994 Northridge earthquakes, *J. Geophys Res*, 102(B8), 18013-18033.

Chen H. Y. (1999) A Correction Generation Algorithm for Carrier Phase-Based GPS Positioning Using Multiple Reference Station Networks. School of Geomatic Engineering, The University of New South Wales Sydney NSW 2052 Australia "Annual Research Seminar, School of Geomatic Engineering, UNSW", 16-17 November 1999.

Chen H. Y. (2000). An instantaneous ambiguity resolution procedure suitable for medium-scale GPS reference station. *Proc. 13th Int. Tech. Meeting of the Satellite Division of the U.S. Inst. of Navigation GPS ION'99*, Salt lake city, Utah, 19-22 September, 1061-1070.

Chen H.Y., Rizos C., and S. Han (1999). Rapid static medium-range GPS positioning techniques for geodynamic applications, *Proc. 4th Australasian Symp. on Satellite Navigation Technology & Applications*, Brisbane, Australia, 20-23 July, paper 49, 12pp.

Chen H.Y., Rizos C., and S. Han (2000). From simulation to practicality: medium-range, low-cost densification of permanent GPS networks in geodetic applications, *Submit to Journal of Geodesy.*

Colombo O.L., Hernández-Pajares M., Juan J.M., and J. Sanz (1999). Resolution of carrier-phase ambiguities on the fly, at more than 100km from nearest reference site, with the help of ionospheric tomography, *Proc. 12th Int. Tech. Meeting of the Satellite Division of the U.S. Inst. of Navigation GPS ION'99*, Nashville, Tennessee, 14-17 September, 1635-1642.

Dai, L., Chen, H.Y., Han, S., Rizos, C., & Kearsley, A.H.W. (2000). Ambiguity recovery for long-range kinematic GPS positioning using a triple-difference-type approach. *Western Pacific Geophysics Meeting*, Tokyo, Japan, 26-30 June.

Gao, Y., Li Z., and J.F. McLellan (1997). Carrier phase based regional area differential GPS for decimeter-level positioning and navigation, *Proc. 10th Int. Tech. Meeting of the Satellite Division of the U.S. Inst. of Navigation GPS ION'97*, Kansas City, Missouri, 16-19 September, 1305-1313.

EUREF (European Reference Frame) (2000). Web page: http://epncb.oma.be/.

GEONET (GPS Earth Observation Network of the Geographical Survey Institute) (2000), Web page: http://mekira.gsi.go.jp/ENGLISH/index.html.

Han S. (1995). Ambiguity Recovery for GPS Long Range Kinematic Positioning. *Proc., 8th Int. Tech. Meeting of The Satellite Division of the U.S. of Navigation ION GPS-95,* Palm Spring, California, 12-15 September, 349-360. Accepted by NAVIGATION, Journal of the U. S. Institute of Navigation.

Han S. (1997a). *Carrier Phase-Based Long-Range GPS Kinematic Positioning*, PhD dissertation, UNISURV rept. no. S-49, School of Geomatic Engineering, The University of New South Wales, 185pp.

Han S. (1997b). Quality control issues relating to ambiguity resolution for real-time GPS kinematic positioning, *Journal of Geodesy,* 71(6), 351-361.

Han S., and C. Rizos (1995a). A suggested procedure for on-the-fly ambiguity resolution for long range kinematic positioning, *4th Int. Conf. on Differential Navigation System*, Bergen, Norway, 24-28 April, Paper no. 67, 8pp.

Han S., and C. Rizos (1995b). A new method of constructing multi-satellite ambiguity combinations for improved ambiguity resolution, *Proc. 8th Int. Tech. Meeting of the Satellite Division of the U.S. Inst. of Navigation GPS ION'95*, Palm Springs, California, 12-15 September, 1145-1153.

Han S., and C. Rizos (1996a). Integrated method for instantaneous ambiguity resolution using new generation GPS receivers, *Proc. IEEE Position Location and Navigation Symp. PLAN'96*, Atlanta, Georgia, 22-26 April, 254-261.

Han S., and C. Rizos (1996b). Improving the computational efficiency of the ambiguity function algorithm, *Journal of Geodesy*, 70, 330-341.

Han S., and C. Rizos (1996c). GPS network design and error mitigation for real-time continuous array monitoring system, *Proc. 9th Int. Tech. Meeting of the Satellite Division of the U.S. Inst. of Navigation GPS ION'96*, Kansas City, Missouri, 17-20 September, 1827-1836.

Han S. and C. Rizos (1997a). Making sense of GPS ambiguity resolution techniques, *GIM, Int. J. of Geomatics*, 11(11), 31-33.

Han S., and C. Rizos (1997b). An instantaneous ambiguity resolution technique for medium-range GPS kinematic positioning, *Proc. 10th Int. Tech. Meeting of the Satellite Division of the U.S. Inst. of Navigation GPS ION'97*, Kansas City, Missouri, 16-19 September, 1789-1800.

Han S., Rizos C. and R. Abbot (1998). Flight testing and data analysis of airborne GPS LADS survey, *Proc. 11th Int. Tech. Meeting of the Satellite Division of the U.S. Inst. of Navigation GPS ION'98,* Nashville, Tennessee, 15-18 September, 1211-1221.

Hernández-Pajares M., and Juan J.M., Sanz J., and O.L. Colombo (2000). Application of ionospheric tomography to real-time GPS carrier phase ambiguities resolution at scales of 400-1000km and with high geomagnetic activity, Accepted *Geophysical Research Letters* (30 March 2000).

Hernández-Pajares M., Juan J.M., Sanz J., and J.G. Solé (1998). Global observation of the ionospheric electronic response to solar events using ground and LEO GPS data, *Journal of Geophysical Research 103 (A9)*, 20789-20796.

Hernández-Pajares M., Juan J.M., Sanz J., and O.L. Colombo (1999). Precise ionospheric determination and its application to real-time GPS ambiguity resolution, *Proc. 12th Int. Tech. Meeting of the Satellite Division of the U.S. Inst. of Navigation GPS ION'99*, Nashville, Tennessee, 14-17 September, 1409-1417.

Hofmann-Wellenhof B., Lichtenegger H., and J. Collins (1998). *GPS Theory and Practice,* Fourth Revised Edition, Springer-Verlag, Wien New York, 355pp.

HVO (Hawaiian Volcano Observatory) (2000). Web page: http://volcanoes.usgs.gov/ About/What/Monitor/Deformation/GPSKilauea.html.

IGS (International GPS Service) (2001). Web page: http://igscb.jpl.nasa.gov.

Kouba, J. (1995), SINEX format version 0.05, e-mail send to all IGS Analysis Centers.

Li Z., and Y. Gao (1998). Improving ambiguity resolution for a regional area DGPS system using multiple days of data, *Proc. 11th Int. Tech. Meeting of the Satellite Division of the U.S. Inst. of Navigation ION GPS'98*, Nashville, Tennessee, 15-18 September, 399-406.

Liu J., and L. Dai (1999). A method to fix ambiguity for GPS long baseline precisely rapid static positioning, *Journal of Wuhan Technical University of Surveying and Mapping*, 24, Suppl. 5-8.

Mervart L. (1995). *Ambiguity Resolution Techniques in Geodetic and Geodynamic Application of the Global Positioning System*, PhD Thesis, Geodätisch-geophysikalische Arbeiten in der Schweiz, Band 53.

Odijk D. (1999). Stochastic modelling of the ionosphere for fast GPS ambiguity resolution, *Abstracts of IUGG'99*, Birmingham, UK, 19-24 July, 406.

Parkinson B.W., Spilker J.J., Axelrad P., and P. Enge (1996). *Global Positioning System: Theory and applications*, American Institute of Aeronautica and Astronautics, Inc., 623pp.

Preliminary Report on the 10/16/1999 M7.1 Hector Mine, California Earthquake. Scientists from the U.S. Geological Survey, Southern California Earthquake Center, and California Division of Mines and Geology. (http://www- socal.wr.usgs.gov /hector/hector_srl.html)

Rabah M. and S. Leinen (1998). Real-time crustal movement determination over long baselines, *Proc. 9th Int. Symp. on Recent Crustal Movements (CRCM'98)*, Cairo, Egypt, 14-19 November, 75-86.

Raquet J.F. (1996). Multiple reference GPS receiver multipath mitigation technique, *Proc. Annual Meeting of The U.S. Institute of Navigation*, Cambridge, Maryland, 18-20 June, 681-690.

Raquet J.F. (1997). Multiple user network carrier-phase ambiguity resolution, *Proc. Int. Symp. on Kinematic Systems in Geodesy, Geomatics and Navigation - KIS97*, Banff, Canada, 3-6 June, 45-55.

Raquet J.F. (1998). *Development of a Method for Kinematic GPS Carrier-Phase Ambiguity Resolution Using Multiple Reference Receivers*, PhD dissertation Report No. 20116, Department of Geomatics Engineering, The University of Calgary.

Raquet J.F., and G. Lachapelle (1996). Determination and reduction of GPS reference station Multipath using multiple receivers, *Proc. 9th Int. Tech. Meeting of the Satellite Division of the U.S. Inst. of Navigation ION GPS'96*, Kansas City, Missouri, 17-20 September, 673-681.

Raquet J.F., and G. Lachapelle (1997). Long-distance kinematic carrier-phase ambiguity resolution using a reference receiver network, *Proc. 10th Int. Tech. Meeting of the Satellite Division of the U.S. Inst. of Navigation GPS ION'97,* Kansas City, Missouri, 16-19 September, 1747-1756.

Raquet J.F., Lachapelle G. and L. Fortes (1998). Use of a covariance analysis technique for predicting performance of regional area differential code and carrier-phase networks, *Proc. 11th Int. Tech. Meeting of the Satellite Division of the U.S. Inst. of Navigation ION GPS'98*, Nashville, Tennessee, 15-18 September, 1345-1354.

Raquet J.F., Lachapelle G., and T. Melgrad (1998). Test of a 400 km x 600 km network of reference receivers for precise kinematic carrier-phase positioning, *Proc. 11th Int. Tech. Meeting of the Satellite Division of the U.S. Inst. of Navigation ION GPS'98*, Nashville, Tennessee, 15-18 September, 407-416.

Remondi B.W. (1988). Kinematic and pseudo-kinematic GPS, *Proc. 1st Int. Tech. Meeting of the Satellite Division of the U.S. Inst. of Navigation GPS ION'88*, Colorado Springs, Colorado, 19-23 September, 115-121.

Rizos C. (1996). *Principles and Practice of GPS Surveying*, Monograph 17, School of Geomatic Engineering, The University of New South Wales, Sydney, Australia, 560pp.

Rizos C., and C. Satirapod (2001). GPS with SA off: How good is it? *Measure & Map*, 12, 19-21.

Rizos C., and S. Han (1998). Status and trends for high precision GPS kinematic positioning, *Proc. 9th Australasian Remote Sensing & Photogrammetry Conf.*, Sydney, Australia, 20-24 July, CD-ROM, paper no.49, 17pp.

Rizos C., Han S., and H.Y. Chen (1998). Carrier phase-based, medium-range, GPS rapid static positioning in support of geodetic applications: algorithms and experimental results, *Proc. Spatial Information Science & Technology (SIST'98),* Wuhan Technical University of Surveying & Mapping, Wuhan, P.R. China, 13-16 December, 7-16.

Rizos C., Han S. and H.Y. Chen (2000). Regional-scale multiple reference stations for real-time carrier phase-based GPS positioning: a correction generation algorithm, *Earth, Planets & Space*, 52(10), 795-800.

Rizos C., Han S., Chen H.Y., and P.C. Goh (1999). Continuously operating GPS reference station networks: new algorithms and applications of carrier phase-based, medium-range, static and kinematic positioning, In *"Quo vadis geodesiaÉ?"*, special publication to celebrate Prof. Erik W. Grafarend's 60th birthday, Dept. of Geodesy & Geoinformatics, University of Stuttgart, ISSN 0933-2839, 367-378.

Rizos C., Han S., Ge L., Chen H.Y., Hatanaka Y., and K. Abe (2000). Low-cost densification of permanent GPS networks for natural hazard mitigation: first tests on GSI's Geonet network, *Earth Planetary Science*, 52(10), 867-871.

Rizos C., Satirapod C., Chen H.Y., and S. Han (1999). GPS with multiple reference stations: surveying scenarios in metropolitan areas, *Proc. 40th Aust. & 6th S.E.Asian Surveyors Congress*, Fremantle, Australia, 30 Oct. - 5 November, 37-49.

Rothacher M., and L. Mervart (1996). *Bernese GPS Software*, Version 4.0, Astronomical Institute, University of Berne, Switzerland, 417pp.

Sagiya T., et al. (1997). Establishment of permanent GPS observation network and crustal deformation monitoring in the Southern Kanto and Tokai areas, GSI Website, (http://www.gsi-mc.go.jp/ENGLISH/RESEARCH/BULLETIN/vol-41/gps.html).

Schaer S., Beutler G., and M. Rothacher (1998). Mapping and predicting the ionosphere, *Proc. of IGS Analysis Center Workshop*, Darmstadt, Germany, 9-11 February, 307-318.

Schaer S., Beutler G., and M. Rothacher (1999). The impact of the atmosphere and other systematic errors on permanent GPS networks, *Abstracts of IUGG'99*, Birmingham, UK, 19-24 July, 406.

Schaer S., Beutler G., Mervart L., Rothacher M., and T.A. Springer (1996). Daily global ionosphere maps based on GPS carrier phase data routinely produced by the CODE analysis center, *Proc. of the IGS Analysis Center Workshop*, Silver Spring, Maryland, USA, 19-21 March, 181-192.

Schaer S., Beutler G., Mervart L., Rothacher M., and U. Wild (1995). Global and regional ionosphere models using the GPS double difference phase observable, *Proc. of the IGS Workshop on Special Tropics and New Directions*, Potsdam, Germany, 15-17 May, 77-92.

SCIGN (Southern California Integrated GPS Network) Analysis Committee Report September (2000), Web page: http://www.scign.org/sac/.

Sun H., Cannon M.E., and T.E. Melgard (1999). Real-time GPS reference network carrier phase ambiguity resolution, *Proc. Institute of Navigation National Technical Meeting*, San Diego, California, 25-27 January, 193-199.

USGS (U.S. Geological Survey) Earthquake Hazards Program-South California, (1999), Web page: http://pasadena.wr.usgs.gov/hector/hector_srl.html.

Wanninger L. (1995). Improved ambiguity resolution by regional differential modelling of the ionosphere, *Proc. 8th Int. Tech. Meeting of the Satellite Division of the U.S. Inst. of Navigation GPS ION'95*, Palm Springs, California, 12-15 September, 55-62.

Wanninger L. (1997). Real-time differential GPS error modelling in regional reference station networks, *Proc. IAG Symp 118*, Rio de Janeiro, Brazil, 86-92.

Wanninger L. (1999). The performance od virtual reference stations in active geodetic GPS-networks under solar maximum conditions, *Proc. 12th Int. Tech. Meeting of the Satellite Division of the U.S. Inst. of Navigation GPS ION'99*, Nashville, Tennessee, 14-17 September, 1419-1428.

Wild U. (1993) Ionosphere and ambiguity resolution, *Proc. of the 1993 IGS Workshop*, Berne, Switzerland, 25-26 March, 361-369.

Wu J.T. (1994). Weighted differential GPS method for reducing ephemeris error, *Manuscripta Geodaetica*, 20, 1-7.

Wübbena G., Bagge A., Seeber G., Böder V. & P. Hankemeier (1996). Reducing distance dependent errors for real-time precise DGPS applications by establishing reference station networks, *Proc. 9th Int. Tech. Meeting of the Satellite Division of the U.S. Inst. of Navigation GPS ION'96,* Kansas City, Missouri, 17-20 September, 1845-1852.

Yu S.B., and H.Y. Chen (1994). Global Positioning System measurements of crustal deformation in the Taiwan arc-continent collision zone, *TAO*, 5, 477-498.

Yu S.B., Chen H.Y., and L.C. Kuo (1995). Velocity field of GPS stations in the Taiwan area (extended abstract), *Proc. Int. Conf. and 3rd Sino-French Symposium on Active Collision in Taiwan*, Taipei, Taiwan, 22-23 March, 317-327.

Yu S.B., Chen H.Y., and L.C. Kuo (1997). Velocity field of GPS stations in the Taiwan area, *Tectonophysics*, 274, 41-59.

Zhang J. (1999). Precise estimation of residual tropospheric delays in a spatial GPS network, *Proc. 12th Int. Tech. Meeting of the Satellite Division of the U.S. Inst. of Navigation*, Nashville, Tennessee, 14-17 September, 1391-1400.

Zhang Q.J., and K.P. Schwarz (1996). Estimating double difference GPS multipath under kinematic conditions. *Proc. IEEE Positioning Location and Navigation Symp. PLAN'96*, Altanta, Georgia, 22-26 April, 285-291.

Publications from the

SCHOOL OF SURVEYING AND SPATIAL INFORMATION SYSTEMS
(formerly: SCHOOL OF GEOMATIC ENGINEERING)

THE UNIVERSITY OF NEW SOUTH WALES
ABN 57 195 873 179

To order, write to:
Publications Officer, School of Surveying and Spatial Information Systems
The University of New South Wales, UNSW SYDNEY NSW 2052, AUSTRALIA

NOTE: ALL ORDERS MUST BE PREPAID. CREDIT CARDS ARE ACCEPTED.
SEE BACKPAGE FOR OUR CREDIT CARD ORDER FORM.

MONOGRAPHS

Australian prices include postage by surface mail and GST.
Overseas prices include delivery by UNSW's air-lifted mail service (~2-4 weeks to Europe and North America).
Rates for air mail through Australia Post on application.

(Prices effective August 2001)

		Price Australia (incl. GST)	**Price** Overseas
M1.	R. S. Mather, "The Theory and Geodetic Use of some Common Projections", (2nd edition), 125 pp, 1978.	$ 16.50	$ 15.00
M2.	R. S. Mather, "The Analysis of the Earth's Gravity Field", 172 pp, 1971.	$ 8.80	$ 8.00
M3.	G. G. Bennett, "Tables for Prediction of Daylight Stars", 24 pp, 1974.	$ 5.50	$ 5.00
M4.	G. G. Bennett, J. G. Freislich & M. Maughan, "Star Prediction Tables for the Fixing of Position", 200 pp, 1974.	$ 8.80	$ 8.00
M8.	A. H. W. Kearsley, "Geodetic Surveying", 96 pp, 1988.	$ 13.20	$ 12.00
M11.	W. F. Caspary, "Concepts of Network and Deformation Analysis", 183 pp, 2000.	$ 27.50	$ 25.00
M12.	F. K. Brunner, "Atmospheric Effects on Geodetic Space Measurements", 110 pp, 1988.	$ 17.60	$ 16.00
M13.	B. R. Harvey, "Practical Least Squares and Statistics for Surveyors", (2nd edition, reprinted with corrections), 319 pp, 1998.	$ 33.00	$ 30.00
M14.	E. G. Masters and J. R. Pollard (Eds.), "Land Information Management", 269 pp, 1991. (Proceedings LIM Conference, July 1991).	$ 22.00	$ 20.00
M15/1	E. G. Masters and J. R. Pollard (Eds.), "Land Information Management - Geographic Information Systems - Advance Remote Sensing Vol. 1", 295 pp, 1993 (Proceedings of LIM & GIS Conference, July 1993).	$ 33.00	$ 30.00
M15/2	E. G. Masters and J. R. Pollard (Eds.), "Land Information Management - Geographic Information Systems - Advance Remote Sensing Vol. 2", 376 pp, 1993 (Proceedings of Advanced Remote Sensing Conference, July 1993).	$ 33.00	$ 30.00
M16.	A. Stolz, "An Introduction to Geodesy", 2nd extended edition, 148 pp, 2000.	$ 24.20	$ 22.00
M17.	C. Rizos, "Principles and Practice of GPS Surveying", 565 pp, 1997.	$ 46.20	$ 42.00

UNISURV REPORTS - S SERIES

(Prices effective August 2001)

Australian Prices *:	S8 - S20		$11.00
	S29 onwards	Individuals	$27.50
		Institutions	$33.00
Overseas Prices **:	S8 - S20		$10.00
	S29 onwards	Individuals	$25.00
		Institutions	$30.00

* Australian prices include postage by surface mail and GST.
** Overseas prices include delivery by UNSW's air-lifted mail service (~2-4 weeks to Europe and North America). Rates for air mail through Australia Post on application.

S8. A. Stolz, "Three-D Cartesian Co-ordinates of Part of the Australian Geodetic Network by the Use of Local Astronomic Vector Systems", Unisurv Rep. S8, 182 pp, 1972.

S14. E. G. Anderson, "The Effect of Topography on Solutions of Stokes` Problem", Unisurv Rep. S14, 252 pp, 1976.

S16. K. Bretreger, "Earth Tide Effects on Geodetic Observations", Unisurv S16, 173 pp, 1978.

S17. C. Rizos, "The Role of the Gravity Field in Sea Surface Topography Studies", Unisurv S17, 299 pp, 1980.

S18. B. C. Forster, "Some Measures of Urban Residential Quality from LANDSAT Multi-Spectral Data", Unisurv S18, 223 pp, 1981.

S19. R. Coleman, "A Geodetic Basis for Recovering Ocean Dynamic Information from Satellite Altimetry", Unisurv S19, 332 pp, 1981.

S29. G. S. Chisholm, "Integration of GPS into Hydrographic Survey Operations", Unisurv S29, 190 pp, 1987.

S30. G. A. Jeffress, "An Investigation of Doppler Satellite Positioning Multi-Station Software", Unisurv S30, 118 pp, 1987.

S31. J. Soetandi, "A Model for a Cadastral Land Information System for Indonesia", Unisurv S31, 168 pp, 1988.

S33. R. D. Holloway, "The Integration of GPS Heights into the Australian Height Datum", Unisurv S33, 151 pp, 1988.

S34. R. C. Mullin, "Data Update in a Land Information Network", Unisurv S34, 168 pp, 1988.

S35. B. Merminod, "The Use of Kalman Filters in GPS Navigation", Unisurv S35, 203 pp, 1989.

S36. A. R. Marshall, "Network Design and Optimisation in Close Range Photogrammetry", Unisurv S36, 249 pp, 1989.

S37. W. Jaroondhampinij, "A Model of Computerised Parcel-Based Land Information System for the Department of Lands, Thailand", Unisurv S37, 281 pp, 1989.

S38. C. Rizos (Ed.), D. B. Grant, A. Stolz, B. Merminod, C. C. Mazur, "Contributions to GPS Studies", Unisurv S38, 204 pp, 1990.

S39. C. Bosloper, "Multipath and GPS Short Periodic Components of the Time Variation of the Differential Dispersive Delay", Unisurv S39, 214 pp, 1990.

S40. J. M. Nolan, "Development of a Navigational System Utilizing the Global Positioning System in a Real Time, Differential Mode", Unisurv S40, 163 pp, 1990.

S41. R. T. Macleod, "The Resolution of Mean Sea Level Anomalies along the NSW Coastline Using the Global Positioning System", Unisurv S41, 278 pp, 1990.

S42. D. A. Kinlyside, "Densification Surveys in New South Wales - Coping with Distortions", Unisurv S42, 209 pp, 1992.

S43. A. H. W. Kearsley (ed.), Z. Ahmad, B. R. Harvey and A. Kasenda, "Contributions to Geoid Evaluations and GPS Heighting", Unisurv S43, 209 pp, 1993.

S44. P. Tregoning, "GPS Measurements in the Australian and Indonesian Regions (1989-1993)", Unisurv S44, 134 + xiii pp, 1996.

S45. W.-X. Fu, "A Study of GPS and Other Navigation Systems for High Precision Navigation and Attitude Determinations", Unisurv S45, 332 pp, 1996.

S46. P. Morgan et al, "A Zero Order GPS Network for the Australia Region", Unisurv S46, 187 + xii pp, 1996.

S47. Y. Huang, "A Digital Photogrammetry System for Industrial Monitoring", Unisurv S47, 145 + xiv pp, 1997.

S48. K. Mobbs, "Tectonic Interpretation of the Papua New Guinea Region from Repeat Satellite Measurements", Unisurv S48, 256 + xc pp, 1997.

S49. S. Han, "Carrier Phase-Based Long-Range GPS Kinematic Positioning", Unisurv S49, 185 + xi pp, 1997.

S50. M. D. Subari, "Low-cost GPS Systems for Intermediate Surveying and Mapping Accuracy Applications", Unisurv S50, 179 + xiii pp, 1997.

S51. L.-S. Lin, "Real-Time Estimation of Ionospheric Delay Using GPS Measurements", Unisurv S51, 199 + xix pp, 1997.

S53. D. B. Lemon, "The Nature and Management of Positional Relationships within a Local Government Geographic Information System", Unisurv S53, 273 + xvi pp, 1997.

S54. C. Ticehurst, "Development of Models for Monitoring the Urban Environment Using Radar Remote Sensing", Unisurv S54, 282 + xix pp, 1998.

S55. S. S. Boey, "A Model for Establishing the Legal Traceability of GPS Measurements for Cadastral Surveying in Australia", Unisurv S55, 186 + xi pp, 1999.

S56. P. Morgan and M. Pearse, "A First-Order Network for New Zealand", Unisurv S56, 134 + x pp, 1999.

S57. P. N. Tiangco, "A Multi-Parameter Radar Approach to Stand Structure and Forest Biomass Estimation", Unisurv S57, 319 + xxii pp, 2000.

S58. M. A. Syafi'i, "Object–Relational Database Management Systems (ORDBMS) for Managing Marine Spatial Data: ADCP Data Case Study", Unisurv S58, 123 + ix pp, 2000.

S59. X.-Q. Lu, "Strategies for Improving the Determination of Displacements of Sea Surface Temperature Patterns Using Consecutive AVHRR Thermal Images", Unisurv S59, 209 + xiii pp, 2000.

S60. G. Dickson, "GPS-Controlled Photography: The Design, Development and Evaluation of an Operational System Utilising Long-Range Kinematic GPS", Unisurv S60, 417 + x pp, 2000.

S61. J. Wang, "Modelling and Quality Control for Precise GPS and GLONASS Satellite Positioning", Unisurv S61, 171 + x pp, 2001.

S62. Y. Wang, "Knowledge-Based Road Extraction from Aerial Images", Unisurv S62, 178 + xi pp, 2001.

S63. L. Ge, "Development and Testing of Augmentations of Continuously-Operating GPS Networks to Improve their Spatial and Temporal Resolution", Unisurv S63, 230 + xvi pp, 2001.

S64. H.-Y. Chen, "A Study on Real-Time Medium-Range Carrier-Phase-Based GPS Multiple Reference Stations", Unisurv S64, 182 + xxiv pp, 2001.

Credit Card Orders / Payment

from / to

School of Surveying and Spatial Information Systems

The University of New South Wales

Name and postal address of ordering person/organisation:

_____

_____

_____

_____

_____

Date : _____

Day time phone number : _____

Credit Card debit for:

_____ $ _____

_____ $ _____

_____ $ _____

_____ $ _____

Total $ _____

Please debit my credit card: ☐ Mastercard ☐ Visa ☐ Bankcard

Card Name: _____ Signature: _____

Card No: | | | | | | | | | | | | | | | | Expiry Date : _____

Note: UNSW requires that you attach a photocopy of your credit card to this order.